Characterisation of expression and function of respiratory epithelial CD1d

Kambez Hajipouran Benam

Merton College
and
Nuffield Department of Clinical Medicine
University of Oxford

A thesis submitted in fulfilment of the requirements for the degree of Doctor of Philosophy

Hilary Term 2011

Supervisor: Dr. Ling-Pei Ho

Contents

Abstract

In this thesis, I examined the expression of CD1d on respiratory epithelial cells (REC) in human and explored its potential role in mucosal immunity in the lungs. Hitherto, there have been no published reports of CD1d expression on REC though it has been observed on other epithelial surface (notably intestinal epithelial cells). This observation, and work in my supervisor's laboratory demonstrating CD1d-restricted natural killer T cells (*i*NKT) cells as early players in the lungs of influenza A virus (IAV)–infected mice prompted my interest in this area. I hypothesized that CD1d is expressed on REC and that it contributes to activation of *i*NKT cells in the lungs via presentation of endogenous or pathogenic glycolipids. I asked following questions – i) is CD1d expressed on REC ii) can this expression be regulated and iii) does CD1d expression on REC have a function.

This thesis provides the first evidence for CD1d expression on human RECs (in cell lines and primary RECs) and also presence of alternatively spliced variants. CD1d expression was inducible by viral-associated signals *in vitro* and despite being non-professional antigen presenting cells, RECs can present glycolipid (α–GC) to, and activate *i*NKT cells in a CD1d-dependent process resulting in production of both T_h1 and T_h2 cytokines. Using whole genome expression profiling, I then showed that *i*NKT cells expressed a distinct profile of genes while in direct contact with α–GC-bound CD1d on RECs compared to cells separated by transwell membrane. Here early biological pathways were dominated by cytokine and chemokine related genes (JAK-STAT signaling pathways, cytokine-responsive elements and cytokine/chemokine genes) and apoptosis-related genes. This

suggested that glycolipid-bound CD1d on REC was capable of inducing a programme of immune activation in *i*NKT cells. I concluded my work by examining if CD1d expression on RECs influenced its active role in immunity. Using wild type and CD1d-deficient transgenic mice challenged with IAV, I showed that CD1d expression is induced on REC *in vivo* after viral challenge, and in the absence of CD1d, mice showed worse outcome. RECs isolated from CD1d-deficient mice had a much stronger gene expression profile for pro-inflammatory genes. This suggested that CD1d expression on REC could have a bi-directional effect – on the RECs that expressed CD1d (preventing excessive immune-related genes activation) and on the *i*NKT cells that it engaged (activation, with pro-immunity effects). The thesis concludes with discussion of the potential implications of these findings and future work to examine hypotheses generated from this work.

Acknowledgement

I would like firstly to thank my supervisor Dr. Ling-Pei Ho for her advice, help, and encouragement throughout my DPhil studies. She always challenged me scientifically and pushed me beyond my comfort zones.

The analysis of the microarray data was performed with help from Helen Lockstone, bioinformatician at the Wellcome Trust Human Genetics Centre.

I would also like to thank other members of Ho group – Wai Ling, Laura, Sharon, Suzanne, and Anjali for their support and friendship, other scientist in WIMM, like Chris Newbold, Simon Brackenridge, and Veronica Chang.

I would like to thank my family (Akram, Jabbar, Kayvan, and Kimia), and my wife Cigdem who have been the greatest source of love during my DPhil. And a final thank for all that helped me achieve this work.

Abbreviations

α–GC	α-galactosylceramide
α1-AT	α1-antitrypsin
aa	Amino acid
Ab	Antibody
Ag	Antigen
AMP	Antimicrobial peptide
AP3/2	Adaptor protein complex-3/2
APC	Antigen presenting cell
APRIL	A proliferation-inducing ligand
ARG1	Arginase 1
ATRA	all-*trans* retinoic acid
β–D–GlcCer	β–D–glucosyl ceramide
β_2m	β_2-microglobulin
βtubIV	β-tubulin IV
BAFF	B cell activating factor of TNF family
BALF	Bronchoalveolar lavage fluid
BM	Bone marrow
bp	Base pair
BP	Biological process
BST2	Bone marrow stromal cell antigen 2
CCK	Cholecystokinin
CD1dKO	CD1d knock out
CDKN1B	cyclin-dependent kinase inhibitor 1B
CLEC4	C-type lectin 4
CRP	C-reactive protein
CRTAM	Cytotoxic and regulatory T cell molecule
CTL	C-type lectin
DAVID	Database for Annotation Visualisation and Integrated Discovery
DC	Dendritic cell
DN	Double negative
DP	Double positive
DUSP6	Dual specificity phosphatase 6
dsRNA	Double stranded RNA
E-cad	Epithelial cadherin
EDTA	Ethylene diamine tetra acetic acid
EpCAM	Epithelial cell adhesion molecule
ER	Endoplasmic reticulum
ES	Enrichment score
FC	Fold change
FDR	False discovery rate
FcRn	Neonatal Fc receptor
FITC	Fluorescein isothiocyanate
GL	Gene list
GMM	Glucose monomycolate
GO	Gene ontology

GPI	Glycosylphosphatidylinositol
GSEA	Gene-Set Enrichment Analysis
GSL	Glycosphingolipid
GZMB	Granzyme B
HA	Haemagglutinin
HBEGF	Heparin binding EGF-like growth factor
hCD1D	Human CD1D
HEG1	HEG homolog 1
Hexb	Hexosaminidae b
HEV	High endothelial venule
HLA	Human leukocyte antigen
HRV-16	Human rhinovirus type 16
HSV-1	Herpes simplex virus type 1
IAV	Influenza A virus
ICAM	Intercellular adhesion molecule
IEC	Intestinal epithelial cell
IER3	Immediate early response 3
iGb3	Isoglobotrihexosylceramide
*i*NKT	Invariant natural killer T cell
imDC	Immature dendritic cell
i.p	Intraperitoneal
IP	Immunoprecipitation
IRF	Interferon response factor
ITAM	Immunoreceptor tyrosine-based activation motif
JAK	Janus kinase
KEGG	Kyoto Encyclopaedia of Genes and Genomics
KSHV	Kaposi sarcoma-associated virus
LAM	lipoarabinomannan
LFA-1	Leukocyte function associated-1
LIF	Leukaemia inhibitory factor
Limma	Linear models for microarray analysis
LRP	Luecine-rich repeat
LRT	Lower respiratory tract
LTA	Lipoteichoic acid / Lymphotoxin alpha
mCD1D	Murine CD1D
MACS	Magnetic activated cell sorting
MDA-5	Melanoma differentiation-associated protein 5
mDC	Mature dendritic cell
MDSC	Myeloid-derived suppressor cell
MIP	Macrophage inflammatory peptide
MD-DC	Monocyte-derived dendritic cell
MF	Molecular function
MLR	Mixed lymphocyte reaction
MTP	Microsomal triglyceride transfer protein
MUC5AC	Mucin 5Ac
MW	Molecular weight
NA	Neuraminidase
NEP	Nuclear export protein
NES	Nuclear export sequence / Normalised enrichment score
NHBE	Normal human bronchial epithelial

NLR	NOD-like receptor
NLS	Nuclear localisation signal
NOS2	Nitric oxide synthase 2
NP	Nucleoprotein
NR4A1	Nuclear receptor 4A1
NS	Non-spliced variant
OLFM4	Olfactomedin 4
OSM	Oncostatin M
PBMC	Peripheral blood mononuclear cell
PC	Phosphatidylcholine
PCK	Pancytokeratin
PDGFRβ	Platelet-derived growth factor receptor beta
PE	Phosphatidylethanolamine
PHA	Phytohaemagglutinin
PI	Phosphatidylinositol
PIM	phosphatidylinositol mannoside
PPARγ	peroxisome proliferator-activated receptor gamma
PR8	Influenza A virus A/Puerto Rico/8/34 strain
PRR	Pathogen recognition receptor
RA	Retinoic acid
REC	Respiratory epithelial cell
RIG-I	Retinoic acid-inducible gene I
RIN	RNA integrity number
RMA	Robust multi-array average
RLR	RIG-I-like receptors
RSV	Respiratory syncytial virus
SA	Sialic acid
SAP	SLAM-associated protein
sIgA	Secretory IgA
SLAM	Signalling lymphocyte activation molecule
SLC26A4	Solute carrier family 26, member A4
SOCS	Suppressor of cytokine signalling
SPP1	Secreted phosphoprotein 1
SP-A/D	Surfactant protein A/D
SP-PIR	Swiss-Prot and Protein Information Resource
ssRNA	Single stranded RNA
STAT	Signal transducer and activator of transcription
T	Cytoplasmic tail
TBCC	Tubulin cofactor C
TCR	T cell receptor
TGN	Trans-Golgi network
TM	Transmembrane
TNFRSF10	TNF receptor superfamily 10
TRAIL	TNF-related apoptosis inducing ligand
URT	Upper respiratory tract
VE-cad	Vascular endothelial cadherin
VLP	Virus-like particle
VSV	Vesicular stomatitis virus
vRNA	Viral RNA
WT	Wild type

Chapter 1. Introduction

1.1 Overview

1.2 CD1d

1.2.1. CD1D genomic organisation
1.2.2. CD1D transcript splicing
1.2.3. Structure of the CD1d protein
1.2.4. CD1d ligands
1.2.5. Assembly and intracellular trafficking of CD1d
1.2.6. Cellular expression and tissue distribution of CD1d
1.2.7. Regulation of CD1d expression

1.3 Natural killer T (NKT) cells

1.3.1. NKT phenotype
1.3.2. Development and selection of NKT cells
1.3.3. Activation and functional characterisation of NKT cells
1.3.4. NKT tissue distribution and recruitment
1.3.5. Role of NKT cells in antimicrobial immunity

1.4 Influenza infection

1.4.1 Influenza virus structure and morphology
1.4.2 Influenza virus assembly and budding
1.4.3 Tissue tropism of influenza virus

1.5 Respiratory epithelial cells

1.5.1. Epithelial cells engagement in active immunity
1.5.2. Epithelial cells interaction with antigen presenting cells
1.5.3. Epithelial cell interaction with lymphocytes

1.6 Aim and hypothesis

Chapter 1.

Introduction

1.1. Overview

CD1d is an MHC class I-like molecule which is expressed predominantly by professional antigen presenting cells, like dendritic cells (DCs), and cells lining the mucosal surfaces, like intestinal epithelial cells. It is best known for its ability to present glycolipid antigens to and activate a distinct subset of T cells called invariant natural killer T (*i*NKT) cells – which are characterised by expression of an invariant TCR α chain. Shortly after stimulation, *i*NKT cells secrete an array of different cytokines and influence the function of both innate and adaptive immune cells. Several mouse studies have identified a pivotal role for *i*NKT cells in antimicrobial immunity, particularly against viruses. This indicates a requirement for CD1d expression in normal immune homeostasis.

Influenza A virus (IAV) is an enveloped segmented RNA virus which belongs to *Orthomyxoviridae* family. Structurally, it is made up of an envelope, a core and an intermediate layer. The assembled viral particle can be pleomorphic but generally adapts a spherical configuration. IAV exhibits natural tropism for infecting respiratory epithelial cells (RECs).

RECs by forming intercellular tight junctions create a passive barrier against entry of exogenous particles and infective agents. However, more evidence on participation of RECs in active immunity is emerging. These cells express pathogen

recognition receptors (PRRs), secrete cytokines, chemokines, and antimicrobial products, and are capable of regulating maturation and function of local DCs, and directly interacting with T cells.

1.2. CD1d

1.2.1. CD1D genomic organisation

The immune system has evolved strategies to recognise both peptide and lipid antigens. Major histocompatibility complex (MHC) class I and II molecules participate in presentation of peptide antigens (Ag) derived from either endogenous (self) or exogenous (foreign) sources, to T lymphocytes. The CD1 family, on the other hand, comprises molecules that have the capacity to present lipid antigens. These were originally identified using monoclonal antibodies to human thymocytes and a number of B lymphoma cell lines [2]. CD1 genes show a high structural homology to MHC class I genes human leukocyte Ag (HLA)-A, -B, and –C, in encoding a single type I integral membrane protein (α heavy chain) that comprises three extracellular domains: α1, α 2, and α3. Similar to HLA, CD1 proteins can non-covalently associate with β_2-microglobulin (β_2m). However, they illustrate limited functional polymorphism, genetic and allelic variation, and are expressed on a more restricted repertoire of cell types, typically professional antigen presenting cells (APC) [3].

In human there are five CD1 genes designated CD1A-E, corresponding to CD1a-e glycoproteins, which are located as a tightly clustered gene set on chromosome 1 q23.1 (Figure 1.2.1.1). CD1 isoforms, on the basis of sequence homology in α1 and α 2 domains, can be divided into three groups: group I comprising CD1a, CD1b, and

CD1c, groups II and III containing only CD1d and CD1e, respectively [4]. Unlike humans, mice lack groups I and III CD1 genes and only contain two CD1D orthologs which are present in a tail-to-tail orientation on chromosome 3 qF1 (Figure 1.2.1.1) [5]. The murine CD1D (mCD1D) genes exhibit highest similarity in the sequence of their α3 exon (>99% [5]) and encode for CD1.d1 and CD1d.2 proteins. The two genes are separated by about 6kb. mCD1d1 corresponds to human CD1d.

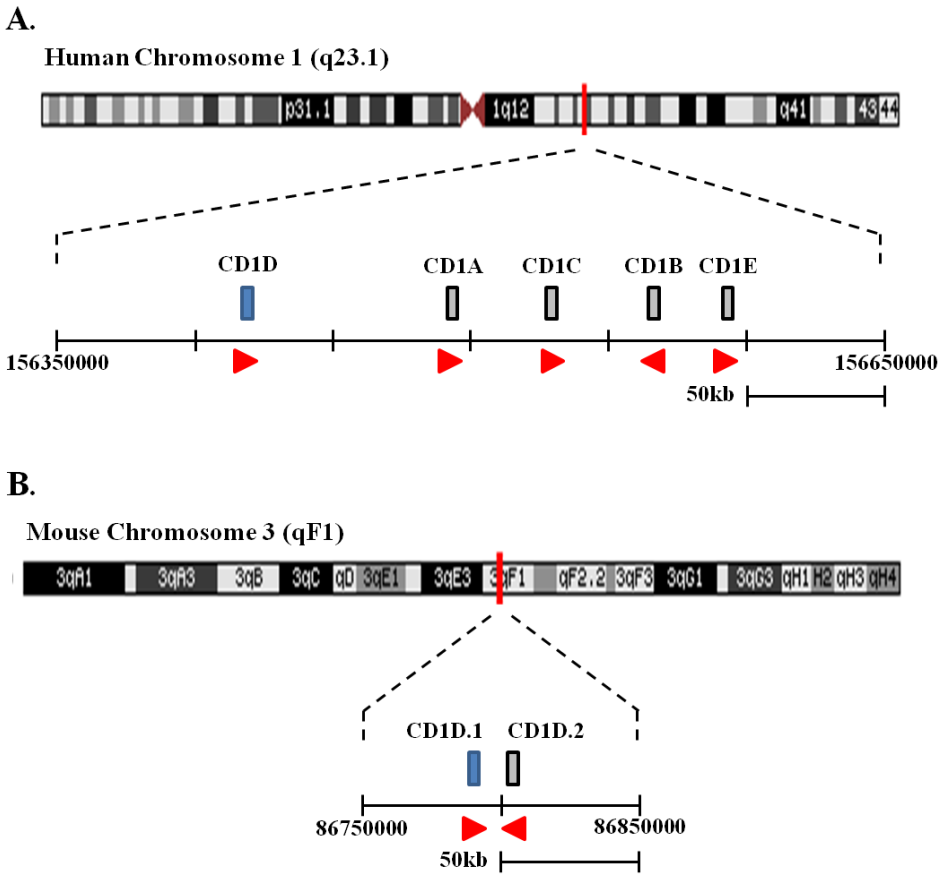

Figure 1.2.1.1. Schematic representation of human and mouse CD1 locus on genome. CD1 genes are illustrated as coloured boxed on appropriate chromosome (human in (A) and mouse in (B)). The scale bar depicts distance on chromosome of 50kb, and red arrowheads highlight direction of transcription. Note tail-to-tail orientation of CD1D1 and CD1D.2 in mouse, and the big gap (~75kb) between hCD1D and other CD1 family members.

Unlike allelic variation and extensive polymorphism which are characteristic of classical MHC class I and II molecules, polymorphism in CD1D is extremely limited. One study has reported different CD1D1 alleles between wild-derived mouse strains,

namely *Mus musculus* (C57BL/6), *Mus castaneus*, and *Mus spretus* [6].The allelic variation was shown to influence ligand presentation by CD1d, and subsequent development and activation of CD1d-restricted T cells [6]. Another study reported a rare polymorphism in exon 2 of human CD1D (hCD1D) resulting in amino acid (aa) replacement of threonine by serine. The frequency of new allele was only 1% in healthy donors [7]. However, genetic variation in CD1D gene across various species studied so far, like human, mouse, rat, is very low and suggests evolutionary conservation of the gene. In addition, to date no clear correlation between CD1D polymorphism, and infection and autoimmunity has been established [3].

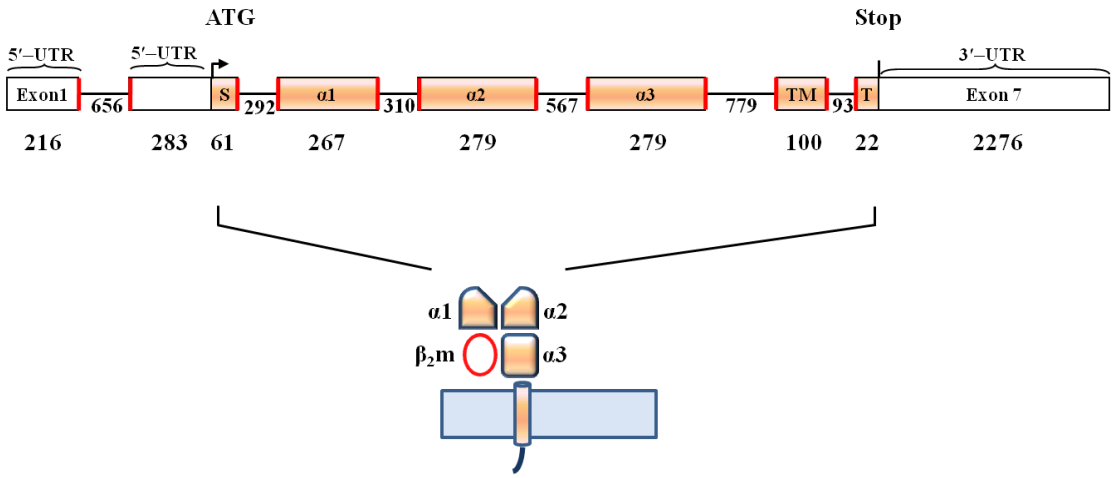

Figure 1.2.1.2. **Graphical representation of human CD1D gene.** Full-length CD1d heavy chain is encoded by up to six exons; each exon corresponds to a distinct domain in the protein. Top: exons are indicated by boxes (coloured: coding; white: non-coding) and introns by horizontal lines separating them. Figures underneath each box or line represent length (bases) of the corresponding segment. Bottom: simplified presentation of full-length CD1d protein in plasma membrane. UTR: untranslated region; S: signal peptide; TM: transmembrane; T: cytosolic tail; β_2m: β_2-microglobulin.

1.2.2. CD1D transcript splicing

In humans, CD1D gene transcribes into seven exons which are separated by six introns. Exons 3–5 encode the α1–α3 extracellular domains, and exon 6 encodes the hydrophobic transmembrane domain. Signal peptide and cytosolic tail of CD1d are encoded by last part of exon 2 and initial segment of exon 7, respectively (Figure

1.2.1.2). Alternative mRNA splicing of CD1D, unlike HLA molecules, such as HLA-G which has limited polymorphism and holds high structural similarity with CD1D [8], and other CD1 family members, like CD1A, CD1C, and CD1E [9,10], has not been extensively studied.

In one report, analysis of CD1D transcripts in healthy human peripheral blood mononuclear cells (PBMCs) identified 8 variants [11]. Four of these variants lacked α3 domain (major β_2m–binding site). The transmembrane domain (necessary for plasma membrane insertion and surface protein expression) was also absent in two of these variants. In addition, the other four variants had partial defects in α1 and/or α2 domains (which form antigen binding groove and are crucial for ligand presentation and downstream activation of CD1d-restricted T cells) [11]. One variant lacked both α3 and transmembrane exons, while α1and α2 domains remained unchanged. Authors later showed in rheumatoid arthritis patients, expression of this variant in PBMCs was significantly lower than healthy controls [12], and levels of soluble CD1d protein coded by this transcript in the plasma followed a similar pattern [13]. However, functional significance of other CD1D mRNA variants and potential tissue-specific regulation of CD1D splicing machinery has not yet been fully addressed.

In a separate study, human choriocarcinoma cell lines JEG-3 and JAR, and placental trophoblast cells were reported to express α3–deficient CD1D variant [14]. Cell–specific expression of this variant was only compared to amnion and MOLT-4 cells. Moreover, no study on modulation of expression of this variant was carried out to explore differential regulation under inflammatory conditions or during infections.

1.2.3. Structure of the CD1d protein

Solving the crystal structure of CD1 proteins, including the mouse and human CD1d [15,16] has helped us improve our understanding of the protein conformation and properties of the ligands that can be presented by these molecules. The overall secondary, tertiary and quaternary structure of mouse CD1d1 was found to be closely related to MHC class I and II molecules and other related proteins like neonatal Fc receptor (FcRn) [16]. Antigen binding groove – formed by α1 and α2 domains, consisted of an eight-stranded anti-parallel β-sheet at the bottom with two α-helical structures sitting on top. However, unlike MHC class I, the groove in mCD1d1 was shown to be substantially narrower – due to relative proximity of α-helices along the longitudinal axis, and deeper – as a result of greater curvature of β-sheet platform, 4–6 Å raised α1 helix and upward kink in α2 helix [16]. The larger groove in mCD1d1 accommodated two major pockets that were lined with hydrophobic amino acid residues capable of forming hydrogen bonds. By analogy to MHC class I, these pockets or channels were designated A′ and F′. Molecular structure of human CD1d later revealed comparable features: a large hydrophobic binding groove and two channels connecting to surface that could accommodate alkyl chains [15]. In both mouse and human, the F′ channel (also called C′ in hCD1d) can accommodate an alkyl chain of up to 18 carbons (C18) long. On the other hand, the maximum length of hydrocarbon chain that can fit in A′ channel is 26 carbon atoms (C26) in hCD1d and 24 (C24) in mCD1d1. Differences between binding grooves and attached pockets serve as a platform to fine-tune ligand binding capabilities across CD1 family members. Human CD1b, for instance, has a larger volume than hCD1d (2200 $Å^3$ versus 1400 $Å^3$) and contains four interconnecting group of channels, namely A′, C′, F′, and T′, that can overall

accommodate alkyl chains of up to 80 carbons long. This translates into differences in the nature of ligands that can potentially load onto CD1s.

Molecular structure of hCD1d associated with exogenous glycolipid α–galactosyl ceramide (α–GC) revealed occupancy of total volume of groove cavities by the ligand hydrocarbon side chains [15]. Viewed from top, one of the α–GC alkyl chains fit in the A′ pocket in an anti-clockwise circular conformation, whereas the other hydrocarbon chain adopted a straighter conformation in C′ channel. The polar head of ligand – galactose ring, was the only part of α–GC that extended above the binding groove and was exposed to recognition by T cell receptor (TCR) on CD1d-restricted T cells.

1.2.4. CD1d ligands

Efforts to identify ligands for CD1 molecules led to discovery of mycolic acid, a non-protein microbial Ag from *Mycobacterium tuberculosis*, that was presented in a CD1b-restricted manner to TCR$\alpha\beta^+$ T cells [17]. To date, a range of endogenous and microbial-derived exogenous fatty acid, glycolipid, phospholipid and lipopeptide antigens that can be presented by CD1a-c have been identified [3,18]. This includes a variety of lipids from mycobacterial cell wall such as glucose monomycolate (GMM), phosphatidylinositol mannoside (PIM), and lipoarabinomannan (LAM) which can be presented by CD1b, and mannosyl-β-1-phosphoisoprenoid and didehroxymycobactin that can be loaded and presented by CD1c and CD1a, respectively. Oligosaccharide-containing sphingolipids like ganglioside GM1 represent a group of self ligands that can be presented by CD1b molecules [3].

The best-characterised CD1d ligand is α–galactosyl ceramide, a glycolipid obtained from marine sponge *Agelas mauritianus*, which can sit tightly in antigen binding groove with high affinity and act as a potent agonist to activate CD1d-restricted T cells. KRN7000, a synthetic analogue of α–GC, is the most widely-used α–galactosyl ceramide experimentally. It comprises a C26 fully saturated fatty acid chain, and a C18 phytosphingosine base which is linked through an α–anomeric bond to galactose ring – polar head of molecule (Figure 1.2.4.1) [1].

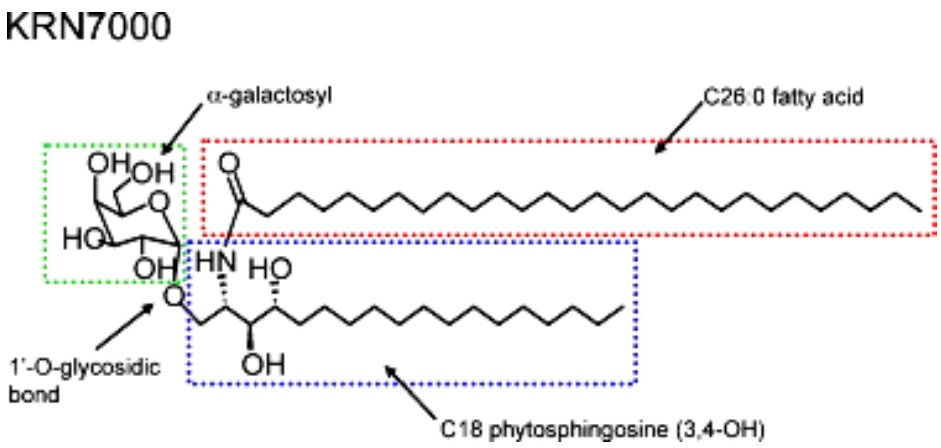

Figure 1.2.4.1. **Structural organisation of KRN7000 – the most widely used α–GC synthetic analogue *in vitro* and *in vivo*.** The polar galactose ring is linked in an alpha configuration to C18 sphingosine chain. The acyl chain moiety of molecule is fully saturated and is 26 carbon atoms long. Picture taken from *Venkataswamy* and *Porcelli* [1].

Advances in identification of other potential CD1d ligands have also led to discovery of a number of normal endogenous, bacterial, and tumour-derived glycolipids [19]. Glycosylphosphatidylinositol (GPI), a glycolipid that can attach C-terminus of cell proteins through its carbohydrate moiety in the process of post-translational modification, was the first natural ligand reported to bind mCD1d1 [20]. Phosphatidylinositol (PI) [21,22], and phosphatidylcholine (PC) [23] were soon after reported as other endogenous CD1d ligands. Due to biochemical challenges in

extracting self ligands, a recent study demonstrated that using protease–cleavable surface, secretory, and endoplasmic reticulum (ER)–confined protein variants, CD1d can survey cellular compartments from ER to secretory pathway, and the most abundantly available lipid sits onto its binding groove [24]. PC was the predominant phospholipid detected on ER-retained CD1d, whereas surface cleavable CD1d bound to sphingomyelin and lysophospholipids (like lyso PC, lyso phosphatidylserine (PS), and lyso phosphatidylethanolamine (PE)) [24]. Sulfatide, a major myelin-derived glycolipid in the nervous system, was also found to be loaded onto CD1d in mouse model of multiple sclerosis and activate a separate group of CD1d-restricted T cells [25]. Overall, self-phospholipids which constitute the majority of cell membranes have been postulated to play a key role in folding and stabilisation of CD1d molecule, and auto-reactivity of CD1d-restricted T cells although it is markedly weaker than stimulation by an exogenous ligand like α–GC [1].

In addition to sulfatide and phospholipids, a few studies have introduced glycosphingolipids (GSLs) as another group of putative natural ligands for CD1d. An initial study reported lack of CD1d-restricted T cell activation by a mouse melanoma cell line (GM-95), which was deficient in β–D–glucosyl ceramide (β–D–GlcCer) synthase and therefore unable to synthesize most of cellular glycosphingolipids [26]. Strikingly, recognition and activation of T cells by GM-95 surface CD1d1 was restored after reconstitution of cells with α–D–GlcCer synthase cDNA [26]. Consistent with this finding, another study using *Hexb*$^{-/-}$ mice, that were deficient in lysosomal GSL degrading enzyme α–hexosaminidae b (Hexb), reported isoglobotrihexosylceramide (iGb3) as the new self CD1d antigen [27]. However, relevance of iGb3, a trigycosylceramide, as an endogenous CD1d ligand has proven controversial. To dissect

complexity of ligand structure, it has been demonstrated that ceramide moiety in iGb3 is linked to proximal sugar of molecule through a β–linkage bond, instead of α–linkage found in other potent ligands like α–GC [28]. On the other hand, trimming of glycolipids in lysosomes by a variety of glycosidases is not required for iGb3 as all the three sugars in the molecule are necessary for activation of CD1d-restricted T cells; hence ruling out the need for lysosomal processing [28]. Absence of iGb3 in thymus and dendritic cells (DCs) of mouse and human tissue further questioned significance of this GSL in development and stimulation of CD1d-restricted T cells [29].

Microbial ligands for CD1d include both ceramide– and diacylglycerol (DAG)–based lipids. Diacyl galactosyl glycerol from *Borrelia burgdorferi* [30], the causative agent of Lyme disease, and α–glycuronosyl ceramide from *Sphingomonas* species [31,32] fall in this category. Apart from bacterial lipids, protozoal-derived antigens have also been demonstrated to activate certain subsets of CD1d-restricted T cells in mice [33,34]. Diacylated PI moiety of lipopeptidophosphoglycan (EhLPPG) antigen from *Entamoeba histolytica* membrane, protozoan responsible for amoebic liver abscess in mice, has been reported to induce IFNγ production from CD1d-restricted T cells and reduce the severity of infection [34]. Lipophosphoglycan from *Leishmania donovani* represents another example of protozoal foreign ligands for CD1d [33].

GD3, a ganglioside that is expressed at high levels on tumours of neuroectodermal origin, like melanomas, but low levels on few normal human or mouse tissues has been studied as a candidate tumour-derived CD1d ligand [35]. Immunising mice with GD^{+} melanoma cell line or syngenic APCs loaded with GD3 induced T cell proliferation in a CD1d-dependent manner [35].

1.2.5. Assembly and intracellular trafficking of CD1d

Following synthesis, CD1d molecules translocate into the lumen of endoplasmic reticulum through signal peptide sequence (Figure 1.2.5.1). N-linked glycosylation and endogenous lipid loading are two key processes affecting CD1d in this cellular compartment. Mouse CD1d1 contains 5 asparagine residues in α1 (N25, N38, N60) and α2 (N128, N183) domains as potential N-glycosylation sites [36]. Because of high amino acid sequence homology in α1 and α2 domains between mouse and human CD1d (60% [37]) only N25 site is absent in hCD1d [36]. Glycosylation, on one hand, enables CD1d molecule to associate with ER chaperones calnexin and calreticulin, as well as thiol oxidoreductase ERp57 [38]. This helps disulfide bond formation and folding of the glycoprotein [38]. On the other hand, glycosylation has been reported essential for biosynthesis and surface expression of mCD1d1, and consequently appropriate stimulation of CD1d-restricted T cells [36].

In parallel, ER provides an environment for self-phospholipids, particularly PC [24], to be loaded onto CD1d binding groove. This is believed to facilitate CD1d folding and stabilise its conformation until the lipid is exchanged for microbial or other exogenous glycolipids in endocytic pathway [39,40]. Microsomal triglyceride transfer protein (MTP) is an ER resident lipid transfer protein that has been shown by *in vitro* lipid loading and immunoprecipitation assays to assist phospholipid transfer onto CD1d [41,42]. Unexpectedly, one study has suggested a more distal role for MTP in antigen presentation by CD1d during the process of recycling from lysosomes to plasma membrane [43].

Association with β_2m occurs next and then CD1d exits ER to reach cell surface. Initial studies reported a requirement for β_2m for functional and stable surface CD1d expression [44]. However, this was challenged as β_2m-independent CD1d expression was later demonstrated, especially on intestinal epithelial cells [45,46].

After leaving ER, CD1d can pass through normal secretory pathway, via Golgi network, to arrive at plasma membrane. Alternatively, it has been suggested that through a separate route CD1d can associate with invariant chain (Ii) and MHC class II complexes in ER [47,48]. Such interaction leads to accumulation of some CD1d molecules in late endosomal/lysosomal compartments – where MHC class II during its transport transiently accumulates [48]. The two identified pathways act independently and lead to antigen presentation and activation of CD1d-restricted T cells [47].

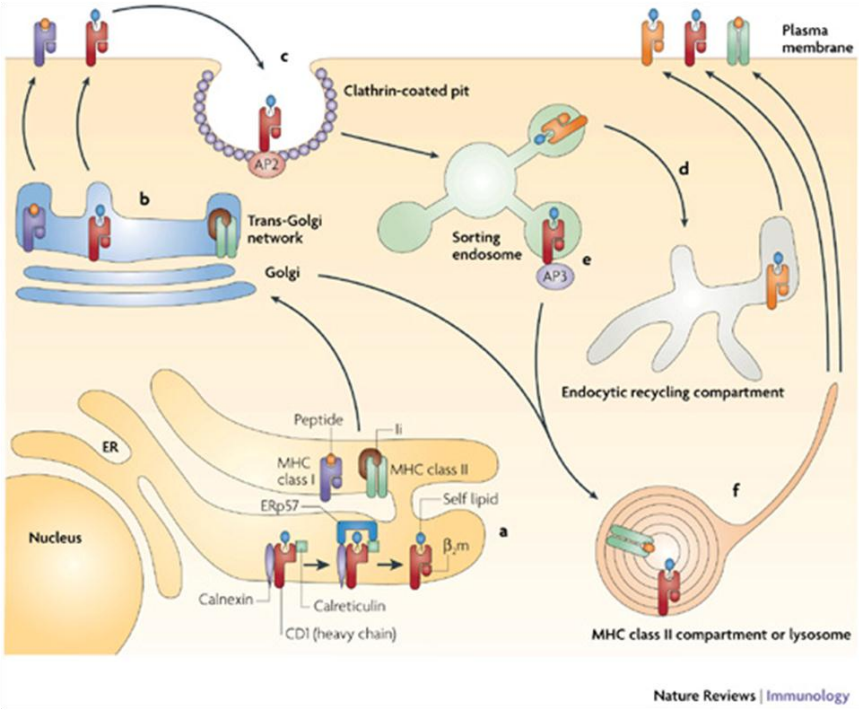

Figure 1.2.5.1. CD1d assembly and trafficking. Following biosynthesis, CD1d is bound to chaperones, calnexin and calreticulin, in ER. CD1d then leaves endoplasmic reticulum, associated with β_2m, for plasma membrane via Golgi. It is internalized through interaction of AP2 with tyrosine motif in its cytoplasmic tail and guided to early/sorting endosomes. From here, CD1d can further traffic to late endosomal or lysosomal compartment and subsequently get recycled back to cell surface. Diagram adapted from Barral DC and Brenner MB, Nature Reviews Immunology, 2007.

Once expressed on the cell surface, tyrosine-based sorting motif in cytosolic tail drives internalisation of CD1d [49,50] which is required for its ability to sample most foreign/microbial antigens in the endocytic pathway. mCD1d1 tail, for example, contains a YQDI (Tyr-Gln-Asp-Ile) amino acid sequence that conforms to YXXΦ (Y= Tyrosine, X= any aa, Φ= bulky hydrophobic aa) consensus motif mediating endosomal localisation of many different surface proteins [49,51]. The tyrosine motif of mouse and human CD1d mainly interacts with μ (one of the four) subunit of adaptor protein complex-3 (AP3) and AP-2, respectively [49]. Via this interaction CD1d joins endocytic vesicles from clathrin-coated pits of plasma membrane. As a consequence of differential AP binding, murine CD1d1 traffics through early and late endosomal compartments to lysosomes, whereas human CD1d has a more limited endosomal and lysosomal distribution [3].

Access to endocytic compartments is important for processing of glycolipid antigens and their presentation by CD1d [22,52]. Saposins are a group of small and heat-stable glycoproteins that catalyse hydrolysis of lysosomal sphingolipids. There are four saposins (A, B, C, and D) which are generated by proteolytic cleavage of a common precursor – prosaposin. It has been reported that saposins, particularly saposin B, act as lysosomal chaperones to mediate lipid loading onto CD1d [52]. This was illustrated by essential role of saposins in mobilising lipids, like α–GC, from lysosomal membrane and facilitate their association with CD1d [22]. Following lipid exchange, CD1d-lipid complexes are recycled back to the cell surface for presentation to CD1d-restricted T cells.

1.2.6. Cellular expression and tissue distribution of CD1d

CD1d expression, in humans, has been well documented on myeloid– and lymphoid–derived haematopoietic cells [53,54]. Amongst myeloid lineage, blood monocytes, monocyte-derived immature (imDC) and mature DCs (mDC), and macrophages were reported to express low levels of CD1d on their surface [54]. Despite such low expression levels, these cells were remarkably potent in presenting α–GC to CD1d-restricetd T cell clones *in vitro* to induce their rapid proliferation [54]. Unlike myeloid lineage cells, circulating and lymph node mantle zone B cells as well as cortical thymocytes express high levels of CD1d on their surface [53]. This was illustrated by flow cytometry and immunohistochemical analysis. Resting peripheral T cells and medullary thymocytes, on the other hand, are CD1d negative or express very low amounts of the protein [53].

CD1d expression has also been characterised in a variety of extra-haematopoietic human tissues [55]. Vascular smooth muscle, and epithelial and parenchymal cells in a range of tissues including liver, kidney, intestine, and skin were reported to be the major cell types to stain positive for anti-CD1d antibodies [55]. Intestinal epithelial cells (IECs) were among the early cell types suggested to express CD1d. Immunoperoxidase staining of snap-frozen surgical specimens from intestine detected CD1d in epithelial cells [56]. In ileum, the protein was present along the length of most villi and crypts, using a rat anti-mouse CD1 antibody (Ab) which cross-reacted with hCD1d. At the cellular level, the protein was most prominently distributed at apical cytoplasm and along the basolateral surface of IECs [56], indicating a potential role for interaction with intraepithelial lymphocytes (IELs). Immunolocalisation of epithelial CD1d on cross-sections of human small bowel and colon, and *in vitro*

polarised IEC line T84 in another study identified a similar pattern of cellular distribution [57]. Freshly isolated IECs pulsed overnight with α–GC were capable of presenting the lipid antigen in a dose-dependent manner to CD1d-restricted T cells to activate them to produce IL-2 [58].

Investigating contribution of non-conventional T cells to psoriasis – a T_h1-biased chronic inflammatory skin disorder, led to characterisation of CD1d on keratinocytes [59,60]. Using a panel of CD1d-sepcific monoclonal Abs (mAbs), CD1d was detected in normal and psoriatic human skin [60]. Notably, basal expression was relatively low and generally restricted to keratinocytes in the three or four outermost layers of epidermis (stratum granulosum) just beneath the lipid rich-stratum corneum. At the cellular level, keratinocytes exhibited a distinct plasma membrane staining pattern for CD1d along the cell boundaries. In line with functional data from IECs, upon co-culture with CD1d- restricted T cell clones and α–GC, keratinocytes activated the T cells to produce IFNγ into the cell culture supernatant [60]. Exploring the role of CD1d in mucosal immunity, expression on other epithelial cells has been also been demonstrated. The lining of human lower reproductive tract, particularly basal and suprabasal cell layers of vaginal, ectocervical, and penile urethral epithelia were strongly immunoreactive with hCD1d-specific mAb [61].

Mice express two CD1D genes, CD1D1 and CD1D2, which share high (90-95%) homology [62]. CD1D2 differs from CD1D1 in 17 amino acid residues in the coding region including a cysteine to tryptophan replacement at position 168 that in conserved in most MHC class I-like molecules [63]. This amino acid substitution ablates ability of CD1D2 to form a disulfide bridge in the α2 domain [64]. CD1D2 mRNA is predominantly expressed in thymus, to a lesser extent in liver, and at low

levels in lymph node and spleen, but the protein is detected only on the surface of thymocytes [64]. CD1D2 is unable to take place of CD1D1 for development and selection of CD1d-restricted T cells in CD1d1$^{-/-}$ mice [64]. Due to limited expression in thymus, most of CD1D outside thymus has been focused on CD1D1.

Similar to human, CD1d1 is expressed on the surface of lymphocytes and professional APCs like DCs and macrophages [65,66]. Using two CD1d-sepcifc mAbs, the protein expression has been demonstrated on the cells from spleen, lymph node, thymus and bone marrow [66]. B cells tend to reduce their surface CD1d1 level as they mature since bone marrow (BM) B220^{+} CD5^{-} B cells (mostly immature) have slightly higher CD1d1 than lymph node (mostly mature) and splenic B cells [65]. On the other hand, in the spleen of mice marginal zone B cells show the highest level of CD1d1 compared to HSA^{hi} BM emigrant and CD21^{int} CD23^{hi} IgM^{low} mature follicular B cells. Murine CD1d1, unlike hCD1d, is found at high levels on the surface of (splenic) CD4^{+} and CD8^{+} T cells [65] and a subset of CD1d-restricted T cells [67]. Outside haematopoietic cells, CD1d1 has also been detected on murine intestinal epithelial cells and hepatocytes [68].

1.2.7. Regulation of CD1d expression

Regulation of CD1d expression, either at mRNA and protein level, has been the subject of a few studies, but conflicting evidences exist in the literature. One study reported reduction in CD1d glycoprotein level on freshly isolated blood monocytes during culture with IL-4 and GM-CSF, a condition used to generate DCs [54]. This was associated with induction of group I CD1 molecules (CD1a, CD1b and CD1c) [53,54,69], and may reveal differential expression regulation between CD1 family

members. Culturing monocytes in the presence of IFNγ, IFNα, IL-1 and TGFβ did not lead to detectable upregulation of CD1d in the same study [54]. In parallel, maturation of DCs by addition of TNFα to cell culture supernatant or co-cultivation with CD40L-bearing cells did not alter CD1d protein levels [54]. However, in another study CD1D transcript level in myeloid DCs was strongly enhanced by stimulation with IFNα and IFNβ in a dose dependent manner, but not IFNγ or TNFα [70]. Activation of toll like receptor (TLR)-7– a receptor for single stranded RNA (ssRNA) molecules, by imiquimod differentially upregulated CD1D mRNA in imDCs, whereas non-viral TLR ligands LPS (TLR-4L), yeast zymosan (TLR-2L) and CpG (TLR-9L) either showed the opposite effect or did not alter CD1D gene expression [70].

Stimulation of peroxisome proliferator-activated receptor gamma (PPARγ) – a lipid-activated transcription factor, by its synthetic ligand rosiglitazone showed an increase in CD1D mRNA and protein content in monocyte-derived DCs [71]. This effect was mediated via induction of enzymes involved in all-*trans* retinoic acid (ATRA) biosynthesis and was coupled with enhanced CD1d-restricted T cell activation [71]. ATRA, active metabolite of vitamin A, at its physiologic dose (10nM) can rapidly induce CD1D transcript in human monocytes in as little as one hour after treatment [72]. The active role of retinoic acid (RA) in modulation of CD1d expression is likely to complement its other regulatory effects on immune system from monocyte maturation and differentiation [73] to T cell–dependent Ab production *in vivo* [74].

Resting human T cells express very low/no surface CD1d when analysed by flow cytometry, but stimulation with phytohaemagglutinin (PHA) induces CD1d protein expression in the cells both on the surface and intracellularly [53,75].

Unlike APCs, CD1d on expression on epithelial cells is somewhat differentially regulated. CD1d on human keratinocytes in normal skin is rapidly inducible in response to physical stress, such as mild trauma, and potent contact-sensitising agents [60]. Exposure to IFNγ for 48h enhances plasma membrane expression of CD1d on a normal human keratinocyte cell line (HaCat) *in vitro* [60]. Similarly, psoriasis – a condition characterised by T_h1-polarised immune response, has been shown to manifest by more extensive CD1d expression in epidermal keratinocytes compared to normal skin [60]. IFNγ–induced upregulation of CD1d on other epithelial cells has also been reported. Immortalised vaginal and penile urethral epithelial cells from human lower reproductive tract exhibit a robust CD1d induction after 24h treatment with IFNγ [61]. IFNγ along with heat shock protein 110 (HSP110) increase surface CD1d on IECs [76,77]. In addition to protein upregulation, semi-quantitative analysis by conventional PCR shows higher CD1D mRNA in IFNγ–treated IECs [76]. HSP110, an intestinal luminal content (LC)-derived agonist for CD1d induction, is prominently expressed by mucosal epithelia, suggesting an autocrine pathway for regulation of surface CD1d by epithelial cells [77].

A number of viruses can modulate CD1d expression in infected host cells. One mechanism by which herpes simplex virus type 1 (HSV-1) evades immune recognition is inhibition of surface CD1d expression on APCs [78]. This downregulation is mediated by prevention of reappearance of CD1d to the cell surface from the endocytic pathway. Trapping of CD1d to large lysosome-like structures intracellularly was evident by immunofluorescent and electron microscopy [78]. In contrast, in another study infection of immature DCs with UV-inactivated HSV for 3 days enhanced both surface density and intracellular content of CD1d compared to untreated DCs [70].

Direct activation of pathogen-associated pattern recognition receptors (PRRs) like TLRs, as opposed to primary effects of proliferating virus may account for such discrepancy in CD1d levels post-infection.

Kaposi sarcoma-associated virus (KSHV) is a gamma-2 herpes virus and causative agent of lymphoproliferative diseases like multicentric Castleman disease, as well as tumours like Kaposi sarcoma (KS). During its lytic stage, KSHV promotes downregulation of surface CD1d on B cell lymphoma cell line [79]. Viral protein modulator of immune recognition (MIR) induces internalisation of surface CD1d through ubiquitination of a unique lysine residue in its cytoplasmic tail [79].

Human immunodeficiency virus 1 (HIV-1) impairs cell surface expression of CD1d via Nef, gp120 and Vpu proteins [80-83]. Nef has been previously reported to reduce surface levels of MHC class I (A and B) and class II molecules, and to inhibit apoptosis in infected cells [81]. Two independent studies demonstrated that Nef can selectively interact with hCD1d cytosolic tail and enhance its internalisation [80,81]. Similarly, HIV gp120 protein downregulates CD1d from the surface of infected monocyte cell line U937 *in vitro* [82]. Vpu is a type I integral membrane protein that mediates proteasomal degradation of CD4 and is required for the release of virions from infected cells [83]. Through inhibition of efficient recycling of CD1d to cell surface, Vpu retains the protein in the early endosomes and decrease its surface expression in infected DCs [83]. Vpu and Nef act co-operatively to downregulate surface CD1d on monocyte derived DCs, as cells infected with mutant virus defective in both proteins exhibit almost a complete lack of CD1d surface reduction [83].

In mice, regulation of CD1d1 expression is somewhat different to human. Murine CD1d level on the surface of bone marrow (BM)-derived macrophages, unlike hCD1d, but similar to human CD1b, is not significantly affected by stimulation with IFNγ but is upregulated with GM-CSF and IL-4 [66].

1.3. Natural killer T (NKT) cells

1.3.1. NKT phenotype

CD1d-restricted T cells can contribute to antimicrobial and antitumour immune responses and influence the balance between autoimmunity and tolerance. They bridge the gap between innate and adaptive immune systems by their unique ability to rapidly secrete cytokines following stimulation to regulate the function of DCs, Natural Killer (NK) cells and other lymphocytes [3]. CD1d-restricted T cells were originally identified in $NK1.1^+$ mouse thymocytes [84] and are classically characterised by co-expression of T cell, like CD3 and TCR, and NK cell, like NK1.1 and DX5 in mice and CD161 in human, surface markers [3]. Consequently, they are often referred to as natural killer T (NKT) cells. However, $NK1.1^+$ $CD3^+$ T cells form a heterogeneous population of cells and not all recognise CD1d molecules. In C57BL/6 (B6) mice, on average 11, 34, 57 and 12% of $NK1.1^+$ $TCR\alpha\beta^+$ cells in thymus, spleen, BM and liver, respectively, did not bind CD1d/α–GC tetramer [85]. In humans, less than 1% of $CD161^+$ $CD3^+$ cells in peripheral blood stain positive with CD1d/α–GC tetramer [86]. Most of the CD1d/α–GC tetramer-binding T cells in B6 mice are $NK1.1^+$ [85], whereas approximately half of the $tetramer^+$ T cells in humans do not express CD161 [86].Moreover, upregulation of NK markers on some conventional T cells post-stimulation *in vitro* and *in vivo* further underlies the inaccuracy of NKT to refer to CD1d-restricted T cells [87].

In addition to NK markers, NKT can express IL-2 receptor β (IL-2Rβ; CD122) in mouse and human and C-type Lectins (CTLs) like CD94 in human. They also show an activated and memory phenotype. In humans and mice, most of the CD1d-restricted T cells are $CD45RO^{+}$ $CD45RA^{-}$ $CD25^{+}$ $CD62L^{-}$ $CCR7^{-}$ and $CD44^{hi}$ $CD69^{int}$ $CD45RB^{hi}$ $CD62L^{low}$ $CCR7^{-}$, respectively [3]. Presence of activated/memory surface phenotype on NKT in germ-free mice and human cord blood suggests that previous exposure to foreign antigens is not required and the phenotype could be a consequence of continuous stimulation by self CD1d ligands [3].

The majority of CD1d-restricted NKT cells express an invariant TCR α chain rearrangement (Vα24-Jα18 in humans; Vα14-Jα18 in mice) and are named canonical or invariant NKT (*i*NKT). They are also called type I NKT. TCR α chain in *i*NKT is predominantly associated with β chain of limited Vβ repertoire: Vβ2, Vβ7 or Vβ8.2 in mice and Vβ11 in humans [3]. At least two subsets of *i*NKT cells exist in mice: $CD4^{+}$ (60% – 90%) and CD4 CD8 double negative (DN) (10% – 40%). Only very few *i*NKT cells appear to express CD8α or CD8β [85]. In contrast, in humans despite high level of donor-to-donor variability all three phenotypes ($CD4^{+}$, $CD8^{+}$, and DN) could be detected [3]. Invariant NKT cells can be readily detected and tracked *in vivo* using CD1d/α–GC tetramer.

As well as *i*NKT cells, a group of CD1d-dependent non-Vα14-Jα18-expressing T cells have also been reported in mice [88,89]. They are commonly referred to as type II or non-invariant NKT, and unlike type I CD1d-restricted T cells express a more diverse TCR on their surface [90]. Due to inability of CD1d/α–GC tetramer to stain them, they are less characterised. CD1d-dependent type II NKT cells are functionally active and are also found in humans [90].

1.3.2. Development and selection of NKT cells

Invariant NKT cells develop in the thymus from the same $CD4^+$ $CD8^+$ (double positive; DP) T cells that also give rise to MHC class I- and class II-restricted T cells [91]. However, unlike conventional T cells the positive selection of *i*NKT cells requires interaction of their Vα14-Jα18 TCR α-chain with CD1d on DP cortical thymocytes, instead of thymic epithelial cells [92]. Extrathymic development of Vα14 TCR^+ T cell in the bone marrow and liver has also been suggested [93]. Evidence for this is supported by findings of high CD1d1 expression on mouse hepatocytes in foetal tissues. Different stages of intrathymic *i*NKT development are as follows.

Upon induction of RORγt-dictated survival signals and expression of Vα14-Jα18 TCR chain on DN thymocytes, *i*NKT precursors interact with self ligands, presumably iGb3, on CD1d-expressing DP cortical thymocytes [92]. Accessory signals provided through SLAM family of receptors, like SLAM and Ly108, recruit SLAM-associated protein (SAP) and protein tyrosine kinase Fyn to activate NFκB signaling cascade. This enhances the precursor's survival during the selection process. Prior to selection, $V\alpha14^+$ cells are present at very low frequencies in thymus and cannot be detected by tetrameric staining, reflecting rarity of TCR rearrangement and low expression on the cell surface. After selection, DP precursors downregulate CD8 and show $CD4^+$ $CD8^-$ $CD24^{hi}$ $CD69^{hi}$ (activated) phenotype. A subset of $CD4^+$ cells (30%–50%) then further downregulates CD4 to produce DN cells. As part of maturation towards the $CD24^{low}$ stage, $V\alpha14^+$ cells initially present with $CD44^{low}$ $NK1.1^-$ and then $CD44^{hi}$ $NK1.1^-$ (memory) phenotype. A few rounds of cellular expansion occur between these two stages before *i*NKT cells leave thymus for periphery, where they acquire NK1.1 receptor. Acquisition of NK1.1 for a minority of mature *i*NKT cells that

reside locally happens within the thymus (Figure 1.3.2.1) [92]. Distinct functional features are detected during different stages of *i*NKT development. For example, upon TCR stimulation CD44^{low} cells exclusively produce IL-4, while CD44^{hi} cells produce both IL-4 and IFNγ and NK1.1+ cells secrete more IFNγ than IL-4 [92].

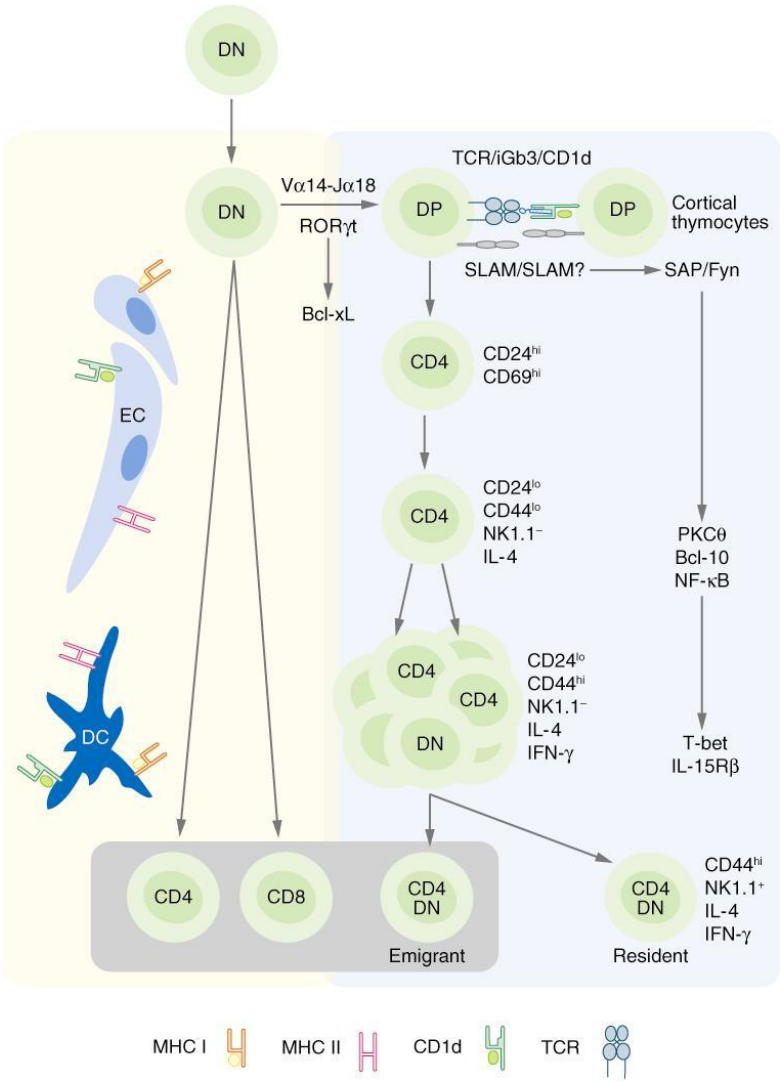

Figure 1.3.2.1. Development of *i*NKT cells in thymus. The precursor NKT cells originate from CD4$^+$ CD8$^+$ (double positive; DP) thymocytes that express Vα14-Jα18 TCR α chain. RORγt expression in these precursor cells stimulates survival signals. Interaction with CD1d loaded endogenous ligands (e.g. iGb3) and accessory molecules, like SLAM family members, on resident DP cortical thymocytes leads to recruitment of SAP and Fyn, and subsequent activation of NFκB pathway (i.e. promoting precursor's survival during selection process). CD8 is then downregulated to produce CD4$^+$ cells with an activated phenotype (CD24^{hi} CD69^{hi}); but nearly half of these cells later downregulate surface CD4 to form a double negative (DN) population. During this process, multiple rounds of cell division occur and cells acquire a memory/effector phenotype (CD44^{hi} NK1.1$^–$) prior to emigration to periphery, where they are thought to start expressing NK lineage receptors, like NK1.1.SLAM: signalling lymphocyte activation molecule; SAP: SLAM-associated protein; Fyn: a protein tyrosine kinase. Diagram taken from Bendelac A, *et al* Annual Reviews Immunology, 2007.

The above model for *i*NKT development is called "TCR instructive model" which states the lineage is instructed after TCR expression and interaction with CD1d endogenous ligands [92]. As opposed to "committed precursor model", in which NKT precursors are committed prior to TCR expression, this model is more widely accepted and is based on the finding that despite rare and stochastic Vα14-Jα18 rearrangement once expressed, *i*NKT TCR drives the full lineage differentiation [92].

Dose-dependent disappearance of *i*NKT cells, when adding α–GC to foetal thymic organ culture, has suggested that CD1d-restricted T cells are also subject to negative selection [94]. Using BM chimeric mice, it was shown that CD1d-expressing bone marrow-derived cells mediate the negative selection of those $V\alpha14^+$ T cells that engage with high-avidity and abundant self antigens [94].

Development of *i*NKT cells, in addition, requires a large number of transcription factors including Runx, GATA3, and T-bet [95,96]. In addition, full complement of ITAMs in CD3 ζ subunit is necessary for its proper development [95]. After birth, CD1d-restricted T cells appear in thymus, liver and spleen at days 5–8, and then their numbers in liver and spleen reach plateau between 4 and 6 weeks of age [3].

1.3.3. Activation and functional characterisation of NKT cells

In mice and humans, *i*NKT cells upon TCR stimulation can rapidly respond and secrete large quantities of both T_h1 and T_h2 type cytokines, such as IFNγ, IL-4, IL-5, and IL-13 [3]. This allows *i*NKT cells to have innate-like properties and distinguishes them from naive MHC class I- or class II-restricted T cells that acquire such cytokine secretion ability during proliferation following initial stimulation. CD1d-restricted T

cells, unlike conventional T_h1 and T_h2 cells, activate constitutive transcription of IL-4 and IFNγ genes during their thymic development [97]. However, no detectable cytokine protein is stored in resting *i*NKT cells before cognate stimulation [98]. Chromatin modification on IL-4 and IFNγ gene loci, in particular histone acetylation which promotes accessibility to transcription factors, initiates during *i*NKT development in the thymus and correlates with abundant IL-4 and IFNγ mRNAs in unchallenged spleen $V\alpha14^+$ T cells [97]. Comparable amounts of cytokine mRNA between *i*NKT and differentiated $CD4^+$ effector T cells supports the potential for *i*NKT cells to act as rapid effector immune cells [97].

Besides T_h1 and T_h2 type cytokines, *i*NKT cells are also capable of producing IL-17 [99,100]. Treatment of mouse splenocytes with anti-CD3 and IL-23 for 24h led to rapid and considerable IL-17 secretion into the supernatant, largely generated in NKT cells in an IL-6-independet manner. Like memory T cells, but unlike NK and naive conventional T cells, NKT cells constitutively express IL-23 receptor (IL-23R) and RORγt [99]. Another study reported α–GC-induced IL-17 production by mouse *i*NKT cells and demonstrated a $NK1.1^-$ subset as the major source of IL-17 production among CD1d-restricted T cells [100].

In addition to rapid and explosive cytokine secretion, mature *i*NKT cells also exhibit cytolytic activity by releasing granzymes and perforin and expressing Fas ligand (FasL; CD178) and TNF-related apoptosis inducing ligand (TRAIL) on their surface [3]. A critical role for IL-12 in activating NK cell-like cytotoxic properties in $NK1.1^+$ $TCR\alpha\beta^+$ T cells, in particular in response to tumours and infections, has been suggested [101,102]. A recent report has demonstrated a direct correlation between *i*NKT cell cytotoxicity and the level of CD1d expression on target cell, as well as, TCR affinity for

the lipid antigen [103]. Using perforin- and CD95 (Fas)-deficient mice, the authors also showed that *in vivo* cytotoxicity of *i*NKT cells is almost exclusively dependent on FasL, rather than granzymes/perforin-meditated cellular toxicity; an opposite trend to what exists in NK cells [103].

Several studies have characterised an important role for co-stimulatory molecules and soluble factors, in addition to direct contact between *i*TCR and CD1d/α–GC complex, to activate *i*NKT cells. α–GC, on one hand, mediates induction of IL-12 production by DCs, and on the other hand, strongly causes upregulation of IL-12 receptor on the surface of *i*NKTs [104]. DC-produced IL-12 and CD40/CD40L interaction during co-culture of $NK1.1^+$ $TCR\alpha\beta^+$ T cells and freshly isolated spleen $CD11c^+$ DCs are essential for IFNγ production by NKT cells [104]. In parallel, another study demonstrated that antigen-activated $CD4^+$ $V\alpha14^+$ T cells preferentially upregulated CD40L that upon engagement with CD40 on the surface of APC stimulated them to produce IL-12 [105]. Production of IL-12 preceded secretion of IFNγ into the cell culture supernatant, and was required for IFNγ but not IL-4 production. Therefore, presentation of α–GC leads to reciprocal activation of both *i*NKT and dendritic cells (Figure 1.3.3.1). CD1d-restricted T cells in mice constitutively express CD28 that through interaction with CD80 and CD86 on the surface of APCs augments cytokine production by *i*NKT following TCR-mediated stimulation [3].

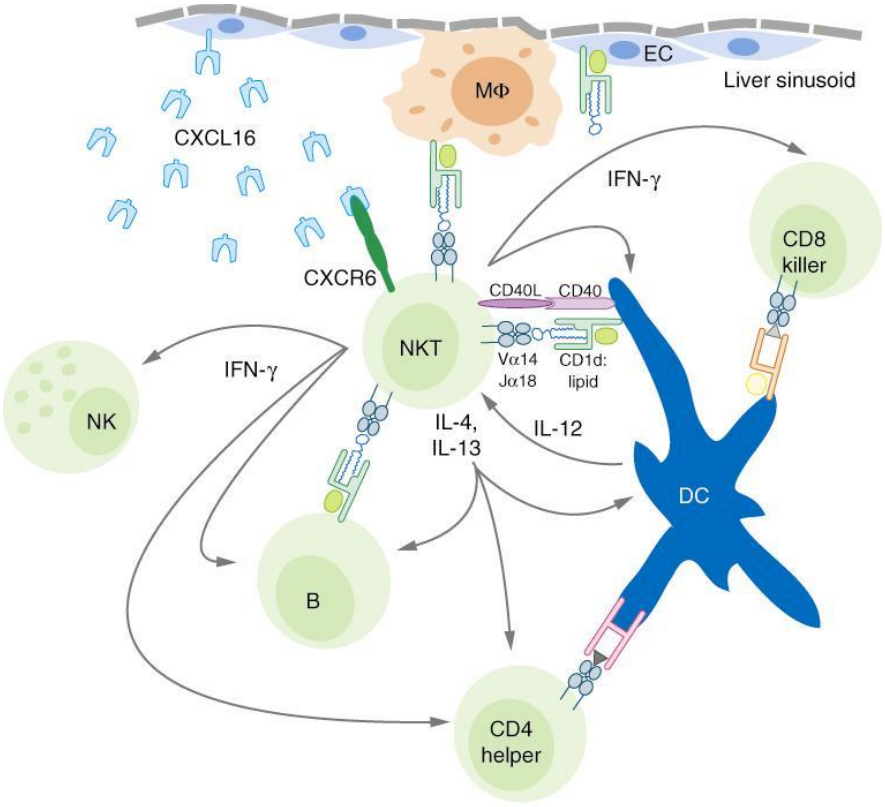

Figure 1.3.3.1. Reciprocal activation of *i*NKT cells and α–GC–loaded APCs. CD1d-ecpressing DCs and macrophages (like liver Kupffer cells) present α–GC to NKT cells and initiate a network of cross-activation. Initially, ligand presentation leads to surface CD40L upregulation, and cytokine (T_h1 and T_h2) and chemokine secretion by NKT cells. CD40L/CD40 interactions and later IFNγ activity modulate IL-12 production and maturity of DCs. NKT cells also influence antibody production by B cells and enhance the cytolytic activity of NK cells. Chemoattractant mediator CXCL16 is important for recruitment of NKT cells to the tissues and provides survival signals for NKT cells. APC: antigen presenting cell; DC: dendritic cell; EC: endothelial cells. Diagram taken from Bendelac A, *et al* Annual Reviews Immunology, 2007.

NKT cells have evolved to contain negative regulatory feedback mechanisms to avoid excessive stimulation after TCR activation. Ly49 comprises a family of NK cell-associated receptors, including Ly49A, C/I, G, and D, which interact with MHC class I molecules [106] and are expressed at varying levels on $NK1.1^+$ $TCR\alpha\beta^+$ T cells from mouse spleen (55%), thymus (68%), and BM (81%) [107]. Expression of Ly49 inversely correlates with NKT responsiveness to α–GC *in vitro*, with highest IFNγ and IL-4 production after stimulation of splenic NKTs [107]. Very low α–GC-induced activation of splenic $Ly49^+$ NKT cells, as opposed to $Ly49^-$ cells, when stimulated with

normal DCs; but potent stimulation of both NKT subsets with TAP-deficient DCs suggest that MHC class I on the surface of APC inhibits NKT activation through engagement with Ly49 [107]. In another study, 2.5 days after intraperitoneal (i.p) administration of α–GC, IFNγ-mediated strong upregulation of Qa-1^b (an MHC class I-b molecule and homologous to human HLA-E) was observed on splenic mononuclear cells [108]. Qa-1^b in turn negatively regulated *i*NKT cell response by interacting with CD94/NKG2A inhibitory receptor [108].

A variety of factors can influence activation of CD1d-restricted T cells *in vitro* and *in vivo* to polarise their response towards T_h1 or T_h2; including 1) cytokines in the microenvironment surrounding *i*NKT cells, 2) NK cell co-receptors, 3) structure and pharmacokinetics of the CD1d ligand, 4) nature of the APC, and 5) multiplicity of antigen administration. IL-12 (produced by DCs), as discussed above, augments NKT IFNγ production, whereas IL-7 and IL-18 favour a T_h2-type cytokine secretion pattern by CD1d-restricted T cells [109,110]. Crosslinking NK1.1 molecules with an immobilised mAb induces IFNγ production by $NK1.1^+$ $CD3^+$ T cells, and NK cells, *in vitro* but unlike TCR crosslinking does not potentiate IL-4 production [111].

In contrast to α–GC which promotes production of both IL-4 and IFNγ by *i*NKT cells, the ability of a CD1d glycolipid antigen to bias cellular response was first reported for an α–GC analogue called OCH [112]. OCH is modified to contain a truncated sphingosine chain (C9 instead of C18 in α–GC) and a slightly shorter acyl side chain (C24 instead of C26); and shifts the *i*NKT response towards T_h2 [112]. Initial studies attributed the preferential T_h2 polarisation by OCH to less stability of the glycolipid in binding CD1d and shorter *i*NKT stimulation [113], and incompetent induction of CD40L on *i*NKT [114]. However, another study revealed differential

kinetics of antigen binding and cell surface localisation as the leading factors driving T_h2-biasing of *i*NKT response [115]. More specifically, various T_h2-polarising α–GC derivatives shared the ability to rapidly and directly load onto surface CD1d and the glycolipid/CD1d complexes were excluded from ganglioside-rich plasma membrane micro-domains (also called lipid rafts) [115]. Longer survival of T_h1-biasing C-glycoside *in vivo* compared with OCH, despite its weaker TCR avidity, has introduced pharmacokinetic properties of glycolipids as another determinant of cytokine skewing of CD1d-restricted T cells when studying systemic cytokine polarity [116].

The type of dendritic cell can influence T_h differentiation of *i*NKT cells *in vitro*. $CD4^+$ $CD3^-$ $CD11c^-$ plasmacytoid dendritic cells (pDCs) enhance differentiation of human cord blood (neonatal) *i*NKT to an IL-4-producing phenotype. In contrast, myeloid-derived DCs promote differentiation of neonatal *i*NKT cells towards IFNγ production [117]. *In vivo,* extracellular stimuli and cytokine environment indirectly via conditioning DCs can influence *i*NKT cell polarisation [118]. Injecting DCs, pre-treated with IL-4 or IFNγ *in vitro,* back into mice led to increased production of T_h1 and T_h2 cytokines by *i*NKT cells, respectively [118]. Single administration of α–GC stimulates mixed IL-4 and IFNγ secretion in mice, while multiple applications tend to elicit a T_h2 bias [3]. Notably, unlike conventional naive $CD4^+$ T cells, pattern of cytokine production by *i*NKT is neither influenced by antigen dose nor the rate of antigen delivery through an osmotic pump, placed under the skin [119].

Early studies demonstrated that soon after *in vivo* stimulation with α–GC, CD1d-restricted T cells start disappearing [98]. However, subsequent reports described activation-induced cell death, similar to what occurs in MHC-restricted T cells, and downregulation of key surface receptors as likely reasons for *i*NKT cells to lose

CD1d/α–GC tetramer staining [120-124]. NK1.1^{+} CD3^{int} T cells in the liver of wild type uninfected B6 mice as early as 3h after i.p α–GC injection showed an enhanced annexin V (apoptotic marker) staining (42%), compared with NK (10%) and conventional T cells (10%) [120]. Increased annexin V expression on NKT cells was also evident when mice were intravenously (i.v) injected with α–GC-pulsed DCs, and could potentially explain the significant drop in the spleen NKT number up to 2 days post-injection [121]. Similar to conventional T cells [125], antigen-activated *i*NKT rapidly down-regulate their surface TCR expression both *in vivo* and *in vitro* [123]. Escape from tetramer staining in CD1d-restricted T cells results from intracellular trapping of TCR complex and decreased recycling of the receptor to the cell surface [123]. Kinetics analysis detected TCR downregulation as quickly as 1h post α–GC i.p injection, peaking at 8h, and then normal surface TCR expression started resuming at 24-48h [123]. In addition to TCR, NKT cells also lose NK1.1 expression upon activation [123,124].

1.3.4. NKT tissue distribution and recruitment

CD1d/α–GC tetramer^{+} T cells in B6 mice represent approximately 0.5% of TCRαβ^{+} T cell population in the peripheral lymph nodes (LNs), bone marrow and blood, 0.5%–1% in the thymus, 1%–2.5% in the spleen, and up to 30% of T cells in the liver [3,85]. Despite low Vα14^{+} NKT frequency in the whole thymus, they represent about 2% of the recent thymic emigrants (almost all TCRαβ^{+} cells) and are predominantly NK1.1$^{–}$ [126]. In humans, CD1d-restricted T cells exhibit a lower frequency and on average about 0.2% of peripheral blood T cells could be detected by either CD1d/α–GC tetramer staining or using anti-Vα24 and Vβ11 mAbs [86,127]. However, the number of Vα24^{+} Vβ11^{+} NKT cells in freshly isolated human PBMCs shows a great variability

(0.01%–1%) across healthy donors [127]. The distribution of *i*NKT cells outside primary and lymphoid organs is poorly characterised; and rather more emphasis has been laid on chemokine and tissue-homing receptors on the surface of these cells.

Unlike chemokine expression which is tightly regulated by cytokines and other immunomodulatory signals that tend to restrict their expression locally within the disturbed microenvironment, expression of chemokine receptors and adhesion molecules on T cells is developmentally regulated [128]. All naive T cells, for example, express CCR7 and L-selectin (CD62L) which mediate their migration into LNs and other lymphoid organs through high endothelial venules (HEVs) [129]. However only 20% of human peripheral blood *i*NKT cells express CCR7; and CXCR5 – a lymphoid follicle-homing receptor, is hardly detectable on the surface of $V\alpha24^+$ $V\beta11^+$ NKT cells [130]. In contrast, chemokine expression profile on human *i*NKT closely resembles that of memory and effector T cells. For instance, high levels of CCR5, CCR6, and CXCR3, and intermediate levels of CXCR4 and CXCR6 on $V\alpha24^+$ NKT cells illustrate a receptor pattern that is often associated with extralymphoid tissue-homing, and T_h1 and $CD8^+$ cell infiltration into the sites of inflammation [130,131]. Several chemokine receptors appear to be differentially expressed by $CD4^+$ and $CD4^-$ subsets of human CD1d-restricted NKT cells. CCR4, for example, is preferentially expressed by $CD4^+$ *i*NKT cells while CXCR6, CCR1, and CCR6 are dominantly expressed by $CD8^+$ and DN *i*NKT cells [130]. This chemokine expression pattern is reflected by robust induction of chemotaxis of $CD4^+$ but poor chemotaxis of $CD8^+$ and DN *i*NKT cells in response to TARC/CCL17 (CCR4 ligand). An opposite trend is evident with MIP-1α (CCR1 ligand) and LARC/CCL20 (CCR6 ligand) [130].

In mice, CXCR6 is expressed on more than 90% of both NK1.1^{+} and NK1.1^{-} Vα14^{+} NKT cells in the spleen [132]. However, less than less than 5% of these cells exhibit migration in response to CXCL16 *in vitro* [132]. Absence of significant chemotaxis in the resting spleen, even in heterozygote mice expressing eGFP/CXCL16 on splenocytes, suggests that this chemokine receptor may be more important for homing of *i*NKT cells during inflammation [132]. On the other hand, accumulation of CD1d-restricted T cells in the mouse liver, where they appear to patrol sinusoids, matches high levels of CXCR6 and CXCL16 on the *i*NKT and endothelial cells, respectively [133]. CXCR3 is expressed on most *i*NKT cells and its expression is consistent with strong chemotactic response to its ligand MIG/CXCL9 [132]. Approximately half of the mouse spleen *i*NKT cells express CXCR4, while CCR6, in contrast to human, is barely detectable on their surface. This expression pattern is in line with functional data from *in vitro* chemotaxis assays [132]. Compared with Vα14^{-} NK1.1^{+} T cells, a larger proportion of α–GC loaded CD1d tetramer^{+} cells in the spleen express CXCR5. Such differential chemokine receptor expression is also evident between NKT cells from different lymphoid organs and consistent with chemotaxis data, as Vα14^{+} NKT cells from spleen, but not liver, BM, or blood, migrate in response to BCA-1/CXCL13 [132]. Very little migratory response from NK1.1^{-} spleen *i*NKT, but significant chemotaxis of NK1.1^{+} Vα14^{+} T cells to SLC/CCL21 suggests down-regulation of CCR7 responsiveness on *i*NKT cells during their maturation in the periphery where they acquire NK1.1 receptor [132].

A few studies have demonstrated critical role of chemokine receptors for recruitment of *i*NKT cells to the sites of inflammation and infection *in vivo*. In the mouse model of sickle cell disease, NY1DD mice have higher numbers of activated

*i*NKT cells expressing CXCR3 in tissues hyperresponsive to hypoxia and reoxygenation damage, compared with wild type controls [134]. Although CXCR3 induction was also observed on other immune cells ($CD4^+$, $CD8^+$, and NK cells), treatment with CD1d-blocking Ab ameliorated the pulmonary damage as did neutralisation of CXCR3 [134]. In another study, following pulmonary infection with *Cryptococcus neoformans*, $V\alpha14^+$ NKT cells accumulated in the lungs from day 1 and reached a peak level on day 7. Recruitment of *i*NKT was dependent on monocyte chemoattractant protein-1 (MCP-1), a ligand for CCR2 [135].

1.3.5. Role of NKT cells in antimicrobial immunity

CD1d-restrict T cells participate in host immune response to a variety of viral, bacterial, parasitic, and fungal pathogens. The outcome of NKT immune contribution and the type of antimicrobial response varies depending on the infectious organism and the disease model. Besides, unlike certain bacteria and parasites, *i*NKT activation during viral infections occurs either through host endogenous lipids or via TCR-independent pathways as viral genomes do not encode for lipid molecules.

NKT cells involvement in active immunity against a number of viruses such as influenza virus, respiratory syncytial virus (RSV), HIV, HSV, encephalomyocarditis virus (EMCV), and Hepatitis virus has been documented. In the context of influenza infection, for example, *i*NKT cells play an important role in cellular and humoral immune defence. An initial study reported that immunisation of wild type (BALB/c) mice with α–GC mixed with H1N1 virus PR8 haemagglutinin (HA) antigen, prior to virus infection, leads to enhanced secretory IgA (sIgA) levels in the lungs and nasal washes, and higher PR8 HA-specific IgG titres in the sera, compared with mice

immunised with HA Ag plus vehicle or vehicle only [136]. Additionally, inoculation of virus into control mice resulted in higher mortality (100% for vehicle group by day 10, and ~60% for HA plus vehicle animals by day 14) than those immunised with HA plus α–GC (<20% by day 14) [136]. Consistent with these findings, another study demonstrated long-term protective immunity in mice after a single dose co-administration of α–GC and inactivated PR8 virus [137]. Interestingly, intranasal (i.n) α–GC alone neither reduced virus titres in the lungs nor mounted PR8-specific IgA or IgG antibody response [137]. Using fluorescent labelled α–GC, *i*NKT cells were found to directly interact with α–GC-loaded DCs in the upper respiratory tract [138].

Detailed dissection of immune consequences of *i*NKT activation was revealed in subsequent studies. Intraperitoneal injection of α–GC at the same time as PR8 i.n inoculation resulted in reduced weight loss and less pulmonary virus titres in wild type B6 mice, compared with control animals inoculated with the virus only [139]. A strikingly rapid increase in the sera IFNγ, IL-4, IL-12, MCP-1 and macrophage inflammatory peptide 2 (MIP-2) levels, and a parallel boost in chemokines MCP-1 and MIP-2 in the bronchoalveolar lavage fluid (BALF) of α–GC-receiving infected mice was observed by day 1. Higher chemokine secretion was reflected with increased polymorphonuclear cell infiltration in the lungs, and enhanced $Gr1^+$ cells (neutrophils), but not $F4/80^+$ macrophages, in the BALF [139]. Infected mice with α–GC injection also exhibited a greater $tetramer^+$ NKT cell expansion in the airways, but unexpectedly the amplification of virus-specific $CD8^+$ T cells in the BALF did not reach significance against infected mice receiving PR8 plus vehicle.

Invariant NKT cells were demonstrated to reduce the suppressive activity of myeloid-derived suppressor cells (MDSCs) – a group of $CD11b^+$ $Gr1^+$ cells comprising

imDCs, immature macrophages and granulocytes and characterised by expression of arginase 1 (ARG1) and nitric oxide synthase 2 (NOS2), in the lungs of influenza-infected mice [140]. This helped restoring PR8-specific immune responses, reducing viral titres and increasing survival rate [140]. However, no report of CD1d-mediated initial priming of *i*NKT cells and its mechanisms has been suggested yet.

RSV is a member of *Paramixoviridiae* family and a common respiratory pathogen causing lower airway inflammation particularly in infants and elderly. Efficient induction of virus-specific $CD8^+$ T cells and early IFNγ production in primary RSV infection *in vivo* was found to be CD1d-dependent [141]. Compared with the wild type, $CD1d^{-/-}$ mice had delayed viral clearance, and treatment of $CD1d^{+/+}$ mice with α–GC improved weight loss profiles and significantly increased IL-4 and IFNγ production leading to greater infiltration of NK and $CD8^+$ T cells into infected lungs. Overall, antigen-activated *i*NKT ameliorated the illness and enhanced the antiviral immune response [141].

Depletion of circulating $V\alpha24^+$ $V\beta11^+$ T cells in humans follows infection with HIV-1 [142,143]. This phenomenon is expected considering CD4 and CCR5 expression, two major targets of the virus [144], on a subset of *i*NKT cells which render NKT cells susceptible to selective and direct infection by the virus. In one study, approximately less than half of the HIV-1-infected patients had undetectable CD1d/α–GC $tetramer^+$ T cells in their PBMCs, while all the healthy controls had at least 0.01% *i*NKT [142]. Nevertheless, the contribution of CD1d-restricted NKT cells to the rate of disease progression remains controversial. In a longitudinal cohort study, despite severe reduction in the number of blood *i*NKT cells, no evidence of contribution of these cells to the course of infection was found [143]. However, in another study, HIV-1 RNA

concentration in the plasma inversely correlated with the number of $CD4^+$ NKT cells [142]. Highly active anti-retroviral therapy (HAART) in HIV-1 –infected individuals results in rapid recovery of conventional $CD4^+$ T, as well as *i*NKT (predominantly $CD4^-$ subtype) cells and may reveal a potential role for NKT in suppressing HIV replication during the combination therapy [145].

Herpesvirus family members, like HSV-1 and KSHV, via downregulation of CD1d on the surface of host cells facilitate their immune evasion. Involvement of NKT in immunity against these viruses is evident with impaired ability to clear HSV-1 SC16 strain and its antigens in $CD1d^{-/-}$ and $J\alpha18^{-/-}$ mice [146]. Additionally, mice lacking iNKT cells presented with higher incidence of skin lesions, viral persistence and more rapid spread of HSV to dorsal root ganglia [146].

NKT cells contribute to immunity to diabetogenic EMCV picornavirus, as $CD1d^{-/-}$ mice exhibited higher susceptibility to the infection, and α–GC-treated wild type mice were protected against EMCV-induced diabetes, encephalitis, and myocarditis [147]. Of interest, CD1d-restricted but α–GC-nonreactive type II NKT cells in the mouse model of hepatitis B virus (HBV) infection are activated in response to HBV Ag-expressing hepatocytes and mediate the acute inflammation [148].

*i*NKT-mediated immune modulation in response to bacterial pathogens can be either independent or dependent on direct recognition of bacterial glycolipids. In *Sphingomonas* infection, wild type mice immunised with DCs pulsed with bacterial glycosphingolipid (GSL-1′sA) potently induced IFNγ production in the liver $V\alpha14^+$ T cells. In parallel, early activation marker CD69 was also upregulated on the $tetramer^+$ T cells, and *i*NKT directly participated in bacterial clearance for significantly higher

numbers of surviving bacteria in the liver of CD1d$^{-/-}$ mice against wild type controls [31]. Notably, at high doses *Sphingomonas* caused rapid mortality in wild type animals, whereas most of the CD1d$^{+/-}$ heterozygotes and *i*NKT-deficient mice survived. The severe lethal outcome in this case was associated with significantly higher serum levels of IFNγ and IL-12 in wild types [149]. Similar to *Sphingomonas*, *in vivo* infection with another Gram-negative, LPS-negative bacterium, *Ehrlichia*, activated *i*NKT cells to secrete IFNγ and increase surface CD69 within 24h post-infection [149]. Furthermore, CD1d$^{-/-}$ and Jα18$^{-/-}$ mice showed delayed clearance of the pathogen compared with heterozygous controls [149]. Diacylglycerol from the spirochete *Borrelia burgdorferi* can be directly recognised by mouse and human *i*NKT cells and induce their proliferation and cytokine secretion *in vitro* [30]. CD1d$^{-/-}$ mice infected with the pathogen manifested with arthritis and increased spirochete DNA in tissues. The knock-out mice also secreted higher titres of a specific IgG2a, commonly associated with disease susceptibility [150]. Hence, *i*NKT cells influence immune response to this spirochete by modulating B cell activation and Ab production.

For a number of bacteria, CD1d-restricted T cells detect microbial invasion or influence systemic immunity through activated APCs. *Salmonella typhimurium*, a Gram-negative LPS-positive bacterium, activates DCs through TLR4 signaling in a MyD88-, Trif-dependent manner to produce IL-12 [149]. Activated DCs in turn present endogenous glycolipid iGb3 to stimulate *i*NKT cells to secrete IFNγ. In support of this, *Hexb*$^{-/-}$ DCs (lacking iGb3 synthesis ability) pulsed with heat-killed *Salmonella* failed to activate NKT in the *in vitro* co-culture system. Moreover, co-addition of IL-12 and LPS to the co-culture was sufficient to replace *Salmonella* [149]. In another model, after intranasal infection with *Pseudomonas aeruginosa*, a Gram-negative bacterium

and an opportunistic pathogen, $CD1d^{-/-}$ mice had markedly impaired pulmonary clearance of the microorganism [151]. The number of bacilli in the lungs, 24h post-inoculation, was 100-times higher in the knockouts compared with the wild type. Pre-treating wild type animals with anti-CD1d blocking Ab also significantly increased viable bacteria in the lungs. In contrast, α–GC-activated *i*NKT cells enhanced clearance of the bacterium at an early stage of infection and prevented pneumonia. This was mediated by increasing *Pseudomonas* uptake by alveolar macrophages, amplified IFNγ and TNFα secretion into the BALF and huge expansion of $tetramer^{+}$ T cells in the airway lumen [151].

Several studies have explored the role of *i*NKT cells during parasitic infections, but their effects remain controversial. One study reported higher parasite burden and defective granuloma formation in response to visceral *Leishmania donovani* in $CD1d^{-/-}$ mice [33]; whereas another study found no significant difference between wild type and $J\alpha18^{-/-}$ mice during the chronic infection [152]. High affinity of *Leishmania* surface lipophosphoglycan and glycoinositol phospholipids for binding CD1d adds to the complexity of CD1d-mediated immunity to this protozoon [33]. In the context of fungal infections, $V\alpha14^{+}$ T cells were demonstrated to accumulate in the lungs after infection with *Cryptococcus neoformans* and participate in T_h1 response and host resistance to this pathogen [135].

1.4. Influenza infection

1.4.1 Influenza virus structure and morphology

Influenza A, B and C viruses belong to *Orthomyxoviridae* family, which encompasses enveloped, negative-stranded, segmented RNA viruses [153]. Influenza A viruses cause annual epidemics and occasionally pandemics in humans, while B viruses cause more limited epidemics and occasionally infect seals. Influenza C viruses are responsible for clinically benign infections in humans and can infect pigs as well [154]. Morphologically, the virus particles (virions) can be pleomorphic but generally adapt a spherical configuration and have an approximate diameter of 100-150 nm [155]. Each virion can be divided into three major sub-viral components : 1) the viral envelope, 2) the intermediate layer, and 3) the core (Figure 1.4.1.1)[153]. The viral envelope consists of a lipid bilayer which has a mosaic structure of lipid raft micro-domains and non-lipid raft regions [156], and contains three transmembrane proteins: HA, neuraminidase (NA), and matrix protein 2 (M2). The lipid rafts are incorporated into the envelope from the host cell membranes, as discrete and well-organised protein/lipid units during the virus assembly process [157]. HA and NA glycoproteins are enriched in the lipid raft domains [157,158]. On the contrary, despite cholesterol binding capacity, only a small fraction of M2 proteins is associated with the envelope detergent-resistant rafts [159].

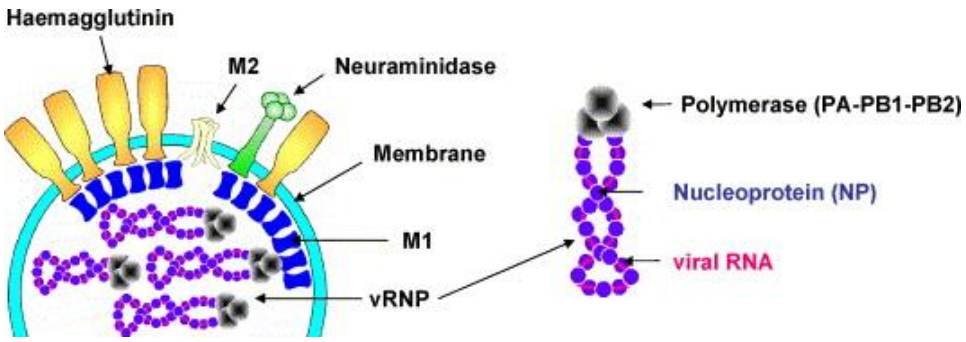

Figure 1.4.1.1. Diagrammatic representation of influenza virion and a viral ribonucleoproteins (vRNP). Picture taken from Boulo S, *et al* Virus Research, 2007.

HA, the major influenza virus envelope protein (~80%) [153], is a rod-shaped trimer of identical subunits, each consisting of two polypeptide chains produced by proteolytic cleavage of a single precursor. It, on one hand, binds sialic acid receptors on the surface of the cells, and on the other hand, mediates virus fusion with the host membrane glycoproteins. More specifically, following internalisation of the receptor-bound viral particle, conformational changes in both HA polypeptides activate fusion of the virus with endosomal membrane [160]. Therefore, HA cleavage is essential for virus infectivity. In addition, membrane fusion by influenza virus is maximal at acidic pH of 5.0 – a pH that is found in endosomes [161-164]. At this low pH, HA undergoes conformational transition and acquires the ability to bind to lipid vesicles and its antigenicity is affected; that is, the acidic endosomal pH is an important step which is crucial for infectivity of the influenza virus [161,162]. To date, 16 HA (H1–H16) subunits for influenza A virus (IAV) have been reported, which phylogenetically are grouped into two [160]. For most HA subtypes, cleavage occurs extracellularly at a single arginine residue. A few trypsin-like proteases from human respiratory epithelium, including TMPRSS2 and HAT, have been suggested to modulate HA cleavage; however, the enzyme(s) involved in this process under natural influenza infection are not yet identified. A few influenza viruses, including highly pathogenic IAVs of H5 and H7 subtypes, contain multiple cleavage motifs R-X-K/R-R (R: arginine; K: lysine; X: any amino acid) which are recognised by ubiquitous and intracellular subtilisin-like proteases [165,166]; hence, higher morbidity with these viruses.

NA, the second most abundant protein in the envelope (~17%) [153], has a mushroom-like configuration and is a tetramer of identical subunits [160]. The mushroom head is suspended from a stalk (~60Å long) on the virus membrane, whose

length varies across different influenza virus strains [160]. Each NA subunit is made up of six anti-parallel β-sheets (blade-like) topologically arranged in a propeller-like format [167]. Through enzymatic activity, that its site is located roughly in the centre of each subunit, NA removes sialic acid from both the virions and cellular glycoproteins and glycolipids. Consequently, newly assembled progeny virus particles are prevented from aggregating together and binding the infected cell, thereby facilitating spread of the infection [160]. On the basis of antigenicity, nine subunits of NA (NA1–NA9) in IAV have been reported so far that, similar to HA, are classified into two groups [160].

M2, the least abundant envelope protein (about 16–20 copies/virion) [153], is a proton-selective ion channel that is required during the early stages of the infection. Following receptor-mediated endocytosis, this disulfide-containing tetramer conducts protons from the lumen of endosome into the virion and lowers pH to facilitate dissociation (uncoating of) the virus matrix. This leads to release of viral ribonucleoproteins (vRNPs) from M1 into the cytoplasm and their availability for subsequent gene expression. M2 is also involved in maturation of HA in acidic cellular compartments, and through interaction with M1 participates in control of virus morphology during budding process [159].

The intermediate layer of influenza virus accommodates the matrix protein 1 (M1). Crystallography revealed a structure consisting of two helical sub-domains, each formed by four α–helices, at N-terminal end of molecule, which are connected through a flexible linker to C-terminal domain [168]. M1 binds the envelope glycoproteins, through its N-terminus, and connects them with the protein-encapsidated viral RNA genome via its C-terminal domain. It particularly functions during the budding process by polymerising and pulling lipid raft micro-domains together to exclude other host cell

proteins from the virus particles [169]. It has been suggested that M1 contains all the necessary information for assembly and budding of influenza virus as its overexpression in eukaryotic cells leads to formation and release of virus-like particles (VLPs) [170]. Additionally, M1 is involved in the nuclear export of RNPs. Stripping off high-affinity binding M1 from the RNPs when the interior of the virus gets acidified in the endosomes, immediately prior to fusion of virus and host membranes, allows RNPs to enter the cell nucleus. Re-association with the M1 at later stages of virus life cycle prevents the import of RNPs back into the nucleus [169,171].

The vRNP in the influenza virus core contains single-stranded negative-sense viral RNAs (vRNAs), nucleoproteins (NPs), three RNA polymerase enzymes (PA, PB1, and PB2), and minor amounts of the nuclear export protein (NEP) [153]. The genome of influenza A and B viruses contains eight vRNA segments, while that of influenza C virus consists of only seven vRNAs [154]. Of note, viral RNPs, but not viral RNAs on their own, are transcriptionally active. Structural conformation of RNPs extracted from IAV revealed twisted rod-like organisations of NP molecules encapsidating each of vRNA segments. RNase-sensitivity assays and crystal structure data suggest that NPs interact with the phosphate backbone of the vRNA and allow the genomic bases to be exposed on the exterior of the RNP. NP is considered to be the major determinant for formation of RNP helical rod-like structure for its ability to form such structures even in the absence of vRNAs [154]. The basic RNA polymerases 1 and 2 (PB1, PB2), and the acidic RNA polymerase (PA) associate together to form heterotrimeric RNA-dependent polymerase complexes (3P complex). These complexes are generally located at, or near, the end of rod-like RNP molecules in close proximity of conserved 5′ and 3′ complementary termini of vRNAs [172]. NEP, also called NS2, is a splicing product of

one of the vRNA segments and is involved in the nuclear export of RNPs after virus transcription and replication. NEP contains a nuclear export signal (NES) motif in its N-terminal domain that interacts with cellular export factor CRM1 and is required for transport of the RNP complexes out of the nucleus [173]. The three largest gene segments in IAV code for RNA polymerases, the medium segments for NP and surface proteins HA and NA. The two shortest vRNA segments each encode two proteins: one (M vRNA) for M1 and M2 and one (NS vRNA) for NS1, an important viral virulence factor, and NEP [174].

The polymerases in influenza virus, on one hand, are responsible for replication and transcription of vRNAs and, on the other hand, due to lack of proofreading activity result in error-prone viral replication affecting all viral proteins from surface glycoproteins to polymerases themselves [174,175]. The latter is crucial for evolution of the virus and its evasion from the host Ab immune response –in a phenomenon called "antigenic drift" [174]. In the infected cells, viral genome is initially copied into a cRNA intermediate and then back into vRNA segments which can act as template for transcription or further replication. In addition to polymerase activity, 3P complex also exhibits endonuclease and cap-snatching properties [174]. Generation of viral mRNAs, unlike replication, is primer-dependent. During transcription, PB2 subunit of the polymerase complex locates the methylguanosine cap at 5′-end of a host nuclear pre-mRNA, and then PA subunit cleaves 10–15 nucleotides downstream. The short capped RNA oligomer acts as an initiating primer upon which PB1 polymerase commences transcription using vRNA as template. Following polyadenylation, the chimeric positive-strand mRNA is then exported from the nucleus for translation in the cytoplasm [174].

1.4.2 Influenza virus assembly and budding

As complete influenza virus particles are not found inside the infected cells, budding and assembly play a crucial role in generating infectious progeny virions [153]. Four sequential steps make up the morphogenesis and budding events involved in the influenza virus life cycle: 1) assembly of the viral components, 2) initiation of budding, 3) bud growth, and 4) bud closing. Although these steps have evolved to ensure survival of the virus, no accurate checkpoint is in place to signal the end of one step before the start of the next, and surprisingly lead to production of both infectious and non-infectious (defective) virus particles from the cell surface [153].

Bud formation requires assembly of various viral constituents either during intracellular transport, or while budding at the cell surface (i.e. the budding site). "Selective packaging" model for assembly of vRNAs assumes presence of specific signals on each viral RNA segment that differentiates them not only from cellular RNAs but also from other vRNAs [176,177]. As opposed to "random packaging", this model enables viruses to selectively incorporate a complete set of 8 vRNAs into the virion of IAVs [154]. Individual contribution of vRNA segments to efficient virion production has been demonstrated by a number of studies [178-180]. The coding region of NA vRNA segment, for instance, both at 5′- and 3′-end is required for the efficient segment incorporation into the virion [178,179]. Similarly, the nucleotide length of the M vRNA segment at 5′-end has been found crucial for incorporation of the segment into the virion [180]. Complete and efficient entry of all viral segments into the virus particle is a consequence of coordinated events involving inter-segmental interactions [154].

Newly assembled RNPs require M1 and NEP for nuclear export [169]. Blockade of virus replication by protein kinase H7, which inhibits production of M1, leads to nuclear trapping of viral ribonucleoproteins [181,182]. NEP contains a luecine-rich nuclear export sequence (NES) and is equally crucial for escort of RNP out of the nucleus. Infecting 293T and MDCK cells with a virus encoding NS1, but not NEP, yielded no virus and led to RNP accumulation within the nucleus [173]. M1 is synthesised by non-membrane-bound polyribosomes in the cytosol and enters the nucleus through its nuclear localisation signal (NLS) motif to interact with C-terminal domain of NEP. Interaction with RNP prevents transcription of vRNAs as only transcriptionally-inactive RNPs with attached 3P polymerase complex are found in the virions [153]. A number of studies supported a CRM1-mediated pathway for RNP nuclear export since treatment with leptomycin B (an inhibitor of CRM1 polypeptide) caused retention of vRNPs and their localisation along the nuclear lamina [183,184]. CRM1, a cellular export receptor, in the presence of Ran-GTP binds to its substrate in the nucleus to form a ternary complex. Following stimulation of the GTP hydrolysis, it then releases the substrate into the cytoplasm [173]. Apical localisation of vRNP is not fully understood. It is likely that at least a fraction of M1-RNP complexes are directed towards the budding site by tail-gating HA glycoprotein along the exocytic pathway [185]. In addition, direct interaction between NP and M1, and cytoskeletal proteins (actin microfilaments) has also been reported [186].

The viral envelope proteins (HA, NA, and M2) use cellular exocytic transport pathway to preferentially accumulate at the budding site; that is, the apical plasma membrane of polarised epithelial cells [187-189]. These proteins contain sorting motifs (determinants) in their transmembrane domain (TMD) both for targeting to apical

plasma membrane and association with lipid-rafts [190,191]. The determinants in NA, for example, despite residing the same region (TMD) of the protein, are not necessarily identical and can vary independently [192]. Moreover, apical sorting signal is not present in a specific amino acid sequence, rather it lies over several peptide regions in NA TMD [192]. Unlike M1 and NP, apical proteins are synthesised by membrane-bound polyribosomes and are transported from ER to trans-Golgi network (TGN), where they leave via transport vesicles for delivery to apical membrane [193].

The site of viral glycoproteins arrival at the cell surface determines where budding would take place [153]. For bud initiation, outward bending of the membrane which involves transition from planar to curved structure is required. Although the precise mechanism is not entirely clear, both lipids and (raft-associated) proteins are likely to contribute to this process. Natural asymmetry in the lipid bilayer can lead to intrinsic curving of one monolayer to the other [153]. In addition, asymmetrical ceramide formation in the inner membrane leaflet, by sphingomyelinase, has been known to induce budding in liposomes [194]. Furthermore, amphiphysin BAR structure, a crescent-shaped dimer that is highly conserved from yeast to human, drives membrane curvature both *in vivo* and *in vitro* [195]. However, individual contribution of each of these mechanisms to influenza virus budding is unknown. As discussed above, M1 facilitates bud formation by polymerisation and pulling lipid rafts, containing viral glycoproteins, together to exclude from other parts of plasma membrane.

The content and size of the nucleocapsid in influenza virus, unlike viruses like vesicular stomatitis virus (VSV) and Semliki forest virus (SFV), are not the principle determinants of bud growth. Instead a pulling and a pushing force seem to influence

this process). On one hand, viral transmembrane proteins as well as M1 provide the pulling force to take the nucleocapsid into the bud. On the other hand, cellular actin filaments interacting with vRNPs which have left the nucleus push the virus core into the bud [153]. During bud development, virus nucleocapsid lies at right angles to the cell surface.

Bud closure is the last step in the virus life cycle and is brought in by fusion of apposing ends of the virus membranes to allow scission of the virus particle from infected cell plasma membrane. Bud closing is an energy-dependent and active process as metabolic inhibitors such as oligomycin and ATP analogous like ATPγS prevent the budding [196]. A number of host and virus factors influence the bud release (Figure 1.4.2.1). M2, for example, may drive merging of the lipid rafts and promote pinching-off of the influenza virus particles from the cell surface [159]. In contrast, cortical actin filaments, while crucial for vRNP incorporation into buds during the growth stage, are inhibitory for bud release and therefore should be removed [153]. Overall, bud release is a highly inefficient process and only a minority (about 10%) of mature buds are released from the cell surface [153].

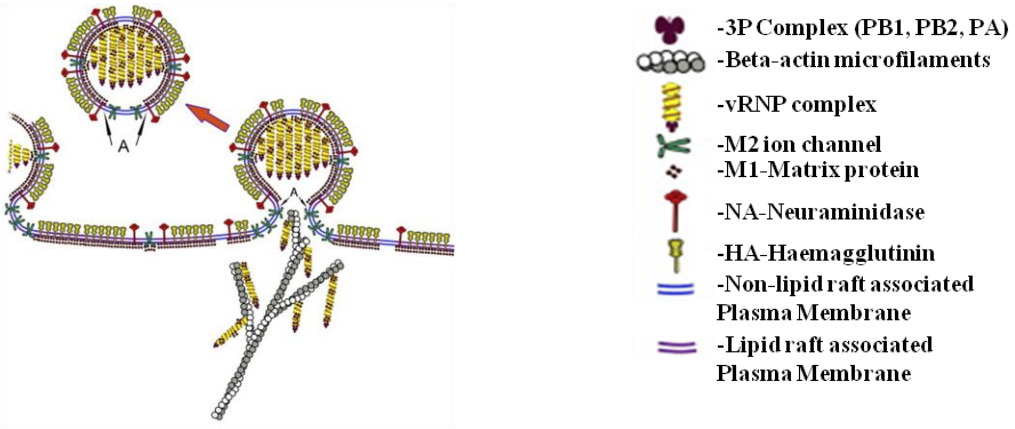

Figure 1.4.2.1. Schematic representation of influenza virus budding off the cell membrane. Budding selectively occurs on the apical domain of polarised epithelial cells. Actin microfilaments facilitate concentration of viral components at the cell surface, and lipid raft micro-domains help in outward bending of plasma membrane and bud initiation. The next stage (bud growth) determines the size and morphology of released virions, and the final step (bud closure) brings about the scission of the bud and release of virus. Diagram taken from Nayak DP *et al* Virus Research 2009.

1.4.3 Tissue tropism of influenza virus

Receptor specificity and binding affinity of haemagglutinin, in the first place, is species-specific [197]. HA isolated from avian and equine species preferentially binds sialic acid (SA) in α2–3 linkage to galactose (SAα2–3Gal), whereas HA from human-tropic influenza A viruses shows preference for cell surface glycans terminating with α2–6 linked SA (SAα2–6Gal).

Sialic acid tissue and cellular distribution is one of the key determinants of influenza virus tropism. In the lungs, SAα2–6Gal is predominantly expressed on non-alveolar epithelial cells [198,199]. Ciliated epithelium from the paranasal sinuses, the pharynx, the trachea and the bronchi stains strongly with *Sambucus nigra* (SAα2–6Gal-specific) lectin. In contrast, SAα2–3Gal expression is more evident in some non-ciliated bronchiolar cells, particularly cuboidal cells at the junction of respiratory bronchioles and alveoli, and type II alveolar pneumocytes [199]. SAα2–6Gal is also present on the M cells of nasopharyngeal lymphoid tissue and upper respiratory tract (URT) goblet cells [198]. Expression pattern of SA receptors in the lungs closely correlates with the clinical manifestation (rhinitis and tracheobronchitis) and sites of IAV infection in humans [198]. With a few exceptions, human SA-binding viruses typically exhibit tropism mostly for lungs, and to a lesser extent for the eyes. However, expression of human IAV receptors on cells and tissues outside respiratory system is poorly characterised.

1.5. Respiratory epithelial cells

1.5.1. Epithelial cells engagement in active immunity

Apical tight junction between respiratory epithelial cells (RECs) enables them to form a physical barrier against harmful particles and microbial pathogens. In addition, respiratory epithelial cell through expression of a host of pathogen recognition receptors (PRRs), secretion of antimicrobial products, cytokines, and chemokines, and interaction with immune cells actively participate in innate and adaptive immune defence.

TLRs recognise conserved microbial structures and have been shows to modulate inducible activation of innate immune response and shaping the subsequent adaptive immunity [200]. At least 13 mammalian TLRs have been identified, to date [201]. Human bronchial epithelial cells express functional TLR-1–6 and TLR-9, as stimulation with appropriate ligands induced IL-6 and IL-8 secretion *in vitro* [202,203]. RT-PCT analysis also detected mRNA transcripts for TLR-1–10 in bronchial epithelial cells [203]. However, the relative expression level and activation potential of each of these receptors vary. In one study double stranded RNA (dsRNA)-activated TLR-3 was the most effective activator to induce upregulation of NFκB signaling pathway genes [203]. On the contrary, low expression levels of TLR-2 and absence of its co-receptor CD36 on normal bronchial epithelial cell line, Beas2B, mediated differential sensitivity of this PRR to corresponding bacterial stimuli [202]. TLR expression is not restricted to bronchial epithelial cells. Human type II alveolar epithelial cells express TLR-2 and TLR-4 and release IL-8 in response to bacterial antigens lipoteichoic acid (LTA) and LPS, respectively [204].

In addition to TLRs, respiratory epithelial cells also express cytosolic pathogen recognition receptors such as RLRs and NLRs. Retinoic acid-inducible gene I (RIG-I) is a member of RIG-I-like receptors (RLR) family of RNA helicases and acts as a sensor for viral 5′-ppp-dsRNA (short, panhandle) in infected cells [205]. RIG-I is highly inducible and its role in signaling antiviral immunity against respiratory viruses such as RSV and IAV has been previously reported [206-209]. In RSV-infected type II pneumocyte cell line, A549, RIG-I molecules bind the virus transcripts in as early as 12h post-infection, and mediate activation of NFκB and interferon response factor 3 (IRF-3) pathways [206]. In parallel, siRNA-induced RIG-I knockout significantly reduced the IFNβ, CCL-5, and IFN-inducible protein 10 (IP-10; CXCL10) expression levels by epithelial cells during the early phase of infection [206]. Similarly, IFNβ production in respiratory epithelial cells after infection with IAV was found to be mediated by RIG-I, and viral protein NS1 was capable of inhibiting RIG-I induced signaling [209]. In addition to RIG-I, melanoma differentiation-associated protein 5 (MDA-5), another member of RLRs which preferentially binds long dsRNA species [205], has also been implicated in antiviral immune response by epithelial cells [209].

Nucleotide-binding oligomerisation domain (NOD)-like receptor (NLR) family comprises more than 20 members which are involved in either sensing intracellular microbial signals or pathogenesis of inflammatory conditions [210]. Structurally, they are characterised by 3 separate domains: i) C-terminal luecine-rich repeat (LRR), ii) central nucleotide binding NACHT, and iii) N-terminal effector domains [210]. Activation of NLRs following direct recognition of bacterial constituents (e.g. peptidoglycan) intracellularly or sensing danger signals (e.g. K^+ efflux) can lead to an inflammatory response (via NFκB), cell death (via caspase 1), or cytokines processing

of pro-IL-1β and pro-IL-18 [210]. *Streptococcus pneumoniae*, an URT-colonising bacterium that typically invades epithelial and endothelial cells, was the first pathogen reported to enhance NOD1 and NOD2 mRNA levels in B6 mouse lungs *in vivo*, and Beas2B epithelial cells *in vitro* [211]. In another study, stimulation of RECs with C12-iE-DAP (NOD1 ligand) enhanced IL-8 and RANTES secretion into the cell culture supernatant, confirming its functional expression [212].

Airway epithelial cells secrete a wide spectrum of molecules with antimicrobial properties ranging from collectins, defensins, and cathelicidins, to lysozymes, lactoferrin, pentraxins, SAA, and SLPI [213]. Collectins are important players of innate immunity and structurally are defined by having a lectin or carbohydrate recognition domain and a collagen-like region [214]. Surfactant proteins A and D (SP-A and SP-D) are well-characterised members of collectin family which are synthesised by type II alveolar epithelial and non-ciliated Clara cells in the lungs [215]. These hydrophilic proteins in Clara cells, for example, are found in the secretory granules which can potentially be released upon infection challenge in the URT during the acute phase reaction [216]. When secreted, SP-A and SP-D then modulate the inflammatory response or alternatively bind the pathogens and either prevent their dissemination, by aggregating them, or act as opsonins to promote their phagocytoses [216]. Both surfactant proteins have been shown to regulate free radical and cytokine production, participate in clearance of the apoptotic cells, inhibit T cell proliferation, and influence DC maturation and Ag presentation [216]. Interactions of SP-A and SP-D with different fungi, like *Cryptococcus neoformans*, bacteria, like *Haemophilus influenza* and *Streptococcus pneumonia*, and viruses like RSV and IAV have been well documented [216]. SP-A, for instance, binds H1N1 and H3N2 IAVs via sialic acid residues in its CTL domain and reduces their infectivity in a dose-dependent manner [217]. SP-D also

strongly inhibits IAV hemagglutination activity and causes viral aggregation. Moreover, binding of neutrophils to IAV is enhanced in the presence of SP-D [218].

Defensins, along with cathelicidins, make up the major antimicrobial peptides (AMP) present in lung mucosal secretions [219]. To date, two main families of defensins have been identified in humans: α– and β–defensins. α–defensins are primarily synthesised by intestinal Paneth cells and neutrophils, whereas epithelial cells are the major source of β–defensins. Among the best-characterised human β–defensins (hBD), hBD-1 is constitutively expressed in human RECs, while expression of hBD-2, -3, and -4 is inducible [219]. β–defensins are cationic peptides with broad antimicrobial activity against fungi, Gram-positive and Gram-negative bacteria, and enveloped viruses [220]. Their activity is mainly of microbicidal nature rather than bacteriostatic, and multiple studies support a role for hBD in permeabilising bacterial membranes [220]. In addition, β–defensins function as chemoattractants for immature DCs and memory T cells via binding CCR6 on their surface [221], neutrophils [222], and macrophages [223]. Cathelicidins comprises a group of structurally diverse α–helical AMPs [219]. RECs express LL-37, a 37-amino acid long peptide, with bactericidal, LPS-neutralising, and chemotaxis-inducing properties [224]. Lysozyme, a main component of lung lavage, is produced by glandular serous and surface epithelial cells as well as professional phagocytes, and exerts its antimicrobial activity by hydrolysing glycosidic bonds in the cell walls of bacteria and fungi [225,226]. Lactoferrin, another constituent of mucosal secretions, by recognising carbohydrate antigens, can agglutinate and kill bacteria, and enhance motility of polymorphonuclear cells and prime superoxide production in neutrophils [227]. Long pentraxin 3 (PTX3) is a soluble pattern recognition receptor and acute phase protein from pentraxin family, whose other

members include C-reactive protein (CRP) and serum amyloid P [228]. PTX3 is expressed by human lung epithelial cells and is strongly upregulated by TNFα in a dose- and time-dependent manner [228]. PTX3 has been previously reported to be important in antifungal immunity in response to pulmonary *aspergillosis* [229], and modulate inflammatory responses by inhibiting phagocytoses of apoptotic neutrophils by DCs and macrophages [228].

1.5.2. Epithelial cells interaction with antigen presenting cells

RECs, on one hand, are capable of inducing DC recruitment to the lungs and, on the other hand, in synchrony with lymphocytes can influence local maturation of monocytes into either plasmacytoid or myeloid DCs [213]. Similar to hBD-2, CCL20 is a potent chemotactic ligand for CCR6-positive imDCs and T cells, and is produced in normal human bronchial epithelial (NHBE) cells [230,231]. CCL20 secretion by NHBE is significantly induced in response to inflammatory and T_h2 cytokines TNFα, IL-1β, IL-4 and IL-13 [231]. IL-17 also stimulates CCL20 secretion dose- and time-dependently from well-differentiated polarised NHBE and mouse RECs *in vitro*, especially into the basolateral compartment [230]. Recruitment of CCR6-expressing cells, mostly imDCs, to the lungs mucosal surfaces is required for innate (NK-mediated) and adaptive (B and T cell-mediated) immunity against viruses and bacteria [232]. In a mouse model of allergic pulmonary inflammation, $CCR6^{-/-}$ mice compared with wild type controls presented with less peri-bronchial eosinophil accumulation, reduced airway hyperreactivity to Ag challenge, and lower IL-5 content in the whole lungs [233]. CCR6 has been reported crucial for DC influx into the lungs following infection with *Aspergillus fumigates* [234]. Furthermore, constant recruitment of DCs to

airways [235] may explain the requirement for steady-state secretion of lung-homing chemokines into the blood.

Lung epithelial cells can regulate the maturation and functional phenotype of locally differentiating DCs. Contact with REC line 16HBE led to higher levels of CD40, CD80 and HLA-DR on DCs while maturating in the presence of IL-4 and GM-CSF. Importantly, cytokine responsiveness and stimulation sensitivity increased in epithelial-conditioned DCs. Co-culture with RECs enhanced TLR-3L-, TLR-4L-, and IFNγ-stimulated IL-12, IL-10, IL-6 and TNFα production by DCs. Additionally, epithelial cells amplified antigen uptake and processing capacity of dendritic cells [236]. IL-15, a multipotent cytokine with biological activities similar to IL-2, can stimulate T cell proliferation and play a key role in survival, development and function of NK cells [237]. Bronchial (Beas2B) and alveolar (A549) epithelial cells have been shown to constitutively synthesise and secrete IL-15, and upregulate its expression when treated with IFNγ, TNFα, and IL-1β. REC-conditioned medium in turn transforms freshly isolated monocytes to grow protruding processes, and increase surface expression of CD80 and CD86 to levels comparable with IL-4/GM-CSF supplemented monocyte-derived DCs [238]. However, on the basis of high expression of CD11c and CD123, and moderate levels of BDCA2, and no CD1a, monocytes differentiated into DCs with both plasmacytoid and myeloid phenotypes [238].

Respiratory epithelial cells interaction with DCs can affect $CD4^+$ T cell (T_h) differentiation locally, via production of thymic stromal lymphoprotein (TSLP) [213]. TSLP is a member of IL-7 family of cytokines that was originally identified for its role in promoting long-term growth of a pre-B cell line *in vitro* [239]. It is produced by RECs and its expression is enhanced in asthmatic airways [240], and in response to

dsRNA [241] and RSV infection [242]. The high affinity TSLP receptor is a heterodimeric complex of IL-7Rα and TSLPR which is expressed on DCs (human) and early T and B cells (mouse) [213]. It has been demonstrated that human respiratory epithelial TSLP potently activated $CD11c^+$ DCs to produce T_h2-attracting chemokines CCL17 and CCL22 [243]. TSLP-primed DCs also differentiated naive $CD4^+$ T cells to T_h2 cells to secrete IL-4, IL-5, IL13, and TNFα, but downregulate IFNγ and IL-10 expression [243].

1.5.3. Epithelial cell interaction with lymphocytes

RECs induce migration of both T_h1 and T_h2 cells to the lungs, via secretion of a variety of chemokines, and engage in direct interaction with T cells [213]. IFNγ strongly induces expression of chemokines CXCL9, CXCL10, and CXCL11 (I-TAC) in primary human bronchial epithelial cells [244]. These ligands are potent chemoattractants for CXCR3-expresssing cells, such as T_h1 and $CD8^+$ T cells, as well as NK and *i*NKT cells [130,131,213,245]. Besides IFNγ, type I and III IFNs, and viral infections can also upregulate CXCR3 ligands in epithelial cells [213]. Human rhinovirus type 16 (HRV-16), for example, amplifies CXCL10 expression in airway cells in a dose- and time-dependent fashion which requires replicating virus and is independent on IFNs [246]. Lymphocytes, through interaction between leukocyte function associated-1 (LFA-1) antigen on their surface and intercellular adhesion molelcule-1 (ICAM-1; CD54) on epithelial cells, can move across bronchial epithelial monolayer stimulated with IFNγ [247]. It has recently been reported that polarised CXCL11 secretion by human RECs creates a chemokine gradient that drives T cell migration across the epithelial barrier [248]. Respiratory epithelial cells, in addition to

T_h1 chemokines, also secrete a range of chemoattractants to recruit T_h2 cells. These include CCL1 (CCR8 ligand), and CCL17 and CCL22 (CCR4 ligands) [213].

Accessory functions of RECs to present microbial antigens and the ability to stimulate T cell proliferation has been suggested by a few studies [249-251]. Mouse type II pneumocytes constitutively express high levels of MHC class II and ICAM-1 on their surface, which along with CD95 are upregulated in *M. tuberculosis*-infected mice [249]. The type II alveolar epithelial cells were able to process and present mycobacterial antigens MHC class II-dependently to $CD4^+$ T cells to stimulate release of IFNγ and IL-2 into the supernatant [249]. Similarly, human RECs can induce peripheral blood T cell proliferation in mixed lymphocyte reaction (MLR) cultures, and activate CD3 associated Fyn, and co-receptors CD4 and CD8 associated lck kinases [250]. Respiratory epithelial cells obtained from surgical specimens of patients undergoing lobectomy induced CFSE-labelled T cell proliferation after seven days *in vitro* co-culture [251]. The REC-induced T cell response was slightly less efficient than that of monocyte derived DCs [251]. RECs were capable of stimulating proliferation of both $CD4^+$ and $CD8^+$ T cells [251].

Antibody production by B cells in the airway mucosa not only is important for protection against pathogens, but also is crucial during pathogenesis of allergic pulmonary disorders [213]. Immunoglobulin (Ig) class switch recombination (CSR) is a process by which B cells are able to shift antibody expression from IgM to other Igs, such as IgE and IgA. Local CSR-mediated IgE production has been reported in nasal and bronchial mucosa of allergic rhinitis and asthmatic patients, respectively [252,253]. CSR on germinal centre B cells can be triggered by CD40 on activating $CD4^+$ T cells [254]. In addition, B cell activating factor of TNF family (BAFF) and a proliferation-

inducing ligand (APRIL) have been shown to promote maturation, survival, and T cell-, CD40-independet CSR Ig production in B cells [255]. RECs express minimal steady-state BAFF and APRIL when unstimulated. However, stimulation with TLR-3L and IFNβ strongly upregulated gene expression and enhanced the soluble and membrane-bound BAFF protein levels in RECs [255]. Furthermore, epithelial cell-derived BAFF was able to induce B cell survival [255]. The BAFF produced by human epithelial cells lining tonsillar crypts stimulates local B cells to secrete polyreactive IgG and IgA [256]. These findings support an active role for respiratory epithelium to influence local humoral immune response.

1.6. Aim

The aim of this project is to investigate whether respiratory epithelial cells express CD1d, and to characterise functional significance of any such expression on *i*NKT cells, and within epithelial cells during influenza virus infection.

Hypothesis

I hypothesize that respiratory epithelial cells express CD1d which is capable of stimulating cytokine secretion from *i*NKT cells. Epithelial CD1d is also important for mounting appropriate immune response during influenza virus infection *in vivo*.

Chapter 2 – Materials and Methods

Chapter 2.

Materials and Methods

2.1. Cell separation, cell staining, and cell growth *in vitro*

2.1.1 Isolation of human bronchial epithelial cells

Primary human bronchial cells were obtained by enzymatic dissociation of lung tissue from patients undergoing lobectomy for localised lung cancer at John Radcliffe Hospital, Oxford, as approved by Local Ethics Committee (Oxford). Tissue fragments distal to the site of tumour were surgically removed and kept in phosphate–buffered saline (PBS). Bronchial cell suspension was generated using a modified protocol [257]. After removal of surrounding parenchymal tissue, airway which was approximately 0.5–1 cm long, was cut into small rings, about 1–2 mm wide, and incubated in dissociation medium [1.4 mg/ml Pronase (Roche); 0.1 mg/ml DNase-I; 110 mM NaCl; 44 mM $NaHCO_3$; 54 mM KCl; 0.25μM FeN_3O_9; 0.9 mM NaH_2PO_4; 1μM sodium Pyruvate; 42μM Phenol Red; pH 7.5; 50U/ml penicillin–streptomycin (Pen/Strep; Lonza)] (all reagents but Pronase and Pen/Strep were purchased from Sigma) for 60 min at 37°C shaking. Pronase digestion was stopped by adding 5 ml foetal calf serum (FCS; Sigma) to 20 ml dissociation medium. Bronchial tissues were rigorously agitated for 5-10 seconds, passed through a 30μm single cell strainer (BD Falcon), washed and treated with 2.5–5 ml RBCLysis^{TM} buffer (Qiagen) for 15 min at RT, and washed again. Following centrifugation, the cell pellet was re-suspended in culture medium [1:1 mix of Nutrient Mixture Ham's F-12:DMEM medium (Invitrogen); 5% FCS; 50U/ml Pen/Strep] and incubated for 3h at 37°C in a 100–mm cell culture plates (BD Falcon) to remove non-epithelial cells like fibroblasts and myeloid cells such as macrophages and

dendritic cells. Non-adherent cells were collected, washed and re-suspended in DMEM medium containing 2mM L-Glutamine (Gln; Lonza) and 50U/ml Pen/Strep before flow cytometry analysis.

2.1.2 Isolation of human peripheral mononuclear cells

Mononuclear cells were separated from whole blood using density gradient centrifugation. Blood was collected directly into heparin-containing tubes. After mixing with an equal volume of RMPI-1640 medium (R0; Invitrogen), diluted blood suspension was layered onto the same volume of Ficoll™ (GE Healthcare) solution and then centrifuged at 850×g for 20 min with no brakes. The interface containing PBMCs was washed in R0 at 300×g for 15 min, re-suspended in R0 and washed again twice. The cells were then re-suspended in R10 (R0 supplemented with 10% FCS, 1% Gln and 1% Pen/Strep) for future use.

2.1.3 Isolation of mouse respiratory epithelial cells

Mice were sacrificed by Schedule 1 method in accordance with Animals Scientific Procedures Act 1986, briefly doused with 70% ethanol, dried, and the whole lungs excised. Adherent tissues, like heart, thymus and thyroid glands were removed before transferring the lungs to DMEM or PBS supplemented with 50U/ml Pen/Strep and 2.5μg/ml amphotericin B (Fungizone; Gibco). Lungs were cut into 1-2 mm pieces and incubated in 1mM EDTA solution in Hanks buffer (Sigma) for 60 min at 37°C, on a shaker. Lung pieces and undigested tissue fragments were further agitated by rigorous shaking for 5-10 seconds and then sequentially filtered through 70–, 40– and 30–μm

nylon meshes (Partec and BD Falcon).The dissociated cells were centrifuged at 550×g for 5 min at RT, incubated in 5 ml RBCLysis^{TM} buffer for 15 min at RT, and then washed in R0. Cell were re-suspended in 0.1 mg/ml of DNase-I in Hanks buffer for 5 min at RT, washed in R0, and depleted of haematopoietic cells by negative magnetic separation with CD45–MicroBeads (Miltenyi Biotech). CD45^{-} cells were re-suspended in culture medium and incubated for 1–2h at 37°C in a 100–mm cell culture plate in order to remove non-epithelial adherent cells (e.g. fibroblasts and macrophages) and to restore surface antigen (Ag) presentation.

2.1.4 Sorting of cells by MACS magnetic beads

Cells were either positively isolated or depleted by magnetic MicroBeads (Miltenyi Biotech) following the manufacturer's protocol (Appendix 1). Single-cell suspensions were obtained. When depleting, up to 10^7 cells were incubated with 90µl MACS buffer (PBS pH7.2, 0.5% BSA and 2mM EDTA) and 10µl MicroBeads at 4°C for 15 min, washed once, and then re-suspended in 2ml MACS buffer for use with one LD column. For positive selection, up to 10^6 cells were incubated with fluorophore-conjugated mAb and 100µl MACS buffer at 4°C for 20 min. Cells were then washed and re-suspended in 80µl MACS buffer and 20µl MicroBeads, and incubated at 4°C for 15 min. Cell suspension was washed and the positively stained population was collected by passing through two MS columns in a magnetic field.

2.1.5 Preparation of cytospin cells and frozen tissue sections from human and mice

Up to 5×10^5 cells were cytospun using Shandon Cytospin® 4 (Thermo Scientific) at 200×g for 3 min onto adhesive glass slides (Surgipath) and left to dry overnight at RT. They were either used for immunofluorescence staining or stored at –20°C for future analysis.

Human lung sections that had been snapped-frozen in liquid nitrogen were partially thawed, immersed in Tissue-Tek® (Raymond A Lamb) and frozen again for sectioning using Cryostat (Leica) at 8μm thickness.

For mouse studies, intact whole lungs were excised from mice after dissecting the trachea just below the larynx. Lungs were intubated and inflated with 4% formaldehyde in PBS for 3-6h using pressure from a 2ml syringe and contained in a sealed 25ml tube topped with the fixative solution (modified from Davies *et al* [258]).

Lungs were incubated in 30% sucrose solution in PBS overnight (for cryoprotection and dehydration), inflated with 1:1 mix of Tissue-Tek ® and PBS, semi-frozen over dry ice, and stored in –80°C until 5–8μm cryosections were prepared.

Figure 2.1.5.1. Fixing whole lungs from mice.

2.1.6 Immunocytochemistry of cells grown on chamber slides

Appropriate cells were seeded at a density of 5×10^4 in 200µl per well in 8-well chamber slides (Thermo Scientific). These were then fixed in 4% formaldehyde/PBS at 37°C for 15 minutes. Non-specific Ab binding sites were blocked with blocking buffer (5% FCS, 1% BSA in PBS) for 30 minutes at RT, before adding the relevant primary Ab. The immunostained primary Ab was then detected by an Alexa Fluor®-conjugated secondary Ab (Invitrogen). Both Ab stainings were performed for 45 minutes at RT and slides were washed three times with blocking buffer between stainings. Cells were covered in Vectashield® Mounting Medium with DAPI (Vector Labs) and visualised by Axiovert S100 inverted microscope (Zeiss).

2.1.7 Immunostaining of cryostat sections and confocal microscopy

Cells were fixed in 4°C cold acetone for 10 minutes and non-specific sites were blocked by incubation with blocking buffer (5% FCS, 1% BSA in PBS) for 30 minutes at RT. Primary and secondary Abs were added consecutively, each for 45 min at RT. Alternatively, cells were incubated with Abs freshly labelled with Alexa Fluor® 488, using Zenon Labelling kit (Invitrogen), for 45 min. Following the manufacturer's protocol, 5µl IgG labelling reagent (Alexa Fluor® 488-conjugated F_{ab} fragments) was added to 1µg Ab and incubated at RT for 5 minutes in dark. Excess unbound F_{ab} were removed by treatment with 5µl of blocking component (5 min) and then used within 30 min. After immunostaining, cells and sections were covered in Vectashield® Mounting Medium with DAPI, covered with Cover Slip and then visualised by confocal

microscope (Bio-Rad). Pictures were taken by Nikon camera and analysed by LaserSharp software (Zeiss).

2.1.8 Flow cytometry

All stainings were performed in 96-well plates. 1–5 × 10^5 cells were washed in FACS buffer (5% FCS, 1% bovine serum albumin (BSA) in PBS) before staining with the relevant Ab at 4°C for 20 min in dark.

For the mouse cells, prior to staining, non-specific Fc receptor binding was blocked with 0.1μg anti-CD16/CD32 Ab in 30μl FACS buffer for 15 min at RT. Cells were then washed twice in 200μl FACS buffer, centrifuged at 300×g for 5 min, and acquired on 3-laser 9-parameter CyAn™ ADP Flow Cytometer (Dako) and analysed using Summit software (Dako).

Dead cells were excluded by incubation with Hoechst 33342 nucleic stain (Sigma), or annexin V and 7-Amino Actinomycin-D (7-AAD; BD Pharmingen) staining.

For intracellular cytokine staining, cells were fixed in 50μl of 1% formaldehyde in PBS for 15 min at RT, washed in permeabilising buffer (0.5% saponin in FACS buffer), and pelleted by centrifugation at 300×g for 5 min. Cells were then stained with appropriate Ab at 4°C for 20 min in dark, washed twice in 200μl permeabilising buffer and acquired on CyAn™ ADP Flow Cytometer.

Abs used in this thesis are listed below:

Antibody	Conjugate	Clone	Host & isotype	Cat. Number	Supplier
Human					
Annexin V	FITC	NA	NA	556419	BD Pharmingen
β–tubulin IV	Unconj.	ONS-1A6	Mse IgG1	MU178-UC	BioGenex
CD1b	AF 647	eBioSN13	Mse IgG1	51-0018-71	eBioscience
CD1d	Unconj.	42	Mse IgG1	550254	BD Pharmingen
CD1d	Unconj.	NOR3.2/13.17	Mse IgG1	Sc-58976	Santa Cruz
CD1d	Unconj.	C3D5	Mse IgG2a	Sc-19632	Santa Cruz
CD1d	Unconj.	H70	Rab pIgG	Sc-21010	Santa Cruz
CD3ε	FITC	HIT3a	Mse IgG2a	11-0039-41	eBioscience
CD4	PB	OKT4	Mse IgG2b	48-0048-42	eBioscience
iNKT TCR Vα24	FITC	6B11	Mse IgG1	558371	BD Pharmingen
IL-1α	FITC	CRM8	Mse IgG1	11-7019-71	eBioscience
IL-4	PE	MP4-25D2	Mse IgG1	12-7048-71	eBioscience
IL-13	FITC	PVM13-1	Mse IgG1	11-7139-41	eBioscience
IL-5	PE	TRFK5	Mse IgG1	12-7052-82	eBioscience
IFNγ	APC	B27	Mse IgG1	554702	BD Pharmingen
Pancytokeratin	Unconj.	Lu-5	Mse IgG1	Ab17155	Abcam
TNFα	PE	MAb11	Mse IgG1	554513	BD Pharmingen
Mouse					
CD16/32 Fc Block	Unconj.	2.4G2	Rat IgG2b	553141	BD Pharmingen
CD45.2	eFluor™ 450	30-F11	Rat IgG2b	48-0451-82	eBioscience
CD45.2	APC	104	Mse IgG2a	17-0454-81	eBioscience
CD140b (PDGF Receptor β)	PE	APB5	Rat IgG2a	12-1402-81	eBioscience
CD144 (VE-cadherin)	AF 488	eBioBV13	Rat IgG1	53-1441-80	eBioscience
CD326 (EpCAM)	Unconj.	G8.8	Rat IgG2a	14-5791-81	eBioscience
CD326	PE	G8.8	Rat IgG2a	12-5791-81	eBioscience
CD324 (E-cadherin)	Unconj.	DECMA-1	Rat IgG1	14-3249-80	eBioscience
CD324	APC	114420	Rat IgG2a	FAB7481A	R&D Systems

Table 2.1.8.1. The antibodies used in the studies described in this thesis. AF: Alexa Fluor®; APC: Allophycocyanin; eFluor™ 450: PB replacement; FITC: Fluorescein Isothiocyanate; PE: Phycoerythrin; PB: Pacific Blue™; Unconj.: Unconjugated; Mse: mouse; Ham: hamster.

2.1.9 Preparation of mouse CD1d-α–GC dimeric complexes

Working stock of α–GC ($C_{50}H_{99}O_9$; Axorra) was prepared by dissolving lyophilised powder in 100µl DMSO, and mixing 20µl of the solution with 980µl vehicle (0.5% Tween-20, 150mM NaCl in distilled water (dH_2O)) to yield 200µg/ml α–GC stock.

Before use, α–GC stock solution was heated at 80°C for 5 min, and sonicated for 3×1 min. The dimers were generated by adding 20µl PBS and 3µg of soluble divalent

mouse CD1d-IgG1 fusion dimer protein (BD Pharmingen) to 0.2μg α–GC, incubating overnight at 37°C on a rotating tube rotator, and then labelled with 1.5μg PE-conjugated rat anti-mouse IgG1 at RT for 1h. The dimeric complex (hereafter referred to as "dimer") was stored at 4°C, up to a week, if not used immediately.

2.1.10 Cell lines and primary cells

The following cell lines were used in this project: Beas-2B (a human bronchial epithelial cell line transformed with Adenovirus-SV40 hybrid virus), A549 (a cancerous human type II alveolar epithelial cell line), Madin-Darby canine kidney (MDCK; a canine normal kidney epithelial cell line), CD1d-expressing EBV-transfected 721.221 B cell line (.221^{+}), Jurkat (a human leukemic T lymphoblast cell line), , MRC5 and IMR90 (normal foetal lung fibroblast cell lines), 16HBE14O^{-} (a differentiated SV40-transformed human bronchial epithelial cell line), TZM-bl (a CD4-expressing HeLa (adenocarcinoma-derived human cervical epithelial) cell line), HaCat (a spontaneously immortalised human keratinocyte cell line), NKer (a human keratinocyte line immortalized using human papilloma virus-16 E6 protein), HCT 116 (a human colon carcinoma epithelial cell line), MOLT4 (a human leukemic T lymphoblast cell line), and THP1 (a human monocytic/macrophage cell line).

All cell lines were purchased from American Type Culture Collection (ATCC), apart from .221^{+}, TZM-bl, HCT116, 16HBE14O^{-}, MOLT4, THP1 received as kind gifts, respectively, from Drs. Demin Lee, Astrid Iversen, Adrian Harris, Alain Townsend, and Vincenzo Cerundolo, all from University of Oxford. NKer was a kind gift from Dr E O'Toole [259] from Northwestern University.

Primary bronchial epithelial cells, NHBE, were purchased from Lonza; or obtained by enzymatic dissociation of normal non-cancerous lung tissue of patients undergoing lobectomy, for localised tumour(s); or brushed bronchial cells from patients undertaking diagnostic clinical bronchoscopy were used.

Human cytokine-secreting *i*NKT clones were obtained as previously described by Ho *et al* [260]. In brief, $V\alpha24^+$ cells in PBMC of a healthy human donor were isolated by MACS separation, seeded onto 96-well plates, stimulated with PHA in RPMI-1640 supplemented with 10% human serum (HS; from First Link) and IL-2 added to their medium on day 3. After 15-20 days, $V\alpha24^+$ $V\beta11^+$ and CD1d/α–GC tetramer$^+$ T cells were further expanded by PHA and allogeneic feeders.

2.1.11 Cell media, reagents, and maintenance

All cells, in this study, were cultured in 37°C incubator in 5% CO_2. Beas-2B was cultured in F12 Nutrient Mixture Kaighn's Modification (F12K), and A549, 16HBE14O$^-$, TZM-bl, HaCat, NK, HCT116, 293 HEK, and MDCK cells in Dulbecco's modified Eagle medium (DMEM). Jurkat, .221+, THP1, and MOLT4 were cultured and passaged in RPMI-1640. All media were supplemented with 10% FCS and 1% Gln and Pen/Strep, and adherent cells were grown in 75-cm^2 flasks (Corning), until seeding into 6-, 12-well tissue-culture plates or 12-well transwell inserts (Corning) for subsequent stimulation with various reagents or co-culture. NHBE and *i*NKT cells were grown in BulletKit (hydrocortisone, bovine pituitary extract, epinephrine, human epidermal growth factor, transferrin, insulin, retinoic acid, triiodothyronine,

gentamicin/amphotericin-B)-supplemented BEGM (Lonza), and RPMI-1640 containing 10% HS, respectively.

2.2. Molecular biology

2.2.1 RNA extraction

Total RNA was extracted by lysing the cells in TRIzol® reagent (Ambion) or using RNeasy Mini Kit (Qiagen), following the manufacturers' protocols. Briefly for the former method, up to 10^7 cells were lysed in 1ml TRIzol® solution – capable of maintaining the RNA integrity while disrupting the cells, incubated at RT for 5 min, centrifuged at 12000×g for 10 min at 4°C to remove cell debris, and mixed well with 100µl bromo-chloropropane (BCP; Sigma). BCP was a less toxic and more stable chloroform substitute which simultaneously phase-isolated the cellular RNA, DNA, and proteins. Following 10 min incubation at RT, spinning at 12000×g for 15 min at 4°C generated two distinct phases: an aqueous phase on the top, which contained RNA, and an organic one at the bottom, that contained proteins. These two were separated by a DNA-rich interface. 500µl of the top phase was removed and mixed well with 500µl isopropanol (Sigma) – to precipitate RNA, centrifuged at 12000×g for 8 min at 4°C, and the pellet was washed in 75% ethanol (7500×g for 5 min) and spun again before dissolving in RNase-free water.

For RNeasy method, up to 4×10^6 cells were lysed in "RLT" – a denaturing guanidine-thiocyanate–containing lysis buffer which inactivates RNases, and cells were further disrupted by passing through a 20-gauge needle for at least 5 times. The lysates were mixed 1:1 with 70% ethanol, centrifuged at 6700×g for 15 sec to allow binding of

RNA to spin column membrane, and washed consecutively in guanidine-thiocyanate–containing ("RW1") and ethanol-containing ("RPE") buffers. The RNA was then eluted off the column by a final wash with RNase-free water at 6700×g for 1 min.

After extraction with either protocol, RNA was incubated with DNase I (Qiagen) for 15 minutes at RT, to remove residual contaminating DNA. The enzyme was inactivated by heating at 65°C for 5 min, and RNA was store at -80°C.

2.2.2 DNA extraction

Total DNA was purified from Beas2B cells using DNeasy Blood & Tissue Kit (Qiagen), following the manufacturer's protocol. For this, 5×10^6 epithelial cells were harvested from tissue culture flask, re-suspended in 200µl PBS, 20µl proteinase K, and 4µl RNase A, and incubated for 2 min at RT. 200µl lysis ("AL") buffer was added and mixed thoroughly with the sample before incubating at 56°C for 10 min. Then 200µl ethanol was added and the mixture centrifuged in spin column at 4300×g for 1 min. Following washes in ethanol-containing ("AW1" and "AW2") buffers, DNA was eluted off the spin column membrane by addition of 100µl low-salt "AE" buffer and centrifuging at 4300×g for 1 min.

2.2.3 cDNA synthesis

The isolated total RNA was subjected to reverse transcription, using SuperScript® Reverse Transcriptase III kit (Invitrogen). cDNA synthesis was primed by mixing 1µl of either oligo-dT (50µM), 1:1 oligo-dT : random hexamers mix (50µM)

or gene-specific primer (1µM), and 1µl of dNTP mix (10mM) with up to 5µg total RNA. The volume of the mixture was brought up to 13µl using RNase-, DNase-free dH_2O, and then heated up at 65°C for 5 min to allow initial annealing of primers with RNA. After this step, 4µl 5×"First Strand buffer", 1µl DTT (0.1M), 1µl RNaseOUT (40U), and 1µl the reverse transcriptase (200U) were added. Enzymatic reaction was initiated by heating at 50°C for 60 min, and then terminated by incubation at 70°C for 15 min. The final volume was 20µl.

2.2.4 Primer/probe design

Unless stated otherwise, primers and probes were designed using either Primer Express® software (Applied Biosystems) or the online Primer3 application (http://frodo.wi.mit.edu/primer3/). As a general guideline and whenever possible, primers' melting temperature (Tm) were designed around 60°C, GC content in the range of 40%–60%, primer's length of 13–25 base pairs (bp), and they were devoid of 5′-end G nucleotide and complementary properties at 3′-end. For real time PCR analysis, the melting temperatures of probes were 10°C higher than the corresponding primers, and the amplicons had a length of 50–150bp.

2.2.5 Reverse-transcription PCR

Two microlitres cDNA was added to 48µl reaction mix containing 2U FastStart Taq DNA Polymerase, 5µl 10 x PCR buffer, 2mM $MgCl_2$, 1µM of each dNTP and 1µM of forward and reverse primers for RT-PCR in a thermocycler (Applied Biosystems, GeneAmp® PCR System 2700). Amplification reactions consisted of an initial 5-

minute denaturation step at 95°C to activate Taq DNA polymerase, and 30-45 cycles of denaturing at 95°C for 30 seconds, annealing at 56-60°C for 1 minute, and extension at 72°C for 1 minute. A final elongation step was performed at 72°C for 10 minutes. PCR products were then electrophoresed on 1.5-2% agarose gel containing ethidium bromide and visualised under ultraviolet transilluminator (UVP, USA).

2.2.6 Real-time PCR

Real time PCR was performed using 7500 Fast real time PCR system (Applied Biosystems, UK). Reactions contained 2µl cDNA added to 10µl Taqman 2×Universal or SYBR Green Master Mix (Applied Biosystems) and appropriate primers and probe. Probes were ordered from Eurogentec. Total reaction volume was adjusted to 20µl, using DNase-free water. PCR conditions for SYBR Green assay were according to default settings: 50°C for 2 minutes, 95°C for 10 minutes, 45 cycles of 95°C for 15 seconds, and 60°C for 1 minute. Dissociation curve was run after the last step to verify product specificity. A single melting temperature peak indicated specific product amplification. Taqman assay conditions were optimised at 95°C for 20 seconds and 45 cycles of 95°C for 3 seconds and 60°C for 30 seconds. In both SYBR Green and Taqman assays, fluorescent signal was collected at the end of extension step of each reaction cycle. Samples were loaded in duplicates or triplicates (when low expression) on the plate and average threshold cycle (Ct) was recorded for each condition. If there were more than 0.5 cycle difference in Ct values for a given sample, the experiment was repeated. The results were quantified using $2^{-\Delta\Delta Ct}$ method [261] (Applied Biosystems). This is a relative quantification approach by which ΔCt ($Ct_{\text{gene of interest}} - Ct_{\text{housekeeping gene}}$) is calculated initially, and then ΔΔCt is obtained by subtracting ΔCt of a

given sample from that of a reference (e.g. untreated cells); i.e. $\Delta\Delta Ct = \Delta Ct_{\text{sample x}} - \Delta Ct_{\text{reference sample}}$. This yields comparative level of sample x against the reference sample. Ultimately, the ΔΔCt value is brought to the power 2; since every cycle on the real-time PCR amplification plot represents a two-fold change in the transcript content. The $2^{-\Delta\Delta Ct}$ method requires comparable amplification efficiencies for both housekeeping genes and genes of interest. This was verified by serial dilution of two target genes against HPRT housekeeping gens.

2.2.7 DNA microarray

The integrity of the total RNA isolated by RNeasy kit from human *i*NKT cells or mouse lung epithelial cells was initially assessed qualitatively with RNA 6000 Nano Reagents kit (Agilent) and analysing with Agilent 2100 Bioanalyser. Where RNA was intact and non-degraded, GeneChip Whole Transcript (WT) Sense Target (ST) Labelling assay (Affymetrix) was followed, starting with 100–300ng RNA, unless stated otherwise. Under the standard protocol, double-stranded cDNA was synthesised using random hexamers attached to a T7 promoter sequence. The ds-cDNA was then used as a template for T7 RNA polymerase to produce multiple copies of antisense cRNA. After clean-up, a second cycle of cDNA synthesis was carried out using random hexamers containing dUTP to yield single-stranded cDNA copies. The ss-cDNA were then treated with uracil DNA glycosylase (UDG) to get fragmented, and were labelled by terminal deoxynucleotidyl transferase (TdT) with biotin. The fragmented targets were hybridised with Human or Mouse Gene 1.0 ST Array chips (Affymetrix), stained and washed using GeneChip Fluidics Station 450, and the fluorescent signals were captured as data image files for analysis with GeneChip Operating Software.

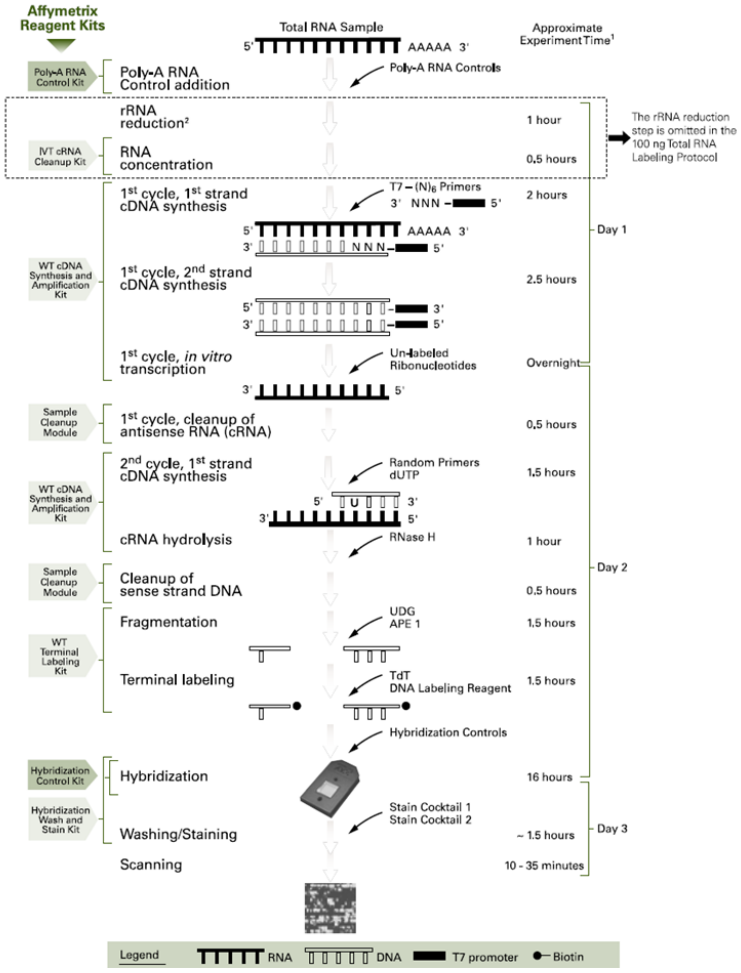

Figure 2.2.6.1. Protocol for whole transcript sense target labelling assay. Obtained from Affymetrix website: (http://media.affymetrix.com/support/downloads/manuals/wt_sensetarget_label_manual.pdf)

2.2.8 DNA sequencing

Nucleotide sequences were detected by in-capillary method using Applied Biosystems 3730 DNA analyser (performed by John Frankland and Tim Rostron).

2.3. Protein analysis

2.3.1 Western blotting

Cells were lysed *in situ* in tissue culture flasks or plates with an ice-cold Ipegal (NP-40)-based Lysis buffer (150mM NaCl; 20mM $MgCl_2$; 0.5% NP-40; 50mM Tris.HCL; pH 7.4) in which Protease Inhibitor Cocktail (Roche; 1 tablet per 7ml buffer) had been dissolved, at 4°C for 30 min. Jurkat or CD1d-transfected .221$^+$ cells were pelleted by spinning at 300×g for 5 min before lysis. The lysates were collected, vortexed vigorously for 10–15 sec, and then centrifuged at 8000×g at 4°C for 10 min. The supernatants were subsequently used for Western blot analysis or immunoprecipitation.

Precast 12% acrylamide 1.0 mm thick Bis-Tris NuPAGE® gels (Invitrogen) were used for protein electrophoresis. The lysates were mixed with 10µl of NuPAGE® lithium dodecyl sulphate (LDS) Loading Buffer (Invitrogen) – for visualising protein migration during electrophoresis, 4µl of NuPAGE® Reducing Agent (Invitrogen) – to reduce protein disulfide bonds, and topped up to 40µl using dH_2O. After loading, the gels were run at 150V constant voltage for 50–70 min in an antioxidant-containing 1×SDS MOPS Running Buffer (0.5ml per 200ml buffer; Invitrogen). Full-range "Rainbow" protein ladder (GE Healthcare) was used in parallel to differentiate the molecular weight (MW) of the protein band on the blot. The proteins were then blotted onto a nitrocellulose membrane (Amersham) that had been pre-soaked in 1×Transfer buffer (10% methanol; 0.1% antioxidant) for 10–15 min, by "wet transfer" using XCell™ II Blot Module (Invitrogen) at 30V constant voltage for 1h. After the blot transfer was complete, the membrane was incubated with Blocking buffer [5% non-fat

dried milk, 0.1% Tween-20 in Tris-Buffered Saline (150mM NaCl; 50mM Tris-HCl; pH 7.5)], called TBS-T, for 1h at RT or at 4°C overnight on a rotator to block non-specific sites. The blot was then probed sequentially with primary and secondary HRP-conjugated Abs in TBS-T either for 1h at RT or at 4°C overnight. After both Ab immunostaining steps, the membrane was washed at least 3 times 10 min each in TBS-T. The protein bands were visualised by incubating the membrane with chemiluminescence reagent (ECL kit; Amersham) at RT for 1 min before exposing to Hyperfilms (Amersham) for 30 sec to 30 min, depending on the intensity of the signal.

2.3.2 Immunoprecipitation

In some experiments CD1d was immunoprecipitated using the following protocol. Cell lysates or lysis buffer alone (negative control) were initially pre-cleared by incubating with 30–50µl Protein A-Sepharose MicroBeads (Sigma) per 2×10^7 starting cells at 4°C for 1h on a rotor. After centrifuging at 10000×g for 10 min, Ab was added to the supernatant, incubated an extra 2h rotating at 4°C, and supplemented with 50µl fresh MicroBeads to crosslink the beads with the Ab-Ag complexes overnight rocking on a shaker. The next day, beads were pelleted, washed 3 times in NET buffer (150mM NaCl; 5mM EDTA; 0.5% NP-40; 50mM Tris.HCL; pH 7.5), boiled in 1×SDS Sample Loading buffer at 90–100 °C for 10 to dissociate the Ab-Ag complexes, and centrifuged at 10000×g for 5 min. The supernatant was then loaded onto precast NuPAGE gels for either western blotting or gel staining.

2.4. Mice

2.4.1 Mouse strains

All mice were kept in the Biological Services Unit, John Radcliffe Hospital, University of Oxford, in accordance with U.K. Home Office regulations and the project was approved by local ethical review committee. Specific-pathogen free C57BL/6 (B6) and CD1d$^{-/-}$ B6 mice [262] of both sexes at 6–8 weeks old were used. Animals were killed using a Schedule 1 method.

2.5. Statistics

Differences in measured variables between groups were determined using Student's t-test where two groups were compared and one-way analysis of variance (ANOVA) where three groups were compared. Data in all graphs are expressed as mean± S.E.M. All statistical analyses were performed with the Prism® software.

Chapter 3. Expression of CD1d on human respiratory epithelial cells

Chapter 3.

Expression of CD1d on human respiratory epithelial cells

3.1. Aims

To characterise CD1D[1] transcript and protein expression in human respiratory epithelial cells (RECs).

3.2. Introduction

RECs are the major site of contact and the primary target of influenza A virus (IAV) due to preferential expression of sialic acid-containing haemagglutinin (HA) receptors in the airways [198,199]. RECs express pathogen recognition receptors (PRRs) [202,204,206,207] and secrete a variety of cytokines, chemokines and antimicrobial peptides [219,220]. They are, therefore, active participants of the local immune and inflammatory defence response [213].

Hitherto, there has been no reports of CD1d expression on RECs. CD1d is typically studied in the context of professional APCs (e.g. macrophages, DCs, and B cells) and monocytes [3,92]. A few reports have shown CD1d expression on intestinal epithelial cells (IECs) [56,57], skin keratinocytes [60], and suprabasal layer epithelium of lower reproductive tract [61]. These findings imply a potential role for this MHC class I-like molecule in mucosal immunity. Intestinal colonisation of bacteria, for example, was found to be regulated by CD1d [263]. $CD1d^{-/-}$ mice had greater colonisation rate of small intestine and increased bacterial translocation across mucosal barrier, compared with wild type (WT) mice. The knock-outs also exhibited defects in

[1] CD1D: gene & mRNA; CD1d: protein

degranulation ability of Paneth cells, and interaction between intestinal crypt cells with *i*NKT cells in the presence of α–GC was sufficient to induce lysozyme secretion [263].

In this chapter, I examine the expression of CD1d at mRNA and protein levels in human RECs.

3.3. Methods

Expression of CD1D mRNA was investigated by RT-PCR initially in human brushed bronchial epithelial cells, and then in Beas2B (a normal human bronchial epithelial cell line transformed with Adenovirus-SV40 hybrid virus) and A549 (an adenocarcinoma-derived human type II alveolar epithelial cell line). Primary bronchial cells were obtained by brushing the lower respiratory tract of patients undergoing bronchoscopy for clinical investigation of a localised mass. Bronchial cells from normal unaffected areas were collected (provided by Dr. Ho). Identity of brushed cells was studied by immunofluorescent staining with pancytokeratin (PCK) and β-tubulin IV (βtubIV) mAbs. Several primer pairs were designed with either Primer Express® software or Primer3 application (Chapter 2.2.4), and RT-PCR was performed as discussed in Materials and Methods (Chapter 2.2.5). A human leukemic T lymphoblast cell line known to express CD1D (Jurkat) was used as a positive control.

Protein expression was studied by flow cytometry using three anti-human CD1d mAbs on Beas2B and A549 epithelial cell lines, and the following primary RECs: commercially-obtained normal human bronchial epithelial (NHBE) cells, and freshly isolated native bronchial epithelia. For the latter, bronchial cells were extracted from

lungs of patients undergoing lobectomy due to localised lung tumours. As described in Materials and Methods (Chapter 2.1.1), non-cancerous tissues distal to the site of tumour were surgically removed and then enzymatically dissociated with pronase/DNase. Cells were then fixed in acetone and permeabilised in saponin before immunostaining with anti-human PCK and CD1d (Chapter 2.1.8).

Protein detection was also carried out by Western blotting on Beas2B, A549, and NHBE. A full-length CD1d-transfected B cell line .221 (hereafter designated as $.221^{+}$; generated by Dr. Li, Oxford University) was used as a positive control.

Immunofluorescent staining and confocal microscopy were used to visualise CD1d in chamber slide-grown NHBE and airway cryosections. For the latter, human lung tissue that had been snapped-frozen in liquid nitrogen was partially thawed, immersed in Tissue-Tek® and frozen again for sectioning by Cryostat at 8μm thickness prior to staining. Cryosections and NHBE were stained as described in Materials and Methods (Chapters 2.1.6 and 2.1.7).

Primer	Sequence (5′→3′)
CD1D	
Forward A.	*CTCGTCCTTCGCCAATAGC*
Reverse A.	*ACCACATCCAGGGTTGCTC*
Forward B.	*CTCGTCCTTCGCCAATAGC*
Reverse B.	*AGCCTGTATGGGTGAAGTGG*
Forward C.	*TTATCGAAGCAGCTTCACCAGG*
Reverse C.	*GATACCATGTCTCGTCAGCATT*
GAPDH	
Forward GAPDH.	*GAGTCAACGGATTTGGTCGT*
Reverse GAPDH.	*TTGATTTTGGAGGGATCTCG*

Table 3.3.1. List of PCR primers used in this chapter and their nucleotide sequence.

3.4. Results

3.4.1 Identification of CD1D mRNA in respiratory epithelial cells

Two sets of primers were designed ("A/A" and "B/B"; Table 3.3.1) to specifically amplify CD1D transcript within its coding exons (Figure 3.4.1.1A). "A/A" spanned α2 exon covering most of α1 and α3 exons, and "B/B" amplified transmembrane (TM) and most of α3 and cytoplasmic tail (T) exons. Using these primers, I first show CD1D is expressed in primary human RECs (brushed bronchial cells) (Figure 3.4.1.1B).

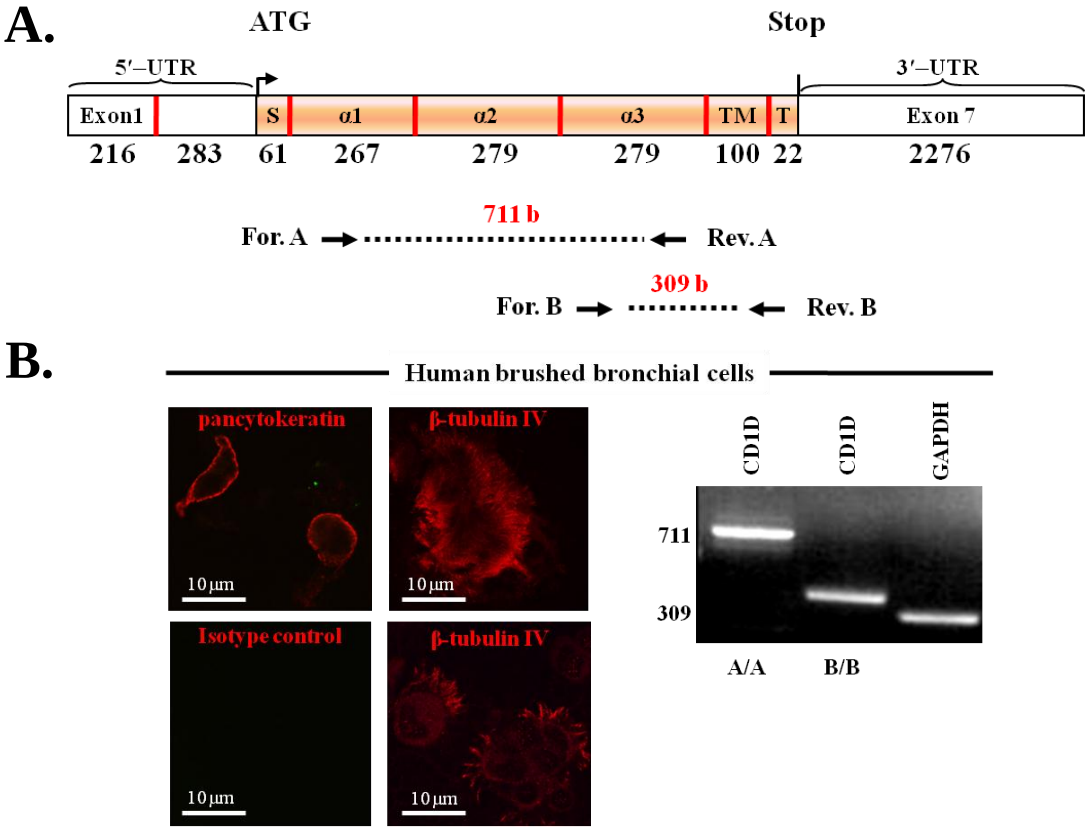

Figure 3.4.1.1. Identification of CD1D mRNA in human brushed bronchial cells. (A) Graphical representation of human CD1D mRNA, showing coding exons in orange, corresponding to peptide domains, and non–coding exons in open boxes. Horizontal arrows illustrate primer sites and expected product sizes in RT-PCR are shown in red**. (B)** Agarose gels showing PCR amplification of CD1D, and representative confocal microscopic pictures demonstrating pancytokeratin and β–tubulin IV staining in human brushed bronchial cells (scale bar: 10µm). ATG: start codon; UTR: untranslated region; S: signal peptide; TM: transmembrane; T: cytoplasmic tail; No-RT: no-reverse transcriptase; For.: forward primer; Rev.: reverse primer.

To confirm that the brushed cells were predominantly REC, the cells were cytospun, and immunostained with PCK and βtubIV. The commercially available PCK mAb (clone Lu-5) was raised against lung cancer cells and reacts with both acidic type I cytokeratins and basic type II cytokeratins. This cytokeratin coverage allows detection of both mucous and ciliated columnar (mainly cytokeratins 7-, 8- & 18-positive), and basal (predominantly cytokeratins 5- & 14-positive) epithelial cells in the airway [264]. βtubIV, on the other hand, was raised against recombinant human β-tubulin isotype IV which is the major β-tubulin in mammalian cilia [265]. Approximately 90% of the cells in any microscopic field stained positive for PCK and 60% for βtubIV (Figure 3.4.1.1B).

Since these cells were not 100% pure, and may have included contaminating sub-epithelial cells, CD1D mRNA was amplified in REC cell lines Beas2B and A549. Using primer pairs "A/A", "B/B", and "C/C" – which spanned α1 to α3 exons, I confirmed CD1D expression in these epithelial cells (Figure 3.4.1.2).

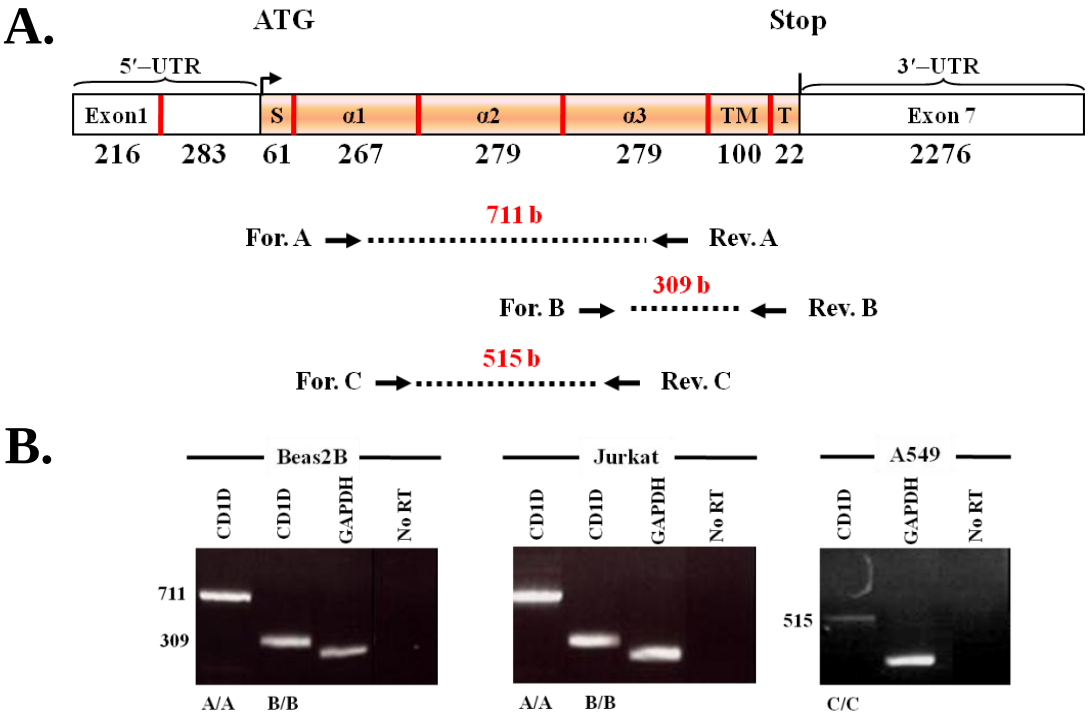

Figure 3.4.1.2. Expression of CD1D mRNA by human REC lines. (A) Graphical illustration of human CD1D mRNA and primer sites. **(B)** RT-PCR amplification of CD1D in Beas2B, A549, and Jurkat.

3.4.2 Flow cytometry detection of CD1d in human respiratory epithelial cells

To determine if these transcripts were translated into protein, three mouse anti-human CD1d mAbs [clones 42 (BD Pharmingen), 51.1.3 (kind gift from Prof. Steven Porcelli; Albert Einstein Medical School) and NOR3.2 (Santa Cruz)] were utilised to determine protein expression on Beas2B and A549 (Figure 3.4.2.1). Flow cytometry analysis detected CD1d on the surface of Beas2B using all the three Abs. However, A549 surface stained positive only with 51.1.3; but, moderate and high levels of intracellular CD1d were identified using clones 42 and NOR3.2, respectively.

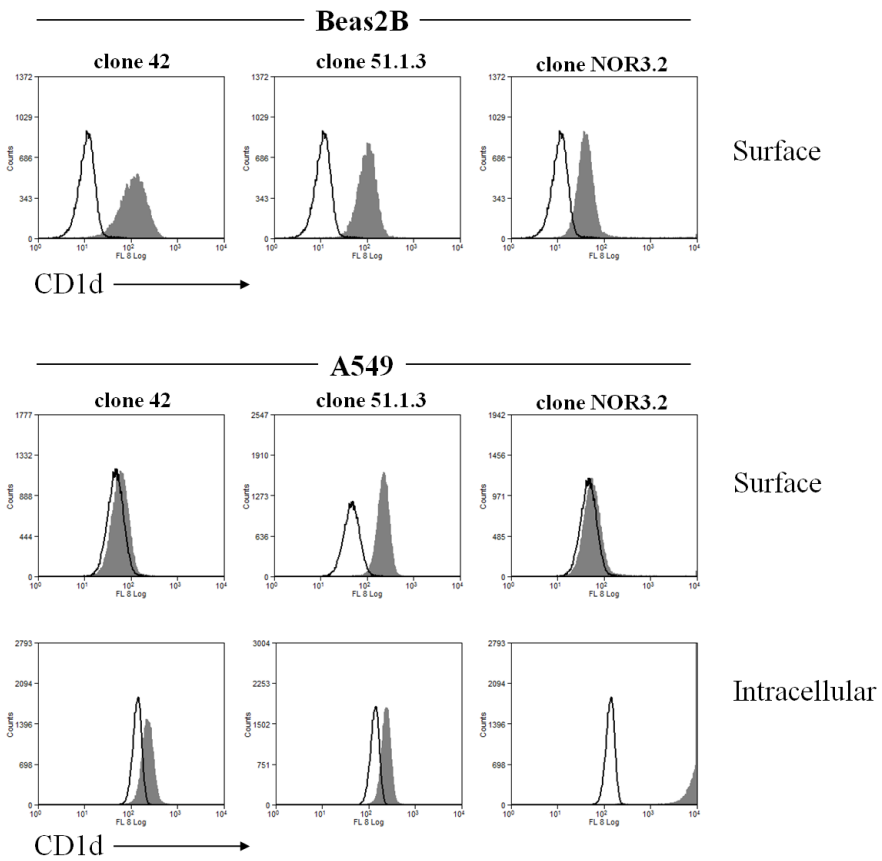

Figure 3.4.2.1. Beas2B and A549 express CD1d. Cells were stained with three mAbs against CD1d. In Beas2B (top panel) all Ab clones detected surface Ag; whereas only clone 51.1.3 detected surface protein on A549 (middle panel). Ab clones 42 and NOR3.2 stained intracellular CD1d in A549 (lower panel). Filled histograms: CD1d; open histograms: isotype control.

The clone 51.1.3 had been previously reported to partially cross-react with CD1b [53]. To verify genuine CD1d detection, Beas2B cells were stained with an anti-CD1b mAb (Figure 3.4.2.2). I found no CD1b expression on Beas2B, whereas the positive control, monocyte-derived dendritic cells (MD-DCs) distinctly expressed CD1b.

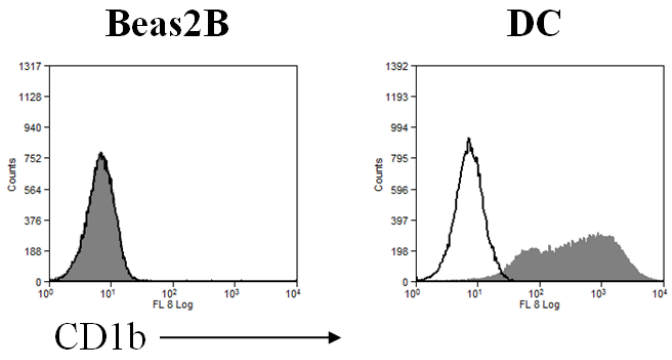

Figure 3.4.2.2. No CD1b is detected on Beas2B. Flow cytometry analysis of Beas2B and monocyte-derived DCs for CD1b expression. Filled histograms: CD1b; open histograms: isotype control.

Beas2B and A549 are cell lines and may not necessarily represent all the actual properties of primary epithelial cells *in vivo*. Therefore, I next characterised CD1d expression in enzymatically-dissociated human airway epithelia and NHBE. Using the three Ab clones (42, 5.1.3, and NOR3.2), I observed intracellular and surface CD1d in PCK^+ and NHBE cells, respectively (Figure 3.4.2.3). The degree of expression, however, varied with different clones of CD1d mAb used. The highest CD1d level, for example, was identified intracellularly with NOR3.2; and on the cell surface with 51.1.3. All CD1d mAb staining were optimised and conditions for highest expression were used.

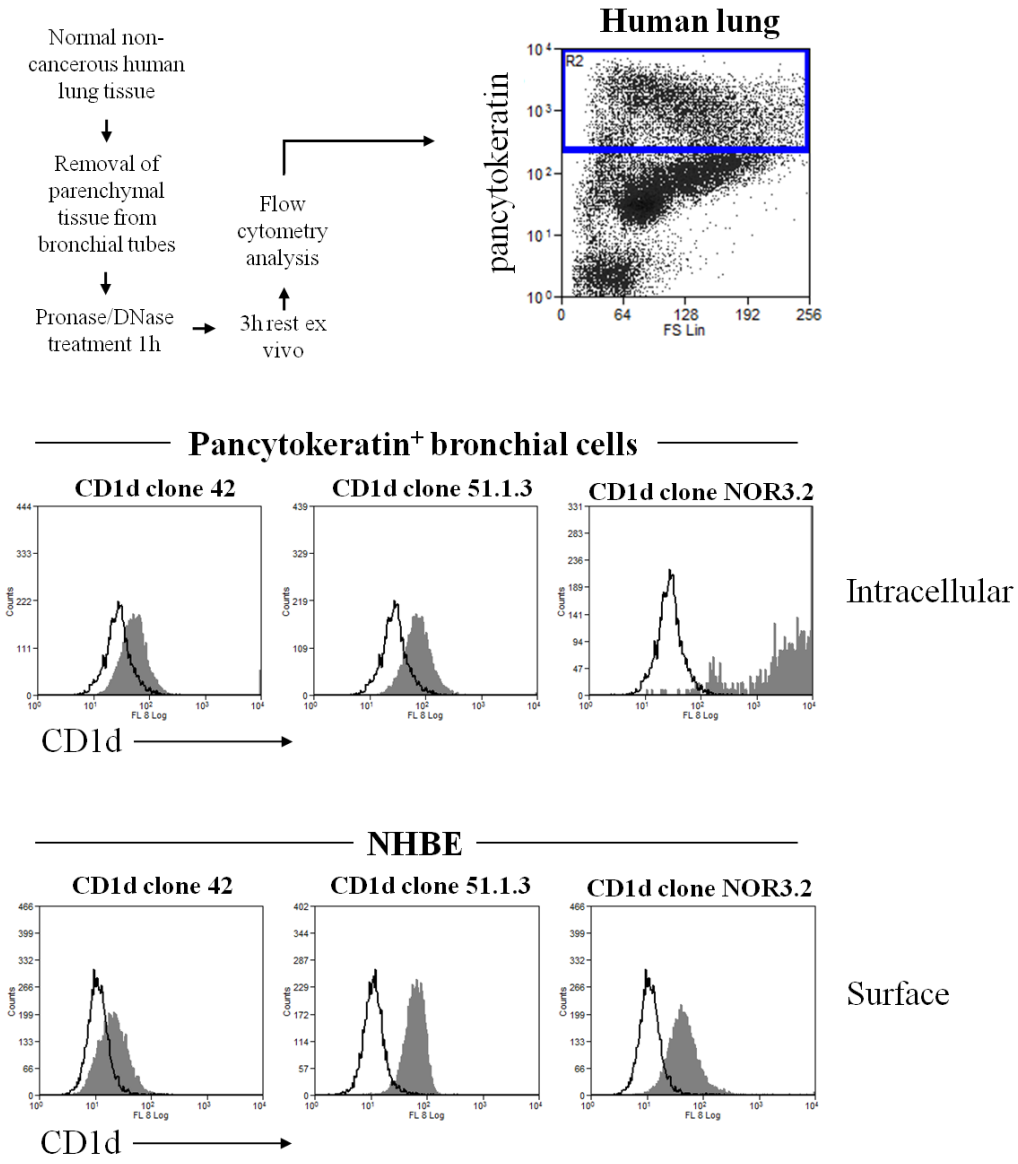

Figure 3.4.2.3. Primary human bronchial epithelial cells express CD1d. (A) Bronchial cells were obtained from human lungs. After enzymatic dissociation, and a brief (3h) incubation period to restore Ag expression, cells were permeabilised and stained with PCK and CD1d. Around 40% of cells were of epithelial origin (PCK^+). **(B)** Flow cytometry analysis detected CD1d using all Ab clones in PCK^+ cells (top panel). Since the cells had to be permeabilised for cytokeratin detection, the observed staining pattern most likely reflects intracellular protein expression. Consistent with the intracellular data on PCK^+ bronchial epithelial cells, surface CD1d was readily identified using all Ab clones in NHBE (bottom panel).

3.4.3 Western blotting and immunoprecipitation of CD1d in human respiratory epithelial cells

Western blot analysis verified presence of CD1d in cell lysates from A549, NHBE and .221^{+} cells using CD1d Ab clone 51.1.3 (Figure 3.4.3.1). Of note, the protein band in NHBE and .221^{+} was around 48 kDa, while the one in A549 was slightly lighter and appeared at about 42 kDa. Human CD1d, depending on its glycosylation state, is expected to have a normal molecular weight (MW) of 37–55 kDa [45,57,266,267].

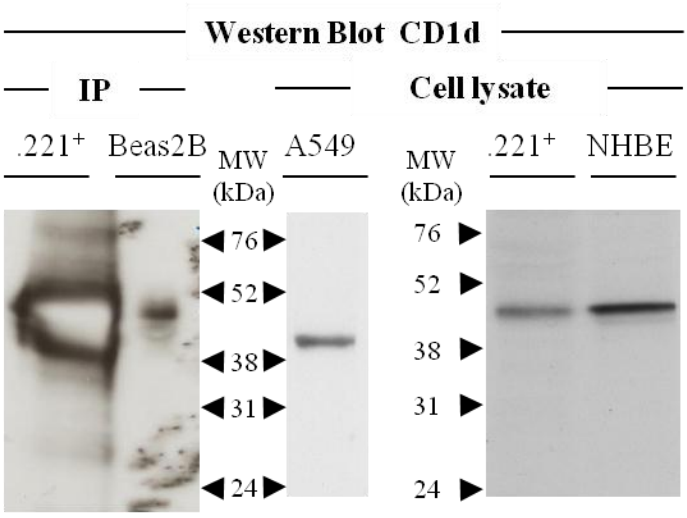

Figure 3.4.3.1. Western blotting and immunoprecipitation identify CD1d in human RECs. CD1d was directly probed using Ab clone 51.1.3 in lysates from A549, NHBE, and .221^{+}. Note the band in A549 (~ 42 kDa) was slightly lighter than the one in NHBE (~ 48 kDa). In Beas2B, CD1d was immunoprecipitated (IP) from cell lysate using Ab clone H70, and then labelled with clone C3D5.

Unlike NHBE and A549, immunoblotting using clones 42, 51.1.3, or NOR3.2 on Beas2B generated a smeared blot (data not shown). This may be due to abundance of non-specific Ab binding sites intrinsic to Beas2B. To overcome this, I immunoprecipitated CD1d (IP) from Beas2B cell lysate using a rabbit pAb (clone H70),

resolved the IP on polyacrylamide gel, and then probed with a new mouse mAb (clone C3D5), which had previously been shown to label CD1d α1 domain specifically on western blots [46]. As Figure 3.4.3.1 demonstrates a major band of approximately 48 kDa, corresponding to mature and glycosylated CD1d glycoprotein, was identifiable in both .221^{+} and Beas2B.

3.4.4 Immunofluorescent staining of CD1d in human respiratory epithelial cells

In another approach to confirm protein expression and define cellular localisation, CD1d was visualised by confocal microscopy in immunostained *in vitro* cultured NHBE cells and cryostat section of human lungs. As shown in Figure 3.4.4.1A, clone NOR3.2 strongly and uniformly stained CD1d in NHBE cells. A weak staining pattern was evident with clone 51.1.3 and no staining occurred with clone 42. PCK was used as a positive control.

CD1d was also observed on human airway cryosections, where the protein was predominantly localised to the apical membrane of ciliated (βtubIV^{+}) epithelial cells (Figure 3.4.4.1B).

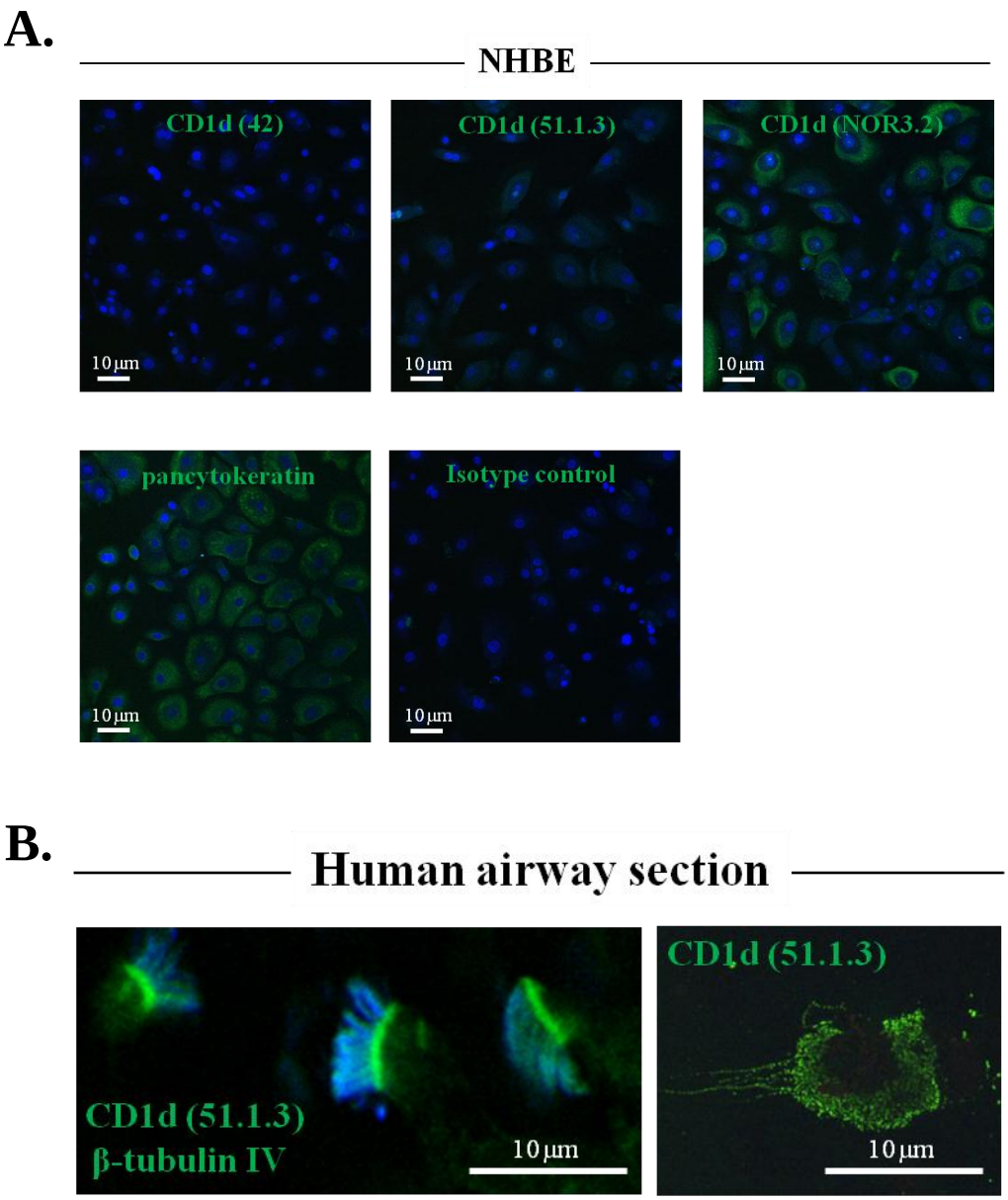

Figure 3.4.4.1. Confocal microscopic visualisation of CD1d in human primary RECs. (A) Chamber slide-grown NHBE cells were stained for CD1d with 42, 51.1.3, and NOR3.2 mAbs (green). NOR3.2 strongly detected the protein and 51.1.3 showed a mild staining pattern. Pancytokeratin and no primary Ab were used as controls. Blue: nuclei (TOPRO); scale bar: 10µm; representative staining of 3 independent experiments are shown. **(B)** Immunostaining revealed CD1d (green) localisation to apical membranes of human airway epithelial cells beneath the cilia (blue). An example of CD1d staining in a cell with numerous dendrite-like processes, presumably a DC, on the same section is illustrated. scale bar: 10µm.

3.5. Discussion

In this chapter, I demonstrate that human RECs express CD1D mRNA and protein. Using multiple approaches and a panel of mAbs, I show that bronchial and alveolar epithelial cell lines, and primary bronchial epithelia constitutively synthesise and express CD1d protein.

Three mAb clones (42, 51.1.3, and NOR3.2) identified surface CD1d on Beas2B, whereas only one (51.1.3) detected surface Ag on A549. CD1d, however, was identified intracellularly using the other two Abs. This may suggest either a genuine differential pattern of protein expression across epithelial lining of the respiratory tract or simply reflect an aberrant expression profile in adenocarcinoma-derived A549.

Of interest, probing CD1d on resolved polyacrylamide gels revealed a smaller product for A549 (~ 42 kDa) than for Beas2B (~ 48 kDa). As CD1d gets glycosylated during maturation, its normal MW ranges from 37 to 55 kDa [45,57,266,267]. Therefore, difference in product size on these gels can potentially be explained by differing glycosylation states of the protein. This is not unexpected. *Sriram et al* recently showed a role for the effect of *N*-linked glycosylation on murine CD1d1 expression on the surface and ability to stimulate *i*NKT cells [36]. The authors concluded that some single or double amino acid (aa) mutated CD1d1 isoforms (at putative glycosylation residues) had lower surface expression than wild types; and the fully unglycosylated isoform was undetectable at the cell surface. This fits in with observations in this chapter where flow cytometry showed that different glycosylation states lead to proteins of different sizes (biochemically distinct forms) with varying surface expression levels in Beas2B and A549. Alternatively, mRNA splicing may

explain the discrepancy in CD1d MW. For instance, an in-frame mutation in which TM exon has been deleted, assuming no change in glycosylation status occurs, can generate a product that is approximately 4 kDa shorter than the full-length variant.

CD1d was readily detectable in native epithelia and primary NHBE cells. Staining by mAb clones 42 and 51.1.3 is particularly notable. Clone 42 has been widely used as a blocking Ab to prevent activation of *i*NKT by CD1d-positive cells [268-270]. On the other hand, previous works by *Kim et al* showed that clone 51.1.3 requires β2m expression to detect CD1d [46,266]. Therefore, flow cytometry results verify presence of (at least) one functional CD1d with the ability to associate with β2m on the surface human bronchial epithelial cells. Stronger CD1d 42 staining on Beas2B, as opposed to NHBE, can potentially translate into a greater functional capability of Beas2B to activate *i*NKT cells *in vitro* (addressed in Chapter 6).

The challenge to identify CD1d consistently across human airway cryosections can be attributed to low protein expression at resting state or potential requirement for Ag retrieval prior to immunostaining. This could explain why earlier studies failed to detect CD1d on respiratory epithelium [55]. In addition, the difference in staining with mAb clone 51.1.3 which showed strong signals on the cryosections, but very weak signals on non-polarised NHBE cells suggests that epithelial polarisation may be required for apical expression of at least one CD1d isoform.

Immunostaining of airway cryosections showed apical distribution of CD1d in ciliated epithelial cells. This places CD1d in an ideal location to load and process luminal Ags and interact with airway-infiltrated *i*NKT cells. It is also in line with previous work on IECs [57].

3.6. Conclusion

In summary, this chapter reports CD1D mRNA and protein expression in human RECs for the first time. Applying RT-PCR, flow cytometry, western blotting and immunofluorescent staining, CD1d was detected in primary epithelial cells, and bronchial and alveolar cell lines of human airway. Differential staining of these CD1d mAb clones suggest presence of CD1d variants which is the subject of study in the next chapter.

Chapter 4. Human respiratory epithelial cells express multiple alternatively spliced CD1D variants

Chapter 4.

Human respiratory epithelial cells express multiple alternatively spliced CD1D variants

4.1. Aims

To investigate the occurrence of CD1D alternative splicing in human respiratory epithelial cells (RECs). To determine relative levels of variants (if any) in RECs, and compare splicing pattern with a selection of other cells types.

4.2. Introduction

Findings from Chapter 3 showed existence of CD1D transcript and potential protein variants in human RECs. Alternative splicing of precursor mRNA is an important mechanism in generating functional diversity of many human multi-exonic genes [271]. CD1D splicing, unlike other CD1 family members (namely, CD1A, CD1C, and CD1E) [9,10], has only been marginally studied. Peripheral blood mononuclear cells (PBMCs), in one study, were reported to express eight CD1D variants [11]. However, PBMCs comprises lymphocytes, monocytes and granulocytes, and therefore it is unclear which cells contained these variants. In addition, the expression of variants was too low to be detected with one-round amplification and required nested PCR. Another study identified an α3–deficient CD1D transcript in placenta-derived trophoblasts [14]. Neither of these studies compared the expression of the spliced

variants across different cells, nor did they investigate relative expression of variants to each other at basal state. It is unknown if CD1D in RECs undergoes alternative splicing.

Different CD1D variants, when translated, can lead to formation of proteins of varying Ag loading and functional capacity (to activate *i*NKT cells), molecular weight (MW), and ability to associate with β_2-microglobulin (β_2m).

In this chapter, I examine alternative splicing on CD1D in human RECs.

4.3. Methods

CD1D splicing was initially examined in human brushed bronchial cells by RT-PCR (Table 4.3.1). As in Chapter 3.3, the bronchial epithelial cells were obtained by brushing the lower airways of patients undergoing clinical bronchoscopy (provided by Dr. Ho). To verify the findings, RT-PCR was also carried out on a REC line, Beas2B, and the primary normal human bronchial epithelial (NHBE) cells. In addition, primers or probes spanning exon-exon boundaries were used to examine the splicing junctions by qPCR (Table 4.3.1). To compare splicing profiles across different cell types, A549, 16HBE14O$^-$ (a differentiated SV40-transformed human bronchial epithelial), NKer (an HPV 16 E6-transduced normal keratinocyte [259]), HaCat (a spontaneously immortalised human keratinocyte), MRC5 and IMR90 (normal foetal human lung fibroblast), TZM-bl (a CD4-expressing HeLa (adenocarcinoma-derived human cervical epithelial)), HCT 116 (a human colon carcinoma epithelial), MOLT4 (a human leukemic T lymphoblast), and THP1 (a human monocytic/macrophage) cell lines were used (Chapter 2.1.10).

To obtain the amino acid (aa) sequence and new position of stop codons in spliced variants, their nucleotide sequence was translated using the online ExPASy tool (http://expasy.org/tools/dna.html). Similarly, the MW of nascent (i.e. unmodified non-glycosylated) peptides was computed using ExPASy pI/Mw tool (http://expasy.org/tools/pi_tool.html) and the potential *N*-glycosylation sited were predicted by NetGlyc 1.0 application (http://www.cbs.dtu.dk/services/NetNGlyc/).

Primer	Sequence (5′→3′)
CD1D	
Forward D.	*CTGCTGTTTCTGCTGCTCTG*
Reverse D.	*GACTCAAGGAGGCCACTGAC*
Forward E.	*TCACCAGGGACGTGAAGGAA*
Reverse E.	*TACATGGAAGAAGTTATTTGAGGCG*
Forward F.	*GCGCTGAAGATCCCTTGGA*
Forward G.	*CTGGGAACGCCTCAAATAAC*
Reverse G.	*ACAGGACGCCCTGATAGGA*
Reverse H	*GAAAGCTGCCTCATGACTGTT*
Forward I1.	*TATCTCCGAGCAACCCTGGA*
Forward I2.	*TCTAGAGGGCCAGGACATCG*
Reverse I1.	*AGGACGCCCTGATAGGAACC*
Forward J1.	*CAAGAGGCCCCACTTTGGT*
Reverse J1.	*GAGACATGGCACACCAGCAG*
Reverse J2.	*CCTGAGACATGGCACACCAG*
Forward K1.	*AACAGTGCAGTGGCTCCTTAATG*
Reverse K1.	*TCCCACCTTGCTTCTTCAGTTC*
Forward L1.	*GTGGACGAGGGAAACAGTGC*
Forward L2.	*GAGGCCCCACTTTGGGTAAA*
Forward L3.	*TGGCCATTCAAGTGCTCAAC*

Primer	Sequence (5′→3′)
CD1D	
Reverse L1.	*CGCCCTGATAGGAACTTGCTT*
Reverse L2.	*CAGGACGCCCTGATAGGAACT*
Forward M1.	*TTTGGAGCAGGTGGGAGCTA*
Reverse M1.	*CGGGAGGTAAAGCCCACAAT*
HPRT	
Forward HPRT.	*GACTTTGCTTTCCTTGGTCAGG*
Reverse HPRT.	*AGTCTGGCTTATATCCAACACTTCG*

Primer	Sequence [5′(FAM)→3′(TAMRA)]
CD1D	
Probe E.	*TGCTACGCTTATCCTATCCCTTGGAGCTCC*
Probe K.	*CCCAATTTGTCAGTGGCCTCCTTGAGT*
Probe L.	*CCCCCAATTTGTCAGTGGCCTCCTT*
Probe M.	*AGTCCTGGCGTGCTTGCTGTTCCTC*
HPRT	
Probe HPRT	*TTTCACCAGCAAGCTTGCGACCTTGAT*

Table 4.3.1. List of PCR primers and probes used in this chapter and their nucleotide sequence.

4.4. Results

4.4.1 Expression of an α1-deficient CD1D transcript by bronchial epithelial cells

Using primer pair "D/D" (Table 4.3.1), which amplifies a 572–base pair (bp) product containing parts of the signal peptide (S) and α2 exons and the whole α1 exon of CD1D, on human brushed bronchial cells (Figure 4.4.1.1A), I observed a 305-bp product, which raised the possibility of existence of an alternatively spliced variant in RECs. Direct nucleotide sequencing confirmed this to be CD1D (Figure 4.4.1.1B, left gel).

To investigate this further, PCR was carried out using "D/D" on oligo–dT reverse transcribed cDNA (i.e. a copy of total mRNA repertoire) from Beas2B cell line. I found two distinct bands – one corresponding to the expected full-length variant (572-bp) and a smaller (305–bp) product (Figure 4.4.1.1B, right gel). To ensure that the smaller band is not a heteroduplex artefact arising from non-specific amplification, I synthesised a CD1D-specific cDNA (using Rev. B primer) from total RNA pool and then repeated the PCR. The smaller band, still present, was excised, purified from gel, and as before nucleotide sequenced. The result showed a CD1D variant lacking α1 exon ("V1"; Figure 4.4.1.1C).

The spliced region in "V1" was 267 bases (i.e. an integer multiple of 3) long. Therefore, no frame shift occurs in this variant (in-frame deletion), and the resultant protein is predicted to be shortened by 89 aa.

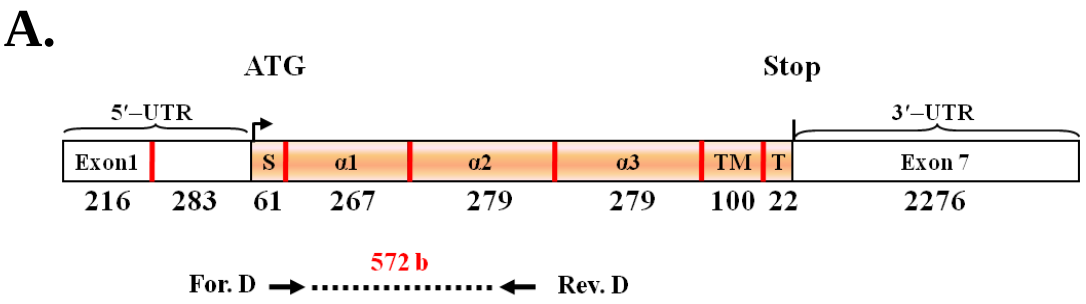

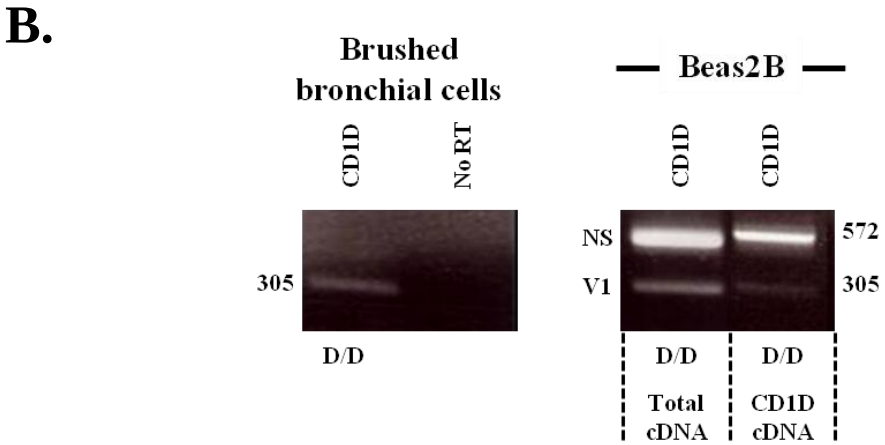

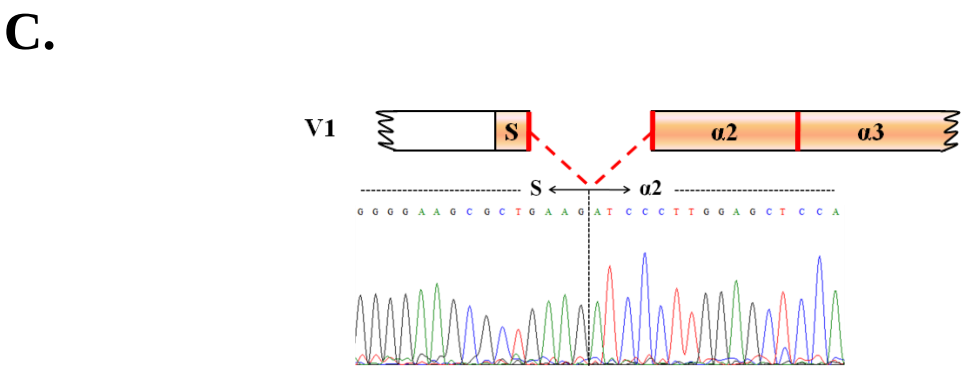

Figure 4.4.1.1. Human bronchial epithelial cells express full-length and α1–deficient CD1D transcripts. (A) Graphical representation of primer pair "D/D" binding sites on CD1D mRNA; orange boxes: coding and open boxes: non–coding exons. Full-length non-spliced (NS) product size is 572-bp. **(B)** PCR amplification by "D/D" detects a smaller band (305-bp) in brushed bronchial cells (left agarose gel). This band was also present in Beas2B cDNA reverse-transcribed either by oligo–dT or a CD1D-specific primer. **(C)** DNA sequencing of the smaller band identifies this as a spliced variant lacking the α1 exon (V1). The nucleotide sequence highlighting the splicing junction between S and α2 exons is illustrated.

I next determined the comparative levels of non-spliced (NS) α1–present to α1–deficient CD1D transcript in Beas2B with qPCR, using a set of primer and probe (Table 4.3.1) designed to amplify the α1–present mRNA (E/E; Figure 4.4.1.2A) and another primer set (F/E) that amplified the α1–deficient transcript. The α1–present CD1D transcript was 39 times higher than α1–spliced variant in resting Beas2B cells (Figure 4.4.1.2B).

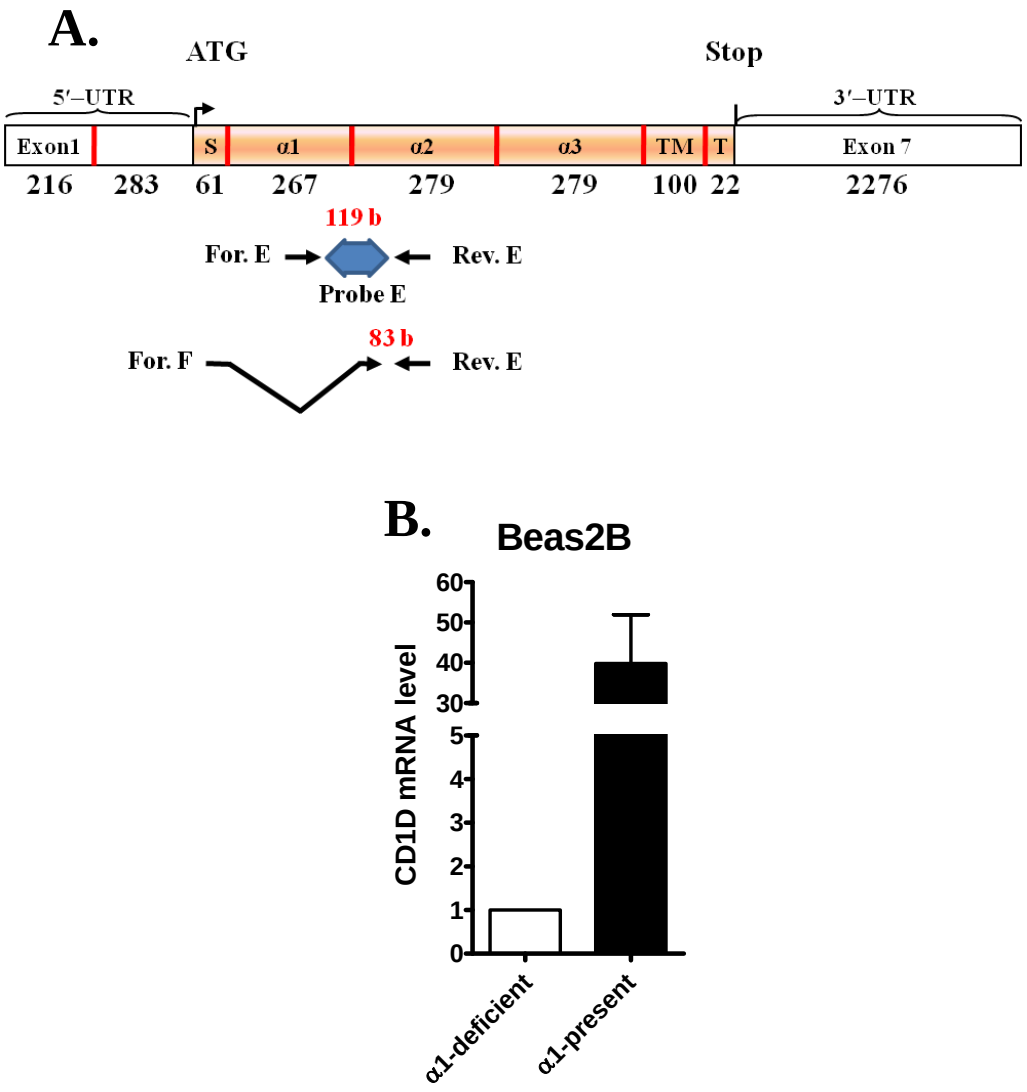

Figure 4.4.1.2. Comparative level of α1–deficient to full-length CD1D in human RECs. **(A)** Primer and probe set E/E amplifies the α1–present variant by spanning α1– α2 exons junction and primer set F/E amplifies the α1–deficient variant by a for. primer skipping α1 exon and spanning S–α2 splicing site. **(B)** Real time PCR detected 39 times higher α1–present than α1–deficient mRNA in resting Beas2B cells. Values represent mean ± S.E.M.; n: 3 independent experiments.

4.4.2 Identification of other alternatively spliced CD1D variants in respiratory epithelial cells

The finding of α1–deficient variant stimulated an interest in other possible spliced variants. In "V1" the spliced region is at the 5′–end of the coding sequence. To delineate whether RECs also expressed other variants, Beas2B cells were studied for spliced transcripts at the middle and 3′–end of the coding sequence.

To do this, I designed two further primer sets – "G/G" and "G/H" (Table 4.3.1). The forward primer in both sets (For. G) originates in the first half of the α2 exon, while the reverse primers Rev. G and Rev. H originate in T and 3′-UTR of exon 7, respectively (Figure 4.4.2.1A). RT-PCR with "G/G" amplified six products with varying lengths (Figure 4.4.2.1B). Only one (NS) corresponded to expected non-spliced transcript (636-bp). To examine whether the other amplified DNAs were spliced forms of CD1D, nucleotide sequence was determined. This confirmed all the PCR products as CD1D. In addition, sequencing revealed the splice junctions for three of the variants: "V4", "V5", and "V6" (Figure 4.4.2.1C). V4 and V5 were defective in α3 (279 bases), and α3-TM (379 bases), respectively; whereas "V6" represented a variant with double splicing events, trimming out the second half of α2 (last 133 out of 279 bases) and most (274 out of 279 bases) of the α3 exon.

"V4" is in-frame, and therefore the consequent protein was predicted to be 93-aa shorter than full-length peptide. In contrast, "V5" and "V6" were out-of-frame. The frame shift resulted in stop codons at nucleotide position 79 in exon 7 (56 bases downstream of the stop codon in full-length variant) and position 89 in TM exon of "V5" and "V6" variants, respectively.

For the "G/H" primers PCR amplified three DNA products (Figure 4.4.2.1B). The largest (793-bp) corresponded to non-spliced transcript, whereas the smaller products, following DNA sequencing, were shown to be α3-TM–deficient "V5" and α2- α3-defective "V6".

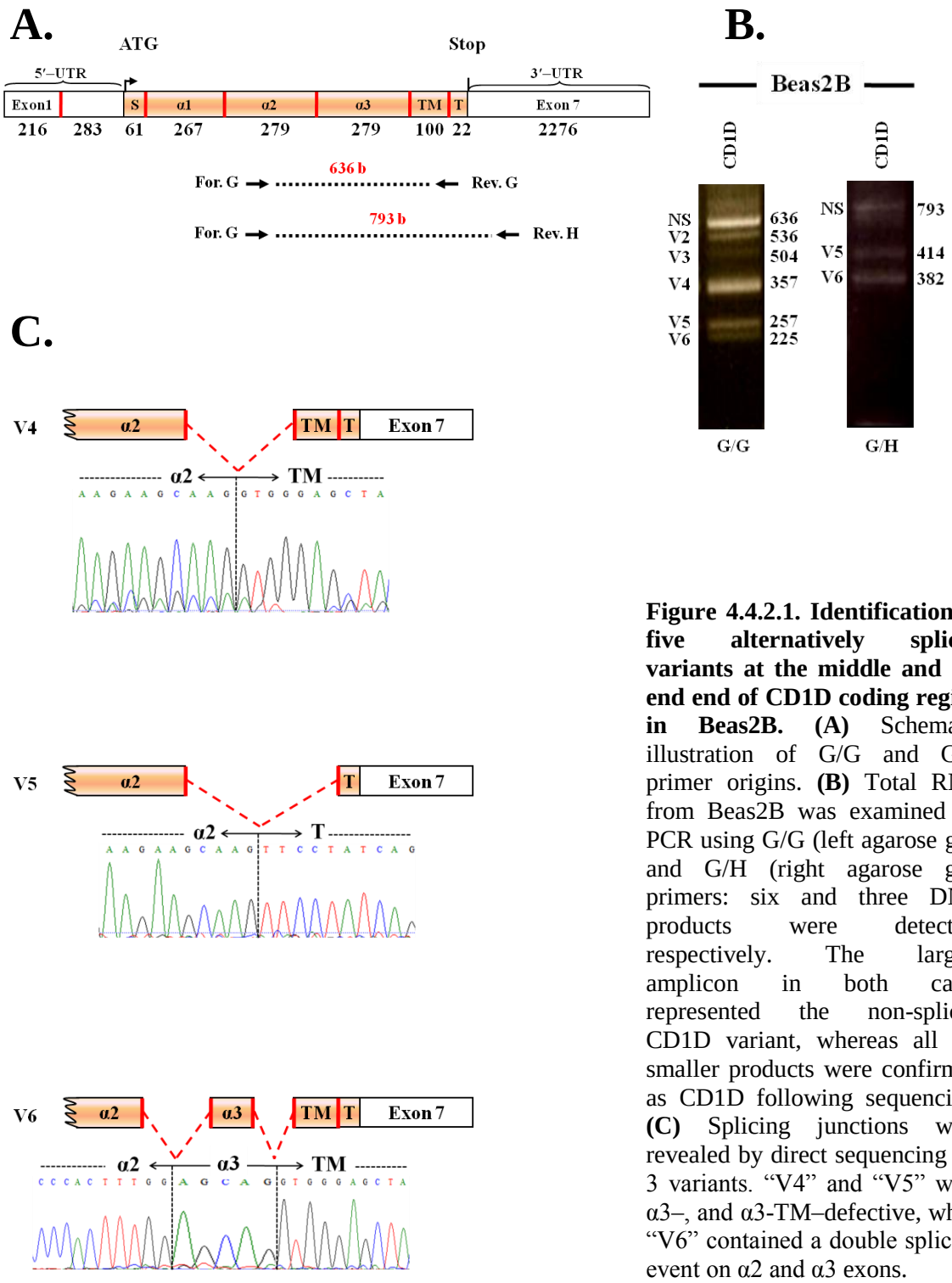

Figure 4.4.2.1. Identification of five alternatively spliced variants at the middle and 3′–end end of CD1D coding region in Beas2B. (A) Schematic illustration of G/G and G/H primer origins. **(B)** Total RNA from Beas2B was examined by PCR using G/G (left agarose gel) and G/H (right agarose gel) primers: six and three DNA products were detected, respectively. The largest amplicon in both cases represented the non-spliced CD1D variant, whereas all the smaller products were confirmed as CD1D following sequencing. **(C)** Splicing junctions were revealed by direct sequencing for 3 variants. "V4" and "V5" were α3–, and α3-TM–defective, while "V6" contained a double splicing event on α2 and α3 exons.

4.4.3 Confirmation of CD1D variant expression by real time PCR

To confirm expression of "V4–6" variants, qPCR was performed using Taqman primer and probe sets (Table 4.3.1), in which one primer spanned the splicing junction, were used (Figure 4.4.3.1A). These primers specifically amplified "V4" and "V6" and yielded single products at expected sizes (Figure 4.4.3.1B). However, a non-specific (as verified by nucleotide sequencing) and larger band was present when amplifying "V5" (Figure 4.4.3.1B).

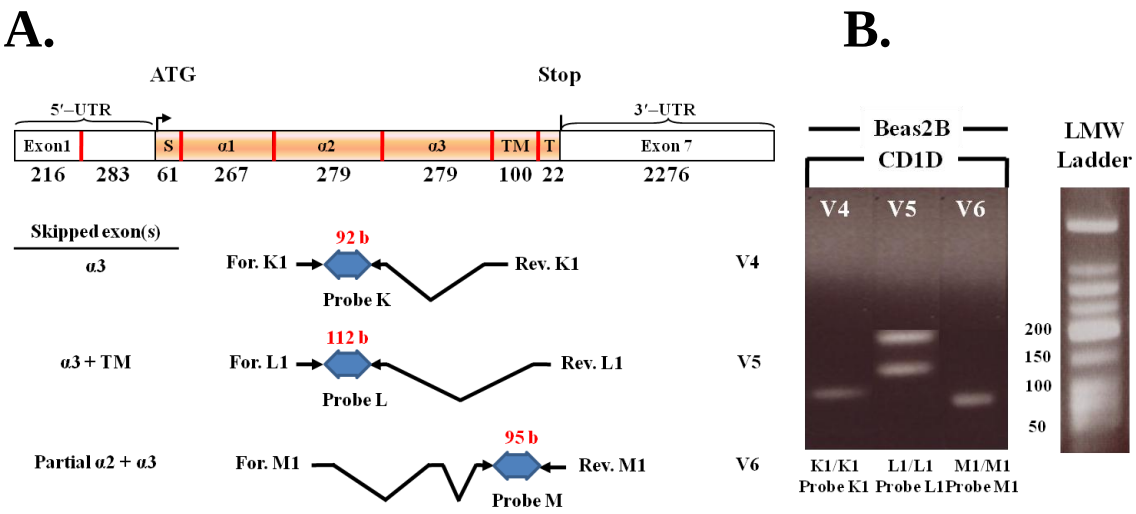

Figure 4.4.3.1. Amplification of "V4-6" CD1D spliced variants by qPCR in Beas2B. (A) K1/K1, L1/L1, and M1/M1were designed to amplify "V4", "V5", and "V6", respectively, in a Taqman assay. The spliced-out exon(s) for each primer and probe set is illustrated. **(B)** qPCR products were run on an agarose gel. "V4" and "V6" were specifically amplified and corresponded to expected product sizes. However, "V5" amplification resulted in two bands – one larger non-specific product, and a smaller product at expected size. LMW: low molecular weight DNA ladder.

Taqman qPCR is generally considered a sensitive assay to amplify (c)DNAs. However, it is compromised by potential formation of cross-dimers between probes and primers, the nature of the target sequence (e.g. multiple and long repeats of a single base or high G/C contents), and lack of suitable primer and probe sets to amplify a given sequence. This may be the cause for the band observed when amplifying "V5".

To overcome this, two new SYBR Green primer sets were designed for "V5", which shared the same reverse primer (Figure 4.4.3.2A; Table 4.3.1). In order to minimise the chances of amplification of NS variant, the reverse primer contained only two bases at its 3′-end. Using both primer sets, qPCR amplified single products at correct sizes (Figure 4.4.3.2B).

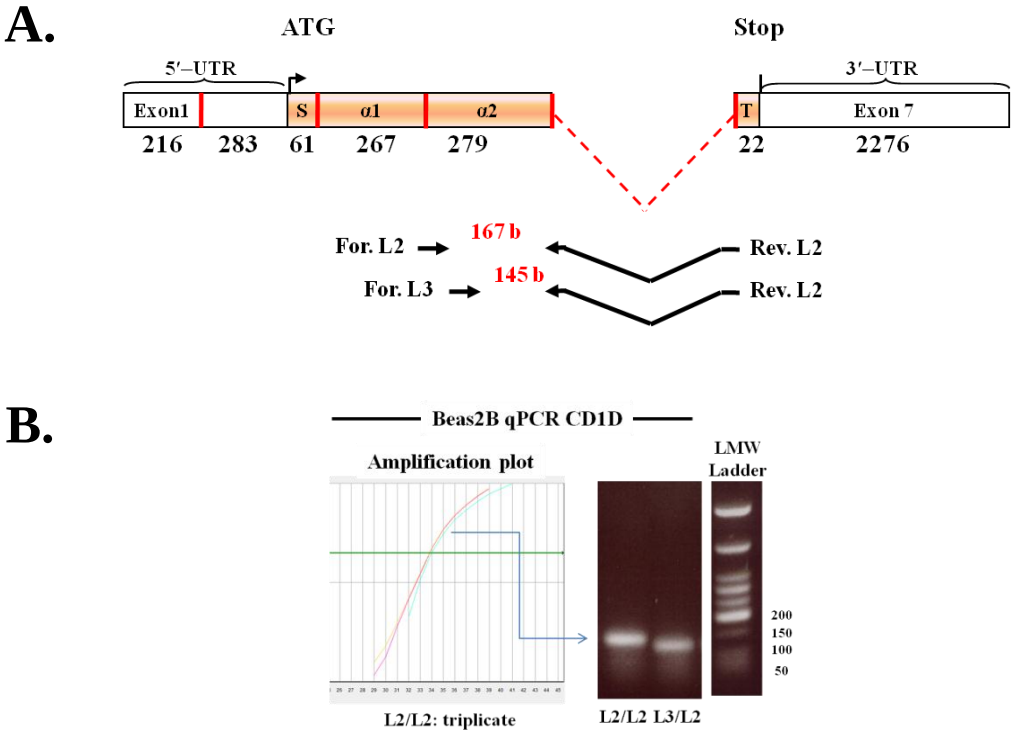

Figure 4.4.3.2. qPCR amplification of "V5" in Beas2B. (A) SYBR Green primer Rev. L2 was designed to span the splicing site in V5, by skipping the α3 and TM exons. It was combined with two forward primers – For. L2 and L3 **(B)** qPCR amplification yielded single products of expected lengths. The primer sets only differed in Ct values and reproducibility of amplification (distance between curves on the plot). L2/L2 exhibited higher reproducibility and lower Ct, compared with L3/L2.

Nucleotide sequencing verified the "V2" and "V3" PCR products as CD1D (Figure 4.4.2.1B; sequencing data not shown). But no reliable data were obtained on possible splicing junctions. Kojo *et al* have previously reported presence of eight CD1D variants in human PBMCs, including a TM–deficient variant (lacking 100 bases) and

one in which the 2nd half of the α2 exon (last 133 bases) was spliced out [11]. Therefore, I hypothesised that "V2" and "V3" represent the TM–deficient and the α2–defective variants, respectively.

To test this hypothesis, I could either clone the PCR products into bacteria and then DNA sequence them, or alternatively, design qPCR primers to amplify the variants. The latter was preferred as it would allow verification of the variants as well as their quantification. Using multiple SYBR Green primer sets, qPCR amplified "V2" and "V3" (Figure 4.4.3.3). The expression level of "V2" was very low. This was evident by late Ct on amplification plot and requirement for multiple replicates to detect the transcript (Figure 4.4.3.3A).

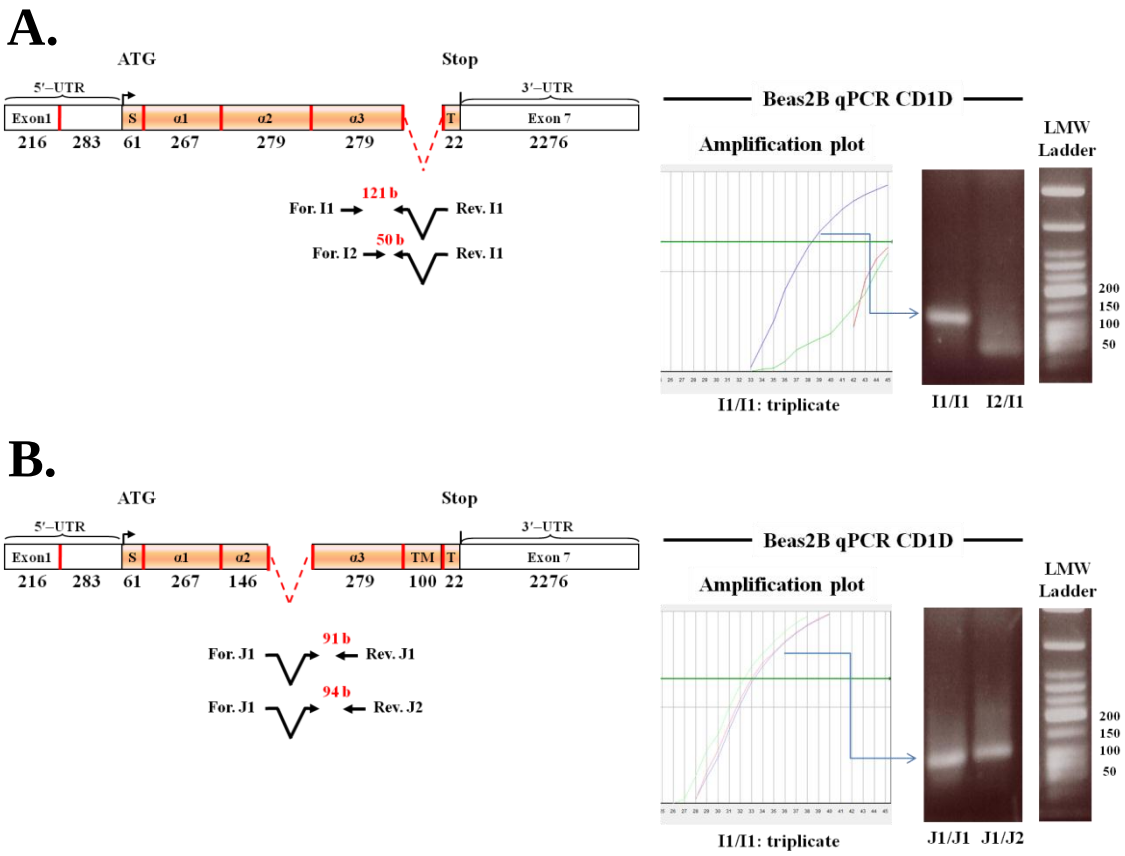

Figure 4.4.3.3. qPCR amplification of "V2" and "V3" variants in Beas2B. (A) The α3-T exon-exon boundary in V2 was targeted for amplification by Rev. I1 primer, which was shared between two SYBR Green primer sets (I1/I1 and I2/I1). The agarose gel illustrates products of qPCR amplification. **(B)** qPCR amplification using SYBR Green primer sets J1/J1 and J1/J2 produced single bands of expected size.

"V2" and "V3" were both out-of-frame, and the newly formed stop codons are positioned at the 79th and 73rd nucleotide in exons 7 and α3, respectively. Therefore, their nascent (unglycosylated) protein products were expected to be around 36, and 21 kDa, instead of 37 kDa for non-spliced full-length variant.

Genomic abnormalities and mutations like deletion, allelic polymorphism, and chromosomal rearrangement can potentially account for existence of defective transcript variants within a cell. To rule out possibility of DNA defects as the cause of diverse CD1D variant formation, genomic DNA was extracted from Beas2B. PCR analysis using "D/D" and "G/G" primer pairs amplified only single bands (Figure 4.4.3.4B).

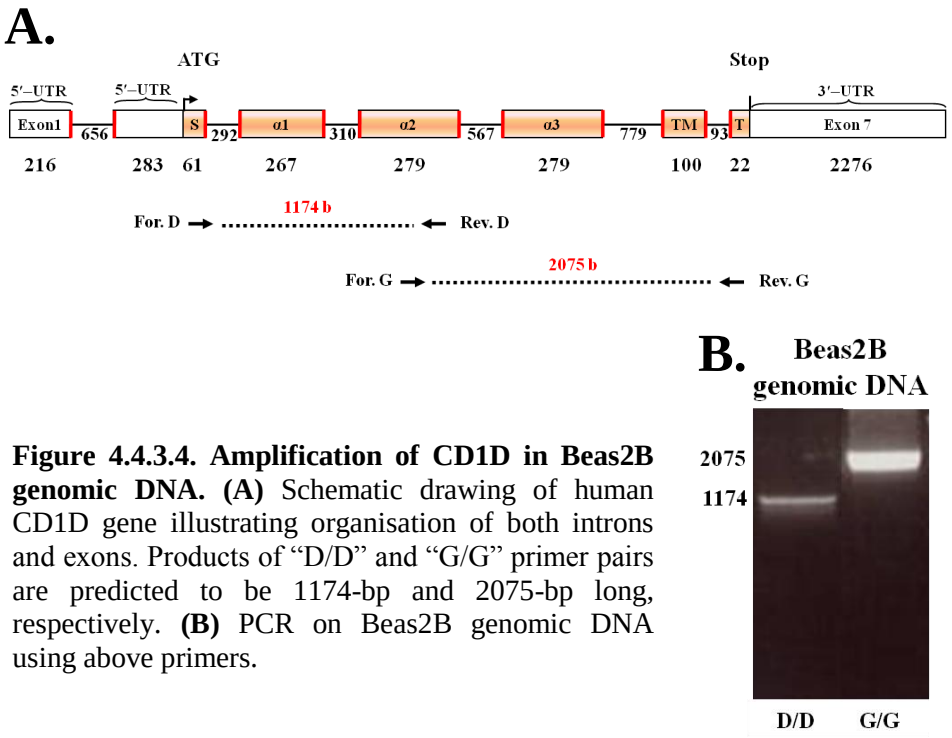

Figure 4.4.3.4. Amplification of CD1D in Beas2B genomic DNA. (A) Schematic drawing of human CD1D gene illustrating organisation of both introns and exons. Products of "D/D" and "G/G" primer pairs are predicted to be 1174-bp and 2075-bp long, respectively. **(B)** PCR on Beas2B genomic DNA using above primers.

A summary of all CD1D variants identified in Beas2B, their frame shift change, likelihood of membrane insertion (based on presence of an intact TM exon), and the

potential ability to bind and present Ag (unaltered sequence of α1 plus α2) is shown in Figure 4.4.3.5.

A.

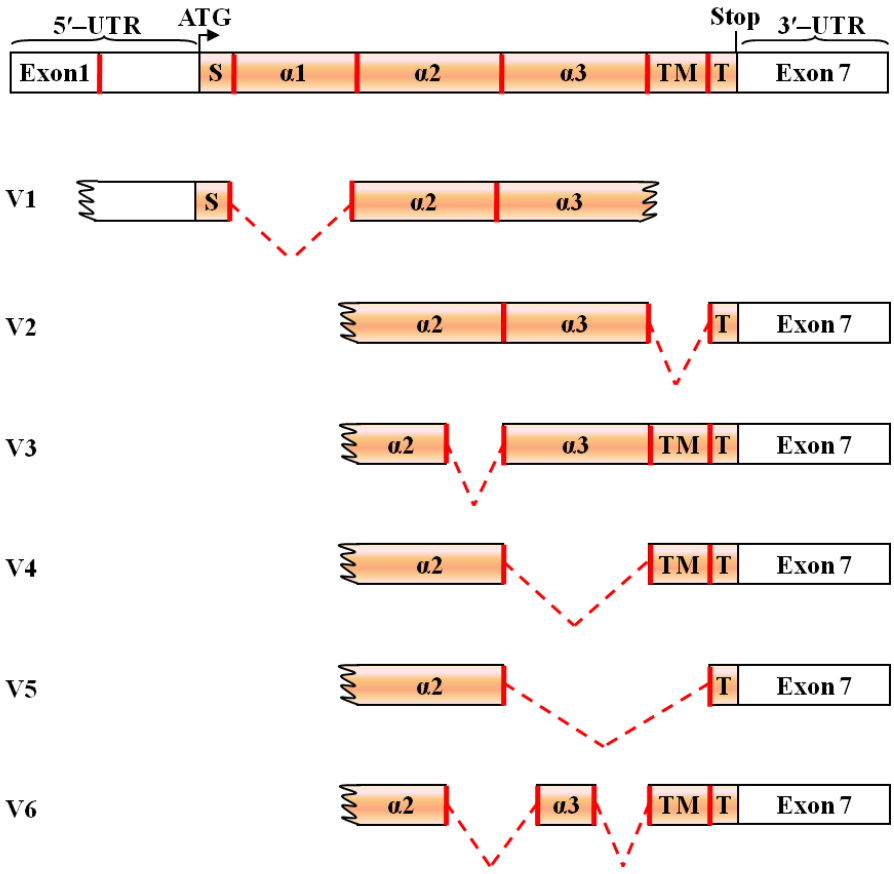

B.

Variant	Spliced sequence	Frame shift	Stop codon position	Membrane insertion	Ag presentation	Predicted MW (kDa)	# of potential *N*-glycosylation sites
V1	α1	In-frame	Unchanged	Likely	Unlikely	27.2	2
V2	TM	Out-of-frame	78th base in exon 7	Unlikely	Unlikely	36.1	4
V3	½ α2	Out-of-frame	1st base in α3 exon	Unlikely	Unlikely	21.4	3
V4	α3	In-frame	Unchanged	Likely	Likely	27.4	4
V5	α3-TM	Out-of-frame	78th base in exon 7	Unlikely	Likely	25.8	4
V6	½ α2 + α3	Out-of-frame	25th base in TM exon	Unlikely	Unlikely	18.9	3
NS	–	–	–	+	+	37.7	4

Figure 4.4.3.5. RECs express at least six alternatively sliced CD1D variants. **(A)** Diagrammatic illustration of splicing junctions of "V1–6" transcripts. **(B)** Frame shift change, new post-splicing stop codon position, likelihood of plasma membrane insertion, and the potential ability to present glycolipid Ags are summarised in the table. The nascent peptide MW and the potential number of *N*-linked glycosylation sites in the predicted peptides are listed as well.

The nucleotide sequence of variants was translated into amino acid sequence, and potential *N*-linked glycosylation sites (Asparagine residues in Asparagine-X-Serine/Threonine, where X represents any aa) as well as MW of nascent peptides were computed. This table shows that "V1" and "V2" were unlikely to participate in Ag presentation, only "V1" and "V4" could be inserted into cell surface membrane, and "V2", "V4", and "V5" were the only variants with all four major glycosylation sites intact.

4.4.4 Relative expression of CD1D variants in respiratory epithelial cells

To determine comparative level of CD1D variants, qPCR was carried out on NHBE. This extrapolates the findings from Beas2B by verifying alternative splicing in primary cells, and also reveals relative expression values of various CD1D transcripts. All the spliced variants apart from "V2", which was hardly detectable, were readily amplified. Compared against the lowest expressed variant ("V1"), "V4" and "V6" showed the highest expression levels – 27 and 16 times of "V1", respectively; whereas "V3" and "V5" were 2 and 3 times higher than "V1" (Figure 4.4.4.1).

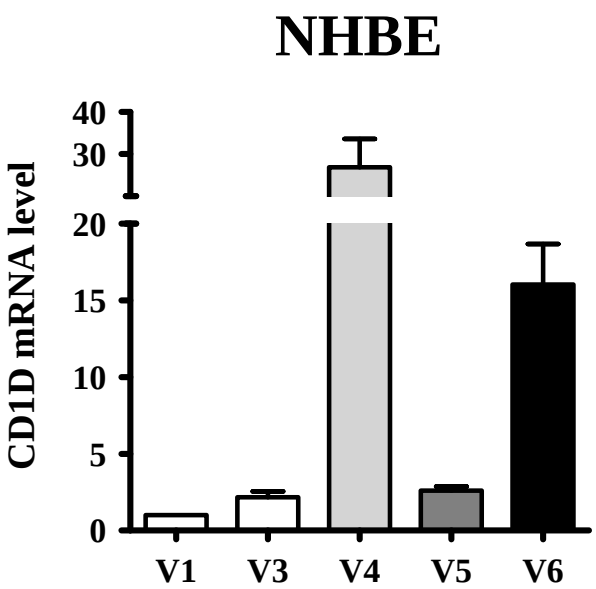

Figure 4.4.4.1. Relative expression level of CD1D variants in RECs. All the variants, but "V2", were amplified in untreated NHBE. Expression values are shown relative to "V1". N: 6 experiments.

4.4.5 Comparison of expression of epithelial CD1D variants with other cell types

Different CD1D variants had been previously reported in PBMCs and trophoblasts [11,14]. I next investigated how CD1D spliced variants in RECs compared with other cell types. I performed RT-PCR using "G/G" primers – that readily identified "V2–6" variants in RECs, on a selection of cell lines from various tissues. Beas2B, 16HBE14O$^-$, A549, NKer, HaCat, MRC5, IMR90, TZM-bl, HCT116, THP1, and MOLT4 were tested (Figure 4.4.5.1). I found similar variant profile across Beas2B, 16HBE14O$^-$, NKer and HaCat. The highest signal intensity belonged to "V4", and MRC5 only expressed one ("V6") variant.

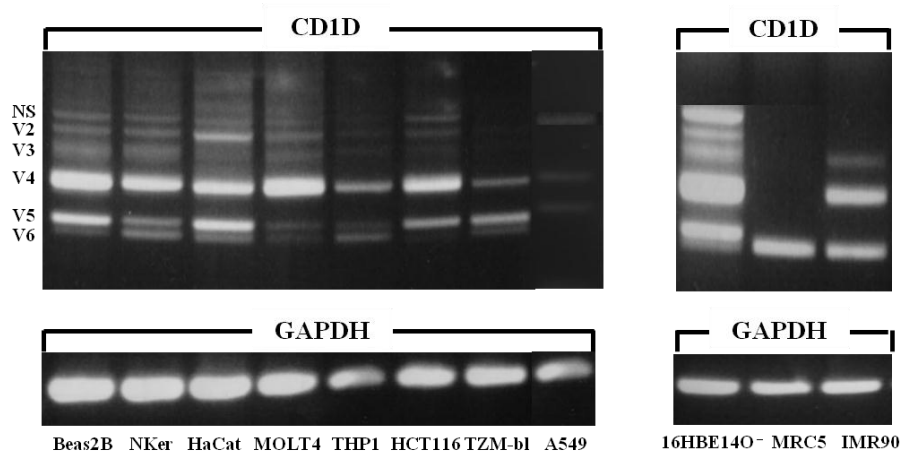

Figure 4.4.5.1. Cell type-specific generation of CD1D "V2–6" variants. RT-PCR using G/G primer was performed on various epithelial (Beas2B, 16HBE14O$^-$, NKer, HaCat, HCT116, and TZM-bl), antigen presenting (THP1), structural (MRC5 and IMR90), and T cells (MOLT4). GAPDH housekeeping gene was amplified in parallel as a positive control.

4.5. Discussion

In this chapter, I demonstrate that CD1D mRNA in human RECs undergoes alternative splicing. Conventional RT-PCR and direct nucleotide sequencing identified six variants. Real time PCR confirmed these variants and allowed their relative quantification. Moreover, a different expression pattern of "V2–6" variants was observed across a selected range of various cell types.

CD1d is required for direct engagement with and activation of *i*NKT cells [3,92]. Alternative splicing represents a potential mechanism for generating proteins of varying sizes and functions. The six variants reported in this chapter exhibited different splicing regions and, may subsequently translate into proteins with different functional properties. Lipid-binding groove in CD1d is formed by α1 and α2 domains [15,16]. "V1" is defective in α1, and therefore the resulting protein is unlikely to participate in Ag loading and presentation.

On the other hand, hydrophobic aa residues encoded by transmembrane exon are required for insertion of the protein into plasma membrane. The TM exon is either completely spliced out, as in "V2" and "V5"; or due to frame-shift mutation which results is early stop codon is impaired or absent, as in "V3" and "V6". So, it is likely that proteins coded by these variants are secreted from the cell (soluble isoform) or retained intracellularly. Woolfson *et al* showed expression of CD1A and CD1C TM-deficient transcripts, and detected corresponding soluble protein isoforms [10]. Similarly, soluble HLA-G, an MHC class I molecule which has limited polymorphism and holds high structural similarity with CD1D [8], has been well established and shown to correlate with the presence of a TM-deficient variant [272,273]. Of all CD1D

variants identified in RECs, "V1" and "V4" were the only ones with intact TM exon; and therefore, potentially capable of cell surface expression.

The α3 domain is the major part of the CD1d peptide required for non-covalent association with β_2m [15,16]. "V4" and "V5" have no α3 exon and their protein products are predicted to lack β_2m binding ability. As "V4" was in-frame and comprised intact TM and cytoplasmic tail (T) exons, it can produce a cell surface-expressed β_2m-free CD1d isoform. This is not unexpected as previous reports have demonstrated stable β_2m-independent CD1d expression on intestinal epithelial cells (IECs) [45,46]. Absence of β_2m, however, can influence the maturity of CD1d protein. While the four potential *N*-glycosylation (asparagine) residues are located in α1 and α2 domains (amino acids 30, 60, 126, and 181), surface CD1d in CD1d-transfected FO-1 human melanoma cells is 3 kDa less heavy than its counterpart in CD1d/β_2m-transfected FO-1. This indicates requirement for β_2m for complete protein maturity and full modification of *N*-linked carbohydrate side chains [46].

I did not carry this part of the project forward as my priority was to investigate the function of CD1d on RECs. However, if I were to, existence of the soluble or intracellular CD1d isoform in epithelial cells could be confirmed by ELISA or immunoprecipitation assays. For the latter, the protein extract of spent medium of RECs can be indirectly labels and quantified [10], whereas the former focuses on precipitation of CD1d in cell lysate of surface Ag-blocked RECs [78]. Verification of cell surface-expressed β_2m-free CD1d is more challenging. One potential approach could be radio-labelling the surface proteins, lysing the cells and immunoprecipitating CD1d, and removing *N*-linked carbohydrates (e.g. by treatment with *N*-glycanase or endoglycosidase-H [46]). The unglycosylated "V4"-encoded CD1d compared with full-

length non-spliced nascent peptide is predicted to be approximately 10 kDa lighter (Figure 4.4.3.5) on autoradiographs of polyacrylamide gels.

This chapter describes the use of qPCR as a powerful tool not only to detect but also to relatively quantify CD1D variants. Assay-optimised primers or probes spanning the exon-exon boundaries were key determinants in this process. All variants, but "V2", were consistently and specifically amplified by qPCR. Low abundance of V2 in epithelial cells, as evident by weak amplicon intensity on agarose gels and late Ct on amplification plots, may account for observed inconsistent detection by qPCR.

Many factors at mRNA level, including transcript abundance, mRNA stability, and presence of enhancer/silencer sequence can regulate protein expression in eukaryotic cells. Therefore, it can be speculated that higher transcript levels of "V4" than "V1", "V3", and "V5" suggests greater likelihood of translation of this variant. Higher availability of "V6" is unlikely to be important as its protein product is defective in α2 and α3, and lacks TM due to an early stop codon. In fact, the final truncated peptide, if any, is predicted to be only 18.9 kDa heavy with only 3 (out of 4) intact potential *N*-glycosylation sites.

Consistent splicing patterns were observed among bronchial epithelial cells 16HBE14O$^-$ and Beas2B. Additionally, normal keratinocytes (NKer) and colon epithelial cells (HCT116) illustrated comparable mRNA profiles as Beas2B. This suggests potential similarity in splicing machinery at resting state across different mucosa-lining epithelial cells. However, cancerous origin of HCT116 or immortalised nature of cell lines may account for this phenomenon. The α3–deficient CD1D variant ("V4"), when present, was the most intensely PCR-amplified transcript in all cell types.

This challenges the need for β_2m for steady-state CD1d expression and function. Of note, foetal fibroblast cells MRC5 only expressed the "V6" variant. This may imply developmental regulation of CD1D mRNA splicing. Nevertheless, its importance remains unclear.

In A549, two CD1D spliced variants were present – "V4" and "V5". These two have predicted MWs of 27.4 and 25.8 kDa (prior to post-translational modification) and their *N*-glycosylation sites remain intact. Even if peptide maturity occurs fully, it does not still explain the discrepancy (6 kDa) in MW of bands observed in CD1d Western Blots of this cell line against NHBE and .221$^+$ (Figure 3.3.4.1 in the last Chapter). The difference in modification of full-length NS peptide is more likely to explain the difference.

4.6. Conclusion

In summary, this chapter provides the first report on CD1D mRNA splicing in human RECs. Applying RT-PCR and qPCR six alternatively spliced variants were detected in RECs. Predicted protein products of α1-deficient "V1" and α3-deficient "V4" were likely to be transported to cell surface. Compared to other variants, "V4" showed the highest expression level at basal level. Additionally, preliminary analysis revealed similar splicing patterns of CD1D among human bronchial, colonic, and skin epithelial cells.

Chapter 5. Human respiratory epithelial CD1d expression can be regulated

Chapter 5.

Human respiratory epithelial CD1d expression can be regulated

5.1. Aims

To determine if CD1d expression on respiratory epithelial cells (RECs) is affected by viral- and bacterial-associated signals, and infection with influenza A virus (IAV).

5.2. Introduction

So far, I have shown that RECs constitutively express CD1d on their surface; but it is unknown if this can be regulated in an immunologic context. Previous studies have demonstrated that inflammatory cytokines, particularly interferons [274], and respiratory pathogens like rhinovirus and respiratory syncytial virus (RSV) [275,276] can modulate surface expression of MHC class I and class II molecules on RECs . In addition, expression of co-stimulatory molecule B7-H1 on airway epithelial cells is induced by IFNγ [251]. These findings suggest APC-like behaviour in RECs.

Expression of CD1d on epithelial cells of the small intestine and keratinocytes has been shown to be upregulated by IFNγ [55,60,76,77]. Furthermore, an overexpression of CD1d occurs in psoriatic skin plaques, which are characterised by high IFNγ production [60]. In addition, immortalised vaginal and penile urethral epithelial cells exhibited robust CD1d induction after 24h treatment with IFN [61]. Together, these suggest a potential for modulation of REC CD1d by specific cytokines and viral infections.

In this chapter, I examine if major viral- or bacterial-associated signals can modulate CD1d expression on RECs.

5.3. Methods

Beas2B cells were separately stimulated with the following cytokines and TLR ligands – IFNγ (1000U/ml for 48h; Roche), IFNα (10 or 100ng/ml for 18h; PeproTech), *E. coli* and *Pseudomonas* LPS (10μg/ml for 48h; Sigma), and pam3CSK4 (1 or 10μg/ml for 18h; InvivoGen), or poly I:C (10 or 25μg/ml for 18h; InvivoGen) in F12 Nutrient Mixture Kaighn's Modification (F12K) medium. After stimulation, cells were detached by treatment with 1mM EDTA solution and analysed by flow cytometry for surface CD1d expression. Some cells were lysed in TRIzol® reagent and their RNA extracted for qPCR analysis (as discussed in Chapters 2.2.1, 2.2.3 and 2.2.6) of IL-8 mRNA, using primers listed in Table 5.3.1. These experiments were also performed in primary RECs (NHBE).

Primer	Sequence (5′→3′)
IL-8	
Forward IL-8.	*CCACCCCAAATTTATCAAAGAA*
Forward IL-8.	*CAGACAGAGCTCTCTTCCATCA*
IFNβ	
Forward IFNβ.	*CGCCGCATTGACCATCTA*
Forward IFNβ.	*GACATTAGCCAGGAGGTTCTCA*

Table 5.3.1. List of PCR primers used in this chapter and their nucleotide sequence.

To determine changes in epithelial CD1d expression after IAV infection, an *in vitro* infection model was set up. Beas2B cells were treated with several titres of influenza A virus A/Puerto Rico/8/34 (PR8) in serum free medium for 2h (adsorption phase), washed three times, and then incubated for 48h (replication/propagation phase). Viral infectivity was measured by expression of envelope haemagglutinin (HA) glycoprotein (Ab was a kind gift from Prof. Alain Townsend, Oxford University), and changes in IL-8 and IFNβ transcript (Table 5.3.1) levels – both established markers of viral infection in RECs [277-279]. Expression of CD1d was studied by flow cytometry and confocal microscopy (Chapters 2.17 and 2.1.8).

5.4. Results

5.4.1 Upregulation of CD1d on respiratory epithelial cells in response to viral-associated danger signals

Stimulation with IFNα, IFNγ, and poly I:C upregulated surface CD1d on Beas2B. However, treatment with pam3CSK4 and LPS did not change the expression of CD1d. Enhanced transcription of IL-8 verified bioactivity of these two reagents. The positive regulatory effect of IFNα and poly I:C was dose-dependent (Figure 5.4.1.1A).

Extrapolating the findings, a similar expression pattern was observed in NHBE, although changes in the protein expression were not as marked as Beas2B (Figure 5.4.1.1B).

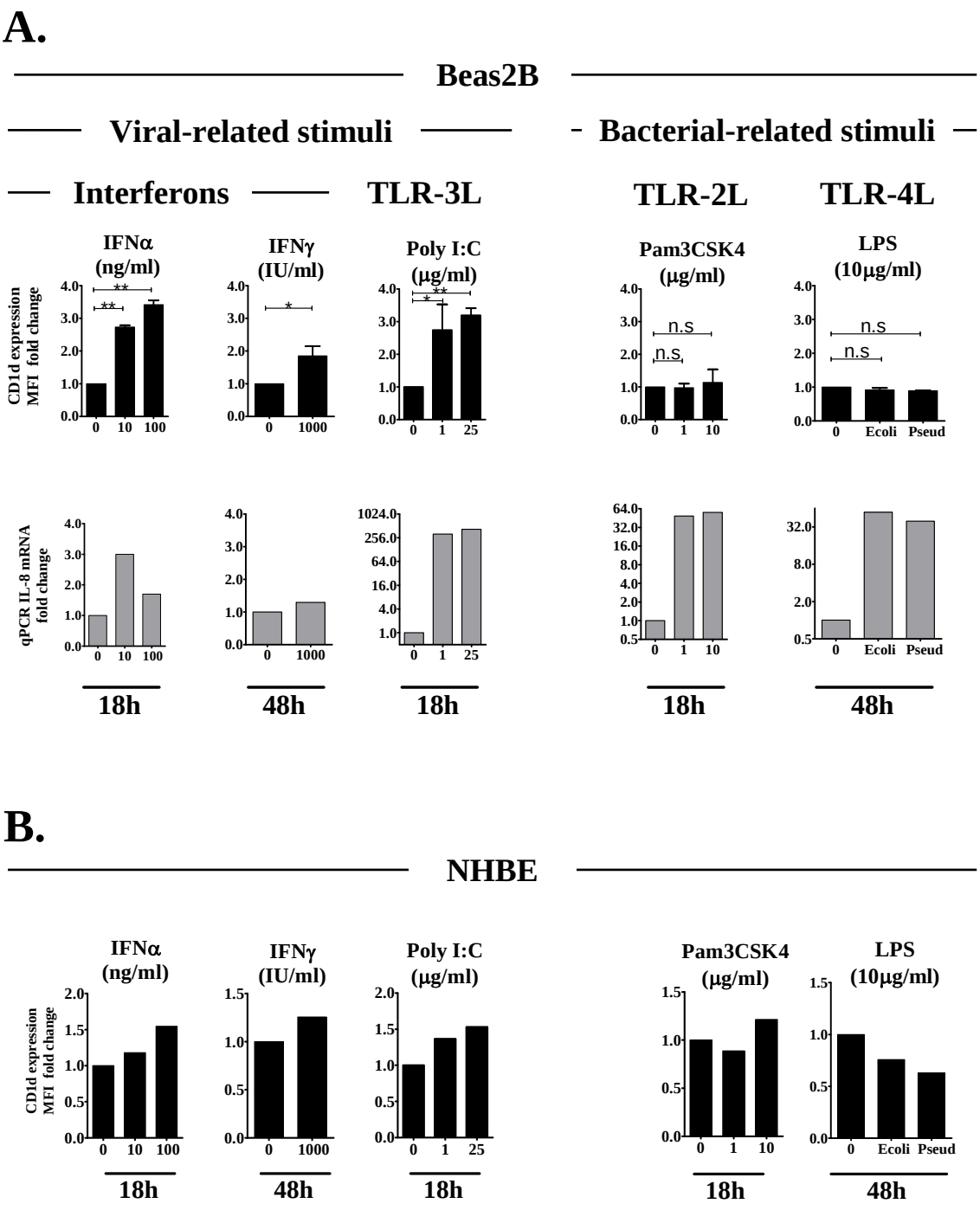

Figure 5.4.1.1. Viral-related stimuli enhance surface CD1d on human RECs. (A) Beas2B cells were exposed to IFNγ (1000U/ml) or LPS (10μg/ml) for 48h or IFNα (10 or 100ng/ml), poly I:C (10 and 25μg/ml), or pam3CSK4 (1 or 10μg/ml) for 18h. Surface CD1d was then determined by FACS (Ab clone 51.1.3) and presented as mean fluorescent intensity (MFI). N= 5 independent experiments. (top panel). IL-8 transcript level was studied by qPCR (bottom panel). Mean of 2 independent experiments is shown. **(B)** Similar protocol as in **(A)** but on NHBE. Mean of 2 independent experiments shown. **: $p < 0.001$; *: $p < 0.05$; n.s.: non-significant.

5.4.2 Modest increase of epithelial CD1d in response to influenza A virus infection

Beas2B cells were treated with 4, 40, or 400HAU/ml of PR8. HA expression in infected cells was evident by immunofluorescent staining (Figure 5.4.2.1). The HA expression was dose-dependent, as 4 HAU/ml wells had very low immunostaining and 400 HAU/ml showed a considerably higher fluorescent signal.

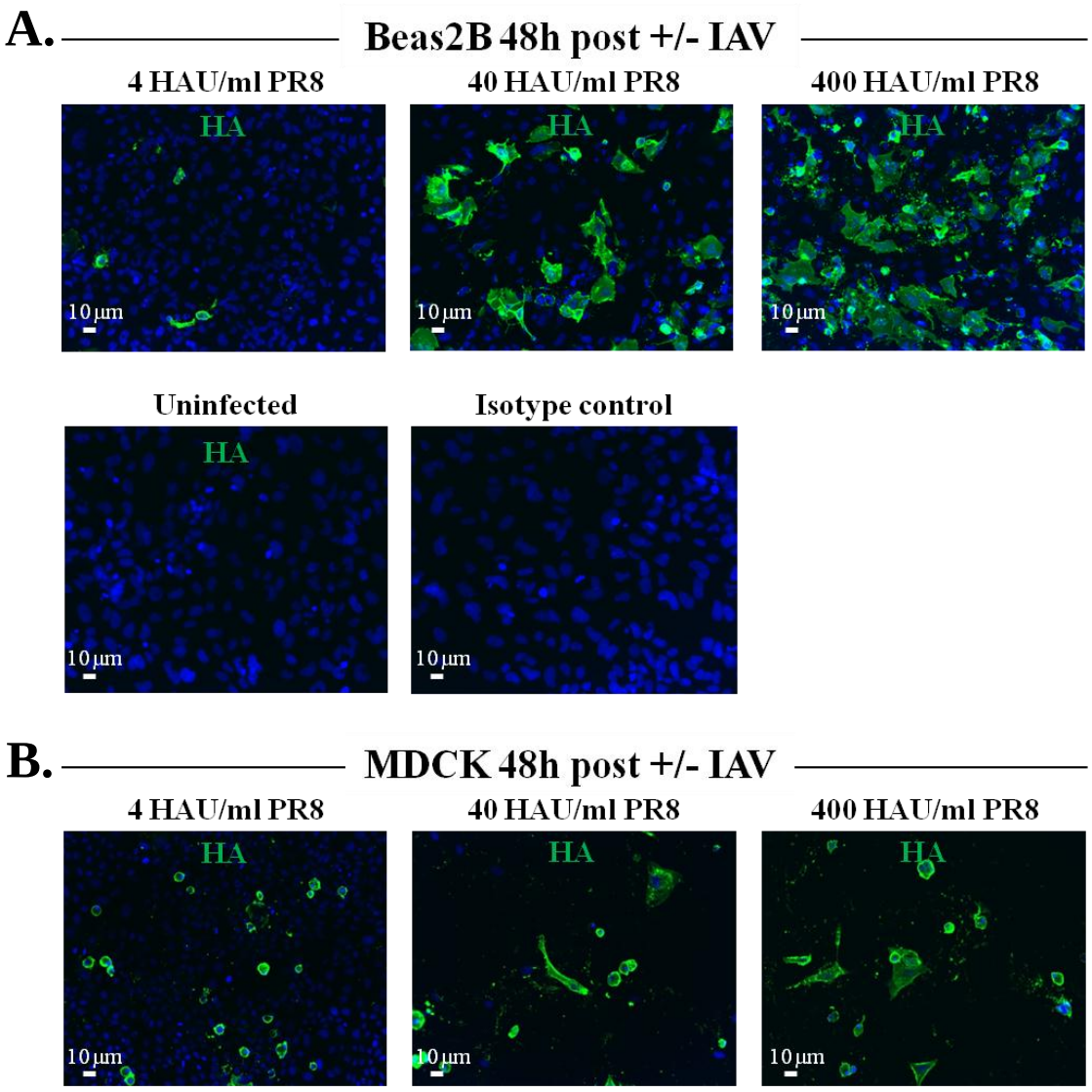

Figure 5.4.2.1. IAV-infected Beas2B express viral antigen HA. (A) Epithelial cells were infected with 4, 40, or 400HAU/ml PR8. 48h post-infection immunofluorescent analysis was performed to visualise HA expression by confocal microscopy. A representative of three independent experiments is shown here. Uninfected and non-specific binding (isotype control) slides represent the negative controls. **(B)** MDCK was utilised as the assay positive control. Substantial levels of MDCK cell death, hence detachment from the culture well, occurred at 40 and 400HAU/ml PR8, indicating high pathogenicity of this virus strain Scale bar: 10µm. Filled histograms: HA; open histograms: isotype control (Iso Ctrl). HA: haemagglutinin; IAV: influenza A virus.

Using 40 HAU/ml as a representative of infectious dose, transcript levels of IFNβ and IL-8 were shown to be enhanced 91 and 7 times respectively in PR8-treated cells compared with uninfected cells (Figure 5.4.2.2).

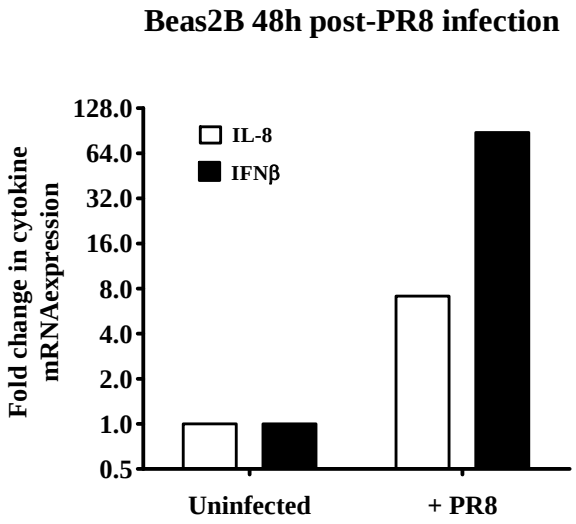

Figure 5.4.2.2. IAV challenge upregulates IL-8 and IFNβ transcripts in Beas2B. qPCR detected 7 and 91 fold increase in IL-8 and IFNβ transcript levels. Mean of two experiments is shown.

PR8 challenge enhanced both cell surface and intracellular CD1d in Beas2B in a dose-dependent manner (Figure 5.4.2.3).

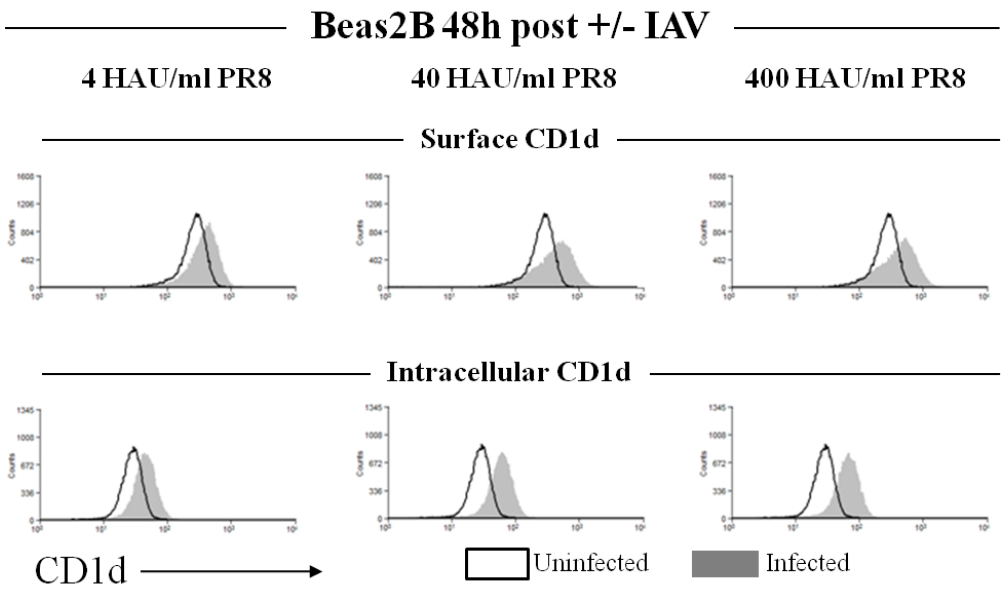

Figure 5.4.2.3. IAV infection enhances CD1d protein levels in Beas2B. Epithelial cells were infected with various titres of PR8. 48h later surface and intracellular CD1d was analysed by flow cytometry (clones 51.1.3 and 42, respectively). Filled histograms: infected cells; open histograms: uninfected cells. The data are representative of two independent experiments.

NHBE cells were studied for inducibility of CD1d expression in response to PR8. Virus-infected cells clearly expressed HA after infection (Figure 5.4.2.4), and the CD1d protein level was modestly increased post-challenge.

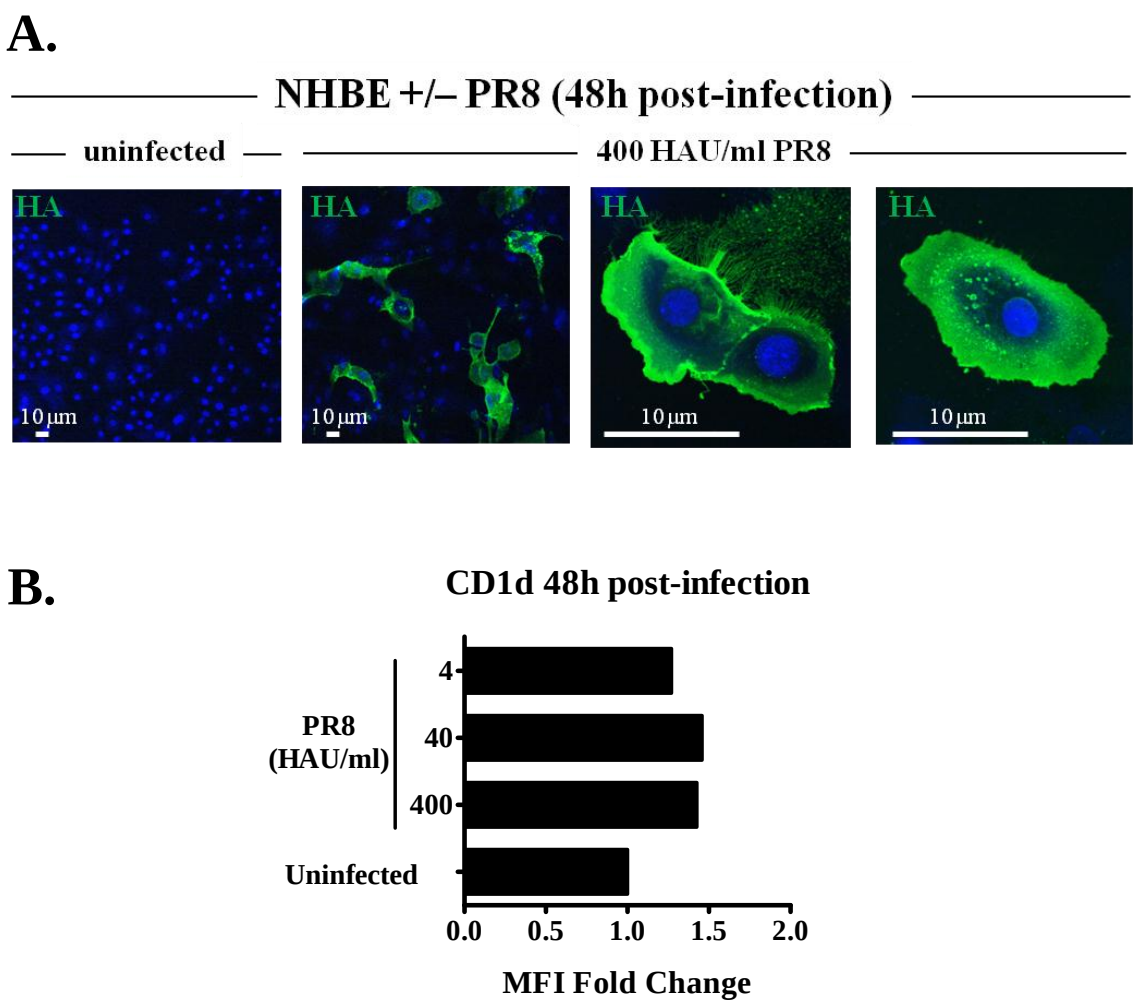

Figure 5.4.2.4. CD1d was modestly upregulated in PR8-infected NHBE cells. (A) Confocal microscopy shows HA expression (especially at the cell periphery) in infected NHBE 48h post-challenge with 400HAU/ml PR8. Stainings are representative of three independent experiments. **(B)** Flow cytometry analysis reveals a modest increase in surface CD1d infection. Mean of two experiments is shown.

In another approach to visualise changes in NHBE CD1d production, cells were immunostained (Abs clone NOR3.2) and analysed by confocal microscopy (Figure 5.4.2.5). Consistent with flow cytometry data a small increase was observed in infected cells.

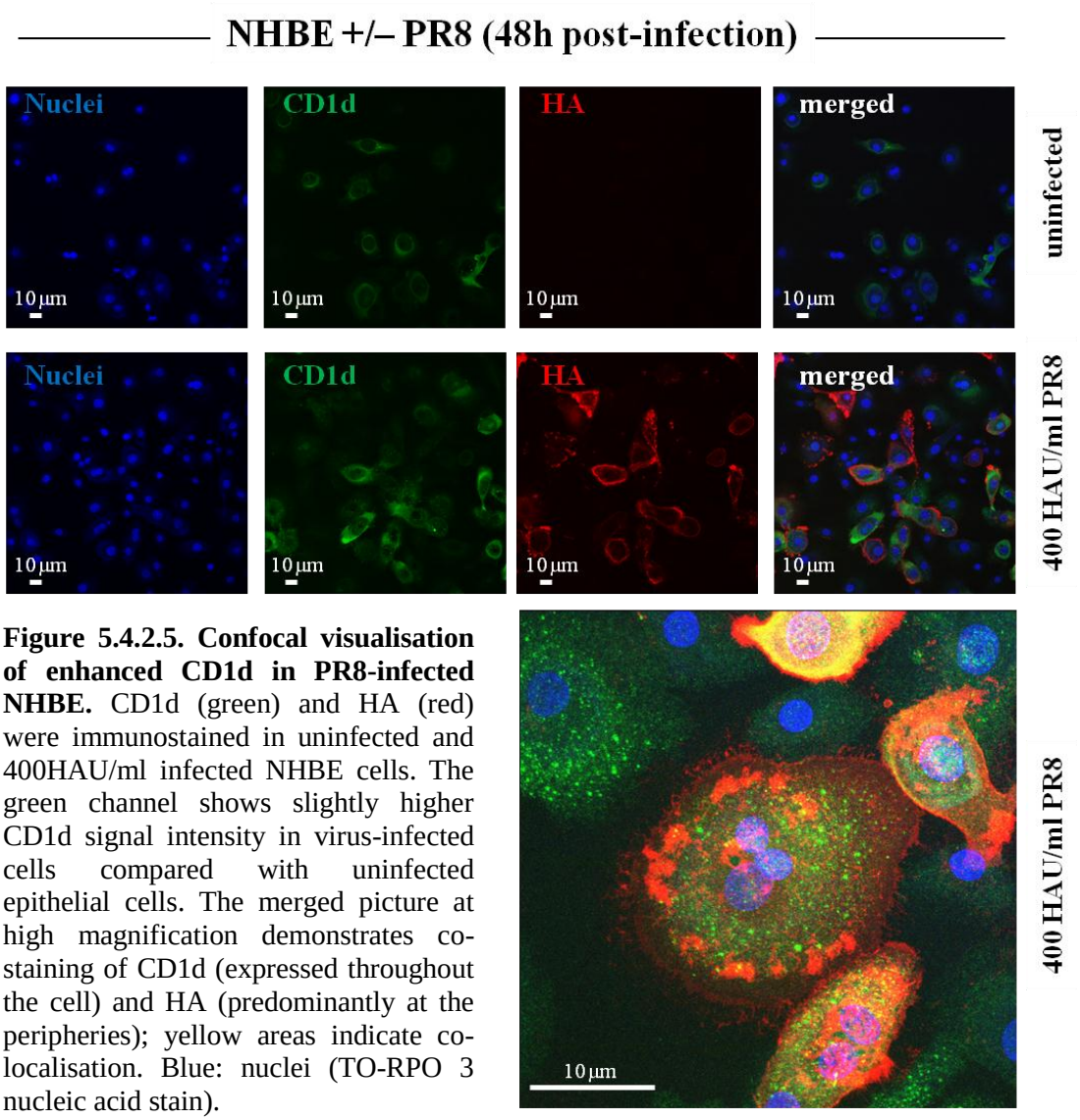

Figure 5.4.2.5. Confocal visualisation of enhanced CD1d in PR8-infected NHBE. CD1d (green) and HA (red) were immunostained in uninfected and 400HAU/ml infected NHBE cells. The green channel shows slightly higher CD1d signal intensity in virus-infected cells compared with uninfected epithelial cells. The merged picture at high magnification demonstrates co-staining of CD1d (expressed throughout the cell) and HA (predominantly at the peripheries); yellow areas indicate co-localisation. Blue: nuclei (TO-RPO 3 nucleic acid stain).

5.5. Discussion

In this chapter I demonstrated that CD1d on human RECs can be induced with viral-associated signals IFNα, IFNγ, and TLR-3L, and to a lesser extent following IAV infection. This is particularly relevant at the respiratory mucosal surface. Bronchial epithelial cells synthesise and secrete type I IFNs upon infection with IAV [280,281]. During infection intraepithelial $CD8^+$ T cells also produce IFNγ [282]. Such positive regulatory loops, be it autocrine via virus-infected epithelial cells or paracrine through neighbouring lymphocytes, suggest control of REC CD1d expression by important players of mucosal immunity. Of note, *i*NKT cells can potentially augment this loop as they secrete IFNγ when activated with APCs [92].

TLR-3, a PRR for dsRNA, is widely expressed on RECs [202]. Upon binding to its ligand, TLR-3 can induce type I IFN production in a range of human cells [283]. IAV is a single-stranded segmented RNA virus belonging to *Orthomyxoviridae* family [153]. However, dsRNA replicative intermediates are formed during viral replication which are critical determinants for outcome in this infection [284,285]. Such intermediates have been identified in IAV-infected cells by RT-PCR and Abs against helical dsRNA [277,284,285]. As the major dsRNA receptor, TLR-3 has been reported to be crucial in the immune response to IAV. For example, compared with wild type mice, TLR-$3^{-/-}$ mice displayed significantly reduced amounts of RANTES, IL-6, and IL-12, and lower $CD8^+$ T cells in their bronchoalveolar space following IAV challenge [286]. Also, in *in vitro* models, TLR-3 in infected human RECs regulates the proinflammatory response [277]. In addition to TLR-3, two other cellular nucleic acid receptors – retinoic acid-inducible gene-I (RIG-I) and melanoma differentiation-associated gene (MDA-5) – contribute to detection of virus and mounting an immune

response [209]. RIG-I mediates the IFN antiviral signaling in infected human bronchial epithelial cells [277]. Therefore, it was reasonable to expect that infection with PR8 would result in activation of TLR-3 and RIG-I-induced IFN signalling pathways with subsequent increase in surface CD1d. However, I only observed a small increase in CD1d expression in PR8 infected RECs.

One possible explanation is that the virus has evolved mechanisms to escape immune activation by suppressing CD1d expression. A report by Yuan *et al* showed downregulation of surface CD1d on herpes simplex virus 1 (HSV-1)-infected cells [78]. Similarly, HIV-1 and Kaposi sarcoma-associated herpes virus (KSHV) have been reported to impair surface CD1d levels [79-83].

Unchanged levels of REC CD1d when treated with LPS and pam3CSK4 suggest that epithelial CD1d is less likely to have a role in certain bacterial infections of airways. A report by Nieuwenhuis *et al* showed that $CD1d^{-/-}$ mice had markedly reduced pulmonary clearance of *Pseudomonas aeruginosa*, a Gram-negative bacterium [151]. The number of bacilli in the lungs, 24h post-inoculation, was 100-times higher in the knockouts compared with the wild types. Activation of *i*NKT cells by α–GC enhanced the clearance of the bacterium and prevented pneumonia. This was mediated by increasing *Pseudomonas* uptake by alveolar macrophages, and amplified IFNα and TNFα secretion into the bronchoalveolar lavage fluid [151]. Therefore, it can be postulated that while REC CD1d has a more dominant role in viral infections (as a consequence of inducibility by IFNs), CD1d on alveolar macrophages is more involved in bacterial infections. These finding suggest a differential contribution of REC CD1d and CD1d expressed on APCs to immune defence in the lungs. In order to define the importance of these cells I will need to separate their relative contributions. One way of

doing this would be to generate a system where CD1d expression is either "silenced" in the epithelium or APCs for example in $CD1d^{-/-}$ /WT bone marrow chimeric mice. This is not reported in this thesis, but will be discussed in Chapter 8.

5.6. Conclusion

This chapter shows that REC CD1d can be upregulated when exposed to type I and type II IFNs, or upon activation of their TLR-3 receptor. It also demonstrates a moderate increase in CD1d expression on REC following IAV infection. Additionally, LPS and pam3CSK4 did not change REC CD1d expression.

Chapter 6. Function of CD1d on respiratory epithelial cells - activation of *i*NKT cells

Chapter 6.

Function of CD1d on respiratory epithelial cells – activation of *i*NKT cells

6.1. Aims

To determine if CD1d expressed on RECs has a function by examining its ability to activate *i*NKT cells and the consequences of this interaction.

6.2. Introduction

The findings from the last three chapters demonstrated constitutive expression of CD1d on human airway epithelial cell lines and primary cells; and that epithelial CD1d can be induced by viral-associated signals. I now question whether CD1d expressed on REC can stimulate *i*NKT cells and use genomic expression profiling to explore other potential functions.

Previous investigators have shown activation of *i*NKT by keratinocytes and intestinal epithelial cells (IECs) *in vitro* [58,60]. Keratinocytes presented lipid Ag to induce IFNγ secretion from human *i*NKT clones in a CD1d-dependent fashion and this effect was partially blocked in the presence of CD1d blocking Ab [60]. Similarly, α–GC-pulsed freshly isolated human IECs stimulated IL-2 secretion from an *i*NKT hybridoma [58]. While conventional $CD3^+$ T cell activation by RECs has been suggested in a number of studies [249-251], there is no report of *i*NKT activation by airway epithelial cells to date. Human RECs can present mycobacterial antigens to $CD4^+$ T cells and stimulate release of IFNγ and IL-2 by these cells [249]. They can also induce T cell proliferation in mixed lymphocyte reaction (MLR) cultures [250]. Oei *et*

al showed that RECs obtained from surgical specimens of patients undergoing lobectomy were capable of stimulating proliferation of both $CD4^+$ and $CD8^+$ T cells [251].

*i*NKT cells play an important role in optimal immunity against respiratory pathogens like influenza A virus (IAV) [139,140]. Inoculation of *i*NKT-deficient mice with IAV results in higher mortality than wild types [139]. Frequency of *i*NKT cells in bronchoalveolar lavage fluid (BALF) of IAV-infected wild type mice is raised within three days of viral challenge [139], suggesting a role for these cells in efficient mucosal immunity to the virus. These *i*NKT cells can reduce the suppressive activity of myeloid-derived suppressor cells (MDSCs) – a group of $CD11b^+$ $Gr1^+$ cells comprising immature DCs, immature macrophages and granulocytes, in the lungs of infected mice [140]; and are thought to help restore IAV-specific immune responses, reduce viral titres, and increase survival rate [140].

Recruitment of activated T cells, including *i*NKTs, to the mucosal surface depends on expression of chemokines CXCL9 (MIG), CXCL10 (IP-10), and CXCL11 (I-TAC) by normal human bronchial epithelial (NHBE) cells [244]. These ligands are potent chemoattractants for CXCR3-expresssing cells, such as *i*NKT cells as well as T_h1 and $CD8^+$ T, and NK cells, and are strongly induced by IFNγ [130,131,213,245]. Besides IFNγ, type I and III interferons (IFNs), and viral infections can upregulate CXCR3 ligands in epithelial cells [213]. Of note, CXCL16 – the sole ligand for CXCR6 (which is present on *i*NKT cells), is expressed by human bronchial epithelial cells [287]. Indeed, the basal expression of CXCL16 by RECs is higher than in other stromal cell compartments in the lungs (e.g. fibroblasts and smooth muscle), and is inducible with IFNγ [287].

In this chapter, I examine first, if RECs can stimulate cytokine secretion from *i*NKT cells, and if this activation depends on CD1d. I will then investigate the gene expression profile and potential molecular pathways that are activated in *i*NKT cells after CD1d-dependent stimulation by RECs.

6.3. Methods

6.3.1. Overall experimental design

In the first experiment, α–GC-pulsed Beas2B epithelial cells were co-cultured with *i*NKT cells, and activation of *i*NKT cells studied by intracellular cytokine (TNFα, IFNγ, IL-13, IL-4, and IL-5) staining. Transwell separation of epithelial-*i*NKT cells and co-addition of CD1d blocking mAb were used to determine if the observations were dependent on CD1d-TCR engagement or physical contact between the two cell types.

To determine if the findings were reproducible in primary RECs, production of TNFα and IFNγ (as representative cytokines) was examined in *i*NKT cells co-incubated with NHBE cells.

Finally, using an NHBE and *i*NKT co-culture system, the whole genome expression profile in *i*NKT cells was examined comparing an early and late time point to baseline *i*NKT cell gene expression.

6.3.2. Cytokine production in epithelial–stimulated *i*NKT cells

Beas2B cells were grown in 12-well tissue culture plates and at 70% confluence were pulsed with 200ng/ml α–GC for 24h. After washing, a previously generated

human *i*NKT cell clone [260] was added at 2:1, 1:1, and 1:2 (*i*NKT: Beas2B) ratios, either directly to the adherent cells or in the top compartment of a transwell insert. CD1d blocking mAb or appropriate isotype control was used in some wells (Figure 6.3.1). Five hours after co-culture, *i*NKT cells were harvested and intracellular IFNγ, TNFα, IL-13, IL-4, and IL-5 staining determined by flow cytometry.

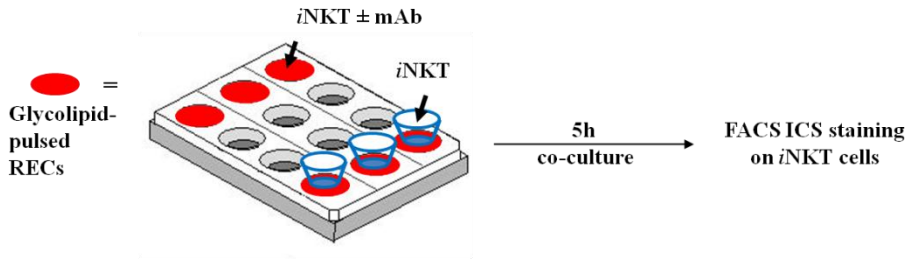

Figure 6.3.1 Study design for epithelial CD1d-mediated activation of *i*NKT cells. For blocking assays, mAb (anti-CD1d (clone 42) or isotype control (Iso Ctrl)) was added together with *i*NKT.

To extrapolate results from Beas2B cell line, primary NHBE cells (passage 3-5) were similarly pulsed with α–GC, and then co-incubated with *i*NKT cells at 1:1 ratio. Five hours after co-culture, intracellular IFNγ and TNFα production in *i*NKT was determined by flow cytometry.

6.3.3. Gene expression analysis of *i*NKT cells

*i*NKT cells were added to adherent NHBE cells as described in Figure 6.3.2, and harvested for RNA isolation. All non-adherent cells were collected at the specified time points – this was the case also for the *i*NKT cells separated by transwell, in order to standardise the potential contaminating non-adherent epithelial cells to collected *i*NKT cells. *i*NKT cells at baseline were the same amount of *i*NKT cells which were not exposed to NHBE. I chose this as baseline since I reasoned that the alternative baseline - *i*NKT cells co-cultured with non-pulsed NHBE will also be stimulated by endogenous

glycolipid. Total RNA was first extracted using RNeasy Mini Kit (Chapter 2.2.1), and its quality assessed using the high-resolution electrophoresis bioanalyser system (Agilent Technologies). Gene expression profiling was performed using the Affymetrix Gene ST 1.0 array which provides probes for whole transcript coverage. Isolated total RNA was then taken through the Affymetrix preparation protocol (www.affymetrix.com; Chapter 2.2.7).

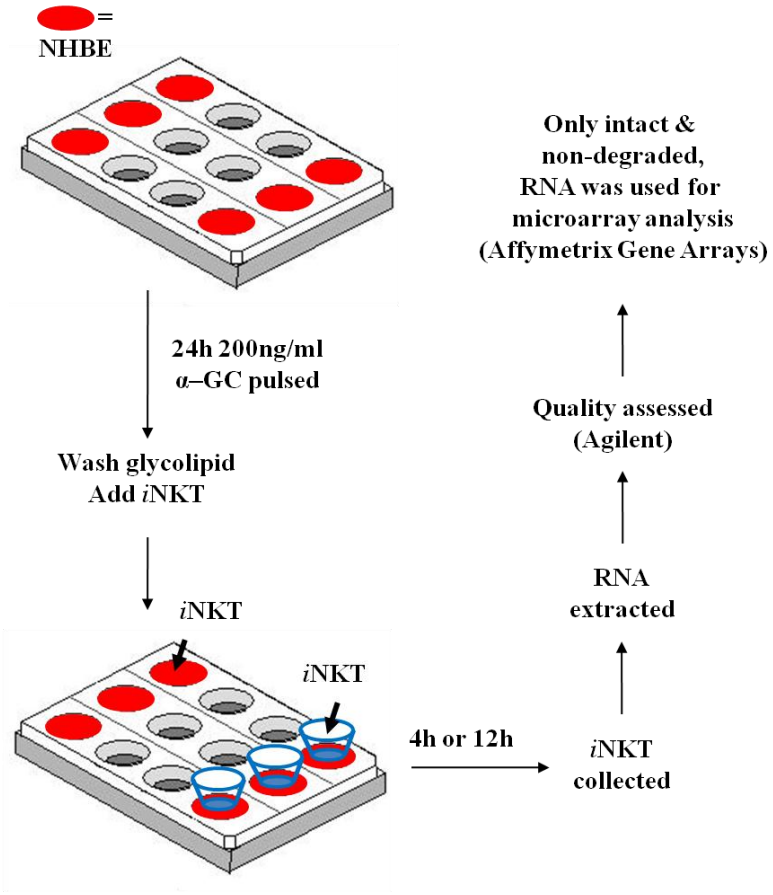

Figure 6.3.2. Experimental design for microarray analysis of REC-activated *i*NKT cells. *i*NKT cells were added at 1:1 ratio either on α–GC-pulsed NHBE cells or onto transwell inserts. At 4h and 12h after co-culture, *i*NKT cells were collected and their RNA extracted.

Raw data were processed using Affymetrix Power Tools (www.affymetrix.com /support/developer/powertools/changelog/index.html) to generate RMA-normalised gene level intensities. Quality control procedures included a comparison of smoothed

histograms and boxplots of RMA normalized expression values between samples, and hierarchical clustering of all samples to identify any potential outliers. Further analysis was performed using the 'R' statistical program (http://www.r-project.org/) (described later).

Prior to statistical analysis, the mean intensity was computed for each probe set and internal control and duplicate probe sets were removed. Bayesian moderated t-test was applied to identify differentially expressed genes between groups using the 'limma' (linear models for microarray analysis) package from Bioconductor (http://www.bioconductor.org/). The Benjamini–Hochberg false discovery rate (FDR) procedure was applied to correct for multiple testing [288]. The inverse log of the absolute $\log_2$ fold change (FC) generated by 'limma' was used to determine the FC between groups. Visualisation of the data using heatmaps and hierarchical clustering was performed using the TMeV4 software and 'R' statistical programme.

6.3.4. Interpretation of data

Three approaches were taken, described in greater detail in the relevant Results sub-headings; but in each, the time point and the condition in the question (e.g. time point 4 hours, cells separated by transwell) was first compared with the baseline (gene expression profile of *i*NKT cells not exposed to NHBE cells), before comparison with cells not separated with transwell at time point 4 hours.

In the first approach, comparisons were made using the two groups of interest and a "Gene List (GL)" was generated – this being the genes that were statistically differentially expressed between the two groups. In the second approach, a more

sophisticated level of steps was designed with 'R' to enhance mathematical significance and interpretation of the final gene list. Finally, since unrestricted comparisons of very large numbers of variables between two groups introduce the problem of multiple testing, where the chance of making a Type I error (falsely identifying single genes as differentially expressed) is increased and relevant sets of genes can be lost to identification because the differences are modest relative to the noise inherent to the microarray technology, the "biological relevant sets of gene approach" was used. For this, I used Gene-Set Enrichment Analysis (GSEA) and Database for Annotation Visualisation and Integrated Discovery (DAVID; an online tool: http://david.abcc.ncifcrf.gov/), to evaluate whether *sets of genes*, grouped together by biological processes, are enriched (over-represented) among the differentially expressed genes.

Analysis with DAVID assists in identifying enriched pathways/gene categories by mapping a given gene list against categorical data from available annotations databases. These include gene ontology (GO) – which itself contains biological process (BP) and molecular function (MF) databanks, Swiss-Prot and Protein Information Resource (SP-PIR), and Kyoto Encyclopaedia of Genes and Genomics (KEGG) [289]. DAVID can discover over-presented annotations; however, it does not take into account change in expression values of individual genes (i.e. does not rank the list), and therefore is not as accurate as GSEA (discussed below).

GSEA is a more powerful analytical tool. It evaluates microarray data at the level of gene sets, which, like DAVID, are defined based on prior biological knowledge. The goal of GSEA is to determine whether members of a gene set tend to occur toward the top (or bottom) of a list of genes ranked in order of their relative

difference expression to the phenotype in question [290]. Processing the list top-to-bottom (upregulated-to-downregulated) against any given set, genes are allocated a positive (running) enrichment score when they are present or penalised by a negative score when absent. The final enrichment score (ES) is the maximum deviation from zero. The higher the ES and the more biased the ES curve is towards a phenotype, the greater is the enrichment of that particular gene set in that phenotype. False discovery rate (FDR) is the probability estimate that indicates if a gene set with a given ES could be a false positive result.

6.4. Results

6.4.1 RECs present exogenous glycolipid to, and activate *i*NKT cells in a CD1d-dependent process

α–GC-pulsed Beas2B cells stimulated IFNγ, TNFα, IL-13, IL-4, and IL-5 production in *i*NKT cells at all tested ratios (Figure 6.4.1.3). This effect was partially blocked in the presence of blocking mAb but was unchanged with isotype control. Cytokine synthesis was completely abolished in the transwell-separated *i*NKT cells, indicating the requirement for direct contact with RECs to initiate cytokine synthesis.

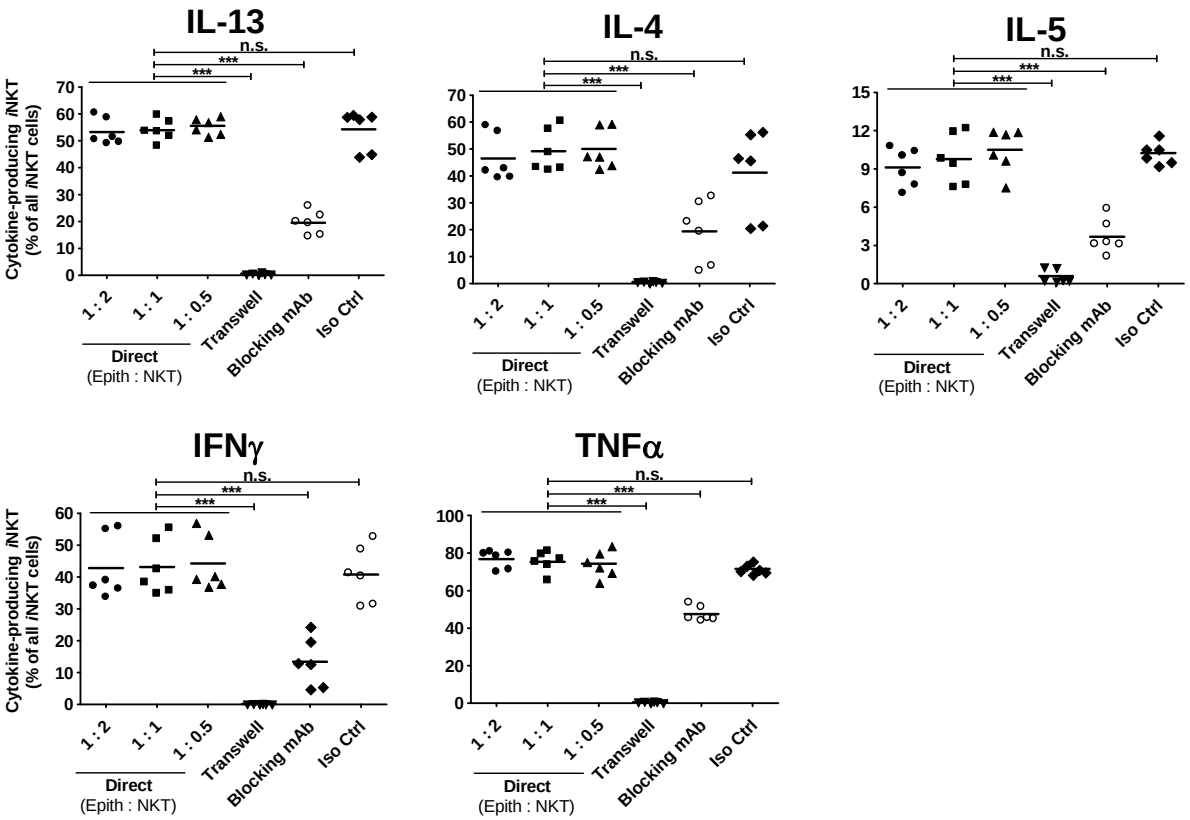

Figure 6.4.1.1. Epithelial-stimulated *i*NKT cells produce TNFα, IFNγ, IL-13, IL-4, and IL-5. (A) Following the protocol in Figure 6.3.1, α–GC-pulsed Beas2B stimulated cytokine production in *i*NKT cells after 5h co-culture. No activation happened in transwell-separated *i*NKTs. The blocking mAb, but not the isotype control, partially blocked the cytokine production. N=6 independent experiments. ***: $p < 0.0001$; n.s.: non-significant.

To test whether interactions via non-CD1d surface molecules could have mediated *i*NKT activation, Beas2B and *i*NKT cells were cultured at 1:1 ratio and production of IFNγ, TNFα, IL-13, and IL-4 as representative cytokines was studied (Figure 6.4.1.2). In addition, isotype control and CD1d blocking mAbs were added to the wells 3h prior to pulsing with α–GC and kept in the medium (until co-culture) in order to improve blocking.

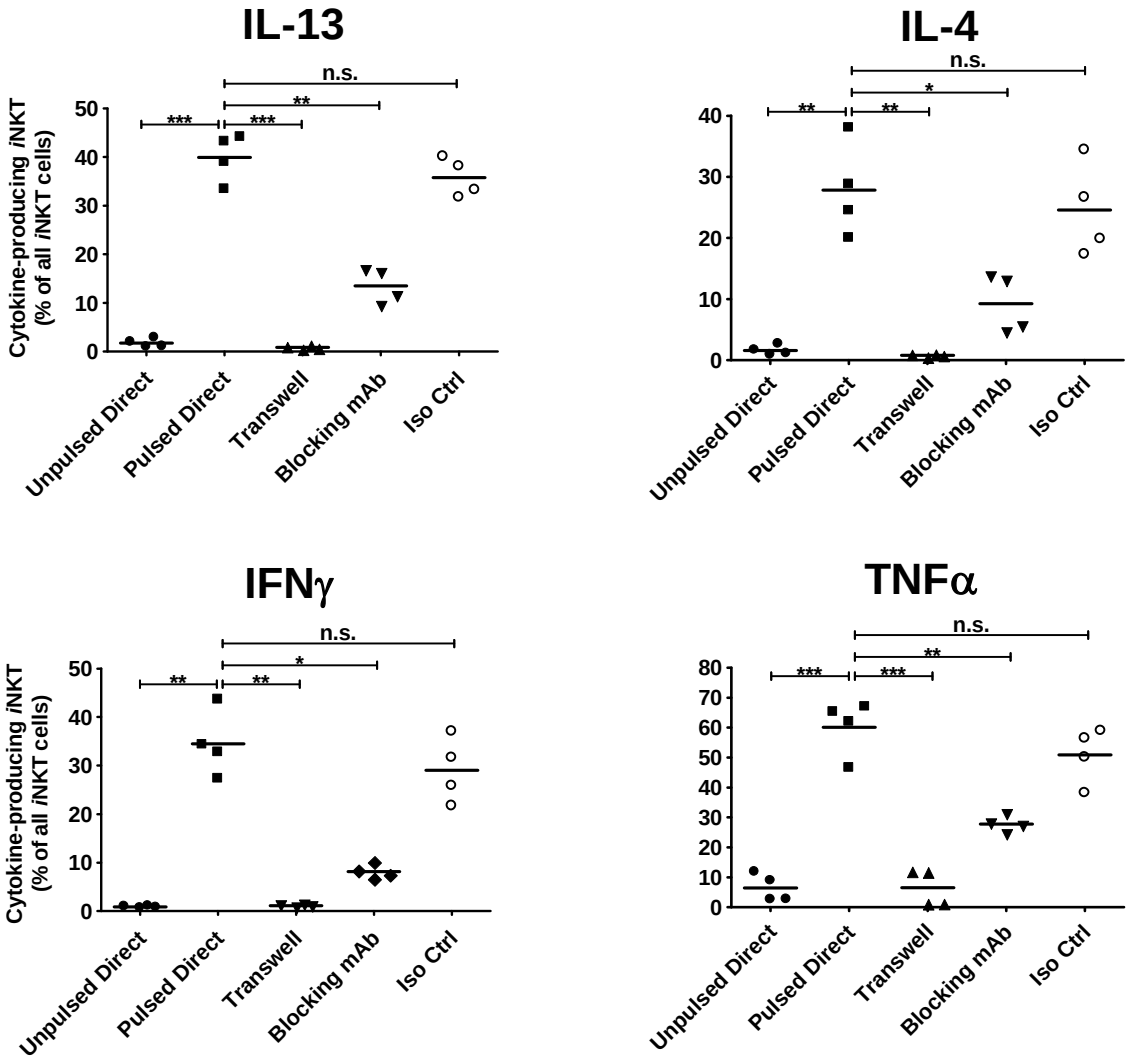

Figure 6.4.1.2. Cytokine production in epithelial-stimulated *i*NKT cells is mediated by direct CD1d-TCR interaction. (A) A protocol similar to Figure 6.4.1.1 was applied. However, an extra well containing unpulsed (with glycolipid loading) Beas2B was studied in parallel to monitor *i*NKT activation through non-CD1dmolecules. Abs were added prior to α–GC pulsing and were washed out before co-culture with *i*NKT (for 5h). N=4 independent experiments. ***: $p < 0.0001$; **: $p < 0.001$; ***: $p < 0.01$; n.s.: non-significant.

Similar to Beas2B, α–GC-pulsed NHBE cells activated *i*NKT cells to produce IFNγ and TNFα. (Figure 6.4.1.3). CD1d blocking mAb partially blocked the cytokine synthesis, and stimulation was absent in both transwell-separated *i*NKT cells, and *i*NKT cells co-cultured with un-pulsed NHBE.

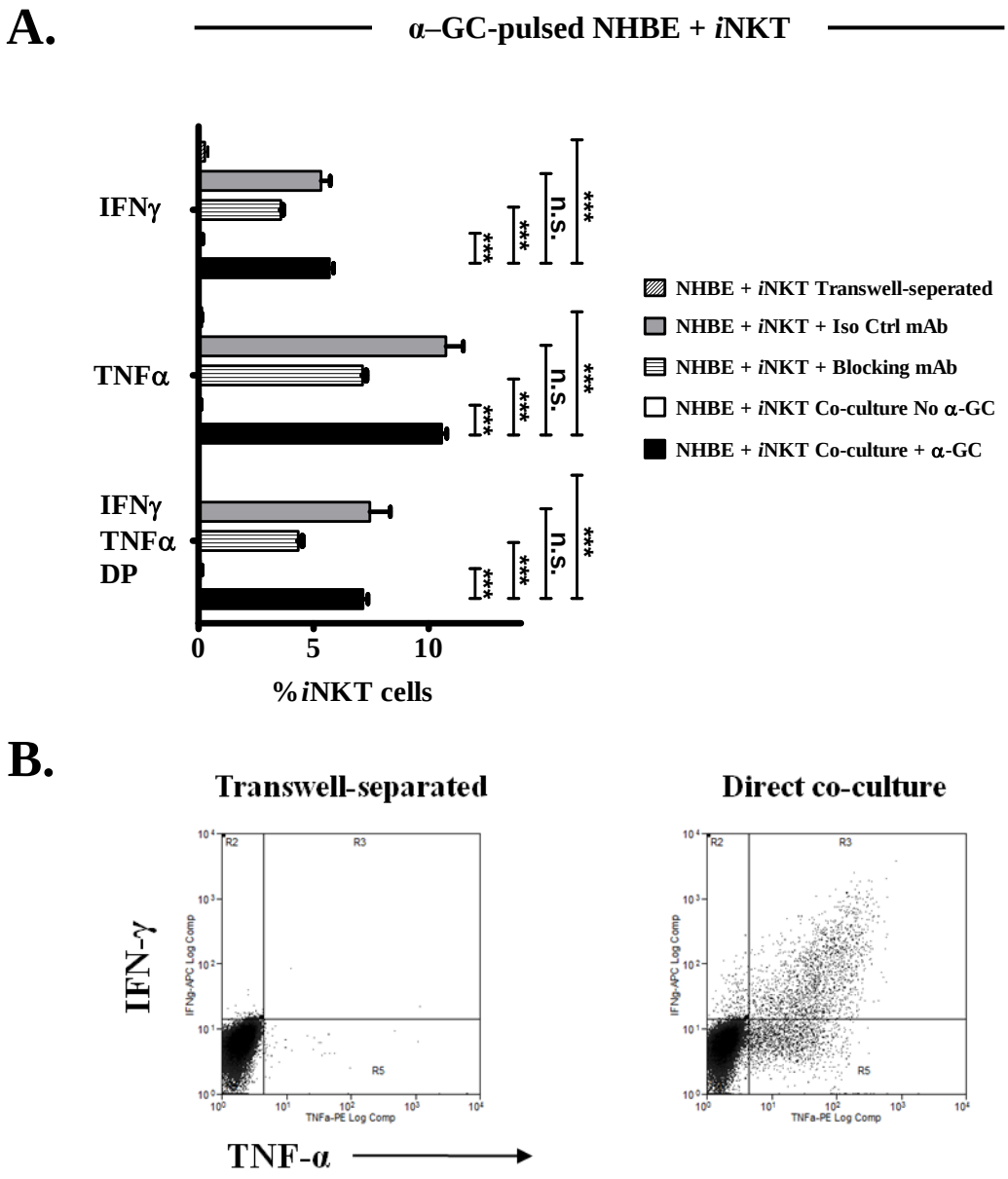

Figure 6.4.1.3. TNFα and IFNγ intracellular cytokine staining in *i*NKT cells after interaction with NHBE cells. (A) Flow cytometry detected cytokine production upon direct engagement of lipid-loaded NHBE CD1d and *i*NKT TCR, which was absent in transwell-separated cells. The cytokine production was partially blocked in the presence of blocking Ab, but was unchanged in isotype control (Iso Ctrl) treated cells. **(B)** Representative dot plots illustrating cytokine expression in *i*NKT. N= 3 experiments. ***: $p < 0.0001$; n.s.: non-significant.

6.4.2 Quality control of samples pre and post DNA microarray chip hybridisation

In addition to robust experimental design, two key processes are required before interpretation of data obtained from gene expression profiling using DNA microarray chip. Firstly, the sample offered for hybridisation has to contain high quality RNA and after hybridisation and scanning of intensity, another important step follows – that of ensuring that there is no unintended bias in the output data. Analysis of the first is performed by assessing the "RNA integrity number" (RIN) of the RNA samples. RIN is an algorithm, produced by Agilent Bioanalyser, which evaluates the entire electrophoretic trace of RNA and determines the sample integrity. The algorithm assigns a score of 1 to 10, where 10 represents completely intact RNA. To ensure there is no unintended bias in the output data, histograms and hierarchical clustering of all the samples according to intensity are carried out.

In this study, sufficient RNA was obtained from all the samples apart from Transwell 12h (T12), therefore, this condition was excluded from further analyses. The RIN values verified high RNA integrity and lack of degradation for all the other samples (Figure 6.4.2.1A).

The histogram of intensity patterns (Figure 6.4.2.1B) demonstrated comparable expression across all samples [Time 0 (0h), Direct 4h (D4), Transwell 4h (T4), and Direct 12h (D12)]. All intensity histograms were unimodal, ruling out potential artefact formation during scanning, high background intensities, or abnormally elevated expression values (as evident in bimodal distributions). Compared with D4, T4 and 0h, the D12 samples showed slightly smaller quantile deviation (i.e. higher concentration

around the median) of normalised intensity expression values on box plots. But, the global median was in line with other samples (Figure 6.4.2.1C).

A.

	0h_1	0h_2	0h_3	D4_1	D4_2	D4_3	T4_1	T4_2	T4_3	D12_1	D12_2	D12_3
RIN	9.6	9.5	9.7	8.9	9.5	9.9	9.7	9.8	9	9.2	9.3	9.1

B. **C.**

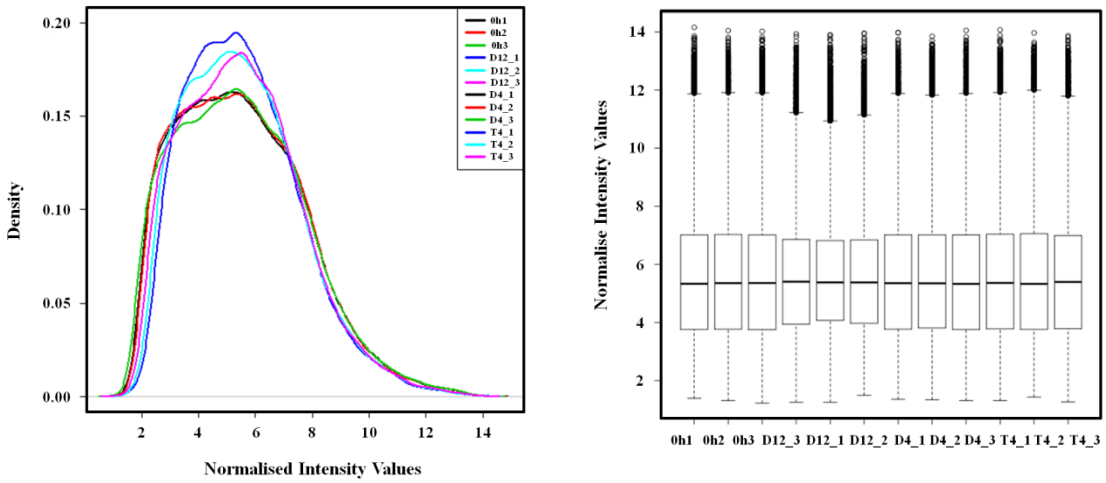

Figure 6.4.2.1. Comparison of RMA-normalised microarray signal intensities from *i*NKT cells. The RIN values obtained for all samples is listed in **(A)**. Expression distribution of all genes from all samples represented as histograms **(B)** or box plots **(C)** after RMA normalisation. In **(C)** the boxes are drawn between the 25th to the 75th percentiles of normalised data, with median (50th percentile) drawn inside. Comparable unimodal distribution patterns of expression intensities were evident. 01–3: *i*NKT at 0h; D4_1–3: *i*NKT directly interacting with NHBE at 4h; T4_1–3: *i*NKT transwell-separated from NHBE at 4h; D12_1–3: *i*NKT directly interacting with NHBE at 12h.

Before further analysis, the natural grouping of similarities and dissimilarities of the samples was examined for unintentional bias (e.g. due to experimental procedures). Unsupervised hierarchical clustering using "complete linkage" method, which computes the maximum distance between any two data points in neighbouring sets (i.e. the minimum of similarity), was employed (Figure 6.4.2.2). As expected, the statistical algorithm grouped the samples on the basis of experimental time point, with D12

(Direct contact, 12th hour) being the most dissimilar from the rest, with no specific bias towards Ts or Ds. This data means there is no unexpected bias, and the groupings fall into the expected clusters. It confers technical reassurance on the data to be analysed.

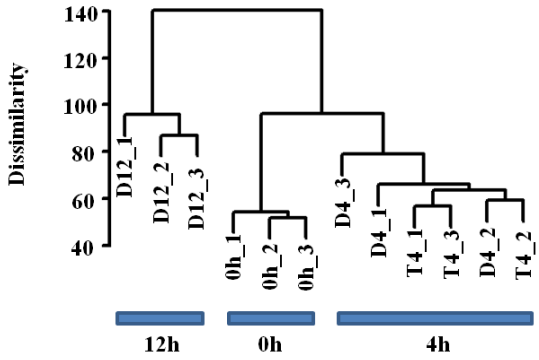

Figure 6.4.2.2. Unsupervised hierarchical clustering of all *i*NKT samples. Clustering was carried out using "complete linkage" distance measure. The output dendrogram shows grouping of data primarily on the basis of experiment time point.

6.4.3 Gene expression profile of *i*NKT cells activated by direct contact with α–GC–pulsed RECs

To elucidate differentially expressed genes in *i*NKT cells 4h after co-culture with NHBE, gene expression data in D4 and T4 samples were compared against 0h. A total of 2637 and 1577 genes with adjusted $p < 0.05$ were identified, respectively (Table 6.4.3.1).

Gene list (GL)	Comparison	No. differentially expressed genes
1	D4 vs. 0h	2637
2	T4 vs. 0h	1577
3	D4 vs. T4	119
4	(D4 vs. 0h) – (T4 vs. 0h)	1315
5	D12 vs. 0h	7964

Table 6.4.3.1. Number of differentially expressed genes in *i*NKT cells comparing the various conditions. Normalised expression values were used as input and only genes with adjusted $p < 0.05$ were considered. 0h: baseline; D4: Direct at 4th hour; T4: Transwell at 4th hour; D12: Direct at 12th hour.

Ordering the genes in Gene Lists 1 and 2 (GL1 and GL2) from the most differentially expressed (p=9.89×E^{-10} and p=3.76×E^{-13}) to the lowest (p=0.05), I found some epithelial-specific genes on top of the lists, such as keratins and secretory leukocyte peptidase inhibitor (SLPI). This was expected since some epithelial cells would have detached during the experiment. Due to this, the more accurate determination of differentially expressed genes in directly activated *i*NKT (D4) against that with no contact (T4), is identified either by comparing "D4 vs. T4" or by obtaining the difference between "D4 vs. 0h" and "T4 vs. 0h". The former produced 119 (GL3) and the latter 1315 (GL4) genes (Table 6.4.3.1). The list of genes in GL3 is shown in Figure 6.4.3.1B.

To visualise the differential expression between D4 and T4 (GL3), TMeV4 was used to construct a heatmap of GL3 (Figure 6.4.3.1A). This gives a visual representation of the differentially expressed genes, which can be further clustered by hierarchical clustering using "complete linkage" method (Pearson Correlation) into four upregulated sub-clusters plus a downregulated sub-cluster. In terms of similarity, genes in sub-cluster 1 were closer to sub-cluster 2, and sub-cluster 3 was more related to sub-cluster 4 (Figure 6.4.3.1A).

Genes in the upregulated sub-clusters were almost all immune-related. They included cytokines, like IL-13, IL-5, TNFα, IL-1α, and oncostatin M (OSM), cytokine receptors, such as IL-2Rα, IL-2Rβ, IL-4R, and GM-CSF receptor beta chain (CSF2Rβ), chemokines, including CCL3, CCL3-like 1 (CCL3L1), and the activation marker CD69 (Figure 6.4.3.1B).

A.

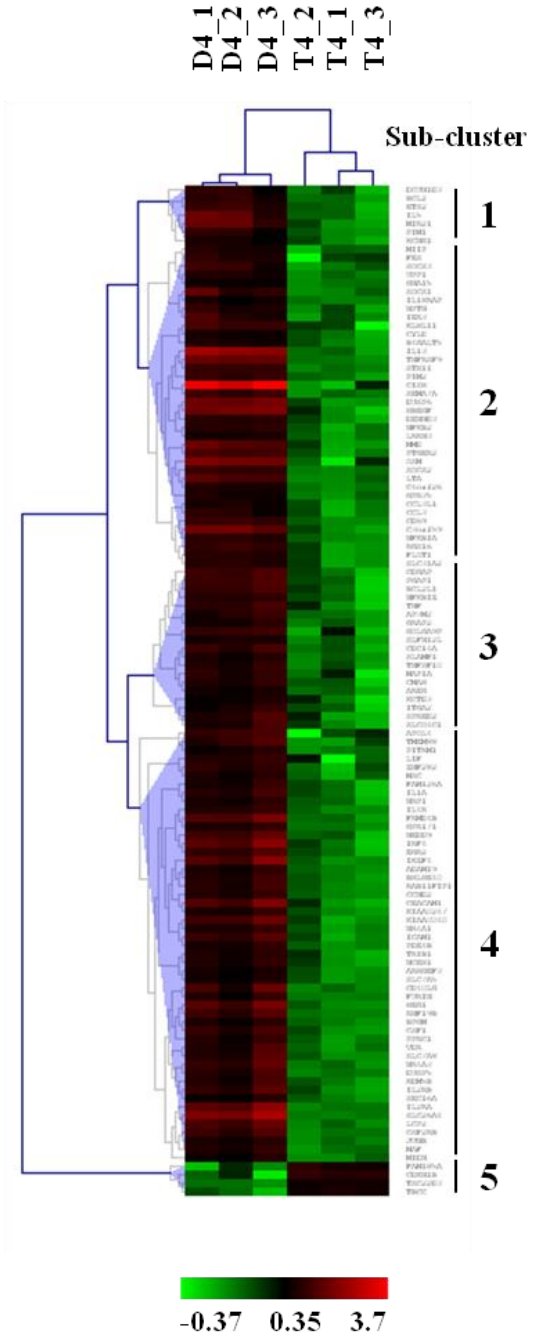

B.

Gene	"D4 vs. T4"	Gene	"D4 vs. T4"
CISH	11.47	*APOL4*	1.92
IL13	4.86	*MAP1A*	1.91
SLC26A4	4.67	*IL4R*	1.90
OSM	3.83	*BCL2*	1.90
DUSP6	3.70	*AP3M2*	1.89
HBEGF	3.65	*SLC31A2*	1.89
IL2RA	3.48	*CCND2*	1.86
IKZF4	3.34	*FES*	1.84
C3orf59	3.30	*ZNF282*	1.83
TNFRSF9	3.20	*GPR171*	1.82
IRF4	3.16	*NFKBIZ*	1.81
MMD	3.10	*FLOT1*	1.80
FRMD4B	3.07	*NR4A1*	1.80
CEACAM1	3.01	*DENND3*	1.79
HEG1	3.01	*FAM126A*	1.79
MIR21	2.82	*ADAM19*	1.78
IL5	2.75	*KIAA0247*	1.78
LCP2	2.69	*NPTN*	1.77
KIAA0040	2.66	*JUNB*	1.77
LTA	2.50	*CMAH*	1.77
NEDD9	2.49	*MAF*	1.76
CDGAP	2.45	*CCL3*	1.76
CD40LG	2.44	*DCUN1D3*	1.74
NR4A3	2.37	*FURIN*	1.74
SOCS1	2.36	*ITGA2*	1.74
PGAP1	2.32	*TNFSF10*	1.74
KLHL11	2.29	*NCEH1*	1.74
PTGER2	2.28	*PIM1*	1.73
RNF19B	2.26	*TRIB1*	1.72
IL2RB	2.26	*PPRC1*	1.72
GOLGA9P	2.25	*UPP1*	1.69
CSF2RB	2.22	*GRAP2*	1.69
BCL2L1	2.21	*SLAMF1*	1.69
ICAM1	2.19	*NRP1*	1.68
SPRED2	2.18	*AREG*	1.68
SEMA7A	2.16	*MIIP*	1.67
CDC14A	2.14	*PDE4B*	1.67
CSF1	2.10	*SLFN12L*	1.65
TNF	2.10	*MSC*	1.65
STX11	2.09	*MIDN*	1.58
CD69	2.08	*PITRM1*	1.57
SOCS3	2.07	*SLC7A5*	1.57
PIM2	2.05	*B4GALT5*	1.57
SOCS2	2.04	*SEC16A*	1.56
SLCO4C1	2.03	*KCTD3*	1.56
TMEM88	2.03	*BPGM*	1.56
EGR2	1.98	*GPR35*	1.55
IER3	1.97	*C4orf26*	1.54
NFKBIA	1.97	*LRRN3*	1.54
NFKB2	1.97	*CCL3L1*	1.54
VDR	1.97	*ARHGEF3*	1.53
ETS2	1.97	*IL18RAP*	1.52
LIF	1.97	*KCNK1*	1.49
RAB11FIP1	1.96	*CYLD*	1.47
BHLHE40	1.96	*GNA15*	1.46
DUSP5	1.95	*TSC22D3*	0.64
IL1A	1.95	*TBCC*	0.62
KDM5B	1.95	*FAM185A*	0.62
RGS16	1.94	*CDKN1B*	0.52
SLC7A8	1.93		

Figure 6.4.3.1. Hierarchical clustering of transcripts differentially expressed in "D4 vs. T4". (A) Using "complete linkage" method, genes and samples from GL3 were clustered into five sub-clusters – four upregulated and one downregulated. Expression levels are coloured red for high and green for low intensities; colour bar values represent the Log_2 of intensities. **(B)** The 119 genes in GL3 are ranked according to expression fold change in D4 vs. T4.

These genes were clustered together, suggesting that they were co-regulated. This lends biological plausibility to the genes that are identified in this gene list. Thus,

T_h1 and T_h2 type cytokines were clustered together since IL-5 and IL-13 were co-expressed in sub-clusters 1 and 2, whereas TNFα and IL-1α were co-expressed in sub-clusters 3 and 4 (discussed below in Figure 6.4.4.2). Similarly, the expression of STAT-induced STAT inhibitors SOCS1–3 was differently regulated from that of cytokine receptors IL-2Rα, IL-2Rβ, IL-4R, and CSF2Rβ. The former were present in sub-cluster 2, and the latter in sub-cluster 4. Interestingly, anti-apoptotic B-cell CLL/lymphoma 2 (BCL2), immediate early response 3 (IER3), PIM1, and PIM2 were co-expressed together in sub-clusters 1+2, whereas pro-apoptotic nuclear receptor 4A1 (NR4A1), TNF receptor superfamily 10 (TNFRSF10), TNFα, and IL-1α located in sub-cluster 3+4.

The downregulated cluster included structural (tubulin cofactor C; TBCC), housekeeping (cyclin-dependent kinase inhibitor 1B; CDKN1B), and hypothetical of unknown function (FAM185A) genes, as well as an immune-related gene coding for a transcription factor (glucocorticoid-induced leucine zipper protein; TSC22D3).

In order to incorporate genes in *i*NKT cells that were specifically activated by contact with NHBE (i.e. to separate those activated by NHBE pulsed with α–GC), a more complex analysis was employed. Here the comparison between *i*NKT cells and baseline *i*NKT cells without contact with NHBE cells was integrated in the input by using GL4 (Table 6.4.3.1). To do this, the following instructions were given to 'R' for computation:

1- From GL1 take out all the genes that are also expressed in GL2 and create GL4. The removed genes are those that are activated by common factors and are shared between both GL1 and GL2. Therefore, GL4 is a list of genes on "D4 vs. 0h" which shows statistically different expression between D4 and 0h but

not between T4 and 0h;

2- Then, tabulate the fold change of genes in GL4 (i.e. “D4 vs. 0h”);

3- Identify genes in the “T4 vs. 0h” *original* (i.e. prior to statistical analysis) list which are present in GL4 and tabulate the fold change for these genes;

4- Put fold change for GL4 (from step 2) on “x” axis, and the same genes for “T4 vs. 0h” (identified in step 3) in “y” axis.

With this output graph (Figure 6.4.3.2), the following can be deduced:

a. In the grey area, genes are downregulated in both “D4 vs. 0h” and “T4 vs. 0h”;

b. In the blue area, genes are upregulated in at least one of “D4 vs. 0h” or “T4 vs. 0h”. To determine the degree of up- or down-regulation in “D4 vs. 0h” relative to “T4 vs. 0h”, look at the axis . For example, IRF4 is upregulated ×3.3 comparing D4 to 0h (“x” axis), but only ×1.1 comparing T4 to 0h (“y” axis);

c. The coloured lines give the subtractive *difference* (as + or –) in fold change in “D4 vs. 0h” compared to “T4 vs. 0h”. For example, the fold change of IRF4 is 3.3 – 1.1 = 2.2 larger in “D4 vs. 0h” compared to “T4 vs. 0h”. The lines are a visual guide to how much higher the genes are in one axis compared to the other (i.e. does not express the proportion or ratio of FC). The proportion of increase of IRF4, in this example, in “D4 vs. 0h” relative to “T4 vs. 0h” is 3.3 ÷ 1.1 = ×3.

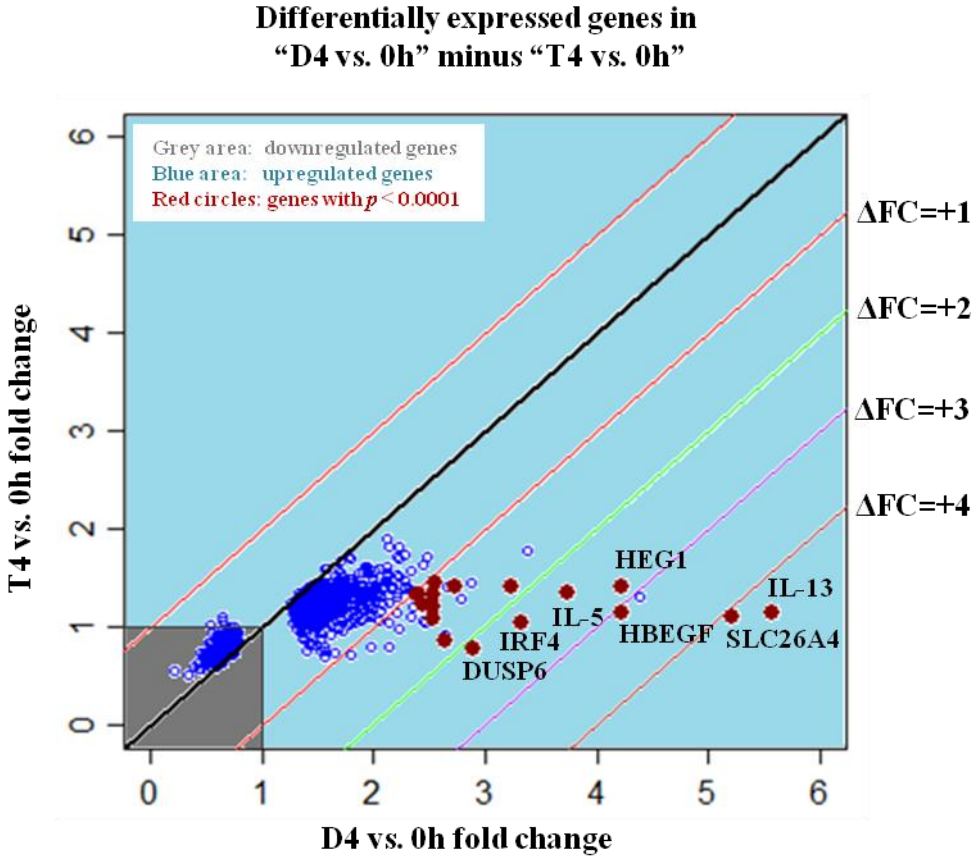

Figure 6.4.3.2. Averaged fold change of differentially expressed genes in D4 and T4 against 0h. Genes of GL2 were taken out from GL1, and the fold change (FC) of remaining genes which had a p of < 0.05 in GL1 together with corresponding FC in "T4 vs. 0h" were plotted (i.e. GL4). Diagonal lines indicate the difference in fold change (ΔFC) of differential expression between the two phenotypes. Filled circles represent highly differentially expressed (p < 0.0001) genes, amongst which, those with ΔFC > 2 are cited on the graph. Grey and pale blue areas contain the downregulated and upregulated genes, respectively.

Nineteen genes were highly differentially (p < 0.0001) expressed (Table 6.4.3.2). All of them were upregulated in "D4 vs. 0h" (skewed to the right on Figure 6.4.3.2 plot). Genes of T_h2 type immune response like IL-13, IL-5, and IL-4R, and pro-inflammatory cytokine IL-1α were present on this list.

Gene Symbol	Ref Seq ID	D4 vs. 0h	T4 vs. 0h	ΔFC	NCBI official full name
IL13	NM_002188	**5.58**	1.15	4.43	interleukin 13
SLC26A4	NM_000441	**5.21**	1.11	4.10	solute carrier family 26, member 4
HBEGF	NM_001945	**4.23**	1.16	3.07	heparin-binding EGF-like growth factor
HEG1	NM_020733	**4.23**	1.4	2.83	HEG homolog 1 (zebrafish)
IL5	NM_000879	**3.73**	1.36	2.37	interleukin 5
IRF4	NM_002460	**3.32**	1.05	2.27	interferon regulatory factor 4
DUSP6	NM_001946	**2.89**	0.78	2.11	dual specificity phosphatase 6
RNF19B	NM_153341	**3.23**	1.42	1.81	ring finger protein 19B
FRMD4B	NM_015123	**2.64**	0.86	1.78	FERM domain containing 4B
PGAP1	NM_024989	**2.53**	1.09	1.44	post-GPI attachment to proteins 1
IL1A	NM_000575	**2.73**	1.4	1.33	interleukin 1 alpha
STX11	NM_003764	**2.53**	1.21	1.32	syntaxin 11
NFKB2	NM_002502	**2.45**	1.24	1.21	nuclear factor of kappa light polypeptide gene enhancer in B-cells 2 (p49/p100)
IL4R	NM_000418	**2.53**	1.33	1.20	interleukin 4 receptor
ITGA2	NM_002203	**2.55**	1.46	1.09	integrin alpha 2
NFKBIZ	NM_031419	**2.41**	1.33	1.08	nuclear factor of kappa light polypeptide gene enhancer in B-cells inhibitor, zeta
NR4A1	NM_002135	**2.39**	1.33	1.06	nuclear receptor subfamily 4, group A, member 1

Table 6.4.3.2. Highly differentially expressed genes in D4 against 0h. Genes from GL4 with p of < 0.0001 are listed. The third and the fourth column show fold change (FC) in D4 and T4 versus 0h, respectively. Genes are ranked according to ΔFC between "D4 vs. 0h" and "T4 vs. 0h".

This analysis identifies the top genes that are directly activated due to contact with α–GC-pulsed NHBE cells. The highest differentially expressed genes are up- (rather than down-) regulated. These are IL-13, solute carrier family 26, member A4 (SLC26A4), heparin binding EGF-like growth factor (HBEGF), HEG homolog 1 (HEG1), IL-5, interferon regulatory factor 4 (IRF4), and dual specificity phosphatase 6 (DUSP6), which all had a p < 0.0001 (Table 6.4.3.2; top seven genes). The potential implication of these genes in *i*NKT function is explored in Discussion at the end of this chapter.

6.4.4 Functional relevance of gene expression profiles in *i*NKT cells activated by RECs

To functionally cluster and categorise genes that are differentially regulated between directly activated *i*NKT cells compared to those separated by transwell, GL3 ("D4 vs. T4") is used for analysis with DAVID. Table 6.4.4.1, shows the outcome derived from three annotated categories – "function", "pathway", and "gene ontology".

The most significantly enriched genes/pathways (i.e. with Benjamini *p* of < 0.05 and of highest "% Input" – i.e. the number of genes identified) were "cytokine", "Janus kinase (JAK)–signal transducer and activator of transcription (STAT) signalling pathway", and "regulation of apoptosis"; which comprised 14, 16, and 22 differentially expressed genes, respectively.

"D4 vs. T4"
Annotation clustering of genes – DAVID

Annotation	Term	Source	%Input	Benjamini *p* value
Function				
	Cytokine	SP-PIR	11.9	1.84E-8
	Cytokine receptor	SP-PIR	3.4	3.80E-3
	Proto-oncogene	SP-PIR	6.8	1.10E-2
Pathway				
	JAK-STAT signalling pathway	KEGG	13.6	6.19E-9
	Cytokine-cytokine receptor interaction	KEGG	15.3	7.34E-8
	Apoptosis	KEGG	5.9	7.16E-3
Gene Ontology				
	Regulation of apoptosis	GO Term-BP	18.6	1.20E-4
	Cytokine activity	GO Term-MF	11	1.36E-6
	TNF receptor binding	GO Term-MF	3.4	4.12E-2

Table 6.4.4.1. Functional clustering of genes in D4 vs. T4, using DAVID. Genes from GL3 (Table 6.4.3.1) were run against SP-PIR (Swiss-Protein and Protein Information Resource), and KEGG (Kyoto Encyclopaedia of Genes and Genomics) libraries, and gene ontology (GO) biological process (BP), and molecular function (MF) databanks. All with a Benjamini *p* of < 0.05 are listed. *%Input shows* the percentage of *genes in the gene list which were present in any given pathway*. In every category, sets or terms were ranked according to %Input, and those with the highest %Input (i.e. the most enriched) were highlighted in red.

Genes present exclusively in these three clusters and those shared between them are depicted in Figure 6.4.4.1. The "cytokine" cluster, for example, contained genes coding for chemokines CCL3 and CCL3L1, pro-inflammatory cytokines IL-1α, TNFα, and lymphotoxin alpha (LTA), and T_h2 type cytokines IL-5 and IL-13, as well as leukaemia inhibitory factor (LIF), CD40LG, and OSM genes. On the other hand, genes for cytokine receptors IL-2Rα, IL-2Rβ, IL-4R, and CSF2Rβ, and three members of the suppressor of cytokine signalling gene family (SOCS1–3) dominated the "JAK-STAT signalling" group. The "regulation of apoptosis" cluster included a combination of anti-

apoptotic genes like BCL2, BCL2-like 1 (BCL2L1), IER3, PIM1 and PIM2, and pro-apoptotic genes such as NR4A1, TNFRSF9, TNFRSF10, TNFα, and IL-1α.

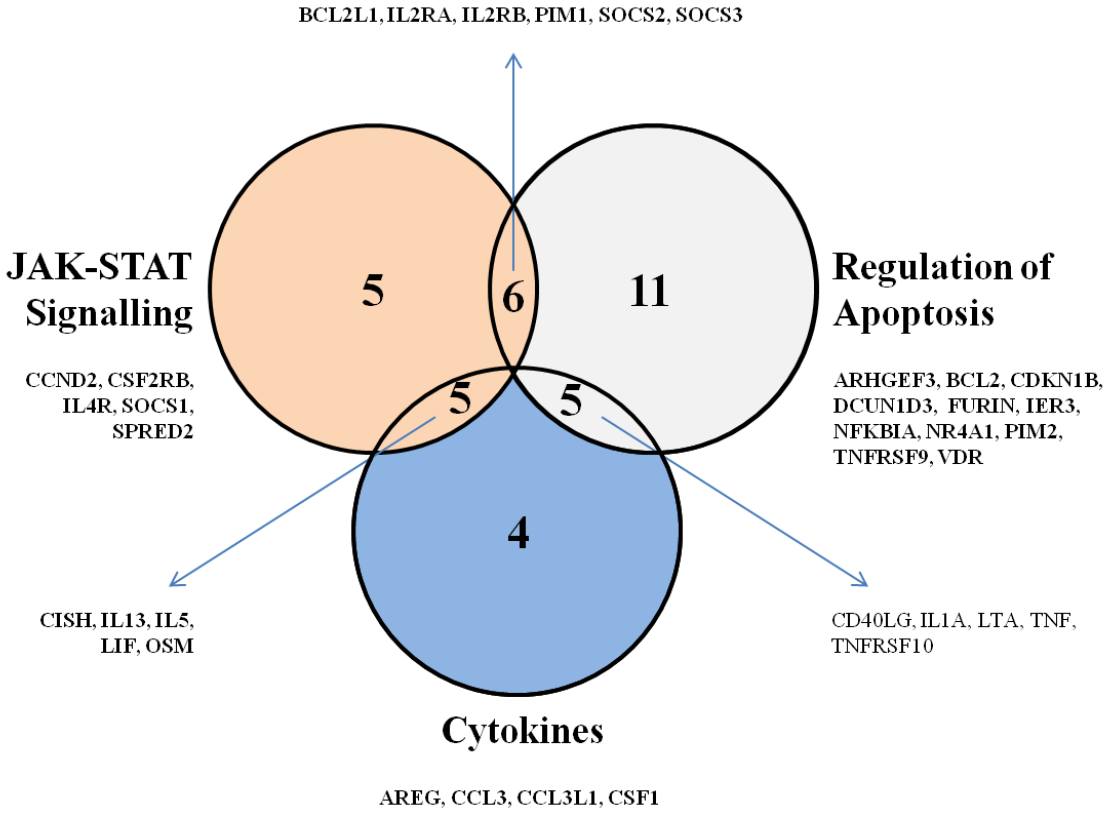

Figure 6.4.4.1. Venn diagram representation of highly enriched DAVID-identified gene clusters in "D4 vs. T4". The most significantly enriched pathways/gene categories from Table 6.4.4.1 are illustrated.

The relative expression of genes between D4 and T4 identified in the above three clusters is shown in Figure 6.4.4.2. The genes are grouped according to the sub-clusters in Figure 6.4.3.1A. As shown, genes of similar function or belonging to the same family (e.g. SOCS) are transcriptionally co-regulated. Furthermore, several of the genes identified in Figure 6.4.3.2, like IL-13 and IL-5, are represented here providing consistency in deductions using different analytical approaches.

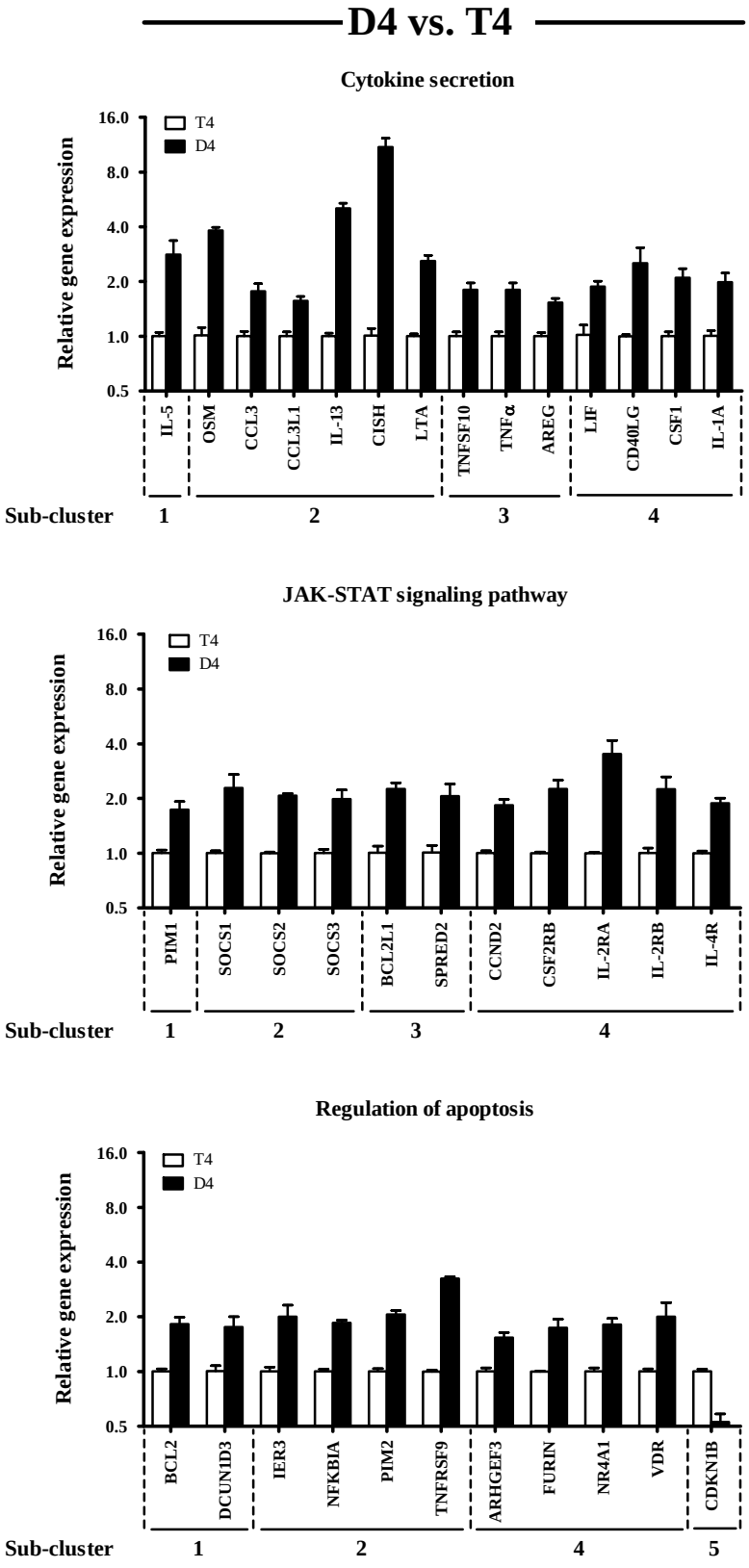

Figure 6.4.4.2. Relative expression of highly enriched DAVID-identified genes in "D4 vs. T4". Comparative expression of those genes in GL3 which were present in the top three DAVID-discovered gene categories – "cytokines", "JAK STAT signalling" and the "regulation of apoptosis" is illustrated. Genes were grouped according to their heatmap sub-cluster location in Figure 6.4.3.1A.

GSEA was also carried out in order to scrutinise the "whole genome" gene expression patterns, rather than focus on genes from a short gene list. Using GO "biological processes" databank, 23 pathways were specifically enriched in D4 compared to T4 (Table 6.4.4.2). Three pathways were related to apoptosis and programmed cell death, four pathways involved immune or inflammatory response, one covered the JAK-STAT signalling cascade, and one was cytokine and chemokine signalling. Example enrichment plots of this list are illustrated in Figure 6.4.4.3. Note the skewing of ES curves towards D4 (left side of the graphs).

"D4 vs. T4"
Gene-Set Enrichment Analysis (GSEA)

Gene Set Name	NES	FDR *q* Value
Inflammatory response	2.08	3.39E-02
Negative regulation of cellular protein metabolic process	2.02	2.53E-02
Regulation of protein amino acid phosphorylation	2.02	3.64E-02
Immune response	2.00	2.70E-02
Negative regulation of apoptosis	1.99	2.35E-02
Negative regulation of programmed cell death	1.97	2.22E-02
Negative regulation of protein metabolic process	1.95	2.42E-02
Response to wounding	1.92	3.54E-02
Negative regulation of developmental process	1.91	3.04E-02
JACK STAT cascade	1.91	3.37E-02
Regulation of small GTPase mediated signal transduction	1.89	3.41E-02
Anti-apoptosis	1.88	3.83E-02
Immune system process	1.87	3.97E-02
Immune effector process	1.86	3.79E-02
Cytokine and chemokine mediated signalling pathway	1.85	3.56E-02
Positive regulation of transduction	1.85	3.65E-02
Hormone secretion	1.85	3.77E-02
Positive regulation of nucleobase nucleoside nucleotide and nucleic acid metabolic process	1.85	3.98E-02
Generation of a signal involved in cell signaling	1.84	3.46E-02
Regulation of peptidyl tyrosine phosphorylation	1.84	3.50E-02
Regulation of protein modification process	1.83	3.53E-02
Response to external stimuli	1.83	3.61E-02
Negative regulation of cell differentiation	1.82	3.56E-02

Table 6.4.4.2. Gene sets enriched in epithelial-activated *i*NKT cells. In GSEA, averaged D4 expression values were compared and ranked against T4, and using GO "biological processes" databank those gene sets with FDR $q < 0.05$ (i.e. significantly enriched) in D4 were extracted. The sets were ranked by NES. FDR: false discover rate (see text); NES: normalised enrichment score (ES corrected for difference in the size of gene sets).

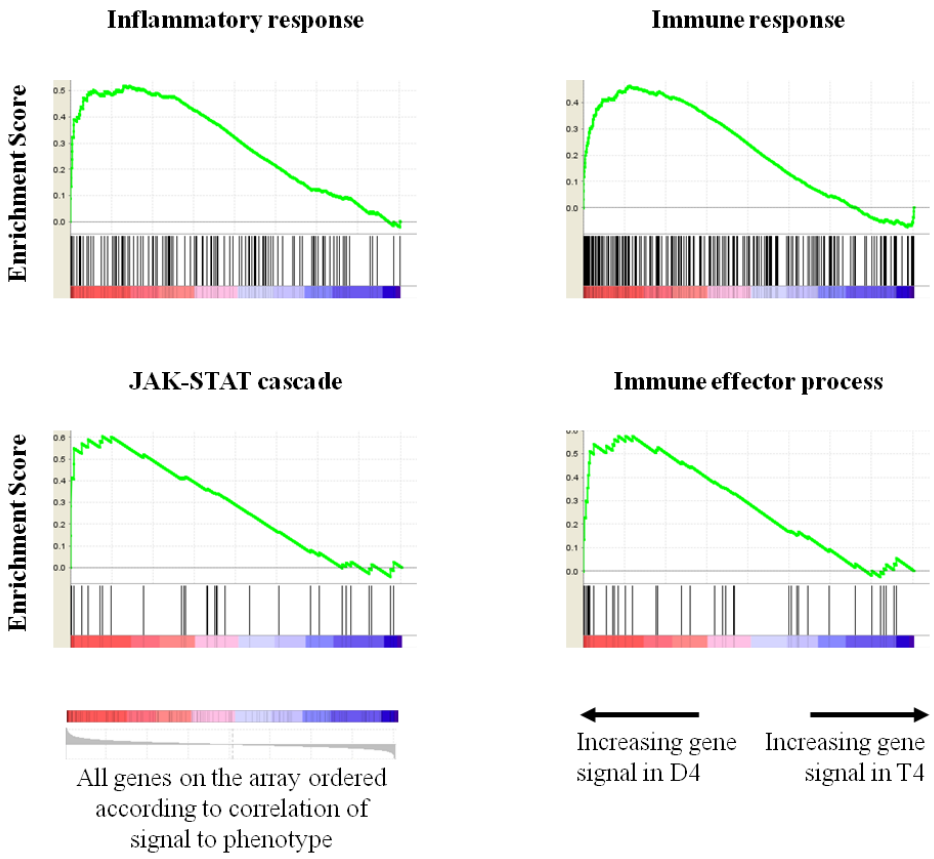

Figure 6.4.4.3. Examples of enrichment plots for four biological processes enriched in epithelial-activated *i*NKT cells. D4 is compared against T4. The red-blue strip represents the 26,626 genes expressed in the samples ranked according to differential expression between the D4 and T4 groups (hence phenotype). Each line in the 'bar code' represents presence of a gene from the GO-defined gene-set (e.g. immune effector process gene set) within the ranked genes. The enrichment score (ES; on "y" axis) is a running-sum statistic which increases when the gene in that particular gene-set is found in the ranked gene list and decreases otherwise. The changes are weighted such that the magnitude is greater if there is a strong correlation of the gene from the defined gene-set with phenotype (i.e. found towards the extreme ends of the ranked list). The leading-edge subset is defined as genes appearing at or before the running sum reaches maximum deviation from zero.

6.4.5 Changes in gene profiles comparing immediate and late time points after activation by RECs

So far, my analysis has been focused on identifying genes and gene sets differentially regulated between *i*NKT cells directly in contact with α–GC conditioned

NHBE-stimulated *i*NKT cells against those not, at an early (4h) time point. To examine whether different sets of genes are activated at a later time point, expression values from samples 12h post-co-culture should be used. Since RNA from T12 was not sufficient for labelling and chip hybridisation, comparisons like "D12 vs. T12", or "(D12 vs. 0h) vs. (T12 vs. 0h)" were not possible. However, the D12 data can be meaningfully analysed by following up the expression of significantly differentially expressed genes identified at 4h. That is, to identify the fold change expression values of "D12 vs. 0h" (i.e. GL5) on "D4 vs. 0h" – for all the 7964 genes and not just the 2637 genes on GL1 (Figure 6.4.5.1).

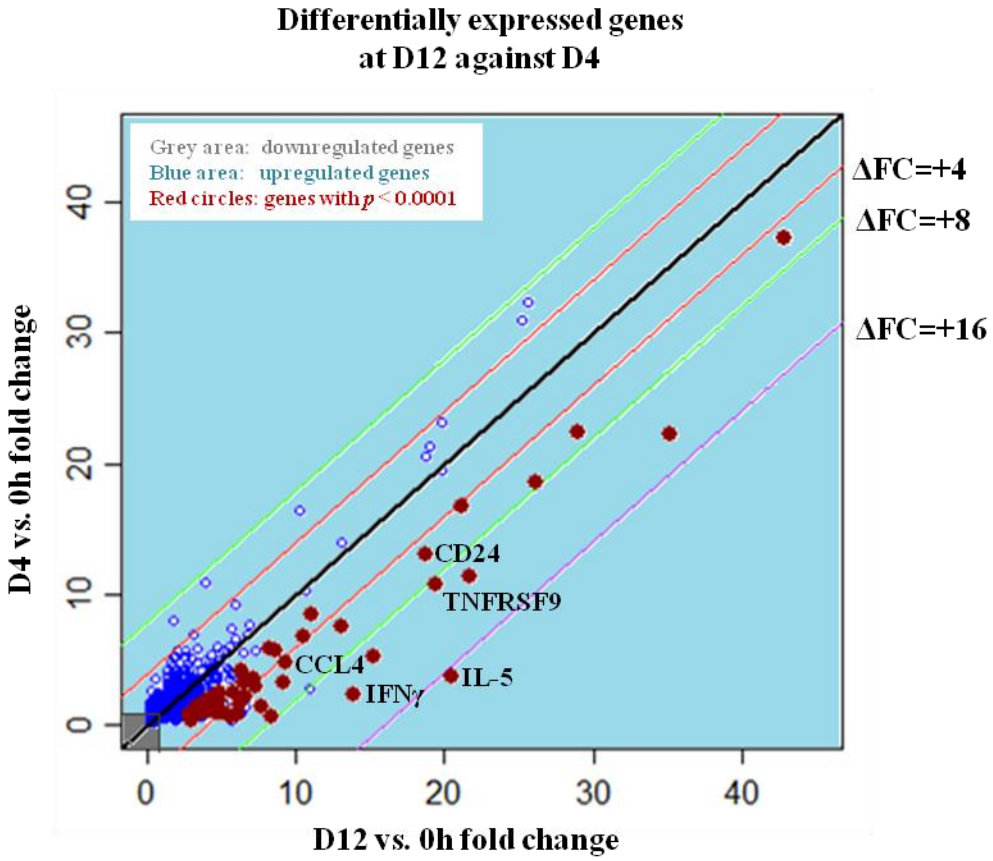

Figure 6.4.5.1. Averaged fold change of differentially expressed genes in D12 and D4 against 0h. GL5 (Table 6.4.3.1) genes were found on "D4 vs. 0h" list and then plotted against each other. Diagonal lines indicate difference in fold change expression (ΔFC). 53 genes were highly expressed ($p < 0.0001$) and had a ΔFC > 2 in D12 (filled circles), of which 13 were immune-related. Highly differentially expressed immune genes with ΔFC > 4 are cited on the graph.

From this analysis, 66 genes had a fold change difference of > 2 in "D12 vs. 0h" compared to "D4 vs. 0h" and were highly significant statistically ($p < 0.0001$) (Figure 6.4.5.1; genes in red). Of these, 13 were immune-related (Table 6.4.5.1). They included genes coding for both T_h1 (IFNγ) and T_h2 (IL-4, IL-5) type cytokines, chemokines (CCL1, CCL4, CXCL10), stimulatory cytokines (CSF2, LTA), an apoptosis-inducing enzyme (granzymes B; GZMB), and TNFRSF9. The non-immune genes and those with an apparent epithelial origin (e.g. keratins) are listed in Table 6.4.5.2.

Gene Symbol	Ref Seq ID	D4 vs. 0h	D12 vs. 0h	ΔFC	NCBI official full name
IL5	NM_000879	3.73	**20.44**	16.71	interleukin 5 (colony-stimulating factor, eosinophil)
IFNG	NM_000619	2.31	**13.95**	11.64	interferon, gamma
TNFRSF9	NM_001561	10.69	**19.44**	8.75	tumour necrosis factor receptor superfamily, member 9
CD24	NM_013230	13.00	**18.71**	5.72	CD24 molecule
CCL1	NM_002981	1.59	**6.27**	4.69	chemokine (C-C motif) ligand 1
CCL4	NM_002984	4.83	**9.31**	4.49	chemokine (C-C motif) ligand 4
IRF6	NM_006147	5.71	**8.58**	2.87	interferon regulatory factor 6
CXCL10	NM_001565	1.08	**3.85**	2.77	chemokine (C-X-C motif) ligand 10
GZMB	NM_004131	2.36	**4.86**	2.5	granzyme B (granzyme 2, cytotoxic T-lymphocyte-associated serine esterase 1)
IL21	NM_021803	1.07	**3.31**	2.24	interleukin 21
LTA	NM_001159740	1.79	**3.86**	2.07	lymphotoxin alpha (TNF superfamily, member 1)
CSF2	NM_000758	1.58	**3.61**	2.03	colony stimulating factor 2 (granulocyte-macrophage)
IL4	NM_000589	1.38	**3.39**	2.01	interleukin 4

Table 6.4.5.1. Highly differentially expressed immune genes in D12 against 0h. Immune-related genes from GL5 (Table 6.4.3.1) with p of < 0.0001 whose expression is > 2 folds greater than D4 are listed.

Gene Symbol	NCBI official full name
S100A8	S100 calcium binding protein A8
SPRR3	small proline-rich protein 3
SLC26A4	solute carrier family 26, member 4
FABP5	fatty acid binding protein 5 (psoriasis-associated)
SCARNA9	small Cajal body-specific RNA 9
KRT6A	keratin 6A
SERPINB2	serpin peptidase inhibitor, clade B (ovalbumin), member 2
PMCH	pro-melanin-concentrating hormone
SERPINB3	serpin peptidase inhibitor, clade B (ovalbumin), member 3
KRT6C	keratin 6C
DSG3	desmoglein 3 (pemphigus vulgaris antigen)
SKIV2L	superkiller viralicidic activity 2-like (S. cerevisiae)
RNU2-1	RNA, U2 small nuclear 1
SNORD116-24	small nucleolar RNA, C/D box 116-24
PRAMEF10	PRAME family member 10
SCARNA9L	small Cajal body-specific RNA 9-like (retrotransposed)
KRT23	keratin 23 (histone deacetylase inducible)
S100A9	S100 calcium binding protein A9
SCEL	sciellin
KRT6B	keratin 6B
SNORD116-15	small nucleolar RNA, C/D box 116-15
SNORD116-20	small nucleolar RNA, C/D box 116-20
TM4SF1	transmembrane 4 L six family member 1
SNORD116-14	small nucleolar RNA, C/D box 116-14
MMP1	matrix metallopeptidase 1 (interstitial collagenase)
UBTFL1	upstream binding transcription factor, RNA polymerase I-like 1
SPINK5	serine peptidase inhibitor, Kazal type 5

Gene Symbol	NCBI official full name
CSTA	cystatin A (stefin A)
FAM74A3	family with sequence similarity 74, member A3
PLS3	plastin 3 (T isoform)
ANKRD20B	ankyrin repeat domain 20B
HEPHL1	hephaestin-like 1
SNORD116-29	small nucleolar RNA, C/D box 116-29
SNORD116-17	small nucleolar RNA, C/D box 116-17
DDR1	discoidin domain receptor tyrosine kinase 1
SNORD4A	small nucleolar RNA, C/D box 4A
NOC3L	nucleolar complex associated 3 homolog (S. cerevisiae)
RPS26	ribosomal protein S26
SNORD14C	small nucleolar RNA, C/D box 14C
KRT17	keratin 17
CT47A6	cancer/testis antigen family 47, member A6
MYO1B	myosin IB
GPR64	G protein-coupled receptor 64
ALDH1A3	aldehyde dehydrogenase 1 family, member A3
LOC442132	similar to hypothetical protein FLJ36144
CEACAM6	carcinoembryonic antigen-related cell adhesion molecule 6
KRT16	keratin 16
SLC7A8	solute carrier family 7, member 8
RNF5P1	ring finger protein 5 pseudogene 1
LOC391742	TBP-associated factor 11 pseudogene
CCHCR1	coiled-coil alpha-helical rod protein 1
PRR13	proline rich 13
CC2D2B	coiled-coil and C2 domain containing 2B

Table 6.4.5.2. Highly differentially expressed non-immune and epithelial-derived genes in D12 against 0h. Genes unlikely to be involved in immune response or with clear epithelial origin from GL5 that had a p of < 0.0001 and ΔFC > 2 in D12 than D4 are listed.

Examining the time-course change in expression of the 13 immune-related genes, all showed an increase at the 12th hour compared to the 4th hour (Figure 6.4.5.2), suggesting a progressive increase in activation. Some genes appear to be activated to near maximal capacity by the 4th hour (the ones that are plateauing – e.g. CD24, IRF6) while others becomes more highly activated later (the ones that show a steep change between 4th and 12th hour e.g. IFNγ, GZMB, CCL1, CCL4).

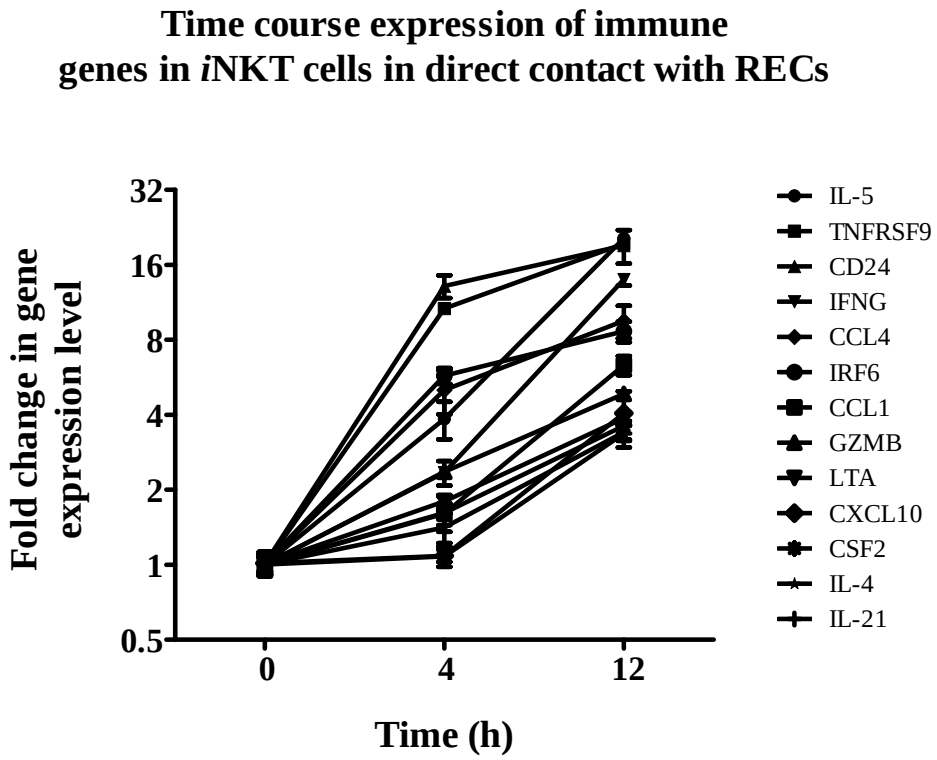

Figure 6.4.5.2. Time course change in expression of highly expressed immune-related genes in D12 and D4 from 0h. Gene had a *p* of < 0.0001 and ΔFC > 2 in D12. N= three samples (normalised microarray data).

6.5. Discussion

In this chapter, I first demonstrated that exogenous glycolipid-loaded CD1d on RECs can directly engage with, and stimulate *i*NKT cells. Epithelial-activated *i*NKTs induced production of a variety of cytokines as shown by intracellular cytokine staining. The activation was absent in transwell-separated *i*NKT cells and was significantly diminished in the presence of CD1d blocking mAb; which indicates the requirement for direct interaction between CD1d and *i*NKT TCR. The cause for the partial reduction in activation with CD1d blocking could be incomplete blocking of the CD1d sites or the possibility that direct CD1d engagement only contributed to some of the *i*NKT cell activation.

It is well established that upon ligation of its invariant TCR by glycolipid presented by CD1d on professional APCs, *i*NKT cells rapidly secrete large quantities of both T_h1 and T_h2 type cytokines [3]. Here, I show that human bronchial epithelial cells can do the same. *i*NKT cells produced high levels of IFNγ, TNFα, IL-4, IL-5, and IL-13 in as short as 4h after co-culture. This lack of polarisation in T_h1 and T_h2 cytokines (Figure 6.4.1.1) contradicts somewhat the finding in Figure 6.4.3.2 where IL-5 and IL-13 was very highly over-expressed. One reason could be that intracellular cytokine staining is a qualitative rather than quantitative measure and may not reflect the relative amount of IL-5 and IL-13 production compared to IFNγ. Another possibility is that stimulation of IL-13 and IL-5 may well be contributed in a greater part by the non-CD1d-TCR activation process e.g. by soluble factors produced by RECs upon stimulation by *i*NKT cells. This path, often referred to as 'indirect *i*NKT cell activation' is increasingly recognised as a major component of *i*NKT cell stimulation [270]. An alternative explanation is that *i*NKT cells activate constitutive transcription of IL-4 and

IFNγ genes during their thymic development [97]. It has been shown that comparable amounts of mRNA for these two cytokines exist between *i*NKT and differentiated $CD4^+$ effector T cells [97]. As a result, it can be expected that during the early hours after stimulation *i*NKT cells IL-4 and IFNγ using the transcript reservoir they acquired during thymic development. But as the stimulation lasts, they start upregulating the gene expression.

The net DNA microarray profile in directly-activated *i*NKT cells provides a wider view of the consequence of *i*NKT cell activation as a result of contact with α–GC-pulsed RECs. I used transwell separation to completely prevent *i*NKT cells contact with RECs, but this has its own limitations. For example, it could be argued that other interactions like CXCR6-CXCL16 between *i*NKT cells and RECs are also abolished by transwell separation. One method of narrowing the output to CD1d-*i*NKT TCR engagement would be to use CD1d blocking mAbs. However, this suffers from the variable effects of incomplete blockade and I reasoned that the composite analysis of α–GC-pulsed REC compared to unstimulated RECs comparing transwell and no transwell use came close to the right study design for my question.

In addition to stimulation of cytokine secretion, whole genome profiling of *i*NKT cells as described, showed upregulation of several genes belonging to JAK-STAT pathway as early as 4h after direct co-culture. The typical pathway is composed a cytokine or a growth factor (GF), a cytokine receptor, and an intracellular signalling cascade (comprising STATs and JAKs) which mediates the transcription of target genes (e.g. SOCS) [291]. In resting state, the STAT proteins (a family comprising seven members, namely STAT1–4, STAT5a, STAT5b, and STAT6 [292]) reside unphosphorylated in the cytosol. Upon cytokine or GF binding to the surface receptor,

JAK kinases (a family of four protein tyrosine kinases, including JAK1–3, and Tyk2 [293]) activate the STATs by phosphorylation and lead to translocation of phospho-STAT dimers to the nucleus, where they function as transcription factors [291]. In conjunction with that, there was a significant enrichment of genes in *i*NKT cells which encode for candidate ligands, receptors, and downstream STAT-induced targets of this pathway; such as OSM, IL-13, CSF2 (GM-CSF), IL-4R, CSF2Rβ, CISH and SOCS1–3. The overall picture is that of rapid engagement of *i*NKT cells with stimulation of a programme of immune activity – evident from the increased expression of pro-immune cytokine-related signalling (JAK-STAT) and cytokines, and apoptosis, a natural consequence of cell activation. The most accurate interpretation is that interaction between *i*NKT cells and RECs is not a passive event – this induces a very robust immune activation in *i*NKT cells. In my experiment, it is very likely at least some and possibly all of this is due to glycolipid presentation by CD1d expressed on RECs.

One interesting gene not previously reported to be expressed or induced in *i*NKT cells is oncostatin M (OSM) (3.8 folds higher in D4 than T4). OSM is a multifunctional cytokine and a member of the IL-6 cytokine family, which also includes IL-6, IL-11, and LIF [294,295]. It is produced by activated T cells and monocytes [295,296] and signals through a heterodimer complex of gp130 (also called CD130) – the common subunit of all IL-6 cytokine family receptors, and LIF receptor (LIFR), or gp130 and OSM receptor β chain (OSMRβ) [297]. Ligation of OSM receptors result in control of differentiation (e.g. of megakaryocytes), function (e.g. induction of inflammatory response or regulation of cholesterol metabolism), and proliferation (e.g. inhibition of tumour cell growth) of the target cells [298]. The gp130 subunit of the receptor is ubiquitously expressed by all cell types [299]; but, OSMRβ is primarily

expressed on keratinocytes [296,300], airway and intestinal epithelial cells [301-303], as well as haematopoietic cells. Therefore, it is possible that OSM produced by *i*NKT cells can act on RECs and possibly modulate the function and proliferation of epithelial cells. Indeed, OSM has been shown to attenuate the growth and proliferation of bronchial epithelial cells in *ex vivo* cultures [303], and to potently stimulate the secretion of α1-antitrypsin (α1-AT) – the main inhibitor of serine proteases and a key player in lung homeostasis, from type II pneumocytes [304,305]. Similarly, OSM reduced HCV viral load and augmented the antiviral activity of IFNα in infected hepatocytes [306].

Another example of a previously unreported family of genes in *i*NKT cells found upregulated in *i*NKT cells after direct contact with α–GC pulsed NHBE cells is the SOCS family of genes. SOCS represents a family of eight SH2-containing proteins (SOCS1–7, CISH) with structural and functional homology [307]. They are cytokine-inducible and act as part of a negative feedback system which regulates cytokine signal transduction. In unstimulated cells, SOCS1–3, for example, are transcribed at low levels; however, they are rapidly induced within minutes to hours upon cytokine stimulation [307]. SOCS1 is the key inhibitor of IFNγ signalling [308,309], whereas SOCS3, together with SOCS1, play a critical role in cellular responsiveness to IL-4 and IL-13 [310-312]. Furthermore, IL-6 signalling through gp130 and the activity of CSF2 is limited by SOCS3 [313-315]. CSF2 signalling is also restricted by CISH and PIM1 [316]. SPRED1 – a negative regulator of Ras-ERK pathway, suppresses IL-5 dependent ERK activation and the cell proliferation in T cells [317]. In my experiments there was induced levels of IFNγ, IL-13, IL-5, CSF2, IL-4R (which binds both IL-4 and IL-13), and CSF2Rβ along with SPRED2, PIM1, CISH and SOCS1–3 in REC-activated *i*NKT

cells. This suggests that stimulated *i*NKTs are triggered to upregulate genes encoding both the cytokines and their receptors for these cytokines. This, in turn, leads to upregulation of downstream regulatory molecules which form a feedback system to control *i*NKT cytokine production (Figure 6.5.1).

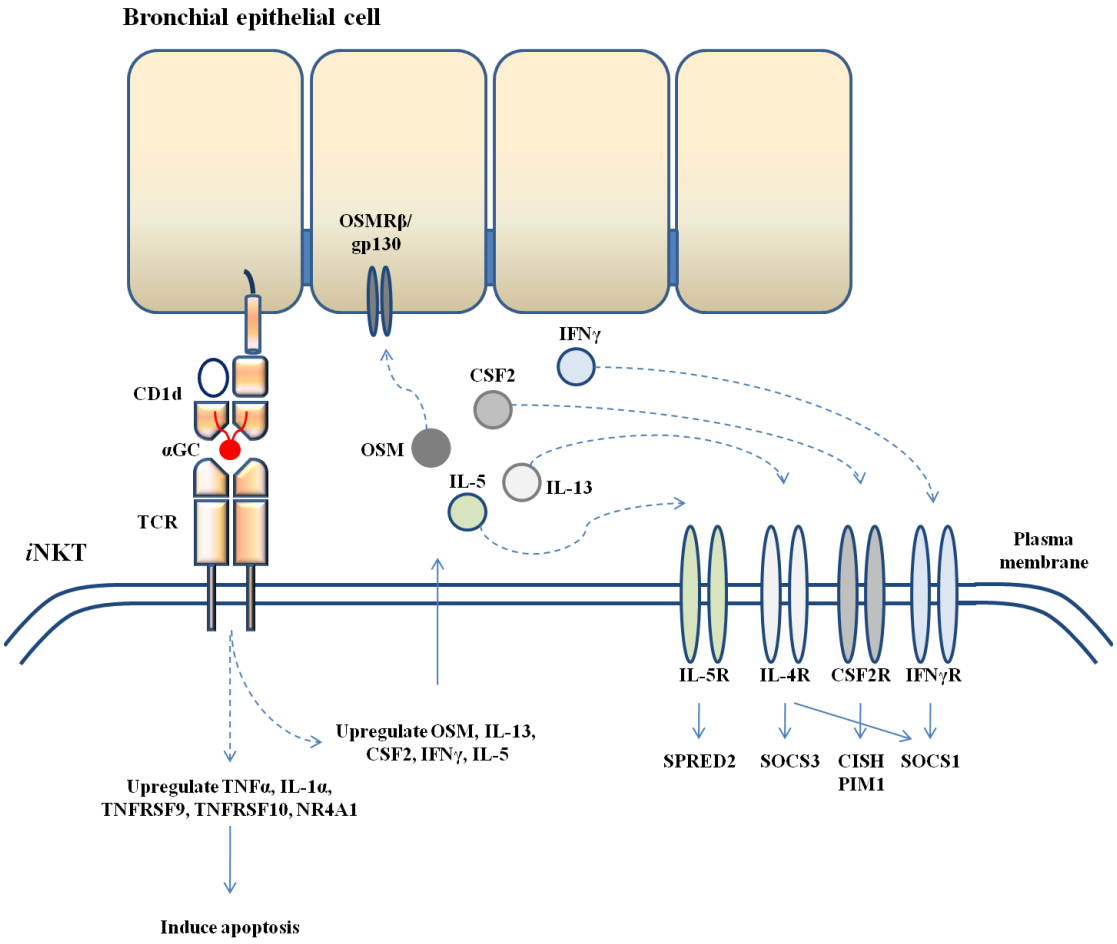

Figure 6.5.1. Summary of one proposed consequence of interaction between REC CD1d and TCR on *i*NKT cells.

The GSEA and DAVID analyses identified enrichment of both pro- and anti-apoptotic genes in *i*NKT cells that were stimulated by direct contact with RECs. Studying the occurrence of apoptosis by flow cytometry using anti-annexin V mAb and DNA dye 7–AAD (Result in Appendix 2). This was placed in Appendix since it is the beginning of validation experiments; the subject of my next project). This helped in

clarifying this paradoxical gene expression patterns by showing that the final outcome is heavier on induction rather than prevention. This is consistent with *in vivo* studies which showed commitment to apoptosis in α–GC-activated *i*NKT cells [120,121]. Since, apoptosis is an interplay between pro- and anti-apoptotic molecules, the upregulation of anti-apoptotic BCL2 genes may be part of a negative regulatory mechanism to control excessive activation of apoptosis [318] or possibly an indirect facilitator of cell death (see below).

Several pro-apoptotic genes were differentially expressed in REC-stimulated *i*NKT cells, including NR4A1, TNFα, IL-1α, TNFRSF9, and TSC22D3. Of these, TNFRSF9 is potentially the most interesting. TNFRSF9 is a T cell costimulatory receptor which is induced on activated T cells [319]. Its natural ligand – TNFSF9 (CD137L; 4-1BBL), is detected on the surface of DCs, macrophages and mature B cells [320,321]. Signalling through TNFRSF9 leads to cytokine secretion and functional maturation of T cells [319,322]. Some studies have suggested a pro-apoptotic role for this receptor, especially when exposed to TNFα [323,324]. Costimulation via TNFRSF9 increases FasL expression in $CD4^+$ T cells which leads to induction of apoptosis in FasL-sensitive target cells [325]. *i*NKT cells are known to have cytolytic function [103] but it is unclear whether this is the function of a subset of the *i*NKT cells or an induced function in all *i*NKT cells. In addition, it is not understood how and what triggers cytolytic *i*NKT cells to kill a target. Upregulation of TNFRSF9 on activated *i*NKTs by induction of CD1d could be a mechanism. It is known that *i*NKT cells exhibit cytolytic activity by secreting granzymes B, or expressing FasL and TNF-related apoptosis inducing ligand (TRAIL) on their surface [3]. The results from 4^{th} vs. 12^{th} hour stimulation show that GZMB was progressively upregulated with time. This supports

the theory of functional plasticity in *i*NKT cells where a cytokine-producing *i*NKT cell acquires cytolytic function later in its activation programme. From another angle, signalling through TNFRSF9 is required for generation and expansion of virus-specific $CD8^+$ T cells after *in vivo* influenza virus challenge [326,327]. It may be interesting to show whether RECs express the appropriate ligand and can interact with $CD8^+$ T cells as well as *i*NKTs.

TSC22D3 was one of the few genes which were downregulated in "D4 vs. T4". The protein product of this gene is reported to protect T cells against IL-2 withdrawal or TCR-induced apoptosis, by downregulating Fas [328] and pro-apoptotic factor BIM [329]. Therefore, it can be deduced that downregulation of this gene is associated with enhanced susceptibility of *i*NKTs to apoptosis induction. This may be beneficial to provide a 'clean' programmed death so that *i*NKT cells activation is associated with minimal inflammation (unlike death from necrosis).

*i*NKT cells exhibited a higher potency for cytokine synthesis (e.g. IFNγ and IL-5) and a stronger response for chemokine production at 12h, compared with 4h, following direct co-culture with RECs. The expression of CCL4 and CCL1, for instance, was more than doubled in "D12 vs. D4". CCL4 (also known as MIP-1β) is a beta chemokine that induces adhesion and migration of various T cell subsets *in vitro* and *in vivo* [330], such as $CD4^+$ $CD25^+$ Tregs [331] and $CD8^+$ T cells [332]. CCL1 is secreted from activated T cells and preferentially chemoattracts monocytes, T_h2 cells, and Tregs to the site of inflammation [333-336]. This suggests that *i*NKTs, after initial interaction with RECs, could potentially influence the local immunity by recruiting Tregs and other inflammatory cells like monocytes.

Besides cytokines and intracellular signaling molecules, the induced expression of CD24, CD69, and CD40L confirms the activation of *i*NKT following direct interaction with REC. CD24 (also known as heat-stable Ag) is rapidly, but transiently, induced on T cells after engagement of TCR-CD3 complex [337] and is required for optimal homeostatic proliferation of both $CD8^+$ and $CD4^+$ T cells *in vivo* [338]. CD69 is a stimulatory receptor which is widely studied as an early activation marker on stimulated *i*NKTs [339-341]. Ag-activated *i*NKT cells upregulate CD40L that after binding with CD40 on the surface of APCs stimulates their IL-12 production [105]. Downregulation of surface CD4 was also observed at the 12^{th} hour after *i*NKT activation. This could be relevant to the idea of functional plasticity described earlier since $CD4^-$ *i*NKT cells have been shown to have greater cytolytic activity than $CD4^+$ cells [260].

Production of IL-13, IL-4, IL-5, IFNγ, and TNFα as studied by flow cytometry validates some of the gene expression array data at protein level. The work here provides a platform for the validation of new hypotheses generated from examination of the gene expression profile. From this work, I would be most interested in validating the expression and examining the role of OSM and TNFRSF9 as described. This is the basis of one of my future projects.

6.6. Conclusion

In conclusion, the results of this chapter show that RECs can present α–GC to, and activate *i*NKT cells in a CD1d-dependent process. Using whole genome expression profiling, it was found that *i*NKT cells express a distinct profile of genes when in direct

contact with α–GC-bound CD1d on RECs, compared to cells separated by transwell membranes. Here early biological pathways were dominated by cytokine and chemokine related genes (JAK-STAT signaling pathways, cytokine-responsive elements and cytokine/chemokine genes) and apoptosis-related genes. This suggests that glycolipid-bound CD1d on REC is capable of inducing a programme of immune activation in *i*NKT cells.

Chapter 7. Function of CD1d on respiratory epithelial cells – influence of CD1d expression on respiratory epithelial cells during influenza virus infection

Chapter 7.

Function of CD1d on respiratory epithelial cells – influence of CD1d expression on respiratory epithelial cells during influenza virus infection

7.1. Aims

The aim of this project is to two fold – to study the consequence of CD1d absence in RECs *in vivo* during influenza A virus (IAV) infection, and to explore differential gene expression patterns in RECs of wild type and CD1d-deficient mice after IAV infection.

7.2. Introduction

The results of the last two chapters demonstrated inducible CD1d expression with viral associated signals in RECs, and the ability of CD1d-expressing REC to activate *i*NKT cells. However, it is unclear if (and how) CD1d expression on REC influence epithelial cell function in an immune context. Very limited literature is available on the function of CD1d in CD1d-expressing cells. Colgan *et al* demonstrated that ligation of intestinal epithelial CD1d mounts an anti-inflammatory response by inducing production of IL-10 [342]. In another study, crosslinking surface CD1d on penile urethral epithelial cells promoted IL-12 and IL-15 production [61]. However, both reports used epithelial cell lines, rather than primary cells, and the results were demonstrated in an *in vitro* system, rather than *in vivo* in the context of inflammation or infection.

In this chapter, I first examine the outcome of IAV infection in CD1d-deficient mice compared with wild type mice, and then set up and use a protocol for purification of RECs to compare gene expression profiles of epithelial cells from CD1d-deficient and wild type mice after viral challenge.

7.3. Methods

7.3.1. Overall experimental design

Wild type C57BL/6 (here after referred to as WT) and $CD1d^{-/-}$ mice on C57BL/6 background (hereafter referred to as CD1dKO) mice were inoculated with a sub-lethal dose of influenza virus A/Puerto Rico/8/34 H1N1 (heron referred to as "PR8") strain, and their weight change monitored for 14 days. After observing a differential outcome between the two groups of mice, a protocol for isolating pure RECs was established. Next, mice were infected with PR8, and RECs on day 0 (no IAV infection), and days 3 and 6 post-viral challenge were purified and analysed for their profiles of gene expression by DNA microarray.

7.3.2. IAV infection in mice and study design

In the first study, WT and CD1dKO mice were intranasally infected with 3.5 HAU/mouse of PR8 in 20µl inoculum (PBS), and monitored daily for weight loss until 14 days after infection. Ten WT and nine CD1dKO mice were used.

For the genomic profiling of REC, 30 mice per group were used. 10 mice from each group were sacrificed prior to viral challenge (D0) and the same again on D3 and

D6 after IAV challenge. At each time point, the RECs from the mice were isolated, purified, and pooled as described in the Results section 7.4.2 below, and RNA extracted and used for microarray analysis (Figure 7.3.3.1).

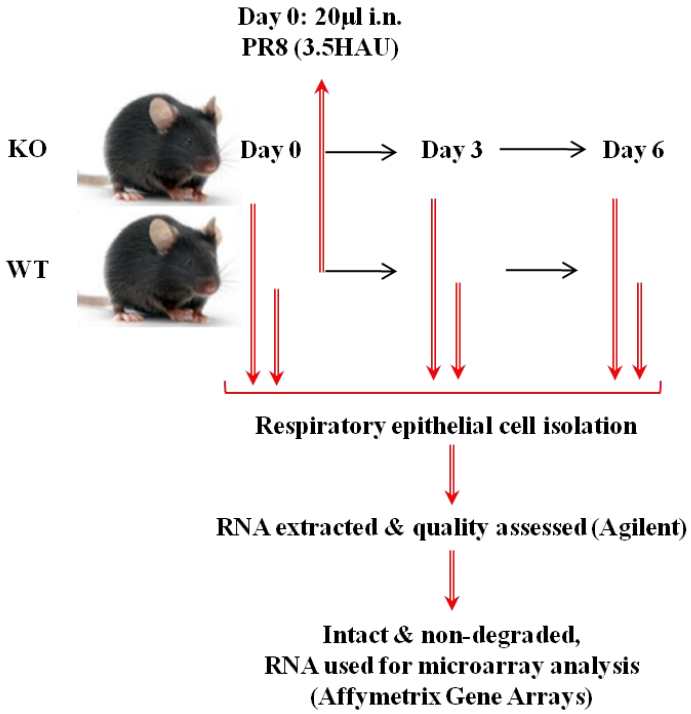

Figure 7.3.3.1. Experimental design for microarray analysis of IAV-infected RECs in WT versus CD1dKO mice. RECs were purified on day 0 prior to challenge, and days 3 and 6 after infection with PR8, from CD1dKO and WT mice, and their RNA extracted.

CD1d presence or absence in the RECs from CD1dKO and WT mice was examined by RT-PCR, using primers designed as described (Chapters 2.2.4 and 2.2.5). The sequence of primers used is listed in Table 7.3.3.

Primer	Sequence (5′→3′)
CD1D1	
Forward mCD1D1.	*GTCCCAGGGCAAGTTGAGTAAC*
Reverse mCD1D1.	*CTTGATCAGCGTTGAGCACTTT*

Table 7.3.2.1. PCR primers used in this chapter and their nucleotide sequence.

7.3.3. Gene expression analysis and interpretation of RECs

RNA extraction, quality control of samples and pre-processing of data for analyses were performed as described in Chapter 6. Identical gene chips (Affymetrix Gene ST 1.0 array, but for mouse rather than human) were used.

As before, three approaches were taken, to interpret the output from the study, described in greater detail in the relevant Results sub-headings. In the first approach, comparisons were made using the two groups of interest and a "Gene List (GL)" was generated – this being the genes that were more than two fold differentially expressed between the two groups. Since there was only one group (comprising 10 mice) per analysis point, no statistical significance could be generated, unlike Chapter 6. In the second approach, a more involved analytical approach was designed with 'R' to enhance mathematical significance and interpretation of the final gene list. Finally, as before, GSEA and DAVID were used to evaluate the biological functions of the differentially expressed genes.

7.4. Results

7.4.1 Transgenic CD1d-deficient mice show poorer outcome after IAV infection

CD1dKO mice had a poorer outcome after IAV infection compared to WT – although no significant difference in weight loss was found, and less mice survived the infection - 4/9 in CD1dKO (44%) vs. 9 of 10 WT survived by day 14. In collaboration with Vincenzo Cerundolo, viral titres (performed by Carmela De Santo) in lung homogenates of CD1dKO mice were significantly higher on day 6 after infection compared to WT [140]. This increase in viral titres was not reversed by adoptive transfer of *i*NKT cells [140], suggesting that deficiency in CD1d rather than loss of *i*NKT cells (also observed in *i*NKT-deficient mice) was responsible for the observations.

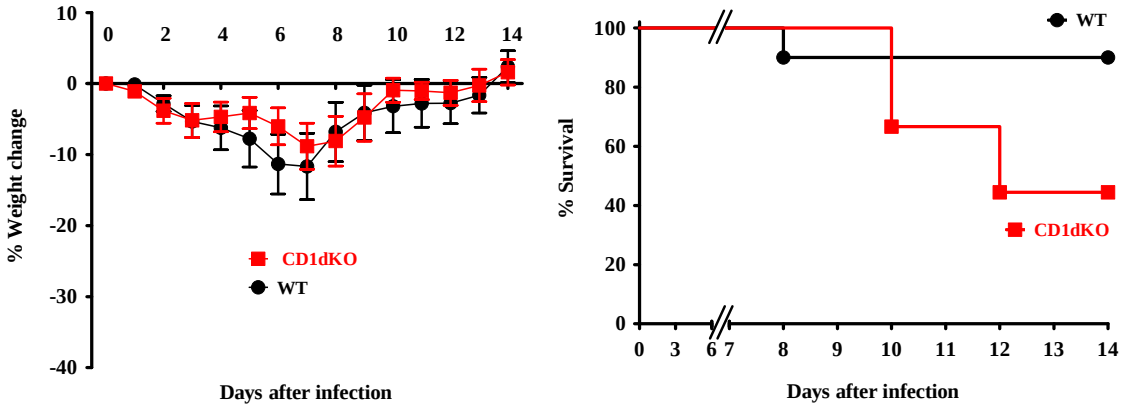

Figure 7.4.1.1. Weight change and survival rate of CD1dKO compared with WT mice after infection with IAV. Comparable results were obtained from three independent experiments. N= 10×WT and 9×CD1dKO.

7.4.2 Isolation of a pure population of mouse RECs

To examine the genomic expression pattern in RECs, it is necessary to obtain a pure population of airway epithelial cells. To do this, a REC-specific Ag which is expressed on the cell surface and does not require cell permeabilisation or fixing is required.

The major epithelial cell types in lungs are ciliated columnar, Goblet (mucous-secreting), Clara (non-ciliated non-mucous secretory), serous, basal, neuroendocrine (containing nerve endings and the ability to secret endocrine hormones), and type I and II alveolar epithelial cells [343-350]. A number of molecules have been reported which specifically localise to different epithelial subtypes. These include β-tubulin IV [265] and cytokeratin 18 [264] for ciliated cells, mucin 5AC (MUC5AC) for mucous and type II alveolar epithelial cells [351], Clara cell-specific protein 10 (CC10) [346], lactoferrin and lysozymes for serous cells [352], cytokeratin 13 and tissue factor for basal cells [345], and cholecystokinin (CCK)-like peptide for neuroendocrine cells [353]. However, most of these molecules are either secreted outside the cell or retained intracellularly, which requires membrane permeabilisation for isolating corresponding cells. The ideal cell marker is expected to be present predominantly on the cell surface.

Surface adhesion molecules are potential candidates which meet this requirement. I tested two adhesion molecules – E-cadherin (E-cad), and epithelial cell adhesion molecule (EpCAM).

E-cad is a member of the cadherin superfamily which is widely expressed on apico-lateral surface of epithelial cells lining the mucosa [354-357]. To verify

epithelial specificity of E-cad, whole lungs were immunostained with anti-E-cad mAb (Figure 7.4.2.1). As expected, only epithelial cells stained positive.

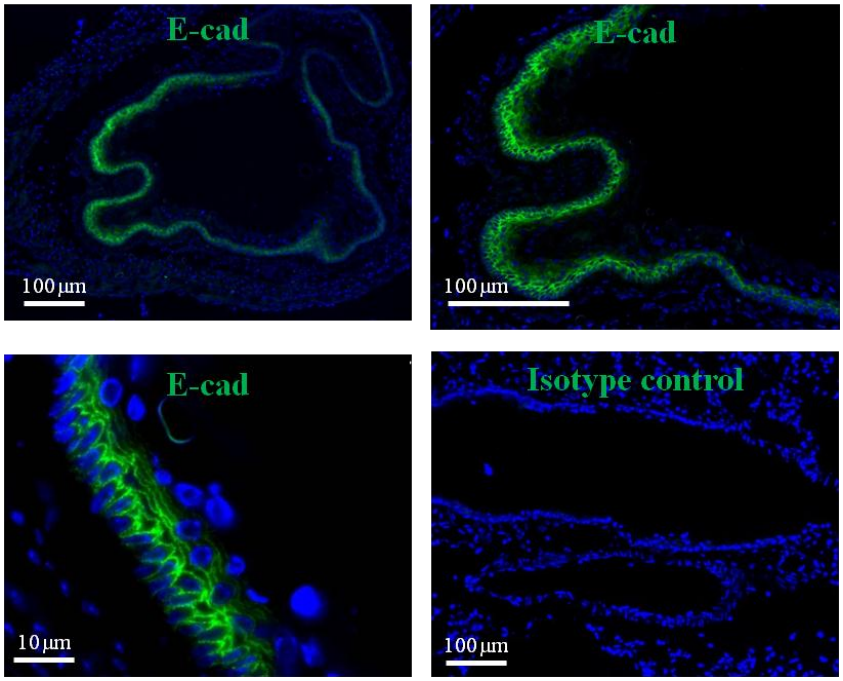

Figure 7.4.2.1. Expression of E-cadherin in mouse lungs. Representative immunofluorescent microscopic pictures demonstrate intense E-cad (green) staining in the linings of airways. Blue: nuclei (DAPI); E-cad: epithelial cadherin; scale bar: 10µm or 100µm.

In the first protocol, mouse lungs were cut into 1–2 mm pieces, incubated with 1.4 mg/ml Pronase (Roche) for 1h, enzyme inactivated with FCS, and after a short (3h) rest the dissociated cells were surface stained by flow cytometry. Abs against E-cad, CD45 (pan-haematopoietic marker), PDGFRβ (fibroblast and smooth muscle cell marker [358]), and VE-cadherin (endothelial cell marker [359]) were used to explore the purity of epithelial and other major contaminating cells. As Figure 7.4.2.2 shows, no positive staining for E-cad was observed suggesting that E-cad may have been cleaved or downregulated upon Pronase treatment.

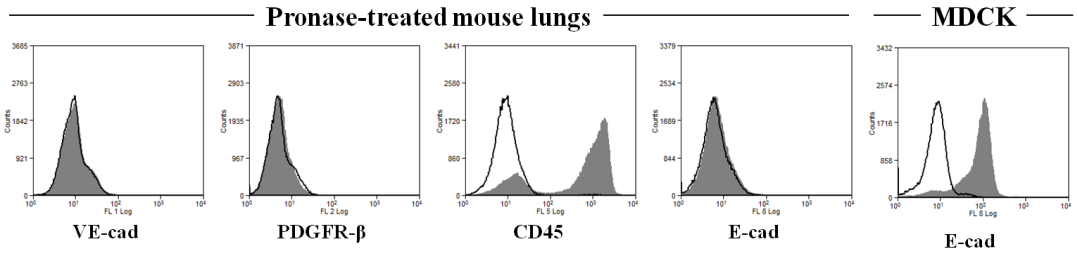

Figure 7.4.2.2. Expression of E-cadherin in Pronase-treated mouse lungs. Enzymatically–dissociated cells were surface stained for Abs against E-cad, VE-cadherin (VE-cad), PDGFRβ, and CD45. MDCK was used as positive control for E-cad expression. Representative histograms of 3 independent experiments are shown.

Next, tissue dissociation by a non-enzymatic means was tested. EDTA is a metal chelator that binds and limits the availability of calcium and magnesium ions that otherwise are required for cell-cell binding and attachment of cells to tissue culture plate. Mouse lungs were dissociated in EDTA (as described in Chapter 2.1.3), the $CD45^+$ compartment – the major contaminating population (Figure 7.4.2.2), was depleted by magnetic beads (Chapter 2.1.4; Figure 7.4.2.3, left panel), and after a 3h rest, cells were stained for surface E-cad. The staining was positive; however, the percentage of $E\text{-}cad^+$ out of the total dissociated cells was low (38%) (Figure 7.4.2.3, middle panel). Applying magnetic separation the $E\text{-}cad^+$ yield increased to 72% (Figure 7.4.2.3, right panel), which is still below the desired purity (> 90%).

The negative population after magnetic separation is likely to be either epithelial cells with low E-cad expression or genuinely $E\text{-}cad^-$ cells, since the majority of $CD45^+$ cells (> 93%) had been depleted (Figure 7.4.2.3, left panel) and contamination by structural cells was minimal (similar to Figure 7.4.2.2). This suggests that E-cad should be replaced with an alternative epithelial surface maker.

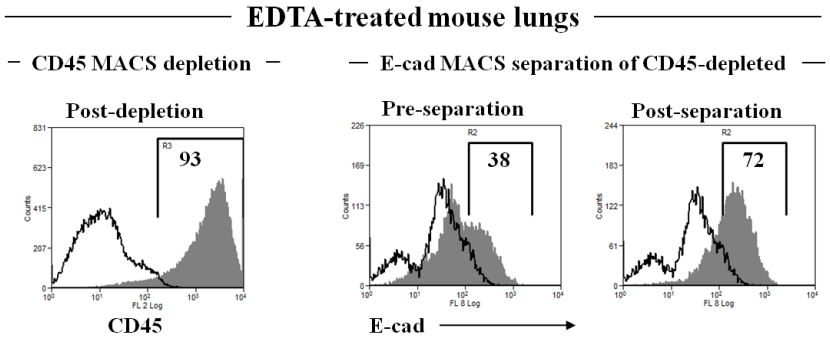

Figure 7.4.2.3. Isolation of E-cad$^+$ cells from mouse lungs. Freshly EDTA-dissociated lungs were depleted of CD45-expression cells (left panel) and then either immediately (middle histogram), or after positive selection by magnetic beads (right histogram) were surface stained for E-cad. Filled histograms: E-cad; open histograms: isotype control.

EpCAM is a transmembrane glycoprotein which is specifically expressed on most of normal epithelia and calcium-independently modulates cell adhesions [360]. A few studies have utilised EpCAM as a marker for purification or detection of epithelial cells from mouse lungs [361-363]. To visualise the distribution of EpCAM expression in airways and assess its suitability as an epithelial specific marker, the whole lungs were fixed and immunostained with a mAb against EpCAM (Figure 7.4.2.4). Lining of primary and secondary airways to a great extent, and bronchiolar and alveolar sacs to a lesser extent, were EpCAM$^+$.

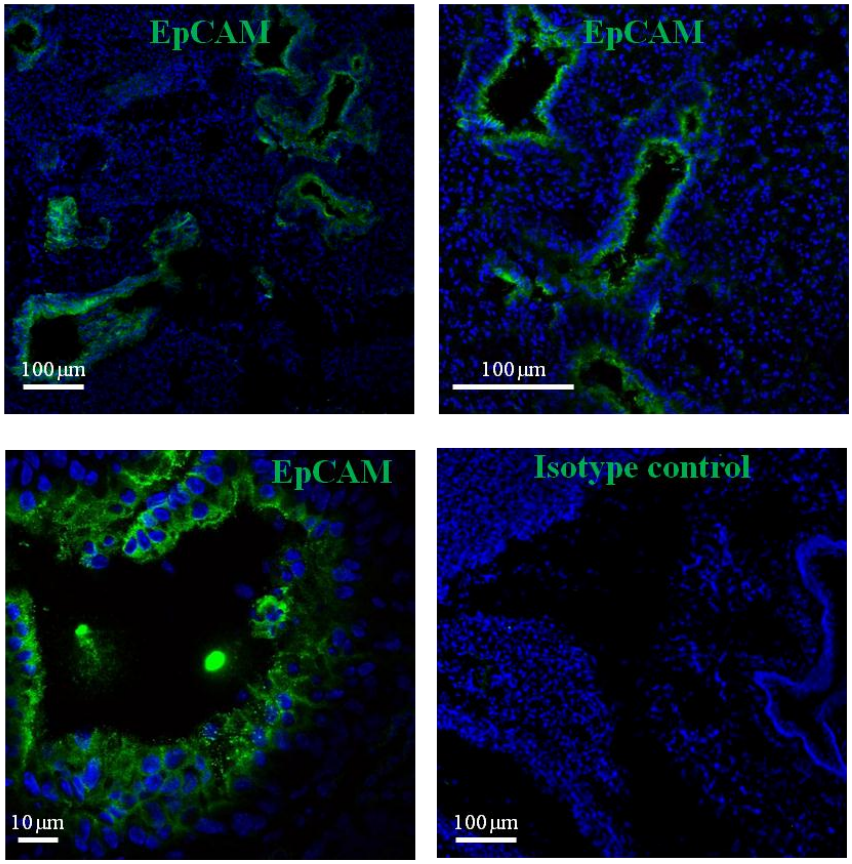

Figure 7.4.2.4. Expression of EpCAM in mouse lungs. Immunofluorescent microscopic pictures show strong EpCAM (green) staining in the linings of major airways and less intense staining in bronchioles and alveolar sacs. Blue: nuclei (DAPI); EpCAM: epithelial cell adhesion molecule; scale bar: 10µm or 100µm.

Next, $EpCAM^+$ cells from ETDA-treated CD45-depleted lungs were isolated by magnetic separation. As Figure 7.4.2.5A shows, prior to separation 84% of cells expressed EpCAM, which was enriched to 90% following sorting. Anatomical distribution of lungs EpCAM from Figure 7.4.2.4 suggested a preferential localisation to bronchial epithelium. Using β-tubulin IV on cytospin preparations of $EpCAM^+$ cells, I found > 80% in any given microscopic field stained with anti- β-tubulin IV (βtubIV; cilia marker) mAb (Figure 7.4.2.5B).

To confirm CD1D1 (murine equivalent of human CD1D) expression or not, on RECs isolated by this method, RT-PCR was performed and showed the presence of transcript in WT but not CD1dKO mice (Figure 7.4.2.5C).

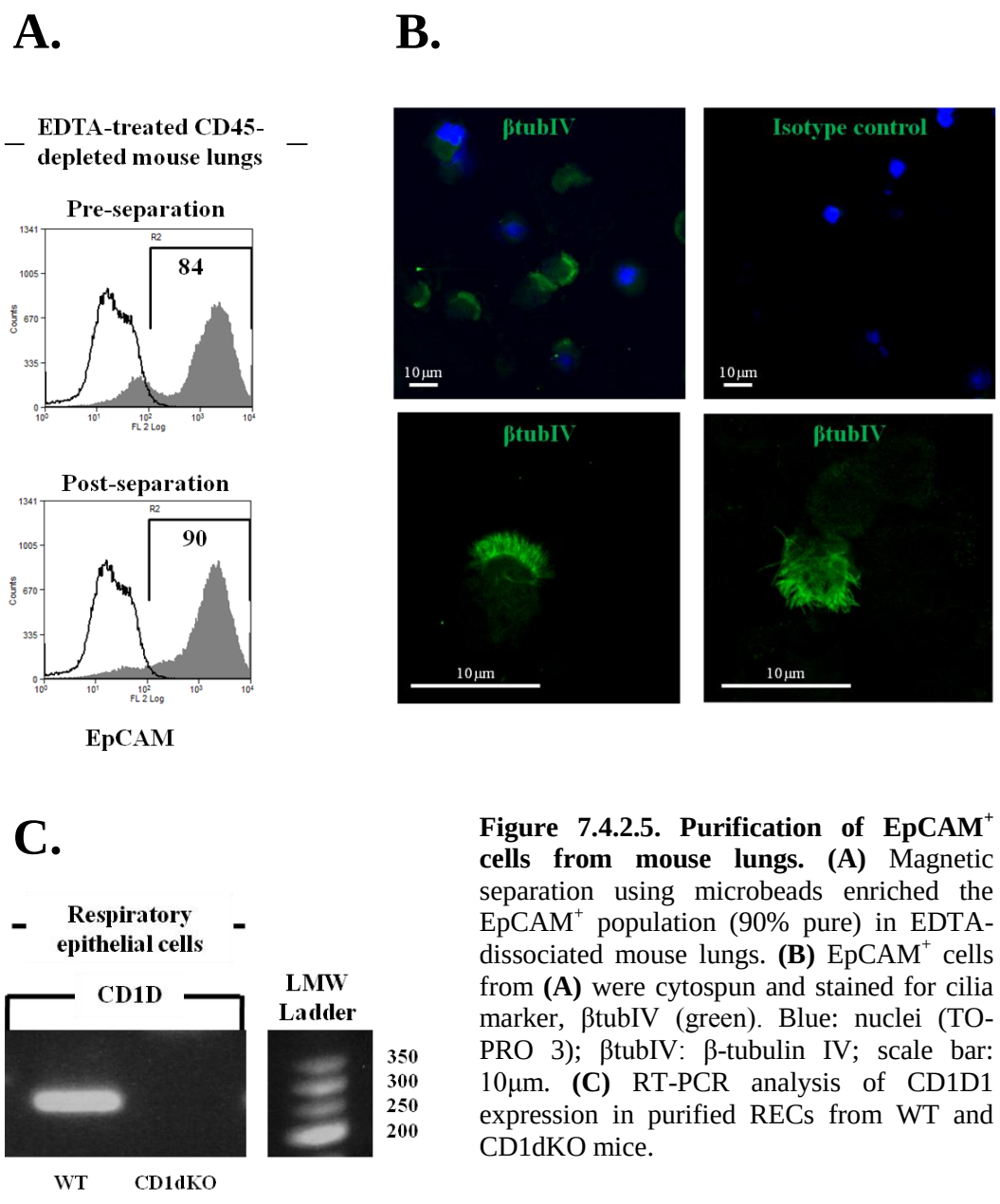

Figure 7.4.2.5. Purification of EpCAM$^+$ cells from mouse lungs. (A) Magnetic separation using microbeads enriched the EpCAM$^+$ population (90% pure) in EDTA-dissociated mouse lungs. **(B)** EpCAM$^+$ cells from **(A)** were cytospun and stained for cilia marker, βtubIV (green). Blue: nuclei (TO-PRO 3); βtubIV: β-tubulin IV; scale bar: 10µm. **(C)** RT-PCR analysis of CD1D1 expression in purified RECs from WT and CD1dKO mice.

The final optimised protocol, therefore uses EDTA for tissue dissociation, and depletes the haematopoietic compartment and stains for EpCAM (Figure 7.4.2.6), is

ideal for isolation of RECs which are the primary targets of IAV; that is, the ciliated bronchial epithelial cells.

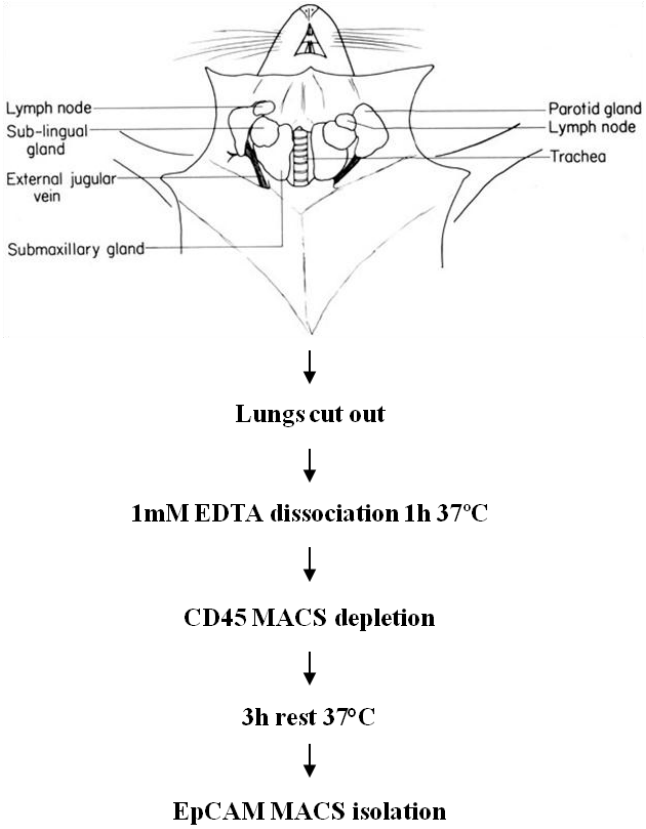

Figure 7.4.2.6. Summary of the protocol to isolate mouse RECs.

7.4.3 Quality control of samples pre and post DNA microarray chip hybridisation

The quality of RNA was assessed by analysing the "RNA integrity number" (RIN) of the samples (discussed in Chapter 6.4.2). Apart from one sample (WT on D3) for which a very low amount of RNA was obtained (i.e. below the threshold of RIN computation on Agilent chip) all other RINs were > 7.60, which indicate good RNA integrity and absence of significant degradation (Figure 7.4.3.1A). After hybridisation and scanning, signal intensities on the DNA chips were summarised using robust multi-array average (RMA) algorithm in 'R' software (discussed in Chapter 6.4.2), and then plotted. Comparable expression patterns were observed across all samples; however, histograms displayed a bimodal Log_2 intensity distribution (Figure 7.4.3.1B). The lower peak was close to background intensity and contained probe sets with absent or low hybridisation. To avoid potential analytical bias and after discussions with the Bioinformatician (Helen Lockstone), those intensity values below five were filtered out (Figure 7.4.3.1C, D).

The natural grouping of similarities and dissimilarities of the samples was examined for unintentional bias (e.g. due to experimental procedures), with particular attention to WT on D3 due to the lack of RIN data. Unsupervised hierarchical clustering using "complete linkage" method (discussed in Chapter 6.4.2) (Figure 7.4.3.2) grouped the samples on the basis of experiment time point, with no significant deviation in WT on D3 from the rest of the samples. Absence of unexpected deviation conferred technical reassurance for these data.

A.

	WT0	WT3	WT6	KO0	KO3	KO6
RIN	7.90	N/A	9.0	7.90	7.90	7.60

B.

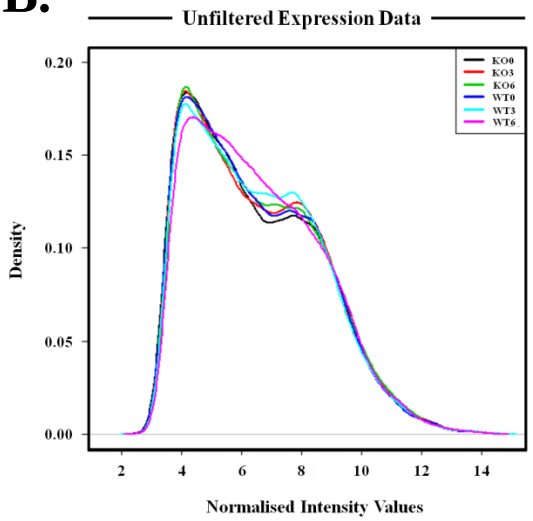

C.

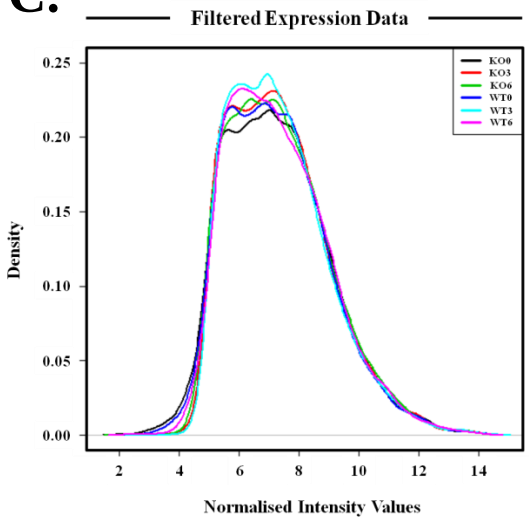

Figure 7.4.3.1. Comparison of RMA-normalised microarray signal intensities from epithelial cells. (A) List of sample RIN values. N/A: no reading available due to low RNA amount. **(B)** Expression distribution of all genes from the six samples is represented as smoothed histograms. Those probe sets with signal intensities < 5 were then filter out to yield a unimodally distributed graph **(C)** and the box plots **(D)**. In **(D)** the boxes are drawn between the 25th to the 75th percentiles of normalised data, with median (50th percentile) drawn inside. KO: CD1dKO BL/6; WT: wild type C57BL/6; 0: prior to PR8 challenge; 3 and 6: days after PR8 inoculation.

D.

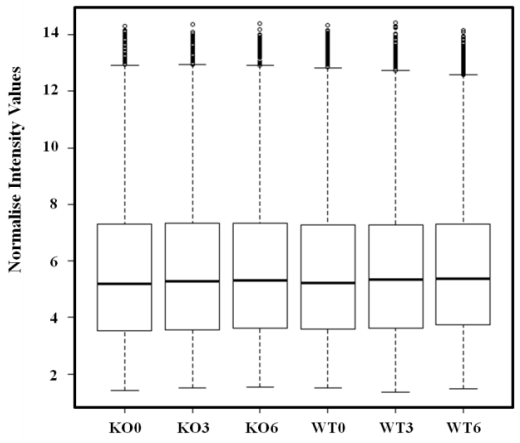

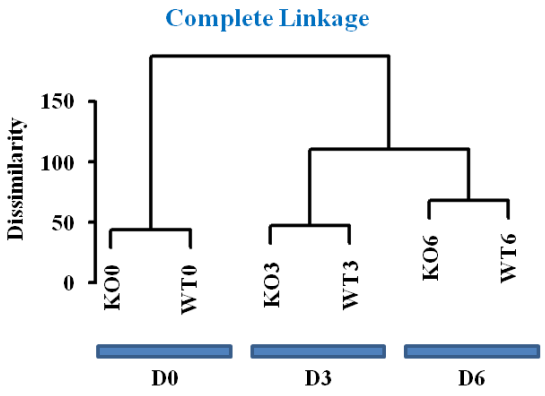

Figure 7.4.3.2. Unsupervised hierarchical clustering of all WT and CD1dKO samples. Clustering was carried out using "complete linkage" distance measures. The output dendrogram shows grouping of data primarily on the basis of experiment time point.

7.4.4 Profile of gene expression in influenza virus-infected RECs of CD1d-deficient compared with wild type mice

To elucidate how absence of CD1d influences the REC gene expression *in vivo* during IAV infection, gene expression profiles in isolated REC were first compared on D3 versus D0 for each phenotype (WT and KO). As there were no *p* values for individual comparisons, those genes whose expression had changed more than 2 folds ($\Delta FC > 2$) were considered to be differentially expressed (Table 7.4.4.1). A total of 2537 genes for WT, and 2136 genes for KO were differentially expressed on D3 compared to D0.

Gene List (GL)	Comparison	No. differentially expressed genes
1	"KO3 vs. KO0"	2136
2	"WT3 vs. WT0"	2537

Table 7.4.4.1. Number of epithelial differentially expressed genes for specific comparisons on day 3. Normalised expression values were used as input and only genes with $\Delta FC > 2$ were considered to be differentially expressed. FC: fold change.

Many genes including immune-related (e.g. IL-1α) and housekeeping (e.g. CCND2) genes were shared between GL1 and GL2. This is not unexpected as no statistical restriction could be applied (only one sample from each time point, albeit from 10 mice) and also changes are likely to be broadly similar in both CD1dKO and WT mice when compared to their uninfected counterparts. However, it does mean that comparing GL1 and GL2, identification of differentially regulated genes between the two phenotypes would be unhelpful. I therefore proceeded to study enrichment of gene sets in "WT3 vs. WT0" and "KO3 vs. KO0" separately by GSEA.

I found that similar biological pathways (e.g. "defence response", "inflammatory response", etc) (Table 7.4.4.2) were enriched on D3 in both WT and CD1dKO mice lung epithelial cells. When genes differentially expressed in "KO3 vs. KO0" were compared to those in "WT3 vs. WT0", no significantly enriched gene sets were found (using GSEA). These findings suggest that very similar changes are occurring in RECs of CD1dKO and WT mice compared to uninfected state; and compared with each other.

GSEA gene set enrichment on day 3

Gene Set Name	NES	FDR *q* Value
"KO3 vs. KO0"		
Defence response	2.45	0
Immune response	2.43	0
Immune system process	2.38	0
Inflammatory response	2.35	0
Response to wounding	2.30	0
Response to external stimulus	2.26	0
Response to other organism	2.18	0
Locomotor behaviour	2.16	0
Behaviour	2.12	0
Cellular defence response	2.09	0
"WT3 vs. WT0"		
Immune response	2.65	0
Defence response	2.65	0
Immune system response	2.61	0
Inflammatory response	2.46	0
Response to external stimulus	2.41	0
Response to wounding	2.40	0
Cellular defence response	2.32	0
Locomotor behaviour	2.31	0
Behaviour	2.27	0
Response to other organism	2.22	0

Table 7.4.4.2. Gene sets enriched in CD1KO and WT mice lung epithelial cells on "D3 vs. D0". In GSEA, expression values of WT3 were compared against WT0, and KO3 against KO0. The top ten most enriched gene sets for both phenotypes are listed. The sets were ranked by NES. FDR (false discovery rate); NES: normalised enrichment score (ES corrected for difference in the size of gene sets).

However, although this is the case, GL1 and GL2 differed considerably in the expression fold change (FC) of certain genes. For example, TLR-13 transcript had

increased 59.71 folds in "KO3 vs. KO0", but had only increased 13.64 folds in "WT3 vs. WT0". To better understand the differential patterns of gene expression between the two phenotypes, (Log_2 FC of) expression values for "WT3 vs. WT0" were plotted against those of "KO3 vs. KO0", using 'R' in order to generate a figure which allows the reader to tell the changes in these groups of mice compared to baseline and compared to each other (Figure 7.4.4.1).

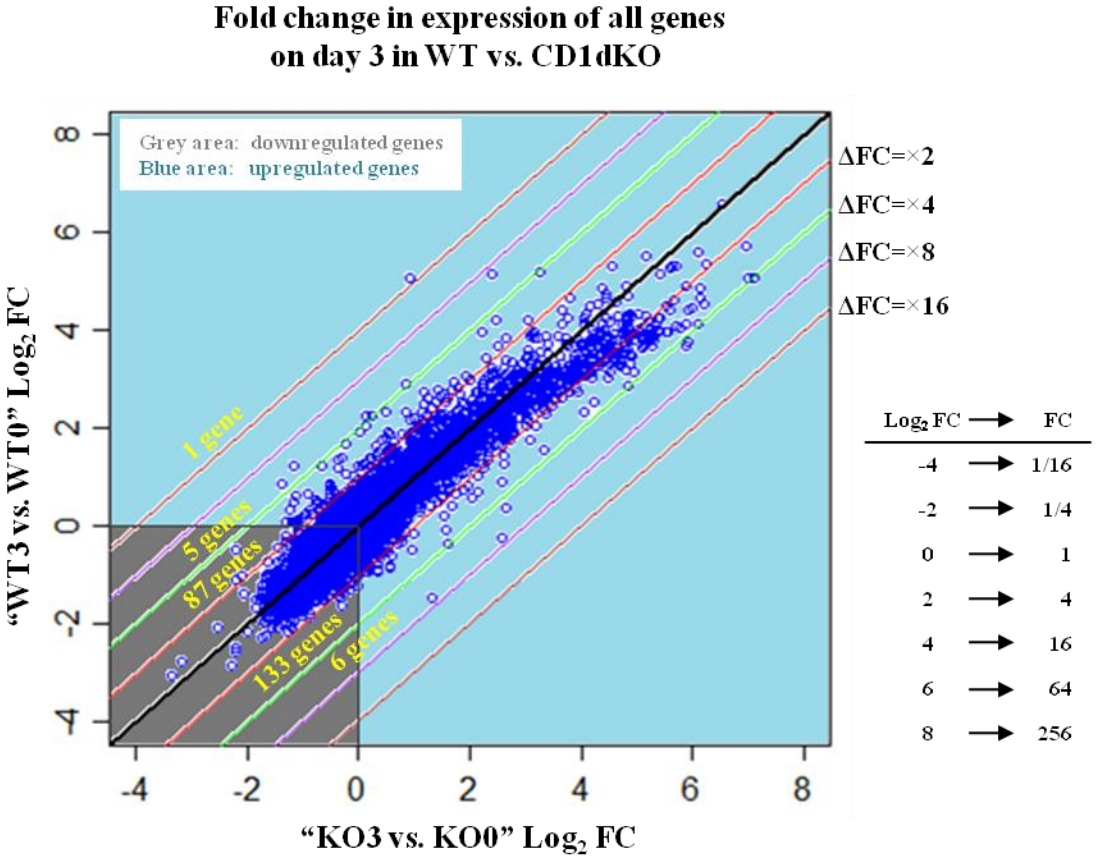

Figure 7.4.4.1. Fold change in gene expression of WT and CD1dKO on D3 against D0. All normalised expression values were compared on "D3 vs. D0" for WT and CD1KO mice, independently, and then the Log_2 fold changes (Log_2 FC) were plotted against each other. Diagonal lines indicate the difference in FC (ΔFC) between the two phenotypes, and the number of genes located between them, when present, is cited on the graph. The table on the right converts the Log_2 FC into equivalent FC values.

Figure 7.4.4.1 shows that on day 3 after viral infection, 139 genes in RECs of CD1dKO (designated as GL3), and 93 genes in RECs of WT (designated as GL4) had

ΔFC > 2 (below and above red slanting lines) when compared to each other. Note here that ΔFC refers to the ratio between the two phenotypes (rather than fold difference in FC between the two groups) as in Chapter 6, but in contrast to Chapter 6, the axis are depicted in Log_2 rather than absolute numbers, therefore ΔFC is really ΔLog_2 FC. This was done because the fold changes were much larger than those observed in Chapter 6. The table in Figure 7.4.4.1 converts Log_2 to absolute numbers.

There were six genes with ΔFC > 4 (i.e. a proportional difference of > 4 comparing the two axes) in each axis (Table 7.4.4.3), including platelet-activating factor receptor (PTAFR), TLR-13, and C-type lectin 4e (CLEC4E) in CD1dKO, and cytotoxic and regulatory T cell molecule (CRTAM) in WT. This means that these genes have exhibited the highest change between the WT and CD1d KO on day 3 (when also compared to uninfected mice).

Gene Symbol	Ref Seq ID	"KO3 vs. KO0"	"WT3 vs. WT0"	ΔFC	NCBI official full name
Higher in KO					
NGP	NM_008694	5.94	0.86	6.91	neutrophilic granule protein
4933409K07RIK	NR_033123	2.48	0.36	6.89	RIKEN cDNA 4933409K07 gene
IGK-V1	Z95477	6.23	1.28	4.87	immunoglobulin kappa chain variable 1 (V1)
PTAFR	**NM_001081211**	**59.30**	**12.91**	**4.59**	**platelet-activating factor receptor**
TLR13	**NM_205820**	**59.71**	**13.64**	**4.38**	**toll-like receptor 13**
CLEC4E	**NM_019948**	**138.14**	**34.06**	**4.06**	**C-type lectin domain family 4, member e**
Higher in WT					
FBP1	NM_019395	1.88	34.06	18.12	fructose bisphosphatase 1
EAR11	NM_053113	5.28	36.00	6.82	eosinophil-associated, ribonuclease A family, member 11
HSPA1A	NM_010479	0.44	2.38	5.41	heat shock protein 1A
SPEER4D	NM_025759	0.38	1.84	4.84	spermatogenesis associated glutamate (E)-rich protein 4d
CRTAM	**NM_019465**	**1.11**	**4.72**	**4.25**	**cytotoxic and regulatory T cell molecule**
A530040E14RIK	ENSMUST00000 093501	1.79	7.41	4.14	RIKEN cDNA A530040E14 gene

Table 7.4.4.3. The most differentially expressed genes in CD1dKO vs. WT and vice versa on day 3 (incorporating comparison to day 0). Genes from Figure 7.4.4.1 with ΔFC > 4 are listed are listed. FC: fold change. Ranking is according to ΔFC.

Similar to day 3, attempts to identify genes that have a fold change of greater than two on day 6 compared to day 0 resulted in lists (Table 7.4.4.4) containing very similar genes.

Gene List (GL)	Comparison	No. differentially expressed genes
5	"KO6 vs. KO0"	4093
6	"WT6 vs. WT0"	4532

Table 7.4.4.4. Number of epithelial differentially expressed genes for specific comparisons on day 6. Normalised expression values were used as input and only genes with ΔFC > 2 were considered to be differentially expressed. FC: fold change.

When GSEA was employed to determine genes enriched in KO6 compared to KO0, 117 gene sets were found to be enriched in "KO6 vs. KO0" (Table 7.4.4.5). This was similar to gene sets that were enriched in WT6 when compared to WT0; i.e. "WT6 vs. WT0".

GSEA gene set enrichment on day 6

Gene Set Name	NES	FDR *q* Value
"KO6 vs. KO0"		
Defence response	2.67	0
Immune response	2.67	0
Immune system process	2.66	0
Inflammatory response	2.49	0
Response to wounding	2.44	0
Response to external stimulus	2.39	0
Locomotor behaviour	2.25	0
Cellular defence response	2.19	0
Positive regulation of multi-cellular organismal process	2.19	0
Lymphocyte activation	2.19	0
"WT6 vs. WT0"		
Immune response	2.87	0
Immune system process	2.86	0
Defence response	2.63	0
Inflammatory response	2.40	0
Cell activation	2.37	0
Lymphocyte activation	2.36	0
Locomotor behaviour	2.35	0
Leukocyte activation	2.33	0
Response to wounding	2.28	0
Cellular defence response		

Table 7.4.4.5. Gene sets enriched in CD1KO and WT mice lung epithelial cells on "D6 vs. D0". In GSEA, expression values of WT6 were compared against WT0 and KO6 against KO0. The top ten most enriched gene sets for both phenotypes are listed. The sets were ranked by NES. FDR (false discovery rate); NES: normalised enrichment score (ES corrected for difference in the size of gene sets).

However, plotting the FC in expression of all genes on "D6 vs. D0" for WT and CD1dKO mice yielded a more informative picture (Figure 7.4.4.2). Of 13539 total genes, 506 had ΔFC > 2 in CD1dKO (designated as GL7), and 165 genes showed ΔFC > 2 in WT (designated as GL8).

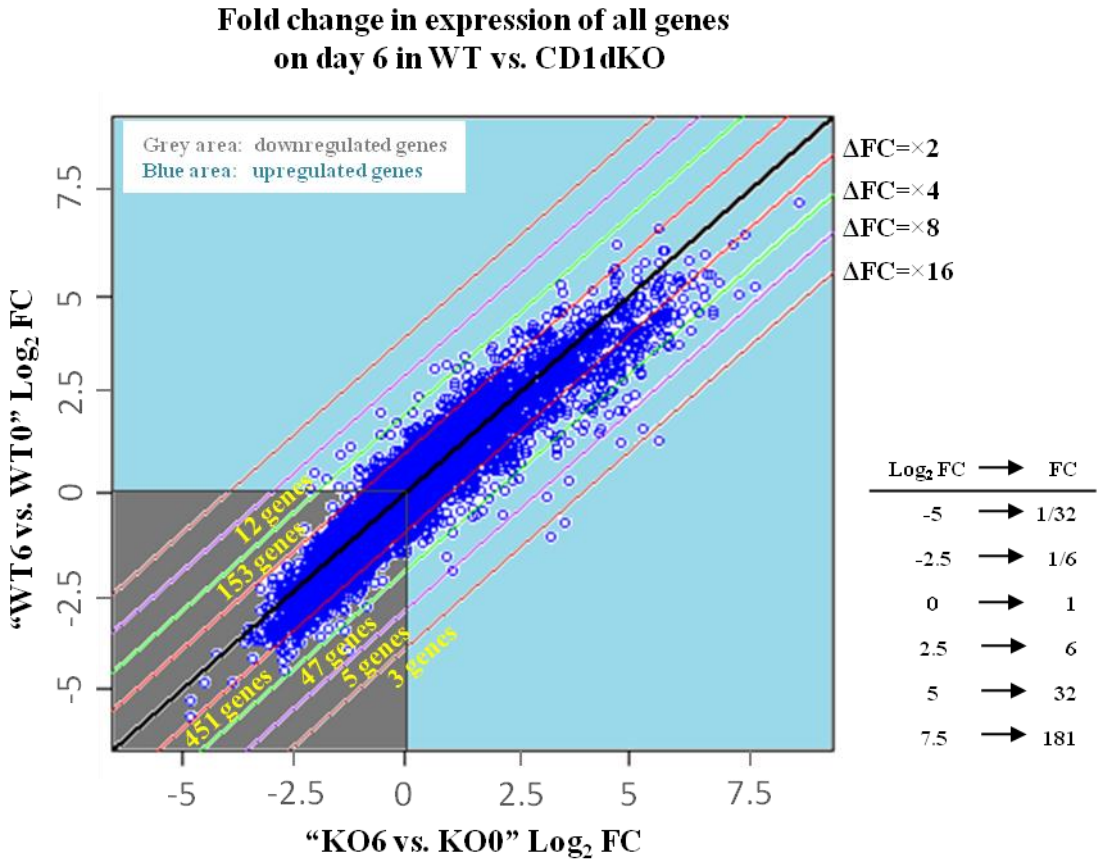

Figure 7.4.4.2. Fold change in gene expression of WT and CD1dKO on D6 against D0. All normalised expression values were compared on "D6 vs. D0" for WT and CD1KO mice, independently, and then the Log_2 fold changes (Log_2 FC) were plotted against each other. Diagonal lines indicate the difference in FC (ΔFC) between the two phenotypes, and the number of genes located between them, when present, is cited on the graph. The table on the right converts the Log_2 FC into equivalent FC values.

There were 55 and 12 genes with ΔFC > 4 in CD1dKO and WT, respectively (Table 7.4.4.6). These included higher levels of CLEC4E, SPP1, and TLR-13 in CD1dKO, and greater expression of CD1D1 in WT (5.35 fold greater on day 6 compared to day 0) which confirms the results from Chapter 5.

Gene Symbol	Ref Seq ID	"KO6 vs. KO0"	"WT6 vs. WT0"	ΔFC	NCBI official full name
Higher in KO					
NGP	NM_008694	9.45	0.45	21.00	neutrophilic granule protein
MMP12	NM_008605	50.91	2.5	20.36	matrix metallopeptidase 12
IGK-V1	Z95477	11.79	0.59	19.98	immunoglobulin kappa chain variable 1 (V1)
GM7609	NM_001081746	39.67	3.03	13.09	predicted gene 7609
CAR4	NM_007607	28.44	2.36	12.05	carbonic anhydrase 4
EAR11	NM_053113	12.64	1.24	10.19	eosinophil-associated, ribonuclease A family, member 11
AWAT1	NM_001081136	9	0.92	9.78	acyl-CoA wax alcohol acyltransferase 1
GM5571	ENSMUST00000103316	2.07	0.24	8.63	predicted gene 5571
ATP6V0D2	NM_175406	30.7	4.2	7.31	ATPase, H+ transporting, lysosomal V0 subunit D2
CHI3L3	NM_009892	20.39	2.91	7.01	chitinase 3-like 3
CES1	NM_021456	0.41	0.06	6.83	carboxylesterase 1
CCL6	NM_009139	20.97	3.12	6.72	chemokine (C-C motif) ligand 6
IGL-V1	M94350	4.5	0.67	6.72	immunoglobulin lambda chain, variable 1
KYNU	NM_027552	27.67	4.26	6.50	kynureninase (L-kynurenine hydrolase)
MRC1	NM_008625	23.92	3.86	6.20	mannose receptor, C type 1
AI607873	BC150711	230.72	37.27	6.19	expressed sequence AI607873
CYBB	NM_007807	34.78	5.7	6.10	cytochrome b-245, beta polypeptide
MFGE8	NM_008594	1.92	0.32	6.00	milk fat globule-EGF factor 8 protein
DAB2	NM_023118	30.7	5.17	5.94	disabled homolog 2 (Drosophila)
CLEC4E	NM_019948	178.53	32.45	5.50	C-type lectin domain family 4, member e
GBGT1	NM_139197	10.56	1.93	5.47	globoside alpha-1,3-N-acetylgalactosaminyltransferase 1
CCL9	NM_011338	15.78	2.95	5.35	chemokine (C-C motif) ligand 9
LPL	NM_008509	12.55	2.38	5.27	lipoprotein lipase
TLR13	NM_205820	69.07	13.64	5.06	toll-like receptor 13
SPP1	NM_009263	117.78	23.43	5.03	secreted phosphoprotein 1
EREG	NM_007950	10.56	2.13	4.96	Epiregulin
MERTK	NM_008587	16.11	3.29	4.90	c-mer proto-oncogene tyrosine kinase
GPNMB	NM_053110	84.45	17.27	4.89	glycoprotein (transmembrane) nmb
EAR1	NM_007894	38.59	7.94	4.86	eosinophil-associated, ribonuclease A family, member 1
MMP19	NM_021412	39.4	8.34	4.72	matrix metallopeptidase 19
CCR1	NM_009912	116.97	25.11	4.66	chemokine (C-C motif) receptor 1
FZD7	NM_008057	3.29	0.72	4.57	frizzled homolog 7 (Drosophila)
F7	NM_010172	18.64	4.11	4.54	coagulation factor VII
MGLL	NM_001166251	4.69	1.04	4.51	monoglyceride lipase
LILRB4	NM_013532	59.71	13.27	4.50	leukocyte immunoglobulin-like receptor, subfamily B, member 4
ABCD2	NM_011994	5.74	1.28	4.48	ATP-binding cassette, sub-family D (ALD), member 2
FBP1	NM_019395	2.99	0.67	4.46	fructose bisphosphatase 1
ITGAX	NM_021334	21.56	4.89	4.41	integrin alpha X
TREM2	NM_031254	5.31	1.21	4.39	triggering receptor expressed on myeloid cells 2
SIRPB1B	NM_001173460	14.42	3.29	4.38	signal-regulatory protein beta 1B
SCD1	NM_009127	0.39	0.09	4.33	stearoyl-Coenzyme A desaturase 1
FSTL1	NM_008047	2.81	0.65	4.32	follistatin-like 1
GP49A	NM_008147	57.28	13.36	4.29	glycoprotein 49 A
LEPR	NM_001122899	2.1	0.49	4.29	leptin receptor
SIGLEC1	NM_011426	23.26	5.54	4.20	sialic acid binding Ig-like lectin 1, sialoadhesin
CTSS	NM_021281	29.65	7.11	4.17	cathepsin S
CHI3L4	NM_145126	0.54	0.13	4.15	chitinase 3-like 4
SLC39A2	NM_001039676	18.38	4.44	4.14	solute carrier family 39 (zinc transporter), member 2
CD84	NM_013489	24.93	6.06	4.11	CD84 antigen
LILRA5	NM_001081239	10.27	2.5	4.11	leukocyte immunoglobulin-like receptor, subfamily A (with TM domain), member 5
SRGN	NM_011157	36.25	8.94	4.05	serglycin
ALOX5	NM_009662	11.16	2.77	4.03	arachidonate 5-lipoxygenase
EAR2	NM_007895	23.92	5.94	4.03	eosinophil-associated, ribonuclease A family, member 2
LY6I	NM_020498	3.61	0.9	4.01	lymphocyte antigen 6 complex, locus I
CLEC4D	NM_010819	95.67	23.92	4.00	C-type lectin domain family 4, member d
Higher in WT					
OTT	NM_011022	0.68	4.14	6.09	ovary testis transcribed
CCL19	NM_011888	0.24	1.39	5.79	chemokine (C-C motif) ligand 19
KLRC2	NM_010653	1.58	8.75	5.54	killer cell lectin-like receptor subfamily C, member 2
2410127L17RIK	NM_026120	0.37	1.93	5.22	RIKEN cDNA 2410127L17 gene
D830030K20RIK	NM_177135	0.43	2.22	5.16	RIKEN cDNA D830030K20 gene
BUB1	NM_001113179	1.92	9.45	4.92	budding uninhibited by benzimidazoles 1 homolog (S. cerevisiae)
HBA-A1	NM_008218	0.23	1.07	4.65	hemoglobin alpha, adult chain 1
CD1D1	NM_007639	1.21	5.35	4.42	CD1d1 antigen
LAG3	NM_008479	2.55	10.93	4.29	lymphocyte-activation gene 3
IFNZ	NM_197889	0.3	1.27	4.23	interferon zeta
TDG	NM_011561	0.68	2.77	4.07	thymine DNA glycosylase
CD4	NM_013488	2.2	8.94	4.06	CD4 antigen

Table 7.4.4.6. The most differentially expressed genes in CD1KO vs. WT and vice versa on day 6. Genes from Figure 7.4.4.2 with ΔFC > 4 are listed are listed. FC: fold change. Ranking is according to ΔFC.

7.4.5 Functional relevance of gene expression profile in RECs from CD1d-deficient mice

Using the GL3 ("KO3 vs. KO0") as input file (Table 7.4.5.1), analysis with DAVID returned enrichment of several functional and gene ontology terms (Table 7.4.5.2).

Gene List (GL)	Comparison	No. differentially expressed genes
3	"KO3 vs. KO0" vs. "WT3 vs. WT0"	139
4	"WT3 vs. WT0" vs. "KO3 vs. KO0"	93

Table 7.4.5.1. Number of epithelial differentially expressed genes for specific comparisons on day 3. Genes with ΔFC > 2 in one group compared to the other were considered to be differentially expressed. FC: fold change.

"CD1dKO vs. WT" on day 3 against day 0 (GL3)
Annotation clustering of genes – DAVID

Annotation	Term	Source	%Input	Benjamini *p* value
Function				
	Cell adhesion	SP-PIR	9.6	3.10E-5
	Immune response	SP-PIR	8.1	3.60E-5
	Chemotaxis	SP-PIR	6.6	4.00E-7
	Cytokine	SP-PIR	6.6	7.30E-5
	Inflammatory response	SP-PIR	5.1	4.20E-4
Gene Ontology				
	Defence response	GO Term-BP	14.0	3.20E-7
	Immune response	GO Term-BP	14.0	7.10E-6
	Chemotaxis	GO Term-BP	10.3	9.90E-9
	Inflammatory response	GO Term-BP	10.3	2.90E-6
	Carbohydrate binding	GO Term-MF	9.6	3.80E-5
	Cytokine activity	GO Term-MF	5.1	2.00E-2
Pathway				
	No enrichment			

Table 7.4.5.2. Functional clustering of differentially expressed genes in CD1dKO vs. WT on D3 against D0, using DAVID. Genes from GL3 were run against SP-PIR (Swiss-Protein and Protein Information Resource) library, and gene ontology (GO) biological process (BP), and molecular function (MF) databanks. A selection of those with Benjamini $p < 0.05$ is listed here. In every category, sets or terms were ranked according to %Input, and those with the highest %Input (i.e. the most enriched) were highlighted in red. No enriched pathway was detected.

This means that on the basis of %Input and Benjamini *p* values, five clusters were highly enriched in RECs of CD1dKO mice on day 3 compared to WT. These

included "chemotaxis", "defence response", "immune response", "carbohydrate binding", and "cell adhesion". According to functional and annotation similarities, I grouped the first three clusters together (as immune-related) and the last two together (as cell adhesion-related), and then scrutinised the genes to identify those exclusively found within or shared between the clusters in each group (Figure 7.4.5.1).

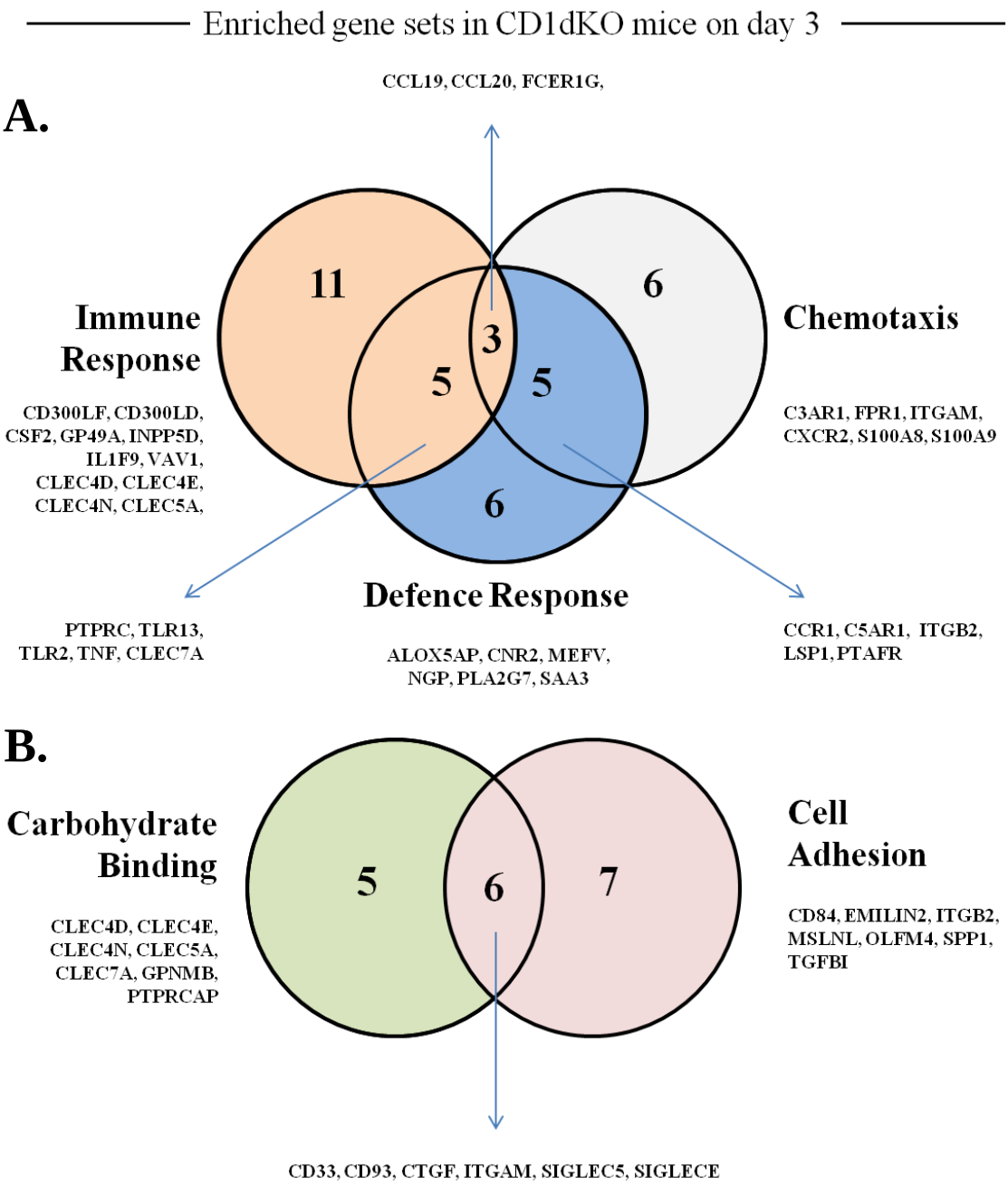

Figure 7.4.5.1. Venn diagram representation of enriched gene clusters in CD1dKO vs. WT on D3. The five highly enriched clusters from Table 7.4.5.2 were grouped into two categories: immune-related **(A)** and cell adhesion-related **(B)**; and then the overlapping genes between clusters in each group were identified.

In the immune-related group, for example, genes coding for two members of the S100 family of calcium binding proteins (S100A8, and S100A9), chemokines (CCL19, CCL20), toll-like receptors (TLR-2, TLR-13), TNFα, and PTAFR were present. The cell adhesion-related group, on the other hand, accommodated genes for five members of C-type lectin superfamily of proteins (CLEC4D, CLEC4D, CLEC4N, CLEC5A, CLEC7A), three members of sialic acid-binding Ig-like lectins (SIGLECE, SIGLEC5, CD33), olfactomedin 4 (OLFM4), and secreted phosphoprotein 1 (SPP1).

Table 7.4.5.3 shows that almost all the genes in Figure 7.4.5.1 were induced in both WT and CD1dKO mice; but, what is different between these two phenotypes is the *magnitude* of induction. Genes for TNFα, IL-1F9, and SPP1, for instance, were upregulated 33.36, 15.24, and 47.18 folds respectively in CD1dKO, but only 14.62, 6.68, and 15.67 folds in WT. This suggests that while the immune response programme was triggered in RECs of both groups of mice, in WT excessive stimulation appears to have been prevented.

	Gene	"KO3 vs. KO0"	"WT3 vs. WT0"	Associated functions and expression sites
C-type lectin receptors	*CLEC4E*	138.14	34.06	Cell adhesion; cell-cell signalling; sensing necrosis; expressed mainly by APCs and activated phagocytes; stimulating inflammatory response to fungi; receptor for mycobacterial TDM glycolipid
	CLEC4D	68.59	17.75	Cell adhesion; cell-cell signalling; expressed by monocytes/macrophages; endocytic receptor;
	CLEC4N	48.84	21.56	Mediates alpha-mannan-induced cytokine production; expressed on DCs and macrophages; important for host defence against *Candida albicans* and induction of Th17 differentiation; mediates *Schistosoma* helminth activation of NLR3 inflammasome and IL-1β production
	CLEC5A	45.57	15.78	Cell adhesion, cell-cell signalling; interacts with DNAX-activating protein 12 to activate cells; causes an inflammatory response; critical for lethal disease caused by Dengue virus
	CLEC7A	33.82	14.52	A receptor for beta 1,3-linked and beta 1,6-linked glucans from pathogenic fungi and bacteria; required for TLR-2-mediated inflammatory response; expressed by keratinocytes and induced in psoriatic epidermis and by IFNs
S100 antimicrobials	*S100A8*	60.13	21.56	Antimicrobial; inhibitor of casein kinase; pro-inflammatory; pro-apoptotic; expressed by phagocytes and bronchial epithelial cells
	S100A9	46.21	22.78	Antimicrobial; inhibitor of casein kinase; pro-inflammatory; pro-apoptotic; expressed by phagocytes and bronchial epithelial cells
TLRs	*TLR13*	59.71	13.64	Poorly characterised TLR; receptor for vesicular stomatitis virus; expressed by DCs and macrophages;
	TLR2	19.70	9.71	A pathogen recognition receptor
Cytokines	*TNF*	33.36	14.62	Pro-inflammatory cytokine
	IL1F9	15.24	6.68	Induced under inflammatory conditions in keratinocytes
	SPP1	47.18	15.67	A cytokine, increases production of IFNγ and IL-12 and reduces synthesis of IL-10; binds to CD44 and fibronectin as a cell adhesion and migration molecule
Chemokines	*CCL20*	5.94	1.88	Ligand for CCR6; has antibacterial activity against *E. coli* and *S. Aureus*
	CCL19	2.97	0.95	Ligand for CCR7 (important both for immunity and tolerance)
Complement receptors	*C5AR1*	25.81	9.71	Receptor of chemotactic and inflammatory C5a
	CD93	22.78	8.94	Receptor for C1q, mannose binding lectin 2 and surfactant protein A; cell adhesion; clearance of apoptotic cells
	C3AR1	18.25	8.94	Receptor of chemotactic and inflammatory C3a
PAF activity	*PTAFR*	59.30	12.91	Receptor for platelet-activating factor (PAF) – a pro-inflammatory phospholipid; potent inflammatory activity; causing vasodilatation and superoxide formation; expressed by RECs; its absence protects against IAV fatality; central to translocation of bacteria across IECs
	PLA2G7	31.12	13.83	A secreted enzyme; degrades PAF and modulates its activity
Cell adhesion molecules	*CD33*	33.82	14.62	Adhesion molecule; mediates sialic acid binding to cells; preferentially binds alpha,-2 6-linked sialic acids; may interact with sialic acid on the same cell surface; inhibitory receptor; induces apoptosis
	OLFM4	2.91	1.16	Expressed in inflamed colonic epithelium; anti-apoptotic; exact function yet unclear
	CTGF	1.30	0.64	A mitogen; secreted by vascular endothelial cells; cell adhesion; promotes proliferation and differentiation of chondrocytes
	TGFBI	29.65	10.06	Cell adhesion; binds several integrins and collagen; induced by TGFβ and inhibits cell adhesion
	EMILIN2	17.88	8.88	Cell adhesion; anchoring smooth muscle cells to elastin fibres
Other immune modulators	*ALOX5AP*	25.28	11.63	Required for leukotriene synthesis; primarily expressed in leukocytes
	MEFV	23.59	10.13	Modulator of innate immunity;
	FPR1	58.49	17.75	Receptor for annexin 1; expressed by neutrophils and DCs; involved in host defence against bacterial and viral infections

Table 7.4.5.3. Example genes from DAVID-identified enriched clusters in CD1DKO and their associated functions Representative genes from Figure 7.4.5.1 were selected and their functions/sites of expression when related to epithelial cells were retrieved from NCBI Pub Med.

Analysis with DAVID using GL4 (i.e. the 93 gene which had ΔFC > 2 in "WT3 vs. WT0" compared with "KO3 vs. KO0"; Table 7.4.5.1) detected fewer enriched gene clusters in WT RECs on day 3 compared to day 0. As Table 7.4.5.4 shows,

"heterodimer", "immune response" and "guanyl ribonucleotide binding" formed the most enriched clusters in GO categories (Figure 7.4.5.2). The overall immune response here is somewhat distinct from that of CD1dKO (Figure 7.4.5.1) in inducing CD1D1, CRTAM, and chemokines like CCL1, CCL17, and CCL24.

"WT vs. CD1dKO" on day 3 against day 0 (GL4)
Annotation clustering of genes – DAVID

Annotation	Term	Source	%Input	Benjamini *p* value
Function				
	Heterotetramer	SP-PIR	6.7	9.10E-6
	Immunoglobulin v region	SP-PIR	4.5	5.90E-4
Gene Ontology				
	Immune response	GO Term-BP	12.4	1.90E-2
	Guanyl ribonucleotide binding	GO Term-MF	14.6	3.40E-4
	Antigen binding	GO Term-MF	5.6	2.40E-4
Pathway				
	No enrichment			

Table 7.4.5.4. Functional clustering of differentially expressed genes in WT vs. CD1dKO on D3 against D0, using DAVID. Genes from GL4 were run against SP-PIR(Swiss-Protein and Protein Information Resource) library, and gene ontology (GO) biological process (BP), and molecular function (MF) databanks. A selection of those with Benjamini $p < 0.05$ is listed here. In every category, sets or terms were ranked according to %Input. No enriched pathway was detected.

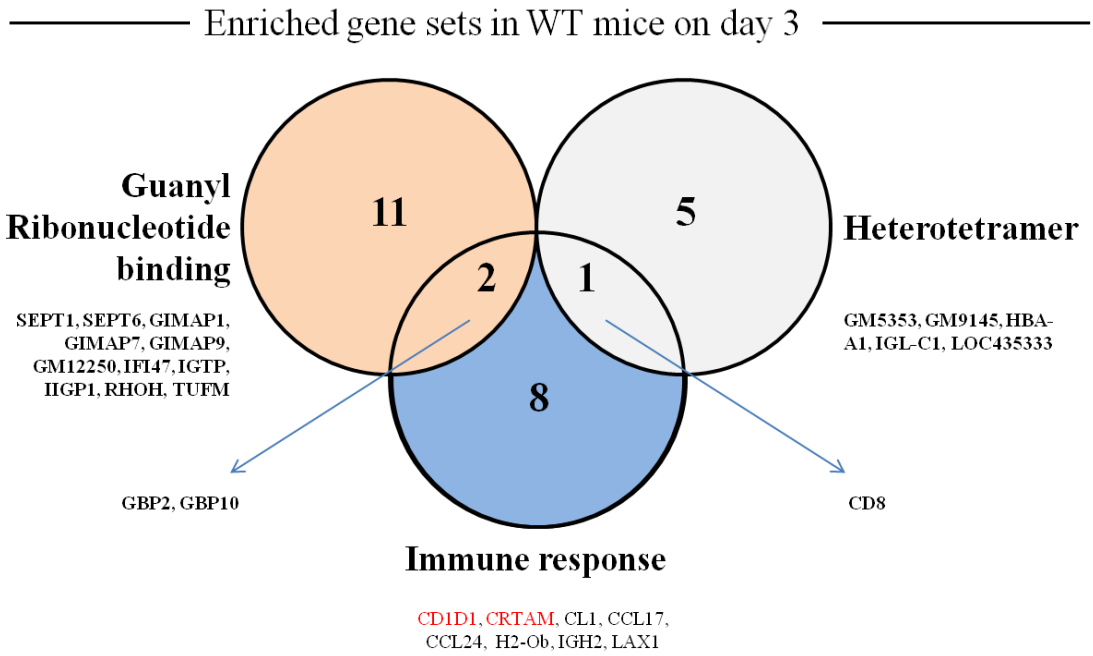

Figure 7.4.5.2. Venn diagram representation of enriched gene clusters in CD1dKO vs. WT on D3. The five highly enriched clusters from Table 7.4.5.4 were grouped into two categories: immune-related **(A)** and cell adhesion-related **(B)**; and then the overlapping genes between clusters in each group were identified.

Analysis with DAVID on day 6 after infection produced similar gene set enrichment as on day 3. However, GSEA analysis by comparing the "KO6 vs. KO0" against "WT6 vs. WT0" for all genes identified significant enrichment of nine sets, including "defence response", "inflammatory response", and "response to external stimulus" (Table 7.4.5.5).

GSEA gene set enrichment on day 6

Gene Set Name	NES	FDR *q* Value
"KO6 vs. KO0" vs. "WT6 vs. WT0"		
Response to wounding	2.23	0
Defence response	2.20	0
Inflammatory response	2.17	0
Response to external stimulus	2.11	0
Cell migration	1.99	3.97E-03
Humoral immune response	1.97	4.75E-03
Cell-cell siganling	1.96	4.21E-03
Lipid metabolic process	1.84	3.20E-02
Behaviour	1.80	4.73E-02
"WT6 vs. WT0" vs. "KO6 vs. KO0"		
No enriched pathway detected		

Table 7.4.5.5. Gene sets enriched in CD1KO and WT mice lung epithelial cells on "D6 vs. D0". In GSEA, comparative expression values of "WT6 vs. WT0" against "KO6 vs. KO0" and vice versa were analysed. The sets were ranked by NES. FDR (false discovery rate); NES: normalised enrichment score (ES corrected for difference in the size of gene sets).

Core-enriched genes (ranked genes in the gene list which appear before running score reaches maximum deviation; i.e. genes that contribute the most to the enrichment result) within the "response to wounding", "defence response", "inflammatory response", "response to external stimulus", and "humoral immune response" pathways were identified (140 genes in total) and those which were > 2 folds higher in CD1dKO than the WT (68 genes) were listed in Table 7.4.5.6. Amongst these genes were those

coding for PTAFR, S100A8, S100A9, IL-1α, IL-1R2, CD86, CXCL9, CXCL11, CCL17, TLR-7, TLR-8, IL-18, and bone marrow stromal cell antigen 2 (BST2) – highlighted in red in the Table.

Gene	Ref Seq ID	"KO6 vs. KO0"	"WT6 vs. WT0"	ΔFC	NCBI official full name
CYBB	NM_007807	34.78	5.7	6.10	cytochrome b-245, beta polypeptide
EREG	NM_007950	10.56	2.13	4.96	Epiregulin
CCR1	NM_009912	116.97	25.11	4.66	chemokine (C-C motif) receptor 1
F7	NM_010172	18.64	4.11	4.54	coagulation factor VII
MGLL	NM_001166251	4.69	1.04	4.51	monoglyceride lipase
TREM2	NM_031254	5.31	1.21	4.39	triggering receptor expressed on myeloid cells 2
CTSS	NM_021281	29.65	7.11	4.17	Cathepsin S
CD84	NM_013489	24.93	6.06	4.11	CD84 antigen
TLR8	NM_133212	17.51	4.38	4.00	toll-like receptor 8
CD86	NM_019388	60.97	15.45	3.95	CD86 antigen
MS4A1	NM_007641	10.41	2.71	3.84	membrane-spanning 4-domains, subfamily A, member 1
TYROBP	NM_011662	47.5	13.09	3.63	TYRO protein tyrosine kinase binding protein
CCL17	NM_011332	4.06	1.12	3.63	chemokine (C-C motif) ligand 17
CFP	NM_008823	15.56	4.44	3.50	complement factor properdin
PTAFR	NM_001081211	89.26	26.17	3.41	platelet-activating factor receptor
BST1	NM_009763	38.05	11.16	3.41	bone marrow stromal cell antigen 1
FPR1	NM_013521	28.64	8.69	3.30	formyl peptide receptor 1
ALOX15	NM_009660	1.41	0.43	3.28	arachidonate 15-lipoxygenase
IL1A	NM_010554	52.71	16.11	3.27	interleukin 1 alpha
CD79A	NM_007655	6.36	2.04	3.12	CD79A antigen (immunoglobulin-associated alpha)
ITGB2	NM_008404	31.78	10.41	3.05	integrin beta 2
SERPINE1	NM_008871	6.45	2.17	2.97	serine (or cysteine) peptidase inhibitor, clade E, member 1
S100A8	NM_013650	73.52	24.93	2.95	S100 calcium binding protein A8 (calgranulin A)
CCL20	NM_016960	1.52	0.52	2.92	chemokine (C-C motif) ligand 20
LSP1	NM_019391	28.64	9.99	2.87	lymphocyte specific 1
CD22	NM_001043317	4.44	1.55	2.86	CD22 antigen
CD36	NM_001159557	0.44	0.16	2.75	CD36 antigen
LY86	NM_010745	35.26	13.18	2.68	lymphocyte antigen 86
RNASE6	NM_030098	9.99	3.76	2.66	ribonuclease, RNase A family, 6
TREM1	NM_021406	51.98	19.97	2.60	triggering receptor expressed on myeloid cells 1
CLEC5A	NM_001038604	56.1	21.56	2.60	C-type lectin domain family 5, member a
IL2RG	NM_013563	56.89	22.16	2.57	interleukin 2 receptor, gamma chain
NCF2	NM_010877	30.48	11.88	2.57	Neutrophil cytosolic factor 2
CCR9	NM_001166625	3.92	1.53	2.56	chemokine (C-C motif) receptor 9
PTPRC	NM_001111316	42.22	16.56	2.55	protein tyrosine phosphatase, receptor type, C
FAIM3	NM_026976	2.97	1.17	2.54	Fas apoptotic inhibitory molecule 3
PLD1	NM_001164056	0.85	0.34	2.50	phospholipase D1
S100A9	NM_009114	56.49	22.63	2.50	S100 calcium binding protein A9 (calgranulin B)
FCGR2B	NM_001077189	20.97	8.46	2.48	Fc receptor, IgG, low affinity IIb
CXCL1	NM_008176	1.51	0.62	2.44	chemokine (C-X-C motif) ligand 1
COLEC12	NM_130449	2.48	1.03	2.41	collectin sub-family member 12
IL6	NM_031168	0.81	0.34	2.38	Interleukin 6
ALOX5AP	NM_009663	20.97	8.88	2.36	arachidonate 5-lipoxygenase activating protein
CTSC	NM_009982	2	0.85	2.35	cathepsin c
IL1R2	NM_010555	56.1	23.92	2.35	interleukin 1 receptor, type II
C5AR1	NM_001173550	22.16	9.51	2.33	complement component 5a receptor 1
IL18	NM_008360	9.13	3.92	2.33	interleukin 18
CXCL11	NM_019494	10.48	4.5	2.33	chemokine (C-X-C motif) ligand 11
LCP2	NM_010696	51.98	22.32	2.33	lymphocyte cytosolic protein 2
TLR7	NM_133211	26.17	11.24	2.33	toll-like receptor 7
ADORA3	NM_009631	7.94	3.43	2.31	adenosine A3 receptor
MX2	NR_003508	10.48	4.56	2.30	myxovirus (influenza virus) resistance 2
C3AR1	NM_009779	58.49	25.46	2.30	complement component 3a receptor 1
F11R	NM_172647	0.59	0.27	2.19	F11 receptor
LILRB3	NM_011095	18.25	8.4	2.17	leukocyte immunoglobulin-like receptor, subfamily B (with TM and ITIM domains), member 3
ARHGDIB	NM_007486	44.63	20.68	2.16	Rho, GDP dissociation inhibitor (GDI) beta
LTF	NM_008522	0.28	0.13	2.15	Lactotransferrin
CCR7	NM_007719	18.13	8.51	2.13	chemokine (C-C motif) receptor 7
UNC119	NM_011676	3.23	1.54	2.10	unc-119 homolog (C. elegans)
SHROOM3	NM_015756	0.44	0.21	2.10	shroom family member 3
RGS1	NM_015811	39.4	18.9	2.08	regulator of G-protein signalling 1
CCL22	NM_009137	3.18	1.55	2.05	chemokine (C-C motif) ligand 22
CXCL9	NM_008599	37.01	18.13	2.04	chemokine (C-X-C motif) ligand 9
PROS1	NM_011173	1.02	0.5	2.04	protein S (alpha)
MALT1	NM_172833	6.87	3.39	2.03	mucosa associated lymphoid tissue lymphoma translocation gene 1
BST2	NM_198095	6.54	3.23	2.02	bone marrow stromal cell antigen 2
SFTPD	NM_009160	-2.34	-3.37	0.69	surfactant associated protein D
AGER	NM_007425	-2.11	-3.35	0.63	advanced glycosylation end product-specific receptor

Table 7.4.5.6. The list of all GSEA-discovered core-enriched immune genes from Table 7.4.5.6. Genes in the "leading-edge subset of "response to wounding", "defence response", "inflammatory response", "response to external stimulus", and "humoral immune response" pathways were identified and their corresponding expression fold change were extracted. Genes were ranked according to ΔFC.

The key message from these analyses is that on both day 3 and day 6 after infection, RECs in both CD1dKO and WT mice exhibited similar programmes of gene activation, mainly those involved in immune response (as expected). It is the magnitude of change that differs between these two phenotypes. Table 7.4.5.4 summarises the fold change in gene expression on day 3 and day 6 of several innate- and proinflammatory-associated genes, which were differentially expressed between WT and CD1dKO (as illustrated in Figure 7.4.5.3).

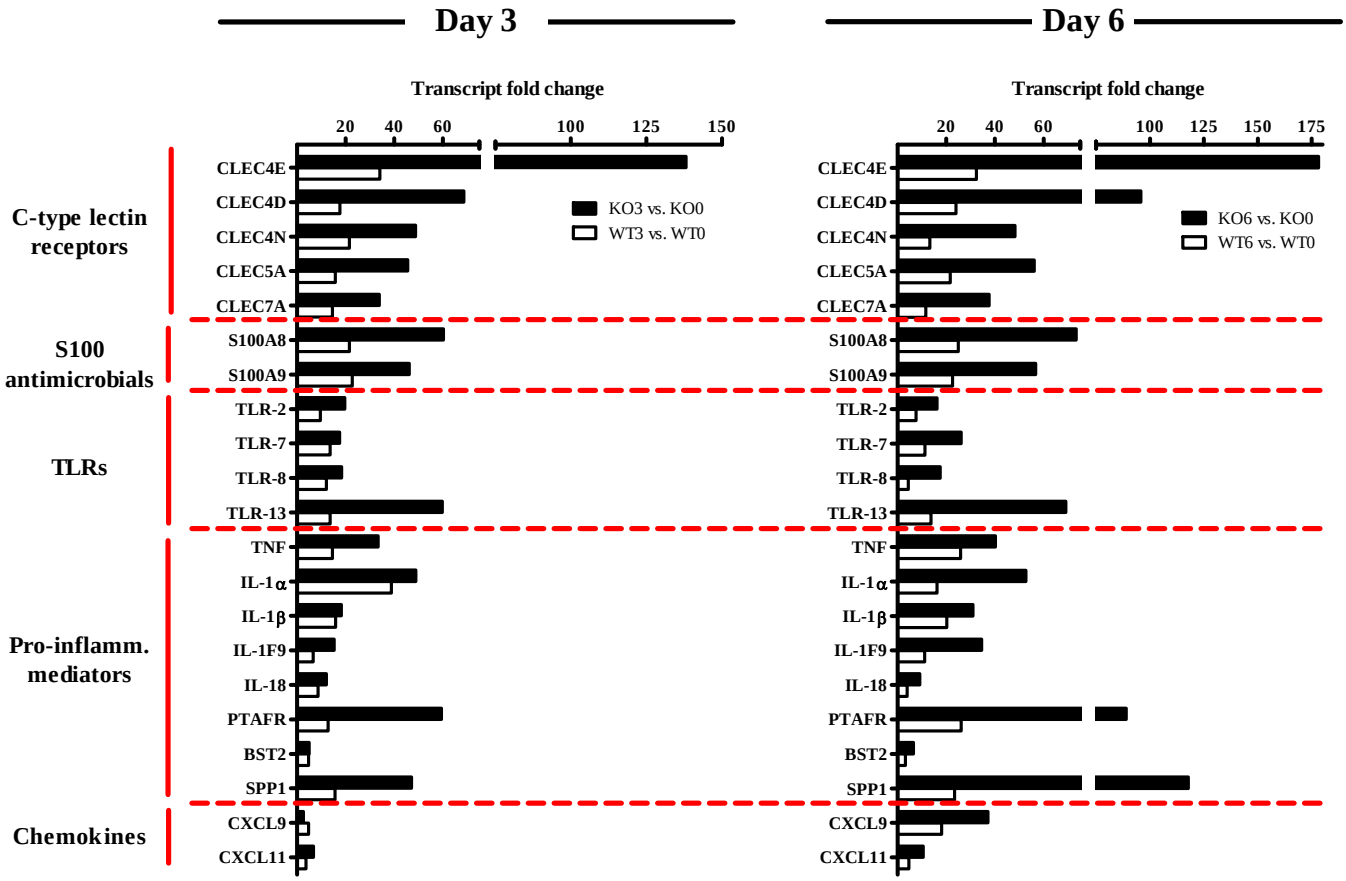

Figure 7.4.5.3. Fold change in expression of several differentially expressed genes in CD1dKO and WT mice on D3 and D6 against D0.

7.5. Discussion

In this chapter, I show that i) in the absence of CD1d, mice have a poorer outcome when infected with sub-lethal doses of PR8, and ii) CD1d expression on RECs is associated with lower induction of innate (e.g. TLR-7/8, S100A8/9) and pro-inflammatory (e.g. TNFα, IL-18) immune responses in lung epithelial cells after *in vivo* challenge with IAV, and higher expression of genes required for airway epithelial remodelling (e.g. CRTAM).

The higher susceptibility of CD1dKO mice to PR8 in my studies is consistent with previous reports [140,364], so it is not unexpected. However, I performed the studies to ensure that this is still the case using the reagents that I would use for my REC gene expression profiling experiment. There are two significant limitations with the use of CD1d KO mice in this context. Firstly, these mice also lacked *i*NKT cells since CD1d expression on thymocytes is required for development of these cells in the thymus. Therefore CD1dKO mice lack both CD1d expression on RECs and *i*NKT cells infiltration to the lungs during IAV infection. Both these factors could have contributed to the observations from this experiment. One argument against the significance of the loss of *i*NKT cells is the finding that adoptively transferred *i*NKT cells to this model do not reverse the excess viral load or mortality observed in these mice. Therefore it would appear that the poorer outcome in CD1dKO mice relates more to the loss of CD1d rather than *i*NKT cells. The other limitation is that CD1dKO mice do not express CD1d on RECs and also other cells, such as antigen-presenting cells like dendritic cells, monocytes and B cells. The relative contribution of CD1d-deficient dendritic cells for example, to the worse outcome in these mice after IAV infection is unknown.

I found no specific genes that were unexpectedly increased or reduced in the experiment, rather the collective results point towards an unexpected lower level of immune-related and pro-inflammatory genes in WT mice. Greater magnitude of induction of innate immune (e.g. TLRs, S100A8, CLECs) and pro-inflammatory genes (SPP1, TNFα, IL-1α), and those coding for chemokines (e.g. CXCL9, CXCL11) and chemokine receptors (e.g. PTAFR) in CD1dKO could explain the contribution of airway cells to higher mortality after IAV infection.

The S100 family of genes were well represented in genes upregulated in CD1dKO. S100A8 (also known as calgranulin A) and S100A9 (also called calgranulin B) are two well-studied members of calcium-binding S100 protein family with known antimicrobial functions [365]. However, their biological activity is very diverse and includes induction of apoptosis and autophagy [366], pro-inflammatory effects [367], and control of microbial growth [368]. While the expression of calgranulins has been predominantly linked to monocytes and neutrophils [365], airway epithelial cells [368], IECs [367,369] and keratinocytes [370] have all been reported to constitutively express S100A8 and enhance its expression following treatment with TNFα, IL-1β, LPS, or exposure to heat-inactivated *P. aueroginosa* [368,371]. Therefore, the more pronounced upregulation of S100A8 in CD1dKO than WT after PR8 infection (60 vs. 22 on D3, and 74 vs. 25 on D6) could be secondary to higher availability of pro-inflammatory mediators like TNFα and IL-1β (both evident in the array results) in the microenvironment surrounding the infected-epithelial cells and may contribute to enhanced apoptosis of RECs [368].

C-type lectins (CLECs) were also amongst the significant fold change outputs in CD1d KO mice. These genes represent a family of carbohydrate-recognising proteins which perform both immune and non-immune functions. By binding endogenous ligands, for example, they facilitate cell-cell bindings and cell-extracellular matrix interactions; whereas via detection of foreign antigens they act as pathogen recognition receptors (PRRs) [214,372,373]. The results of this chapter demonstrate that infection with PR8 strongly upregulates transcripts for five members of CLEC family – CLEC4E, CLEC4D, CLEC4N, CLEC5A, and CLEC7A, in both mouse phenotypes; however, the induction in CD1dKO was at least twice ($\Delta FC > 2$) as high as WT. CLEC4E (also known as MINCLE) is a FcRγ-associated activating surface receptor which senses damaged cells [374], and also signals presence of pathogenic fungal ligands [375] and mycobacterial antigens [376]. CLEC4D (also known as MCL), that lacks intracellular signalling motif, functions as an endocytic receptor [377], and CLEC4N (also known as DECTIN-2) works as a receptor for exogenous (e.g. fungal, mycobacterial) [373,378,379] and endogenous (e.g. surface molecules on $CD4^+$ $CD25^+$ Treg) [380] ligands. Of interest, CLEC5A (also known as MDL-1) is a receptor for Dengue virus [381]. These observations suggest that RECs in CD1dKO mice trigger a stronger antimicrobial response after IAV infection than WT; possibly due to the greater viral burden. Higher CLEC4E expression (highest fold change compared to WT on day 3 and day 6 – Figure 7.4.5.3) could indicate greater abundance of damaged cells in CD1dKO mice.

SSP1 (also called osteopontin) showed near to 110 fold change in KO6 against KO0 (compared to 28 fold change in WT6 against WT0). This gene encodes a secreted protein which binds integrins or CD44 to exert its biological effects [382]. It is

produced by many different cell types and its expression is upregulated during inflammation and tissue injury [382]. SPP1 is reported to be required for T_h1 polarisation of immune response [383-385], and SPP1-CD44 interaction has been shown to inhibit IL-10 production [386]. Additionally, SPP1 is a chemoattractant for DCs, macrophages and T cells [382]. Binding to its receptor, SSP1 results in increased production of IFNα and other cytokines, like IL-12 and TNFα [383]. A number of potential hypotheses could be generated from this observation. One of them is that lack of CD1d expression on RECs result in higher SSP1 production and T_h1 polarisation of immune responses and/or increased recruitment of inflammatory cells to the site of inflammation with resultant augmentation of pro-inflammatory cytokine production from immune cells.

The transcript levels of the pro-apoptotic and pro-inflammatory TNFα cytokine was also more than doubled in CD1dKO than WT mice on day 3 (33 vs. 15). Additionally, the expression of genes coding for ligands and receptors of the IL-1 protein family was induced to a greater extent in CD1dKO mice. For example, IL-1α transcript on day 3 against day 0 showed a fold change of 49 in CD1dKO, compared with 39 in WT. Similarly, IL-1F9 (also known as IL-1 epsilon) had increased 15 fold in CD1dKO on day 3, whereas only a 7-fold increase was observed in WT. Comparable fold change differences also occurred on day 6 versus day 0. IL-1F9 has been demonstrated to be expressed by keratinocytes and epithelial-rich tissues. Its expression is induced in inflammatory conditions (e.g. by TNFα, and IL-1β), and causes activation of NFκB [387]. Exposure to heat-inactivated *P. auerοginosa* or treatment with TNFα has been shown to induce IL-1F9 expression in primary bronchial epithelial cells [368], indicating a role for this cytokine in mucosal immunity. As a result, greater induction of

TNFα, IL-1α, and IL-1F9 suggests a more severe inflammatory and pro-apoptotic response by RECs after IAV infection in CD1dKO mice. All these point towards a greater and less-controlled immune activation by the RECs which could trigger a more severe host immune response. This did not correlate with better control of viral load, rather an increased mortality; suggesting that a possibility for death in these mice might be the occurrence of a phenomenon like the "cytokine storm" observed in severe IAV infection in humans [388].

In the same vein, expression of several chemokines (e.g. CXCL9, CXCL11) was robustly induced after PR8 infection, particularly in CD1dKO mice on D6. CXCL9 and CXCL11 are prototypical examples of IFN-induced chemokines [244,389]. Therefore, their higher levels in CD1dKO indicate greater abundance of (type I and II) IFNs in the microenvironment surrounding epithelial cells. Polarised expression of CXCL11 on respiratory epithelium has been reported to mediate T cell egression from lung interstitium into the lumen [248], therefore, in the absence of CD1d epithelial cells could promote a greater migration of T cells into the airways, which could contribute to increased lung pathology and subsequent higher mortality in these mice.

A number of genes were selectively more expressed in WT than CD1dKO mice, including CRTAM. The product of this gene is a member of immunoglobulin superfamily which was originally identified for its restricted expression on T cells [390]. However, it later became evident that NK and epithelial cells also express CRTAM [391,392]. In fact, CRTAM is expressed on the lateral membrane of epithelial cells and is important for cell-cell adhesions and the maintenance of transepithelial electrical resistance in *in vitro* cultures [391]. Therefore, the unchanged levels of CRTAM in CD1dKO, compared with 4.7 folds increase in WT could indicate lowered ability of

epithelial cells in CD1dKO mice to interact with each other and form a monolayer; hence, less remodelling ability.

The findings have provided novel hypotheses which I will now examine. The key to which to prioritise would be the validation of gene expression by RT-PCR and protein expression in mice RECs or human epithelial cells.

7.6. Conclusion

In summary the results of this chapter indicate that CD1d-deficient mice have a poorer outcome after IAV infection. The innate and defence immune response repertoires in RECs of CD1dKO mice, compared with WT, were more strongly induced after IAV infection. This selective induction included genes coding for TLRs (TLR-7, TLR-8, TLR-13), antimicrobial peptides (S100A8, S100A9), cell adhesion molecules (CLECs), chemokines (CXCL9, CXCL11), and pro-inflammatory cytokines and receptors (TNFα, IL-1α, SPP1, IL-18, PTAFR), and overall may be a contributing factor to mortality in CD1d-deficient mice.

Chapter 8. Discussion, future directions, and final conclusions

Chapter 8.

Discussion, future directions, and final conclusions

8.1. Discussion

This project has five main findings: 1) respiratory epithelial cells (RECs) express CD1D mRNA and protein; 2) CD1D mRNA undergoes alternative splicing to produce at least six variants; 3) viral-associated molecules like type I and type II interferons, and TLR-3L; and infection with influenza A virus (IAV) upregulate surface CD1d expression on REC 4) α–GC pulsed RECs are capable of activating *i*NKT cells and finally 5) lack of CD1d expression on RECs is associated with increased activation of pro-inflammatory immune pathway genes in RECs after IAV infection *in vivo*.

This is the first report of CD1d finding in REC, in contrast to reports on intestinal epithelial cells which first surfaced in 1990 [68], was in 2003 when it was postulated that RECs may express CD1d [393] One reason for the lack of demonstration for this could be the low number of transcripts at baseline (although, considering the area of respiratory airways, a small increase could be rapidly translated to a large consequence); and presence of CD1D variants. My findings showed that there are at least six transcripts in epithelial cells and we are still unclear which were identified by the available CD1d mAbs. There was differential ability by the various CD1d mAbs to detect these variants, and a number of primers I first designed (not reported here) were not able to identify CD1D transcripts. No investigators have shown expression of CD1d proteins on RECs of mice to date, and using the mAbs currently available commercially and from collaborators, I was also unable to do this. However,

the transcript was clearly present in mice RECs (Chapter 7.4.2) and genomic profiling showed a five-fold increase in amount expressed after IAV infection (Chapter 7.4.4).

The potential implications of this finding were suggested in the Discussion section of Chapter 5. In the main, this raises the prospects of different CD1d variants being involved in different cellular function and only some of these being inducible during IAV infection.

As my over-riding priority was to investigate the potential functional contribution of REC CD1d to mucosal immunity and it had already taken me about a year to prove the existence of CD1d expression on REC, I went on to work on the rest of the project rather than define the individual role of the CD1d variants.

Previous studies from my supervisor's laboratory and other investigators have demonstrated a role for *i*NKT cells in protection against influenza infection. However, it is unclear how these cells are activated during IAV infection and how they infiltrate the airways. My findings suggest that inducible CD1d on RECs can activate *i*NKT cells and could be responsible for presentation of self or exogenous glycolipids to *i*NKT cells in the lungs during IAV infection. The *in vitro* studies on NHBE cells used α–GC, which is not a natural ligand (rather a prototype 'superagonist') for *i*NKT cells. Despite numerous efforts to identify exogenous glycolipid ligands for CD1d, only a handful of bacterial and protozoal lipids, from *Borrelia*, *Sphingomonas*, *Entamoeba*, and *Leishmania* species, have been discovered to load onto CD1d [30-34]. There has been no report of viral-derived CD1d ligands to date. This is not surprising since the genome of viruses, like IAV, does not code for lipid antigens; instead their envelope lipids originate from the host cell lipid repertoire. Therefore, the candidate ligand for

epithelial CD1d during IAV infection is possibly a self ligand. The other possibility is that the *i*NKT cells are activated indirectly; that is, without engagement of its TCR – via soluble factors like IL-12. Brigl *et al* proposed that weak responses to CD1d-presented self antigens could be amplified by IL-12 made by dendritic cells in response to microbial products, resulting in potent IFNγ secretion [270]. Theoretically, to detect the identity of this lipid, I could infect the primary NHBE cells *in vitro*, lyse the cells, phase-separate the aqueous and hydrophobic components of epithelial extract, and fractionate the hydrophobic factors on the basis of size (by passing through filters of varying molecular weights). By pulsing RECs with different water-insoluble fractions, I will then be able to see which one can load on to CD1d and subsequently stimulate *i*NKT cells.

One of the signalling molecules that induced CD1d expression was the poly I:C – a TLR-3 ligand and surrogate for dsRNA. IAV is a single-stranded segmented RNA virus [153]; however, dsRNA replicative intermediates are formed during viral replication which are important for the outcome of the infection [284,285]. TLR-3 – the host cell's major dsRNA receptor, is widely expressed on RECs [202], and upon binding by its ligand induces strong type I IFN production [283]. Therefore, IAV infection could activate the TLR-3 signalling cascade and other viral sensors (e.g. retinoic acid-inducible gene-I; RIG-I) leading to type -1 IFN production by REC, and subsequently enhanced surface CD1d.

However, I did note that CD1d upregulation in IAV-infected RECs was at a lower magnitude than when the cells were treated with IFNs. One possible explanation

is that the virus has evolved mechanisms to escape immune activation by suppressing CD1d expression. Indeed, Yuan *et al* showed that herpes simplex virus 1 (HSV-1) downregulated surface CD1d on infected cells [78]; purportedly by preventing the reappearance of endocytosed CD1d on the cell surface via redistribution of endocytosed CD1d to the lysosome limiting membrane. This would impair antigen-presentation and therefore activation of *i*NKT cells. In Yuan's study, this occurred as early as 9 hours after contact with the virus, which is within my 48 hour IAV-stimulation time frame. HIV-1 and Kaposi sarcoma-associated herpes virus (KSHV) have also been shown to impair surface CD1d levels [79-83]. In the case of IAV infection, reduction of CD1d could be considerably counteracted by virus–induced cytokines which then indirectly activate *i*NKT cells.

My findings on the ability of REC to stimulate *i*NKT cells are in keeping with studies showing that RECs are an active component of host defence in the lungs. From the adaptive immunity point, human RECs have been reported to present mycobacterial antigens to $CD4^+$ T cells and stimulate release of IFNγ and IL-2 by these cells [249]. RECs were also able to induce T cell proliferation in mixed lymphocyte reaction (MLR) cultures [250]. Oei *et al* showed that epithelial cells obtained from surgical specimens of patients undergoing pulmonary lobectomy stimulated proliferation of both $CD4^+$ and $CD8^+$ T cells [251]. However, there has been no report of *i*NKT cell activation by airway epithelial cells to date. I show that *i*NKT cells exposed to α–GC-pulsed REC rapidly produced both T_h1 and T_h2 cytokines, like IFNγ, TNFα, IL-4, IL-5, and IL-13, and its genomic profile exhibited enrichment of genes and biological pathways involved in cytokine and chemokine activity, cytokine signalling (JAK-STAT pathway), and apoptosis. These cytokines could further impact on REC function and its

contribution to mucosal immunity. For example, IFNγ by *i*NKT cells could enhance MHC class II and co-stimulatory molecules expression on RECs [251,394] and promote secretion of IL-7 and IL-15 – two key T cell growth factors [282]. Oncostatin M (OSM), (first reported in this thesis to be expressed in *i*NKT cells) could stimulate the secretion of α1-antitrypsin (α1-AT) from RECs – the main inhibitor of serine proteases and a key player in lung homeostasis and anti-inflammatory processes [304,305].

Results from Chapter 7 suggest that CD1d expression on RECs could have a 'bi-directional' effect – on the *i*NKT cells by presenting antigens to these cells and on itself, the RECs. The key finding in the latter is that CD1d expression appears to modulate the immune activation genes in REC with resultant improvement in viral burden and outcome in IAV-infected mice. Although this appears a paradox, in fact, this fits with prevailing thoughts that it is an optimum rather than strong immune response that leads to the best outcome in IAV infection. Vigorous immune response in young patients (30-45 years) from the 1918 IAV pandemic, and more recently in the 2009 pandemic, are thought to be the cause of a "cytokine storm" that accompanied excess deaths in this age group. Therefore it is appealing to speculate that CD1d-mediated signalling in REC is a component of the mucosal immunity that prevents this response. This seems the case in these mice but more definitive studies (in progress, and described later) will have to be performed to confirm/support this hypothesis.

8.2. Future directions

The study has allowed me to prove the expression of CD1d in RECs both in humans (mRNA and protein) and mice (mRNA), and show that there was at least

partial contribution from CD1d expressed on RECs to *i*NKT cell activation. The genomic studies strengthened the idea that *i*NKT cell are activated by RECs and given me an overview of other potential consequence of contact between *i*NKT cells and α–GC pulsed RECs. It has allowed me to generate several interesting hypotheses.

Two studies that I would like to perform first before tackling the hypotheses discussed in Chapter 6 and 7, concern the consequence of CD1d ligation on RECs, and relative contribution of CD1d expression on APCs and RECs, to protection from IAV infection.

For the first question, I will ask how CD1d ligand presentation to TCR, alone and without interference from cytokines secreted by activated *i*NKT cells, influence the function of RECs? This can be studied by crosslinking surface CD1d molecules, using specific Abs, and then monitor cellular responses. Ligating CD1d on the surface of IECs, for example, has been shown to induce an anti-inflammatory response by upregulating IL-10 production [342]. This would support the idea that CD1d expression on REC has a consequence on the REC. Indeed, delineation of an anti-inflammatory response will support my hypothesis that CD1d expressed on REC is involved in modulating the magnitude of immune response to IAV.

For the second question, I will ask how important is the expression of CD1d on epithelial cells compared with CD1d on APCs, like DCs and macrophages, in protection against IAV infection? This can be studied by generating a conditional knockout mouse in which CD1d is selectively deleted in RECs. Alternatively, bone marrow chimeric mice can be created in which CD1d expression is absent either in structural or haematopoietic cells and subject these mice to IAV infection (I have generated these

mice). This would allow me to decide the importance of CD1d expression on RECs to protection from severe disease after IAV infection.

8.3. Final conclusions

In summary, this thesis provides the first evidence for inducible CD1d expression on RECs. RECs are able to present α–GC to, and activate *i*NKT cells in a CD1d dependent process. Activated *i*NKT cells upregulate genes involved in cytokine/chemokine signalling and apoptosis. During IAV infection CD1d-expressing RECs showed a smaller magnitude of immune genes activation, which may have implications in preventing immune-mediated pathology in the lungs.

[1] Venkataswamy MM, Porcelli SA. Lipid and glycolipid antigens of CD1d-restricted natural killer T cells. Semin Immunol 2010;22:68-78.
[2] McMichael AJ, Pilch JR, Galfre G, Mason DY, Fabre JW, Milstein C. A human thymocyte antigen defined by a hybrid myeloma monoclonal antibody. Eur J Immunol 1979;9:205-210.
[3] Brigl M, Brenner MB. CD1: antigen presentation and T cell function. Annu Rev Immunol 2004;22:817-890.
[4] Barral DC, Brenner MB. CD1 antigen presentation: how it works. Nat Rev Immunol 2007;7:929-941.
[5] Bradbury A, Milstein C, Kozak CA. Chromosomal localization of Cd1d genes in the mouse. Somat Cell Mol Genet 1991;17:93-96.
[6] Zimmer MI, Nguyen HP, Wang B, Xu H, Colmone A, Felio K, Choi HJ, Zhou P, Alegre ML, Wang CR. Polymorphisms in CD1d affect antigen presentation and the activation of CD1d-restricted T cells. Proc Natl Acad Sci U S A 2009;106:1909-1914.
[7] Han M, Hannick LI, DiBrino M, Robinson MA. Polymorphism of human CD1 genes. Tissue Antigens 1999;54:122-127.
[8] Bainbridge D, Ellis S, Le Bouteiller P, Sargent I. HLA-G remains a mystery. Trends Immunol 2001;22:548-552.
[9] Angenieux C, Salamero J, Fricker D, Cazenave JP, Goud B, Hanau D, de La Salle H. Characterization of CD1e, a third type of CD1 molecule expressed in dendritic cells. J Biol Chem 2000;275:37757-37764.
[10] Woolfson A, Milstein C. Alternative splicing generates secretory isoforms of human CD1. Proc Natl Acad Sci U S A 1994;91:6683-6687.
[11] Kojo S, Adachi Y, Tsutsumi A, Sumida T. Alternative splicing forms of the human CD1D gene in mononuclear cells. Biochem Biophys Res Commun 2000;276:107-111.
[12] Kojo S, Tsutsumi A, Goto D, Sumida T. Low expression levels of soluble CD1d gene in patients with rheumatoid arthritis. J Rheumatol 2003;30:2524-2528.
[13] Segawa S, Goto D, Yoshiga Y, Hayashi T, Matsumoto I, Ito S, Sumida T. Low levels of soluble CD1d protein alters NKT cell function in patients with rheumatoid arthritis. Int J Mol Med 2009;24:481-486.
[14] Jenkinson HJ, Wainwright SD, Simpson KL, Perry AC, Fotiadou P, Holmes CH. Expression of CD1D mRNA transcripts in human choriocarcinoma cell lines and placentally derived trophoblast cells. Immunology 1999;96:649-655.
[15] Koch M, Stronge VS, Shepherd D, Gadola SD, Mathew B, Ritter G, Fersht AR, Besra GS, Schmidt RR, Jones EY, Cerundolo V. The crystal structure of human CD1d with and without alpha-galactosylceramide. Nat Immunol 2005;6:819-826.
[16] Zeng Z, Castano AR, Segelke BW, Stura EA, Peterson PA, Wilson IA. Crystal structure of mouse CD1: An MHC-like fold with a large hydrophobic binding groove. Science 1997;277:339-345.
[17] Beckman EM, Porcelli SA, Morita CT, Behar SM, Furlong ST, Brenner MB. Recognition of a lipid antigen by CD1-restricted alpha beta+ T cells. Nature 1994;372:691-694.
[18] Moody DB. The surprising diversity of lipid antigens for CD1-restricted T cells. Adv Immunol 2006;89:87-139.
[19] Brutkiewicz RR. CD1d ligands: the good, the bad, and the ugly. J Immunol 2006;177:769-775.
[20] Joyce S, Woods AS, Yewdell JW, Bennink JR, De Silva AD, Boesteanu A, Balk SP, Cotter RJ, Brutkiewicz RR. Natural ligand of mouse CD1d1: cellular glycosylphosphatidylinositol. Science 1998;279:1541-1544.
[21] De Silva AD, Park JJ, Matsuki N, Stanic AK, Brutkiewicz RR, Medof ME, Joyce S. Lipid protein interactions: the assembly of CD1d1 with cellular phospholipids occurs in the endoplasmic reticulum. J Immunol 2002;168:723-733.
[22] Park JJ, Kang SJ, De Silva AD, Stanic AK, Casorati G, Hachey DL, Cresswell P, Joyce S. Lipid-protein interactions: biosynthetic assembly of CD1 with lipids in the endoplasmic reticulum is evolutionarily conserved. Proc Natl Acad Sci U S A 2004;101:1022-1026.
[23] Giabbai B, Sidobre S, Crispin MD, Sanchez-Ruiz Y, Bachi A, Kronenberg M, Wilson IA, Degano M. Crystal structure of mouse CD1d bound to the self ligand phosphatidylcholine: a molecular basis for NKT cell activation. J Immunol 2005;175:977-984.
[24] Yuan W, Kang SJ, Evans JE, Cresswell P. Natural lipid ligands associated with human CD1d targeted to different subcellular compartments. J Immunol 2009;182:4784-4791.
[25] Jahng A, Maricic I, Aguilera C, Cardell S, Halder RC, Kumar V. Prevention of autoimmunity by targeting a distinct, noninvariant CD1d-reactive T cell population reactive to sulfatide. J Exp Med 2004;199:947-957.

[26] Stanic AK, De Silva AD, Park JJ, Sriram V, Ichikawa S, Hirabyashi Y, Hayakawa K, Van Kaer L, Brutkiewicz RR, Joyce S. Defective presentation of the CD1d1-restricted natural Va14Ja18 NKT lymphocyte antigen caused by beta-D-glucosylceramide synthase deficiency. Proc Natl Acad Sci U S A 2003;100:1849-1854.
[27] Zhou D, Mattner J, Cantu C, 3rd, Schrantz N, Yin N, Gao Y, Sagiv Y, Hudspeth K, Wu YP, Yamashita T, Teneberg S, Wang D, Proia RL, Levery SB, Savage PB, Teyton L, Bendelac A. Lysosomal glycosphingolipid recognition by NKT cells. Science 2004;306:1786-1789.
[28] Yin N, Long X, Goff RD, Zhou D, Cantu C, 3rd, Mattner J, Mezard PS, Teyton L, Bendelac A, Savage PB. Alpha anomers of iGb3 and Gb3 stimulate cytokine production by natural killer T cells. ACS Chem Biol 2009;4:199-208.
[29] Speak AO, Salio M, Neville DC, Fontaine J, Priestman DA, Platt N, Heare T, Butters TD, Dwek RA, Trottein F, Exley MA, Cerundolo V, Platt FM. Implications for invariant natural killer T cell ligands due to the restricted presence of isoglobotrihexosylceramide in mammals. Proc Natl Acad Sci U S A 2007;104:5971-5976.
[30] Kinjo Y, Tupin E, Wu D, Fujio M, Garcia-Navarro R, Benhnia MR, Zajonc DM, Ben-Menachem G, Ainge GD, Painter GF, Khurana A, Hoebe K, Behar SM, Beutler B, Wilson IA, Tsuji M, Sellati TJ, Wong CH, Kronenberg M. Natural killer T cells recognize diacylglycerol antigens from pathogenic bacteria. Nat Immunol 2006;7:978-986.
[31] Kinjo Y, Wu D, Kim G, Xing GW, Poles MA, Ho DD, Tsuji M, Kawahara K, Wong CH, Kronenberg M. Recognition of bacterial glycosphingolipids by natural killer T cells. Nature 2005;434:520-525.
[32] Sriram V, Du W, Gervay-Hague J, Brutkiewicz RR. Cell wall glycosphingolipids of Sphingomonas paucimobilis are CD1d-specific ligands for NKT cells. Eur J Immunol 2005;35:1692-1701.
[33] Amprey JL, Im JS, Turco SJ, Murray HW, Illarionov PA, Besra GS, Porcelli SA, Spath GF. A subset of liver NK T cells is activated during Leishmania donovani infection by CD1d-bound lipophosphoglycan. J Exp Med 2004;200:895-904.
[34] Lotter H, Gonzalez-Roldan N, Lindner B, Winau F, Isibasi A, Moreno-Lafont M, Ulmer AJ, Holst O, Tannich E, Jacobs T. Natural killer T cells activated by a lipopeptidophosphoglycan from Entamoeba histolytica are critically important to control amebic liver abscess. PLoS Pathog 2009;5:e1000434.
[35] Wu DY, Segal NH, Sidobre S, Kronenberg M, Chapman PB. Cross-presentation of disialoganglioside GD3 to natural killer T cells. J Exp Med 2003;198:173-181.
[36] Sriram V, Willard CA, Liu J, Brutkiewicz RR. Importance of N-linked glycosylation in the functional expression of murine CD1d1. Immunology 2008;123:272-281.
[37] Porcelli SA. The CD1 family: a third lineage of antigen-presenting molecules. Adv Immunol 1995;59:1-98.
[38] Kang SJ, Cresswell P. Calnexin, calreticulin, and ERp57 cooperate in disulfide bond formation in human CD1d heavy chain. J Biol Chem 2002;277:44838-44844.
[39] Kang SJ, Cresswell P. Saposins facilitate CD1d-restricted presentation of an exogenous lipid antigen to T cells. Nat Immunol 2004;5:175-181.
[40] Zhou D, Cantu C, 3rd, Sagiv Y, Schrantz N, Kulkarni AB, Qi X, Mahuran DJ, Morales CR, Grabowski GA, Benlagha K, Savage P, Bendelac A, Teyton L. Editing of CD1d-bound lipid antigens by endosomal lipid transfer proteins. Science 2004;303:523-527.
[41] Brozovic S, Nagaishi T, Yoshida M, Betz S, Salas A, Chen D, Kaser A, Glickman J, Kuo T, Little A, Morrison J, Corazza N, Kim JY, Colgan SP, Young SG, Exley M, Blumberg RS. CD1d function is regulated by microsomal triglyceride transfer protein. Nat Med 2004;10:535-539.
[42] Dougan SK, Salas A, Rava P, Agyemang A, Kaser A, Morrison J, Khurana A, Kronenberg M, Johnson C, Exley M, Hussain MM, Blumberg RS. Microsomal triglyceride transfer protein lipidation and control of CD1d on antigen-presenting cells. J Exp Med 2005;202:529-539.
[43] Sagiv Y, Bai L, Wei DG, Agami R, Savage PB, Teyton L, Bendelac A. A distal effect of microsomal triglyceride transfer protein deficiency on the lysosomal recycling of CD1d. J Exp Med 2007;204:921-928.
[44] Brutkiewicz RR, Bennink JR, Yewdell JW, Bendelac A. TAP-independent, beta 2-microglobulin-dependent surface expression of functional mouse CD1.1. J Exp Med 1995;182:1913-1919.
[45] Balk SP, Burke S, Polischuk JE, Frantz ME, Yang L, Porcelli S, Colgan SP, Blumberg RS. Beta 2-microglobulin-independent MHC class Ib molecule expressed by human intestinal epithelium. Science 1994;265:259-262.

[46] Kim HS, Garcia J, Exley M, Johnson KW, Balk SP, Blumberg RS. Biochemical characterization of CD1d expression in the absence of beta2-microglobulin. J Biol Chem 1999;274:9289-9295.
[47] Jayawardena-Wolf J, Benlagha K, Chiu YH, Mehr R, Bendelac A. CD1d endosomal trafficking is independently regulated by an intrinsic CD1d-encoded tyrosine motif and by the invariant chain. Immunity 2001;15:897-908.
[48] Kang SJ, Cresswell P. Regulation of intracellular trafficking of human CD1d by association with MHC class II molecules. EMBO J 2002;21:1650-1660.
[49] Lawton AP, Prigozy TI, Brossay L, Pei B, Khurana A, Martin D, Zhu T, Spate K, Ozga M, Honing S, Bakke O, Kronenberg M. The mouse CD1d cytoplasmic tail mediates CD1d trafficking and antigen presentation by adaptor protein 3-dependent and -independent mechanisms. J Immunol 2005;174:3179-3186.
[50] Chiu YH, Park SH, Benlagha K, Forestier C, Jayawardena-Wolf J, Savage PB, Teyton L, Bendelac A. Multiple defects in antigen presentation and T cell development by mice expressing cytoplasmic tail-truncated CD1d. Nat Immunol 2002;3:55-60.
[51] Bonifacino JS, Traub LM. Signals for sorting of transmembrane proteins to endosomes and lysosomes. Annu Rev Biochem 2003;72:395-447.
[52] Yuan W, Qi X, Tsang P, Kang SJ, Illarionov PA, Besra GS, Gumperz J, Cresswell P. Saposin B is the dominant saposin that facilitates lipid binding to human CD1d molecules. Proc Natl Acad Sci U S A 2007;104:5551-5556.
[53] Exley M, Garcia J, Wilson SB, Spada F, Gerdes D, Tahir SM, Patton KT, Blumberg RS, Porcelli S, Chott A, Balk SP. CD1d structure and regulation on human thymocytes, peripheral blood T cells, B cells and monocytes. Immunology 2000;100:37-47.
[54] Spada FM, Borriello F, Sugita M, Watts GF, Koezuka Y, Porcelli SA. Low expression level but potent antigen presenting function of CD1d on monocyte lineage cells. Eur J Immunol 2000;30:3468-3477.
[55] Canchis PW, Bhan AK, Landau SB, Yang L, Balk SP, Blumberg RS. Tissue distribution of the non-polymorphic major histocompatibility complex class I-like molecule, CD1d. Immunology 1993;80:561-565.
[56] Blumberg RS, Terhorst C, Bleicher P, McDermott FV, Allan CH, Landau SB, Trier JS, Balk SP. Expression of a nonpolymorphic MHC class I-like molecule, CD1D, by human intestinal epithelial cells. J Immunol 1991;147:2518-2524.
[57] Somnay-Wadgaonkar K, Nusrat A, Kim HS, Canchis WP, Balk SP, Colgan SP, Blumberg RS. Immunolocalization of CD1d in human intestinal epithelial cells and identification of a beta2-microglobulin-associated form. Int Immunol 1999;11:383-392.
[58] van de Wal Y, Corazza N, Allez M, Mayer LF, Iijima H, Ryan M, Cornwall S, Kaiserlian D, Hershberg R, Koezuka Y, Colgan SP, Blumberg RS. Delineation of a CD1d-restricted antigen presentation pathway associated with human and mouse intestinal epithelial cells. Gastroenterology 2003;124:1420-1431.
[59] Nickoloff BJ, Wrone-Smith T, Bonish B, Porcelli SA. Response of murine and normal human skin to injection of allogeneic blood-derived psoriatic immunocytes: detection of T cells expressing receptors typically present on natural killer cells, including CD94, CD158, and CD161. Arch Dermatol 1999;135:546-552.
[60] Bonish B, Jullien D, Dutronc Y, Huang BB, Modlin R, Spada FM, Porcelli SA, Nickoloff BJ. Overexpression of CD1d by keratinocytes in psoriasis and CD1d-dependent IFN-gamma production by NK-T cells. J Immunol 2000;165:4076-4085.
[61] Kawana K, Matsumoto J, Miura S, Shen L, Kawana Y, Nagamatsu T, Yasugi T, Fujii T, Yang H, Quayle AJ, Taketani Y, Schust DJ. Expression of CD1d and ligand-induced cytokine production are tissue specific in mucosal epithelia of the human lower reproductive tract. Infect Immun 2008;76:3011-3018.
[62] Balk SP, Bleicher PA, Terhorst C. Isolation and expression of cDNA encoding the murine homologues of CD1. J Immunol 1991;146:768-774.
[63] Gozalbo-Lopez B, Perez-Rosado A, Parra-Cuadrado JF, Martinez-Naves E. Identification of a new mouse Cd1d2 allele. Eur J Immunogenet 2004;31:1-3.
[64] Chen YH, Wang B, Chun T, Zhao L, Cardell S, Behar SM, Brenner MB, Wang CR. Expression of CD1d2 on thymocytes is not sufficient for the development of NK T cells in CD1d1-deficient mice. J Immunol 1999;162:4560-4566.
[65] Roark JH, Park SH, Jayawardena J, Kavita U, Shannon M, Bendelac A. CD1.1 expression by mouse antigen-presenting cells and marginal zone B cells. J Immunol 1998;160:3121-3127.

[66] Mandal M, Chen XR, Alegre ML, Chiu NM, Chen YH, Castano AR, Wang CR. Tissue distribution, regulation and intracellular localization of murine CD1 molecules. Mol Immunol 1998;35:525-536.
[67] Hameg A, Apostolou I, Leite-De-Moraes M, Gombert JM, Garcia C, Koezuka Y, Bach JF, Herbelin A. A subset of NKT cells that lacks the NK1.1 marker, expresses CD1d molecules, and autopresents the alpha-galactosylceramide antigen. J Immunol 2000;165:4917-4926.
[68] Bleicher PA, Balk SP, Hagen SJ, Blumberg RS, Flotte TJ, Terhorst C. Expression of murine CD1 on gastrointestinal epithelium. Science 1990;250:679-682.
[69] Kasinrerk W, Baumruker T, Majdic O, Knapp W, Stockinger H. CD1 molecule expression on human monocytes induced by granulocyte-macrophage colony-stimulating factor. J Immunol 1993;150:579-584.
[70] Raftery MJ, Winau F, Giese T, Kaufmann SH, Schaible UE, Schonrich G. Viral danger signals control CD1d de novo synthesis and NKT cell activation. Eur J Immunol 2008;38:668-679.
[71] Szatmari I, Pap A, Ruhl R, Ma JX, Illarionov PA, Besra GS, Rajnavolgyi E, Dezso B, Nagy L. PPARgamma controls CD1d expression by turning on retinoic acid synthesis in developing human dendritic cells. J Exp Med 2006;203:2351-2362.
[72] Chen Q, Ross AC. Retinoic acid regulates CD1d gene expression at the transcriptional level in human and rodent monocytic cells. Exp Biol Med (Maywood) 2007;232:488-494.
[73] Chen Q, Ross AC. Retinoic acid regulates cell cycle progression and cell differentiation in human monocytic THP-1 cells. Exp Cell Res 2004;297:68-81.
[74] DeCicco KL, Youngdahl JD, Ross AC. All-trans-retinoic acid and polyriboinosinic : polyribocytidylic acid in combination potentiate specific antibody production and cell-mediated immunity. Immunology 2001;104:341-348.
[75] Salamone MC, Rabinovich GA, Mendiguren AK, Salamone GV, Fainboim L. Activation-induced expression of CD1d antigen on mature T cells. J Leukoc Biol 2001;69:207-214.
[76] Colgan SP, Morales VM, Madara JL, Polischuk JE, Balk SP, Blumberg RS. IFN-gamma modulates CD1d surface expression on intestinal epithelia. Am J Physiol 1996;271:C276-283.
[77] Colgan SP, Pitman RS, Nagaishi T, Mizoguchi A, Mizoguchi E, Mayer LF, Shao L, Sartor RB, Subjeck JR, Blumberg RS. Intestinal heat shock protein 110 regulates expression of CD1d on intestinal epithelial cells. J Clin Invest 2003;112:745-754.
[78] Yuan W, Dasgupta A, Cresswell P. Herpes simplex virus evades natural killer T cell recognition by suppressing CD1d recycling. Nat Immunol 2006;7:835-842.
[79] Sanchez DJ, Gumperz JE, Ganem D. Regulation of CD1d expression and function by a herpesvirus infection. J Clin Invest 2005;115:1369-1378.
[80] Chen N, McCarthy C, Drakesmith H, Li D, Cerundolo V, McMichael AJ, Screaton GR, Xu XN. HIV-1 down-regulates the expression of CD1d via Nef. Eur J Immunol 2006;36:278-286.
[81] Cho S, Knox KS, Kohli LM, He JJ, Exley MA, Wilson SB, Brutkiewicz RR. Impaired cell surface expression of human CD1d by the formation of an HIV-1 Nef/CD1d complex. Virology 2005;337:242-252.
[82] Hage CA, Kohli LL, Cho S, Brutkiewicz RR, Twigg HL, 3rd, Knox KS. Human immunodeficiency virus gp120 downregulates CD1d cell surface expression. Immunol Lett 2005;98:131-135.
[83] Moll M, Andersson SK, Smed-Sorensen A, Sandberg JK. Inhibition of lipid antigen presentation in dendritic cells by HIV-1 Vpu interference with CD1d recycling from endosomal compartments. Blood 2010;116:1876-1884.
[84] Bendelac A, Lantz O, Quimby ME, Yewdell JW, Bennink JR, Brutkiewicz RR. CD1 recognition by mouse NK1+ T lymphocytes. Science 1995;268:863-865.
[85] Hammond KJ, Pellicci DG, Poulton LD, Naidenko OV, Scalzo AA, Baxter AG, Godfrey DI. CD1d-restricted NKT cells: an interstrain comparison. J Immunol 2001;167:1164-1173.
[86] Gumperz JE, Miyake S, Yamamura T, Brenner MB. Functionally distinct subsets of CD1d-restricted natural killer T cells revealed by CD1d tetramer staining. J Exp Med 2002;195:625-636.
[87] Assarsson E, Kambayashi T, Sandberg JK, Hong S, Taniguchi M, Van Kaer L, Ljunggren HG, Chambers BJ. CD8+ T cells rapidly acquire NK1.1 and NK cell-associated molecules upon stimulation in vitro and in vivo. J Immunol 2000;165:3673-3679.
[88] Behar SM, Podrebarac TA, Roy CJ, Wang CR, Brenner MB. Diverse TCRs recognize murine CD1. J Immunol 1999;162:161-167.
[89] Cardell S, Tangri S, Chan S, Kronenberg M, Benoist C, Mathis D. CD1-restricted CD4+ T cells in major histocompatibility complex class II-deficient mice. J Exp Med 1995;182:993-1004.

[90] Godfrey DI, MacDonald HR, Kronenberg M, Smyth MJ, Van Kaer L. NKT cells: what's in a name? Nat Rev Immunol 2004;4:231-237.
[91] Gapin L, Matsuda JL, Surh CD, Kronenberg M. NKT cells derive from double-positive thymocytes that are positively selected by CD1d. Nat Immunol 2001;2:971-978.
[92] Bendelac A, Savage PB, Teyton L. The biology of NKT cells. Annu Rev Immunol 2007;25:297-336.
[93] Makino Y, Yamagata N, Sasho T, Adachi Y, Kanno R, Koseki H, Kanno M, Taniguchi M. Extrathymic development of V alpha 14-positive T cells. J Exp Med 1993;177:1399-1408.
[94] Chun T, Page MJ, Gapin L, Matsuda JL, Xu H, Nguyen H, Kang HS, Stanic AK, Joyce S, Koltun WA, Chorney MJ, Kronenberg M, Wang CR. CD1d-expressing dendritic cells but not thymic epithelial cells can mediate negative selection of NKT cells. J Exp Med 2003;197:907-918.
[95] Becker AM, Blevins JS, Tomson FL, Eitson JL, Medeiros JJ, Yarovinsky F, Norgard MV, van Oers NS. Invariant NKT cell development requires a full complement of functional CD3 zeta immunoreceptor tyrosine-based activation motifs. J Immunol 2010;184:6822-6832.
[96] Egawa T, Eberl G, Taniuchi I, Benlagha K, Geissmann F, Hennighausen L, Bendelac A, Littman DR. Genetic evidence supporting selection of the Valpha14i NKT cell lineage from double-positive thymocyte precursors. Immunity 2005;22:705-716.
[97] Stetson DB, Mohrs M, Reinhardt RL, Baron JL, Wang ZE, Gapin L, Kronenberg M, Locksley RM. Constitutive cytokine mRNAs mark natural killer (NK) and NK T cells poised for rapid effector function. J Exp Med 2003;198:1069-1076.
[98] Matsuda JL, Naidenko OV, Gapin L, Nakayama T, Taniguchi M, Wang CR, Koezuka Y, Kronenberg M. Tracking the response of natural killer T cells to a glycolipid antigen using CD1d tetramers. J Exp Med 2000;192:741-754.
[99] Rachitskaya AV, Hansen AM, Horai R, Li Z, Villasmil R, Luger D, Nussenblatt RB, Caspi RR. Cutting edge: NKT cells constitutively express IL-23 receptor and RORgammat and rapidly produce IL-17 upon receptor ligation in an IL-6-independent fashion. J Immunol 2008;180:5167-5171.
[100] Michel ML, Keller AC, Paget C, Fujio M, Trottein F, Savage PB, Wong CH, Schneider E, Dy M, Leite-de-Moraes MC. Identification of an IL-17-producing NK1.1(neg) iNKT cell population involved in airway neutrophilia. J Exp Med 2007;204:995-1001.
[101] Cui J, Shin T, Kawano T, Sato H, Kondo E, Toura I, Kaneko Y, Koseki H, Kanno M, Taniguchi M. Requirement for Valpha14 NKT cells in IL-12-mediated rejection of tumors. Science 1997;278:1623-1626.
[102] Takahashi M, Ogasawara K, Takeda K, Hashimoto W, Sakihara H, Kumagai K, Anzai R, Satoh M, Seki S. LPS induces NK1.1+ alpha beta T cells with potent cytotoxicity in the liver of mice via production of IL-12 from Kupffer cells. J Immunol 1996;156:2436-2442.
[103] Wingender G, Krebs P, Beutler B, Kronenberg M. Antigen-specific cytotoxicity by invariant NKT cells in vivo is CD95/CD178-dependent and is correlated with antigenic potency. J Immunol 2010;185:2721-2729.
[104] Kitamura H, Iwakabe K, Yahata T, Nishimura S, Ohta A, Ohmi Y, Sato M, Takeda K, Okumura K, Van Kaer L, Kawano T, Taniguchi M, Nishimura T. The natural killer T (NKT) cell ligand alpha-galactosylceramide demonstrates its immunopotentiating effect by inducing interleukin (IL)-12 production by dendritic cells and IL-12 receptor expression on NKT cells. J Exp Med 1999;189:1121-1128.
[105] Tomura M, Yu WG, Ahn HJ, Yamashita M, Yang YF, Ono S, Hamaoka T, Kawano T, Taniguchi M, Koezuka Y, Fujiwara H. A novel function of Valpha14+CD4+NKT cells: stimulation of IL-12 production by antigen-presenting cells in the innate immune system. J Immunol 1999;163:93-101.
[106] George T, Yu YY, Liu J, Davenport C, Lemieux S, Stoneman E, Mathew PA, Kumar V, Bennett M. Allorecognition by murine natural killer cells: lysis of T-lymphoblasts and rejection of bone-marrow grafts. Immunol Rev 1997;155:29-40.
[107] Maeda M, Lohwasser S, Yamamura T, Takei F. Regulation of NKT cells by Ly49: analysis of primary NKT cells and generation of NKT cell line. J Immunol 2001;167:4180-4186.
[108] Ota T, Takeda K, Akiba H, Hayakawa Y, Ogasawara K, Ikarashi Y, Miyake S, Wakasugi H, Yamamura T, Kronenberg M, Raulet DH, Kinoshita K, Yagita H, Smyth MJ, Okumura K. IFN-gamma-mediated negative feedback regulation of NKT-cell function by CD94/NKG2. Blood 2005;106:184-192.

[109] Hameg A, Gouarin C, Gombert JM, Hong S, Van Kaer L, Bach JF, Herbelin A. IL-7 up-regulates IL-4 production by splenic NK1.1+ and NK1.1- MHC class I-like/CD1-dependent CD4+ T cells. J Immunol 1999;162:7067-7074.
[110] Leite-De-Moraes MC, Hameg A, Pacilio M, Koezuka Y, Taniguchi M, Van Kaer L, Schneider E, Dy M, Herbelin A. IL-18 enhances IL-4 production by ligand-activated NKT lymphocytes: a pro-Th2 effect of IL-18 exerted through NKT cells. J Immunol 2001;166:945-951.
[111] Arase H, Arase N, Saito T. Interferon gamma production by natural killer (NK) cells and NK1.1+ T cells upon NKR-P1 cross-linking. J Exp Med 1996;183:2391-2396.
[112] Miyamoto K, Miyake S, Yamamura T. A synthetic glycolipid prevents autoimmune encephalomyelitis by inducing TH2 bias of natural killer T cells. Nature 2001;413:531-534.
[113] Oki S, Chiba A, Yamamura T, Miyake S. The clinical implication and molecular mechanism of preferential IL-4 production by modified glycolipid-stimulated NKT cells. J Clin Invest 2004;113:1631-1640.
[114] Oki S, Tomi C, Yamamura T, Miyake S. Preferential T(h)2 polarization by OCH is supported by incompetent NKT cell induction of CD40L and following production of inflammatory cytokines by bystander cells in vivo. Int Immunol 2005;17:1619-1629.
[115] Im JS, Arora P, Bricard G, Molano A, Venkataswamy MM, Baine I, Jerud ES, Goldberg MF, Baena A, Yu KO, Ndonye RM, Howell AR, Yuan W, Cresswell P, Chang YT, Illarionov PA, Besra GS, Porcelli SA. Kinetics and cellular site of glycolipid loading control the outcome of natural killer T cell activation. Immunity 2009;30:888-898.
[116] Sullivan BA, Nagarajan NA, Wingender G, Wang J, Scott I, Tsuji M, Franck RW, Porcelli SA, Zajonc DM, Kronenberg M. Mechanisms for glycolipid antigen-driven cytokine polarization by Valpha14i NKT cells. J Immunol 2010;184:141-153.
[117] Kadowaki N, Antonenko S, Ho S, Rissoan MC, Soumelis V, Porcelli SA, Lanier LL, Liu YJ. Distinct cytokine profiles of neonatal natural killer T cells after expansion with subsets of dendritic cells. J Exp Med 2001;193:1221-1226.
[118] Minami K, Yanagawa Y, Iwabuchi K, Shinohara N, Harabayashi T, Nonomura K, Onoe K. Negative feedback regulation of T helper type 1 (Th1)/Th2 cytokine balance via dendritic cell and natural killer T cell interactions. Blood 2005;106:1685-1693.
[119] Matsuda JL, Gapin L, Baron JL, Sidobre S, Stetson DB, Mohrs M, Locksley RM, Kronenberg M. Mouse V alpha 14i natural killer T cells are resistant to cytokine polarization in vivo. Proc Natl Acad Sci U S A 2003;100:8395-8400.
[120] Osman Y, Kawamura T, Naito T, Takeda K, Van Kaer L, Okumura K, Abo T. Activation of hepatic NKT cells and subsequent liver injury following administration of alpha-galactosylceramide. Eur J Immunol 2000;30:1919-1928.
[121] Fujii S, Shimizu K, Kronenberg M, Steinman RM. Prolonged IFN-gamma-producing NKT response induced with alpha-galactosylceramide-loaded DCs. Nat Immunol 2002;3:867-874.
[122] Hayakawa Y, Takeda K, Yagita H, Kakuta S, Iwakura Y, Van Kaer L, Saiki I, Okumura K. Critical contribution of IFN-gamma and NK cells, but not perforin-mediated cytotoxicity, to anti-metastatic effect of alpha-galactosylceramide. Eur J Immunol 2001;31:1720-1727.
[123] Wilson MT, Johansson C, Olivares-Villagomez D, Singh AK, Stanic AK, Wang CR, Joyce S, Wick MJ, Van Kaer L. The response of natural killer T cells to glycolipid antigens is characterized by surface receptor down-modulation and expansion. Proc Natl Acad Sci U S A 2003;100:10913-10918.
[124] Chen H, Huang H, Paul WE. NK1.1+ CD4+ T cells lose NK1.1 expression upon in vitro activation. J Immunol 1997;158:5112-5119.
[125] Schonrich G, Kalinke U, Momburg F, Malissen M, Schmitt-Verhulst AM, Malissen B, Hammerling GJ, Arnold B. Down-regulation of T cell receptors on self-reactive T cells as a novel mechanism for extrathymic tolerance induction. Cell 1991;65:293-304.
[126] McNab FW, Berzins SP, Pellicci DG, Kyparissoudis K, Field K, Smyth MJ, Godfrey DI. The influence of CD1d in postselection NKT cell maturation and homeostasis. J Immunol 2005;175:3762-3768.
[127] Gadola SD, Dulphy N, Salio M, Cerundolo V. Valpha24-JalphaQ-independent, CD1d-restricted recognition of alpha-galactosylceramide by human CD4(+) and CD8alphabeta(+) T lymphocytes. J Immunol 2002;168:5514-5520.
[128] Johnston B, Butcher EC. Chemokines in rapid leukocyte adhesion triggering and migration. Semin Immunol 2002;14:83-92.
[129] Kim CH, Butcher EC, Johnston B. Distinct subsets of human Valpha24-invariant NKT cells: cytokine responses and chemokine receptor expression. Trends Immunol 2002;23:516-519.

[130] Kim CH, Johnston B, Butcher EC. Trafficking machinery of NKT cells: shared and differential chemokine receptor expression among V alpha 24(+)V beta 11(+) NKT cell subsets with distinct cytokine-producing capacity. Blood 2002;100:11-16.
[131] Thomas SY, Hou R, Boyson JE, Means TK, Hess C, Olson DP, Strominger JL, Brenner MB, Gumperz JE, Wilson SB, Luster AD. CD1d-restricted NKT cells express a chemokine receptor profile indicative of Th1-type inflammatory homing cells. J Immunol 2003;171:2571-2580.
[132] Johnston B, Kim CH, Soler D, Emoto M, Butcher EC. Differential chemokine responses and homing patterns of murine TCR alpha beta NKT cell subsets. J Immunol 2003;171:2960-2969.
[133] Geissmann F, Cameron TO, Sidobre S, Manlongat N, Kronenberg M, Briskin MJ, Dustin ML, Littman DR. Intravascular immune surveillance by CXCR6+ NKT cells patrolling liver sinusoids. PLoS Biol 2005;3:e113.
[134] Wallace KL, Marshall MA, Ramos SI, Lannigan JA, Field JJ, Strieter RM, Linden J. NKT cells mediate pulmonary inflammation and dysfunction in murine sickle cell disease through production of IFN-gamma and CXCR3 chemokines. Blood 2009;114:667-676.
[135] Kawakami K, Kinjo Y, Uezu K, Yara S, Miyagi K, Koguchi Y, Nakayama T, Taniguchi M, Saito A. Monocyte chemoattractant protein-1-dependent increase of V alpha 14 NKT cells in lungs and their roles in Th1 response and host defense in cryptococcal infection. J Immunol 2001;167:6525-6532.
[136] Ko SY, Ko HJ, Chang WS, Park SH, Kweon MN, Kang CY. alpha-Galactosylceramide can act as a nasal vaccine adjuvant inducing protective immune responses against viral infection and tumor. J Immunol 2005;175:3309-3317.
[137] Youn HJ, Ko SY, Lee KA, Ko HJ, Lee YS, Fujihashi K, Boyaka PN, Kim SH, Horimoto T, Kweon MN, Kang CY. A single intranasal immunization with inactivated influenza virus and alpha-galactosylceramide induces long-term protective immunity without redirecting antigen to the central nervous system. Vaccine 2007;25:5189-5198.
[138] Kamijuku H, Nagata Y, Jiang X, Ichinohe T, Tashiro T, Mori K, Taniguchi M, Hase K, Ohno H, Shimaoka T, Yonehara S, Odagiri T, Tashiro M, Sata T, Hasegawa H, Seino KI. Mechanism of NKT cell activation by intranasal coadministration of alpha-galactosylceramide, which can induce cross-protection against influenza viruses. Mucosal Immunol 2008;1:208-218.
[139] Ho LP, Denney L, Luhn K, Teoh D, Clelland C, McMichael AJ. Activation of invariant NKT cells enhances the innate immune response and improves the disease course in influenza A virus infection. Eur J Immunol 2008;38:1913-1922.
[140] De Santo C, Salio M, Masri SH, Lee LY, Dong T, Speak AO, Porubsky S, Booth S, Veerapen N, Besra GS, Grone HJ, Platt FM, Zambon M, Cerundolo V. Invariant NKT cells reduce the immunosuppressive activity of influenza A virus-induced myeloid-derived suppressor cells in mice and humans. J Clin Invest 2008;118:4036-4048.
[141] Johnson TR, Hong S, Van Kaer L, Koezuka Y, Graham BS. NK T cells contribute to expansion of CD8(+) T cells and amplification of antiviral immune responses to respiratory syncytial virus. J Virol 2002;76:4294-4303.
[142] Motsinger A, Haas DW, Stanic AK, Van Kaer L, Joyce S, Unutmaz D. CD1d-restricted human natural killer T cells are highly susceptible to human immunodeficiency virus 1 infection. J Exp Med 2002;195:869-879.
[143] van der Vliet HJ, von Blomberg BM, Hazenberg MD, Nishi N, Otto SA, van Benthem BH, Prins M, Claessen FA, van den Eertwegh AJ, Giaccone G, Miedema F, Scheper RJ, Pinedo HM. Selective decrease in circulating V alpha 24+V beta 11+ NKT cells during HIV type 1 infection. J Immunol 2002;168:1490-1495.
[144] Moore JP, Trkola A, Dragic T. Co-receptors for HIV-1 entry. Curr Opin Immunol 1997;9:551-562.
[145] van der Vliet HJ, van Vonderen MG, Molling JW, Bontkes HJ, Reijm M, Reiss P, van Agtmael MA, Danner SA, van den Eertwegh AJ, von Blomberg BM, Scheper RJ. Cutting edge: Rapid recovery of NKT cells upon institution of highly active antiretroviral therapy for HIV-1 infection. J Immunol 2006;177:5775-5778.
[146] Grubor-Bauk B, Simmons A, Mayrhofer G, Speck PG. Impaired clearance of herpes simplex virus type 1 from mice lacking CD1d or NKT cells expressing the semivariant V alpha 14-J alpha 281 TCR. J Immunol 2003;170:1430-1434.
[147] Exley MA, Bigley NJ, Cheng O, Tahir SM, Smiley ST, Carter QL, Stills HF, Grusby MJ, Koezuka Y, Taniguchi M, Balk SP. CD1d-reactive T-cell activation leads to amelioration of disease caused by diabetogenic encephalomyocarditis virus. J Leukoc Biol 2001;69:713-718.

[148] Baron JL, Gardiner L, Nishimura S, Shinkai K, Locksley R, Ganem D. Activation of a nonclassical NKT cell subset in a transgenic mouse model of hepatitis B virus infection. Immunity 2002;16:583-594.
[149] Mattner J, Debord KL, Ismail N, Goff RD, Cantu C, 3rd, Zhou D, Saint-Mezard P, Wang V, Gao Y, Yin N, Hoebe K, Schneewind O, Walker D, Beutler B, Teyton L, Savage PB, Bendelac A. Exogenous and endogenous glycolipid antigens activate NKT cells during microbial infections. Nature 2005;434:525-529.
[150] Kumar H, Belperron A, Barthold SW, Bockenstedt LK. Cutting edge: CD1d deficiency impairs murine host defense against the spirochete, Borrelia burgdorferi. J Immunol 2000;165:4797-4801.
[151] Nieuwenhuis EE, Matsumoto T, Exley M, Schleipman RA, Glickman J, Bailey DT, Corazza N, Colgan SP, Onderdonk AB, Blumberg RS. CD1d-dependent macrophage-mediated clearance of Pseudomonas aeruginosa from lung. Nat Med 2002;8:588-593.
[152] Stanley AC, Zhou Y, Amante FH, Randall LM, Haque A, Pellicci DG, Hill GR, Smyth MJ, Godfrey DI, Engwerda CR. Activation of invariant NKT cells exacerbates experimental visceral leishmaniasis. PLoS Pathog 2008;4:e1000028.
[153] Nayak DP, Balogun RA, Yamada H, Zhou ZH, Barman S. Influenza virus morphogenesis and budding. Virus Res 2009;143:147-161.
[154] Noda T, Kawaoka Y. Structure of influenza virus ribonucleoprotein complexes and their packaging into virions. Rev Med Virol 2010.
[155] Fujiyoshi Y, Kume NP, Sakata K, Sato SB. Fine structure of influenza A virus observed by electron cryo-microscopy. EMBO J 1994;13:318-326.
[156] Scheiffele P, Rietveld A, Wilk T, Simons K. Influenza viruses select ordered lipid domains during budding from the plasma membrane. J Biol Chem 1999;274:2038-2044.
[157] Radiukhin VA. [The concept of transmembrane asymmetry of lateral domains in biomemranes and influenza virus envelope fine structure]. Mol Biol (Mosk) 2009;43:579-589.
[158] Zhang J, Pekosz A, Lamb RA. Influenza virus assembly and lipid raft microdomains: a role for the cytoplasmic tails of the spike glycoproteins. J Virol 2000;74:4634-4644.
[159] Schroeder C, Heider H, Moncke-Buchner E, Lin TI. The influenza virus ion channel and maturation cofactor M2 is a cholesterol-binding protein. Eur Biophys J 2005;34:52-66.
[160] Gamblin SJ, Skehel JJ. Influenza hemagglutinin and neuraminidase membrane glycoproteins. J Biol Chem 2010;285:28403-28409.
[161] Skehel JJ, Bayley PM, Brown EB, Martin SR, Waterfield MD, White JM, Wilson IA, Wiley DC. Changes in the conformation of influenza virus hemagglutinin at the pH optimum of virus-mediated membrane fusion. Proc Natl Acad Sci U S A 1982;79:968-972.
[162] Daniels RS, Douglas AR, Skehel JJ, Wiley DC. Analyses of the antigenicity of influenza haemagglutinin at the pH optimum for virus-mediated membrane fusion. J Gen Virol 1983;64 (Pt 8):1657-1662.
[163] Huang RT, Rott R, Klenk HD. Influenza viruses cause hemolysis and fusion of cells. Virology 1981;110:243-247.
[164] Maeda T, Ohnishi S. Activation of influenza virus by acidic media causes hemolysis and fusion of erythrocytes. FEBS Lett 1980;122:283-287.
[165] Stieneke-Grober A, Vey M, Angliker H, Shaw E, Thomas G, Roberts C, Klenk HD, Garten W. Influenza virus hemagglutinin with multibasic cleavage site is activated by furin, a subtilisin-like endoprotease. EMBO J 1992;11:2407-2414.
[166] Klenk HD, Garten W. Host cell proteases controlling virus pathogenicity. Trends Microbiol 1994;2:39-43.
[167] Varghese JN, Laver WG, Colman PM. Structure of the influenza virus glycoprotein antigen neuraminidase at 2.9 A resolution. Nature 1983;303:35-40.
[168] Timmins J, Ruigrok RW, Weissenhorn W. Structural studies on the Ebola virus matrix protein VP40 indicate that matrix proteins of enveloped RNA viruses are analogues but not homologues. FEMS Microbiol Lett 2004;233:179-186.
[169] Boulo S, Akarsu H, Ruigrok RW, Baudin F. Nuclear traffic of influenza virus proteins and ribonucleoprotein complexes. Virus Res 2007;124:12-21.
[170] Gomez-Puertas P, Albo C, Perez-Pastrana E, Vivo A, Portela A. Influenza virus matrix protein is the major driving force in virus budding. J Virol 2000;74:11538-11547.
[171] Whittaker G, Bui M, Helenius A. Nuclear trafficking of influenza virus ribonuleoproteins in heterokaryons. J Virol 1996;70:2743-2756.
[172] Murti KG, Webster RG, Jones IM. Localization of RNA polymerases on influenza viral ribonucleoproteins by immunogold labeling. Virology 1988;164:562-566.

[173] Neumann G, Hughes MT, Kawaoka Y. Influenza A virus NS2 protein mediates vRNP nuclear export through NES-independent interaction with hCRM1. EMBO J 2000;19:6751-6758.
[174] Boivin S, Cusack S, Ruigrok RW, Hart DJ. Influenza A virus polymerase: structural insights into replication and host adaptation mechanisms. J Biol Chem 2010;285:28411-28417.
[175] Drake JW. Rates of spontaneous mutation among RNA viruses. Proc Natl Acad Sci U S A 1993;90:4171-4175.
[176] Duhaut SD, McCauley JW. Defective RNAs inhibit the assembly of influenza virus genome segments in a segment-specific manner. Virology 1996;216:326-337.
[177] Odagiri T, Tashiro M. Segment-specific noncoding sequences of the influenza virus genome RNA are involved in the specific competition between defective interfering RNA and its progenitor RNA segment at the virion assembly step. J Virol 1997;71:2138-2145.
[178] Fujii Y, Goto H, Watanabe T, Yoshida T, Kawaoka Y. Selective incorporation of influenza virus RNA segments into virions. Proc Natl Acad Sci U S A 2003;100:2002-2007.
[179] Fujii K, Fujii Y, Noda T, Muramoto Y, Watanabe T, Takada A, Goto H, Horimoto T, Kawaoka Y. Importance of both the coding and the segment-specific noncoding regions of the influenza A virus NS segment for its efficient incorporation into virions. J Virol 2005;79:3766-3774.
[180] Ozawa M, Maeda J, Iwatsuki-Horimoto K, Watanabe S, Goto H, Horimoto T, Kawaoka Y. Nucleotide sequence requirements at the 5' end of the influenza A virus M RNA segment for efficient virus replication. J Virol 2009;83:3384-3388.
[181] Martin K, Helenius A. Nuclear transport of influenza virus ribonucleoproteins: the viral matrix protein (M1) promotes export and inhibits import. Cell 1991;67:117-130.
[182] Bui M, Wills EG, Helenius A, Whittaker GR. Role of the influenza virus M1 protein in nuclear export of viral ribonucleoproteins. J Virol 2000;74:1781-1786.
[183] Elton D, Simpson-Holley M, Archer K, Medcalf L, Hallam R, McCauley J, Digard P. Interaction of the influenza virus nucleoprotein with the cellular CRM1-mediated nuclear export pathway. J Virol 2001;75:408-419.
[184] Ma K, Roy AM, Whittaker GR. Nuclear export of influenza virus ribonucleoproteins: identification of an export intermediate at the nuclear periphery. Virology 2001;282:215-220.
[185] Ali A, Avalos RT, Ponimaskin E, Nayak DP. Influenza virus assembly: effect of influenza virus glycoproteins on the membrane association of M1 protein. J Virol 2000;74:8709-8719.
[186] Avalos RT, Yu Z, Nayak DP. Association of influenza virus NP and M1 proteins with cellular cytoskeletal elements in influenza virus-infected cells. J Virol 1997;71:2947-2958.
[187] Hughey PG, Compans RW, Zebedee SL, Lamb RA. Expression of the influenza A virus M2 protein is restricted to apical surfaces of polarized epithelial cells. J Virol 1992;66:5542-5552.
[188] Jones LV, Compans RW, Davis AR, Bos TJ, Nayak DP. Surface expression of influenza virus neuraminidase, an amino-terminally anchored viral membrane glycoprotein, in polarized epithelial cells. Mol Cell Biol 1985;5:2181-2189.
[189] Roth MG, Compans RW, Giusti L, Davis AR, Nayak DP, Gething MJ, Sambrook J. Influenza virus hemagglutinin expression is polarized in cells infected with recombinant SV40 viruses carrying cloned hemagglutinin DNA. Cell 1983;33:435-443.
[190] Kundu A, Avalos RT, Sanderson CM, Nayak DP. Transmembrane domain of influenza virus neuraminidase, a type II protein, possesses an apical sorting signal in polarized MDCK cells. J Virol 1996;70:6508-6515.
[191] Lin S, Naim HY, Rodriguez AC, Roth MG. Mutations in the middle of the transmembrane domain reverse the polarity of transport of the influenza virus hemagglutinin in MDCK epithelial cells. J Cell Biol 1998;142:51-57.
[192] Barman S, Nayak DP. Analysis of the transmembrane domain of influenza virus neuraminidase, a type II transmembrane glycoprotein, for apical sorting and raft association. J Virol 2000;74:6538-6545.
[193] Wandinger-Ness A, Bennett MK, Antony C, Simons K. Distinct transport vesicles mediate the delivery of plasma membrane proteins to the apical and basolateral domains of MDCK cells. J Cell Biol 1990;111:987-1000.
[194] Holopainen JM, Angelova MI, Kinnunen PK. Vectorial budding of vesicles by asymmetrical enzymatic formation of ceramide in giant liposomes. Biophys J 2000;78:830-838.
[195] Peter BJ, Kent HM, Mills IG, Vallis Y, Butler PJ, Evans PR, McMahon HT. BAR domains as sensors of membrane curvature: the amphiphysin BAR structure. Science 2004;303:495-499.
[196] Hui EK, Nayak DP. Role of ATP in influenza virus budding. Virology 2001;290:329-341.
[197] Rogers GN, Paulson JC. Receptor determinants of human and animal influenza virus isolates: differences in receptor specificity of the H3 hemagglutinin based on species of origin. Virology 1983;127:361-373.

[198] Kumlin U, Olofsson S, Dimock K, Arnberg N. Sialic acid tissue distribution and influenza virus tropism. Influenza Other Respi Viruses 2008;2:147-154.
[199] Shinya K, Ebina M, Yamada S, Ono M, Kasai N, Kawaoka Y. Avian flu: influenza virus receptors in the human airway. Nature 2006;440:435-436.
[200] Coll RC, O'Neill LA. New insights into the regulation of signalling by toll-like receptors and nod-like receptors. J Innate Immun 2010;2:406-421.
[201] Brikos C, O'Neill LA. Signalling of toll-like receptors. Handb Exp Pharmacol 2008:21-50.
[202] Mayer AK, Muehmer M, Mages J, Gueinzius K, Hess C, Heeg K, Bals R, Lang R, Dalpke AH. Differential recognition of TLR-dependent microbial ligands in human bronchial epithelial cells. J Immunol 2007;178:3134-3142.
[203] Sha Q, Truong-Tran AQ, Plitt JR, Beck LA, Schleimer RP. Activation of airway epithelial cells by toll-like receptor agonists. Am J Respir Cell Mol Biol 2004;31:358-364.
[204] Armstrong L, Medford AR, Uppington KM, Robertson J, Witherden IR, Tetley TD, Millar AB. Expression of functional toll-like receptor-2 and -4 on alveolar epithelial cells. Am J Respir Cell Mol Biol 2004;31:241-245.
[205] Yoneyama M, Fujita T. Recognition of viral nucleic acids in innate immunity. Rev Med Virol 2010;20:4-22.
[206] Liu P, Jamaluddin M, Li K, Garofalo RP, Casola A, Brasier AR. Retinoic acid-inducible gene I mediates early antiviral response and Toll-like receptor 3 expression in respiratory syncytial virus-infected airway epithelial cells. J Virol 2007;81:1401-1411.
[207] Kato H, Takeuchi O, Sato S, Yoneyama M, Yamamoto M, Matsui K, Uematsu S, Jung A, Kawai T, Ishii KJ, Yamaguchi O, Otsu K, Tsujimura T, Koh CS, Reis e Sousa C, Matsuura Y, Fujita T, Akira S. Differential roles of MDA5 and RIG-I helicases in the recognition of RNA viruses. Nature 2006;441:101-105.
[208] Pichlmair A, Schulz O, Tan CP, Naslund TI, Liljestrom P, Weber F, Reis e Sousa C. RIG-I-mediated antiviral responses to single-stranded RNA bearing 5'-phosphates. Science 2006;314:997-1001.
[209] Opitz B, Rejaibi A, Dauber B, Eckhard J, Vinzing M, Schmeck B, Hippenstiel S, Suttorp N, Wolff T. IFNbeta induction by influenza A virus is mediated by RIG-I which is regulated by the viral NS1 protein. Cell Microbiol 2007;9:930-938.
[210] Fritz JH, Ferrero RL, Philpott DJ, Girardin SE. Nod-like proteins in immunity, inflammation and disease. Nat Immunol 2006;7:1250-1257.
[211] Opitz B, Puschel A, Schmeck B, Hocke AC, Rosseau S, Hammerschmidt S, Schumann RR, Suttorp N, Hippenstiel S. Nucleotide-binding oligomerization domain proteins are innate immune receptors for internalized Streptococcus pneumoniae. J Biol Chem 2004;279:36426-36432.
[212] Berube J, Bourdon C, Yao Y, Rousseau S. Distinct intracellular signaling pathways control the synthesis of IL-8 and RANTES in TLR1/TLR2, TLR3 or NOD1 activated human airway epithelial cells. Cell Signal 2009;21:448-456.
[213] Kato A, Schleimer RP. Beyond inflammation: airway epithelial cells are at the interface of innate and adaptive immunity. Curr Opin Immunol 2007;19:711-720.
[214] Drickamer K. Two distinct classes of carbohydrate-recognition domains in animal lectins. J Biol Chem 1988;263:9557-9560.
[215] Haagsman HP, van Golde LM. Synthesis and assembly of lung surfactant. Annu Rev Physiol 1991;53:441-464.
[216] Haagsman HP, Hogenkamp A, van Eijk M, Veldhuizen EJ. Surfactant collectins and innate immunity. Neonatology 2008;93:288-294.
[217] Benne CA, Kraaijeveld CA, van Strijp JA, Brouwer E, Harmsen M, Verhoef J, van Golde LM, van Iwaarden JF. Interactions of surfactant protein A with influenza A viruses: binding and neutralization. J Infect Dis 1995;171:335-341.
[218] Hartshorn KL, Crouch EC, White MR, Eggleton P, Tauber AI, Chang D, Sastry K. Evidence for a protective role of pulmonary surfactant protein D (SP-D) against influenza A viruses. J Clin Invest 1994;94:311-319.
[219] Hiemstra PS. The role of epithelial beta-defensins and cathelicidins in host defense of the lung. Exp Lung Res 2007;33:537-542.
[220] Schutte BC, McCray PB, Jr. [beta]-defensins in lung host defense. Annu Rev Physiol 2002;64:709-748.
[221] Yang D, Chertov O, Bykovskaia SN, Chen Q, Buffo MJ, Shogan J, Anderson M, Schroder JM, Wang JM, Howard OM, Oppenheim JJ. Beta-defensins: linking innate and adaptive immunity through dendritic and T cell CCR6. Science 1999;286:525-528.

[222] Niyonsaba F, Ogawa H, Nagaoka I. Human beta-defensin-2 functions as a chemotactic agent for tumour necrosis factor-alpha-treated human neutrophils. Immunology 2004;111:273-281.
[223] Garcia JR, Jaumann F, Schulz S, Krause A, Rodriguez-Jimenez J, Forssmann U, Adermann K, Kluver E, Vogelmeier C, Becker D, Hedrich R, Forssmann WG, Bals R. Identification of a novel, multifunctional beta-defensin (human beta-defensin 3) with specific antimicrobial activity. Its interaction with plasma membranes of Xenopus oocytes and the induction of macrophage chemoattraction. Cell Tissue Res 2001;306:257-264.
[224] Tjabringa GS, Rabe KF, Hiemstra PS. The human cathelicidin LL-37: a multifunctional peptide involved in infection and inflammation in the lung. Pulm Pharmacol Ther 2005;18:321-327.
[225] Ibrahim HR, Thomas U, Pellegrini A. A helix-loop-helix peptide at the upper lip of the active site cleft of lysozyme confers potent antimicrobial activity with membrane permeabilization action. J Biol Chem 2001;276:43767-43774.
[226] Bals R, Wang X, Zasloff M, Wilson JM. The peptide antibiotic LL-37/hCAP-18 is expressed in epithelia of the human lung where it has broad antimicrobial activity at the airway surface. Proc Natl Acad Sci U S A 1998;95:9541-9546.
[227] Klebanoff SJ, Waltersdorph AM. Prooxidant activity of transferrin and lactoferrin. J Exp Med 1990;172:1293-1303.
[228] Han B, Mura M, Andrade CF, Okutani D, Lodyga M, dos Santos CC, Keshavjee S, Matthay M, Liu M. TNFalpha-induced long pentraxin PTX3 expression in human lung epithelial cells via JNK. J Immunol 2005;175:8303-8311.
[229] Garlanda C, Hirsch E, Bozza S, Salustri A, De Acetis M, Nota R, Maccagno A, Riva F, Bottazzi B, Peri G, Doni A, Vago L, Botto M, De Santis R, Carminati P, Siracusa G, Altruda F, Vecchi A, Romani L, Mantovani A. Non-redundant role of the long pentraxin PTX3 in anti-fungal innate immune response. Nature 2002;420:182-186.
[230] Kao CY, Huang F, Chen Y, Thai P, Wachi S, Kim C, Tam L, Wu R. Up-regulation of CC chemokine ligand 20 expression in human airway epithelium by IL-17 through a JAK-independent but MEK/NF-kappaB-dependent signaling pathway. J Immunol 2005;175:6676-6685.
[231] Reibman J, Hsu Y, Chen LC, Bleck B, Gordon T. Airway epithelial cells release MIP-3alpha/CCL20 in response to cytokines and ambient particulate matter. Am J Respir Cell Mol Biol 2003;28:648-654.
[232] Stick SM, Holt PG. The airway epithelium as immune modulator: the LARC ascending. Am J Respir Cell Mol Biol 2003;28:641-644.
[233] Lukacs NW, Prosser DM, Wiekowski M, Lira SA, Cook DN. Requirement for the chemokine receptor CCR6 in allergic pulmonary inflammation. J Exp Med 2001;194:551-555.
[234] Phadke AP, Akangire G, Park SJ, Lira SA, Mehrad B. The role of CC chemokine receptor 6 in host defense in a model of invasive pulmonary aspergillosis. Am J Respir Crit Care Med 2007;175:1165-1172.
[235] Holt PG, Haining S, Nelson DJ, Sedgwick JD. Origin and steady-state turnover of class II MHC-bearing dendritic cells in the epithelium of the conducting airways. J Immunol 1994;153:256-261.
[236] Rate A, Upham JW, Bosco A, McKenna KL, Holt PG. Airway epithelial cells regulate the functional phenotype of locally differentiating dendritic cells: implications for the pathogenesis of infectious and allergic airway disease. J Immunol 2009;182:72-83.
[237] Waldmann TA, Tagaya Y. The multifaceted regulation of interleukin-15 expression and the role of this cytokine in NK cell differentiation and host response to intracellular pathogens. Annu Rev Immunol 1999;17:19-49.
[238] Regamey N, Obregon C, Ferrari-Lacraz S, van Leer C, Chanson M, Nicod LP, Geiser T. Airway epithelial IL-15 transforms monocytes into dendritic cells. Am J Respir Cell Mol Biol 2007;37:75-84.
[239] Friend SL, Hosier S, Nelson A, Foxworthe D, Williams DE, Farr A. A thymic stromal cell line supports in vitro development of surface IgM+ B cells and produces a novel growth factor affecting B and T lineage cells. Exp Hematol 1994;22:321-328.
[240] Ying S, O'Connor B, Ratoff J, Meng Q, Mallett K, Cousins D, Robinson D, Zhang G, Zhao J, Lee TH, Corrigan C. Thymic stromal lymphopoietin expression is increased in asthmatic airways and correlates with expression of Th2-attracting chemokines and disease severity. J Immunol 2005;174:8183-8190.
[241] Kato A, Favoreto S, Jr., Avila PC, Schleimer RP. TLR3- and Th2 cytokine-dependent production of thymic stromal lymphopoietin in human airway epithelial cells. J Immunol 2007;179:1080-1087.

[242] Qiao J, Li A, Jin X. TSLP from RSV-stimulated rat airway epithelial cells activates myeloid dendritic cells. Immunol Cell Biol 2010.
[243] Soumelis V, Reche PA, Kanzler H, Yuan W, Edward G, Homey B, Gilliet M, Ho S, Antonenko S, Lauerma A, Smith K, Gorman D, Zurawski S, Abrams J, Menon S, McClanahan T, de Waal-Malefyt Rd R, Bazan F, Kastelein RA, Liu YJ. Human epithelial cells trigger dendritic cell mediated allergic inflammation by producing TSLP. Nat Immunol 2002;3:673-680.
[244] Sauty A, Dziejman M, Taha RA, Iarossi AS, Neote K, Garcia-Zepeda EA, Hamid Q, Luster AD. The T cell-specific CXC chemokines IP-10, Mig, and I-TAC are expressed by activated human bronchial epithelial cells. J Immunol 1999;162:3549-3558.
[245] Kobayashi N, Kondo T, Takata H, Yokota S, Takiguchi M. Functional and phenotypic analysis of human memory CD8+ T cells expressing CXCR3. J Leukoc Biol 2006;80:320-329.
[246] Spurrell JC, Wiehler S, Zaheer RS, Sanders SP, Proud D. Human airway epithelial cells produce IP-10 (CXCL10) in vitro and in vivo upon rhinovirus infection. Am J Physiol Lung Cell Mol Physiol 2005;289:L85-95.
[247] Taguchi M, Sampath D, Koga T, Castro M, Look DC, Nakajima S, Holtzman MJ. Patterns for RANTES secretion and intercellular adhesion molecule 1 expression mediate transepithelial T cell traffic based on analyses in vitro and in vivo. J Exp Med 1998;187:1927-1940.
[248] Porter JC, Falzon M, Hall A. Polarized localization of epithelial CXCL11 in chronic obstructive pulmonary disease and mechanisms of T cell egression. J Immunol 2008;180:1866-1877.
[249] Debbabi H, Ghosh S, Kamath AB, Alt J, Demello DE, Dunsmore S, Behar SM. Primary type II alveolar epithelial cells present microbial antigens to antigen-specific CD4+ T cells. Am J Physiol Lung Cell Mol Physiol 2005;289:L274-279.
[250] Kalb TH, Yio XY, Mayer L. Human airway epithelial cells stimulate T-lymphocyte lck and fyn tyrosine kinase. Am J Respir Cell Mol Biol 1997;17:561-570.
[251] Oei E, Kalb T, Beuria P, Allez M, Nakazawa A, Azuma M, Timony M, Stuart Z, Chen H, Sperber K. Accessory cell function of airway epithelial cells. Am J Physiol Lung Cell Mol Physiol 2004;287:L318-331.
[252] Diaz-Sanchez D, Dotson AR, Takenaka H, Saxon A. Diesel exhaust particles induce local IgE production in vivo and alter the pattern of IgE messenger RNA isoforms. J Clin Invest 1994;94:1417-1425.
[253] Ying S, Humbert M, Meng Q, Pfister R, Menz G, Gould HJ, Kay AB, Durham SR. Local expression of epsilon germline gene transcripts and RNA for the epsilon heavy chain of IgE in the bronchial mucosa in atopic and nonatopic asthma. J Allergy Clin Immunol 2001;107:686-692.
[254] Fagarasan S, Honjo T. T-Independent immune response: new aspects of B cell biology. Science 2000;290:89-92.
[255] Kato A, Truong-Tran AQ, Scott AL, Matsumoto K, Schleimer RP. Airway epithelial cells produce B cell-activating factor of TNF family by an IFN-beta-dependent mechanism. J Immunol 2006;177:7164-7172.
[256] Xu W, He B, Chiu A, Chadburn A, Shan M, Buldys M, Ding A, Knowles DM, Santini PA, Cerutti A. Epithelial cells trigger frontline immunoglobulin class switching through a pathway regulated by the inhibitor SLPI. Nat Immunol 2007;8:294-303.
[257] Davidson DJ, Gray MA, Kilanowski FM, Tarran R, Randell SH, Sheppard DN, Argent BE, Dorin JR. Murine epithelial cells: isolation and culture. J Cyst Fibros 2004;3 Suppl 2:59-62.
[258] Davies LA, Seguela C, Varathalingam A, Cheng SH, Hyde SC, Gill DR. Identification of transfected cell types following non-viral gene transfer to the murine lung. J Gene Med 2007;9:184-196.
[259] Sung CC, O'Toole EA, Lannutti BJ, Hunt J, O'Gorman M, Woodley DT, Paller AS. Integrin alpha 5 beta 1 expression is required for inhibition of keratinocyte migration by ganglioside GT1b. Exp Cell Res 1998;239:311-319.
[260] Ho LP, Urban BC, Jones L, Ogg GS, McMichael AJ. CD4(-)CD8alphaalpha subset of CD1d-restricted NKT cells controls T cell expansion. J Immunol 2004;172:7350-7358.
[261] Livak KJ, Schmittgen TD. Analysis of relative gene expression data using real-time quantitative PCR and the 2(-Delta Delta C(T)) Method. Methods 2001;25:402-408.
[262] Mendiratta SK, Martin WD, Hong S, Boesteanu A, Joyce S, Van Kaer L. CD1d1 mutant mice are deficient in natural T cells that promptly produce IL-4. Immunity 1997;6:469-477.
[263] Nieuwenhuis EE, Matsumoto T, Lindenbergh D, Willemsen R, Kaser A, Simons-Oosterhuis Y, Brugman S, Yamaguchi K, Ishikawa H, Aiba Y, Koga Y, Samsom JN, Oshima K, Kikuchi M, Escher JC, Hattori M, Onderdonk AB, Blumberg RS. Cd1d-dependent regulation of bacterial colonization in the intestine of mice. J Clin Invest 2009;119:1241-1250.

[264] Endres M, Leinhase I, Kaps C, Wentges M, Unger M, Olze H, Ringe J, Sittinger M, Rotter N. Changes in the gene expression pattern of cytokeratins in human respiratory epithelial cells during culture. Eur Arch Otorhinolaryngol 2005;262:390-396.
[265] Renthal R, Schneider BG, Miller MM, Luduena RF. Beta IV is the major beta-tubulin isotype in bovine cilia. Cell Motil Cytoskeleton 1993;25:19-29.
[266] Kim HS, Colgan SP, Pitman R, Hershberg RM, Blumberg RS. Human CD1d associates with prolyl-4-hydroxylase during its biosynthesis. Mol Immunol 2000;37:861-868.
[267] Gerlini G, Hefti HP, Kleinhans M, Nickoloff BJ, Burg G, Nestle FO. Cd1d is expressed on dermal dendritic cells and monocyte-derived dendritic cells. J Invest Dermatol 2001;117:576-582.
[268] Gansert JL, Kiessler V, Engele M, Wittke F, Rollinghoff M, Krensky AM, Porcelli SA, Modlin RL, Stenger S. Human NKT cells express granulysin and exhibit antimycobacterial activity. J Immunol 2003;170:3154-3161.
[269] Van Rhijn I, Young DC, Im JS, Levery SB, Illarionov PA, Besra GS, Porcelli SA, Gumperz J, Cheng TY, Moody DB. CD1d-restricted T cell activation by nonlipidic small molecules. Proc Natl Acad Sci U S A 2004;101:13578-13583.
[270] Brigl M, Bry L, Kent SC, Gumperz JE, Brenner MB. Mechanism of CD1d-restricted natural killer T cell activation during microbial infection. Nat Immunol 2003;4:1230-1237.
[271] Nilsen TW, Graveley BR. Expansion of the eukaryotic proteome by alternative splicing. Nature 2010;463:457-463.
[272] Fujii T, Ishitani A, Geraghty DE. A soluble form of the HLA-G antigen is encoded by a messenger ribonucleic acid containing intron 4. J Immunol 1994;153:5516-5524.
[273] Moreau P, Carosella E, Teyssier M, Prost S, Gluckman E, Dausset J, Kirszenbaum M. Soluble HLA-G molecule. An alternatively spliced HLA-G mRNA form candidate to encode it in peripheral blood mononuclear cells and human trophoblasts. Hum Immunol 1995;43:231-236.
[274] Cunningham AC, Zhang JG, Moy JV, Ali S, Kirby JA. A comparison of the antigen-presenting capabilities of class II MHC-expressing human lung epithelial and endothelial cells. Immunology 1997;91:458-463.
[275] Wang SZ, Hallsworth PG, Dowling KD, Alpers JH, Bowden JJ, Forsyth KD. Adhesion molecule expression on epithelial cells infected with respiratory syncytial virus. Eur Respir J 2000;15:358-366.
[276] Papi A, Stanciu LA, Papadopoulos NG, Teran LM, Holgate ST, Johnston SL. Rhinovirus infection induces major histocompatibility complex class I and costimulatory molecule upregulation on respiratory epithelial cells. J Infect Dis 2000;181:1780-1784.
[277] Le Goffic R, Pothlichet J, Vitour D, Fujita T, Meurs E, Chignard M, Si-Tahar M. Cutting Edge: Influenza A virus activates TLR3-dependent inflammatory and RIG-I-dependent antiviral responses in human lung epithelial cells. J Immunol 2007;178:3368-3372.
[278] Choi AM, Jacoby DB. Influenza virus A infection induces interleukin-8 gene expression in human airway epithelial cells. FEBS Lett 1992;309:327-329.
[279] Matsukura S, Kokubu F, Noda H, Tokunaga H, Adachi M. Expression of IL-6, IL-8, and RANTES on human bronchial epithelial cells, NCI-H292, induced by influenza virus A. J Allergy Clin Immunol 1996;98:1080-1087.
[280] Chan RW, Yuen KM, Yu WC, Ho CC, Nicholls JM, Peiris JS, Chan MC. Influenza H5N1 and H1N1 virus replication and innate immune responses in bronchial epithelial cells are influenced by the state of differentiation. PLoS One 2010;5:e8713.
[281] Khaitov MR, Laza-Stanca V, Edwards MR, Walton RP, Rohde G, Contoli M, Papi A, Stanciu LA, Kotenko SV, Johnston SL. Respiratory virus induction of alpha-, beta- and lambda-interferons in bronchial epithelial cells and peripheral blood mononuclear cells. Allergy 2009;64:375-386.
[282] Hirosako S, Goto E, Fujii K, Tsumori K, Hirata N, Tsumura S, Kamohara H, Kohrogi H. Human bronchial intraepithelial T cells produce interferon-gamma and stimulate epithelial cells. Clin Exp Immunol 2009;155:266-274.
[283] Matsumoto M, Seya T. TLR3: interferon induction by double-stranded RNA including poly(I:C). Adv Drug Deliv Rev 2008;60:805-812.
[284] Jacobs BL, Langland JO. When two strands are better than one: the mediators and modulators of the cellular responses to double-stranded RNA. Virology 1996;219:339-349.
[285] Majde JA. Viral double-stranded RNA, cytokines, and the flu. J Interferon Cytokine Res 2000;20:259-272.

[286] Le Goffic R, Balloy V, Lagranderie M, Alexopoulou L, Escriou N, Flavell R, Chignard M, Si-Tahar M. Detrimental contribution of the Toll-like receptor (TLR)3 to influenza A virus-induced acute pneumonia. PLoS Pathog 2006;2:e53.
[287] Day C, Patel R, Guillen C, Wardlaw AJ. The chemokine CXCL16 is highly and constitutively expressed by human bronchial epithelial cells. Exp Lung Res 2009;35:272-283.
[288] Reiner A, Yekutieli D, Benjamini Y. Identifying differentially expressed genes using false discovery rate controlling procedures. Bioinformatics 2003;19:368-375.
[289] Dennis G, Jr., Sherman BT, Hosack DA, Yang J, Gao W, Lane HC, Lempicki RA. DAVID: Database for Annotation, Visualization, and Integrated Discovery. Genome Biol 2003;4:P3.
[290] Subramanian A, Tamayo P, Mootha VK, Mukherjee S, Ebert BL, Gillette MA, Paulovich A, Pomeroy SL, Golub TR, Lander ES, Mesirov JP. Gene set enrichment analysis: a knowledge-based approach for interpreting genome-wide expression profiles. Proc Natl Acad Sci U S A 2005;102:15545-15550.
[291] Li WX. Canonical and non-canonical JAK-STAT signaling. Trends Cell Biol 2008;18:545-551.
[292] Darnell JE, Jr. STATs and gene regulation. Science 1997;277:1630-1635.
[293] Yeh TC, Pellegrini S. The Janus kinase family of protein tyrosine kinases and their role in signaling. Cell Mol Life Sci 1999;55:1523-1534.
[294] Gomez-Lechon MJ. Oncostatin M: signal transduction and biological activity. Life Sci 1999;65:2019-2030.
[295] Tanaka M, Miyajima A. Oncostatin M, a multifunctional cytokine. Rev Physiol Biochem Pharmacol 2003;149:39-52.
[296] Boniface K, Diveu C, Morel F, Pedretti N, Froger J, Ravon E, Garcia M, Venereau E, Preisser L, Guignouard E, Guillet G, Dagregorio G, Pene J, Moles JP, Yssel H, Chevalier S, Bernard FX, Gascan H, Lecron JC. Oncostatin M secreted by skin infiltrating T lymphocytes is a potent keratinocyte activator involved in skin inflammation. J Immunol 2007;178:4615-4622.
[297] Mosley B, De Imus C, Friend D, Boiani N, Thoma B, Park LS, Cosman D. Dual oncostatin M (OSM) receptors. Cloning and characterization of an alternative signaling subunit conferring OSM-specific receptor activation. J Biol Chem 1996;271:32635-32643.
[298] Pelletier JP, Martel-Pelletier J. Oncostatin M: foe or friend? Arthritis Rheum 2003;48:3301-3303.
[299] Heinrich PC, Behrmann I, Haan S, Hermanns HM, Muller-Newen G, Schaper F. Principles of interleukin (IL)-6-type cytokine signalling and its regulation. Biochem J 2003;374:1-20.
[300] Kasraie S, Niebuhr M, Baumert K, Werfel T. Functional effects of interleukin 31 in human primary keratinocytes. Allergy 2011.
[301] Chattopadhyay S, Tracy E, Liang P, Robledo O, Rose-John S, Baumann H. Interleukin-31 and oncostatin-M mediate distinct signaling reactions and response patterns in lung epithelial cells. J Biol Chem 2007;282:3014-3026.
[302] Dambacher J, Beigel F, Seiderer J, Haller D, Goke B, Auernhammer CJ, Brand S. Interleukin 31 mediates MAP kinase and STAT1/3 activation in intestinal epithelial cells and its expression is upregulated in inflammatory bowel disease. Gut 2007;56:1257-1265.
[303] Loewen GM, Tracy E, Blanchard F, Tan D, Yu J, Raza S, Matsui S, Baumann H. Transformation of human bronchial epithelial cells alters responsiveness to inflammatory cytokines. BMC Cancer 2005;5:145.
[304] Boutten A, Venembre P, Seta N, Hamelin J, Aubier M, Durand G, Dehoux MS. Oncostatin M is a potent stimulator of alpha1-antitrypsin secretion in lung epithelial cells: modulation by transforming growth factor-beta and interferon-gamma. Am J Respir Cell Mol Biol 1998;18:511-520.
[305] Sallenave JM, Tremblay GM, Gauldie J, Richards CD. Oncostatin M, but not interleukin-6 or leukemia inhibitory factor, stimulates expression of alpha1-proteinase inhibitor in A549 human alveolar epithelial cells. J Interferon Cytokine Res 1997;17:337-346.
[306] Larrea E, Aldabe R, Gonzalez I, Segura V, Sarobe P, Echeverria I, Prieto J. Oncostatin M enhances the antiviral effects of type I interferon and activates immunostimulatory functions in liver epithelial cells. J Virol 2009;83:3298-3311.
[307] Dalpke A, Heeg K, Bartz H, Baetz A. Regulation of innate immunity by suppressor of cytokine signaling (SOCS) proteins. Immunobiology 2008;213:225-235.
[308] Alexander WS, Starr R, Fenner JE, Scott CL, Handman E, Sprigg NS, Corbin JE, Cornish AL, Darwiche R, Owczarek CM, Kay TW, Nicola NA, Hertzog PJ, Metcalf D, Hilton DJ. SOCS1 is a critical inhibitor of interferon gamma signaling and prevents the potentially fatal neonatal actions of this cytokine. Cell 1999;98:597-608.

[309] Starr R, Metcalf D, Elefanty AG, Brysha M, Willson TA, Nicola NA, Hilton DJ, Alexander WS. Liver degeneration and lymphoid deficiencies in mice lacking suppressor of cytokine signaling-1. Proc Natl Acad Sci U S A 1998;95:14395-14399.
[310] Albanesi C, Fairchild HR, Madonna S, Scarponi C, De Pita O, Leung DY, Howell MD. IL-4 and IL-13 negatively regulate TNF-alpha- and IFN-gamma-induced beta-defensin expression through STAT-6, suppressor of cytokine signaling (SOCS)-1, and SOCS-3. J Immunol 2007;179:984-992.
[311] Hebenstreit D, Luft P, Schmiedlechner A, Duschl A, Horejs-Hoeck J. SOCS-1 and SOCS-3 inhibit IL-4 and IL-13 induced activation of Eotaxin-3/CCL26 gene expression in HEK293 cells. Mol Immunol 2005;42:295-303.
[312] Hebenstreit D, Luft P, Schmiedlechner A, Regl G, Frischauf AM, Aberger F, Duschl A, Horejs-Hoeck J. IL-4 and IL-13 induce SOCS-1 gene expression in A549 cells by three functional STAT6-binding motifs located upstream of the transcription initiation site. J Immunol 2003;171:5901-5907.
[313] Croker BA, Krebs DL, Zhang JG, Wormald S, Willson TA, Stanley EG, Robb L, Greenhalgh CJ, Forster I, Clausen BE, Nicola NA, Metcalf D, Hilton DJ, Roberts AW, Alexander WS. SOCS3 negatively regulates IL-6 signaling in vivo. Nat Immunol 2003;4:540-545.
[314] Lang R, Pauleau AL, Parganas E, Takahashi Y, Mages J, Ihle JN, Rutschman R, Murray PJ. SOCS3 regulates the plasticity of gp130 signaling. Nat Immunol 2003;4:546-550.
[315] Croker BA, Metcalf D, Robb L, Wei W, Mifsud S, DiRago L, Cluse LA, Sutherland KD, Hartley L, Williams E, Zhang JG, Hilton DJ, Nicola NA, Alexander WS, Roberts AW. SOCS3 is a critical physiological negative regulator of G-CSF signaling and emergency granulopoiesis. Immunity 2004;20:153-165.
[316] Lehtonen A, Matikainen S, Miettinen M, Julkunen I. Granulocyte-macrophage colony-stimulating factor (GM-CSF)-induced STAT5 activation and target-gene expression during human monocyte/macrophage differentiation. J Leukoc Biol 2002;71:511-519.
[317] Inoue H, Kato R, Fukuyama S, Nonami A, Taniguchi K, Matsumoto K, Nakano T, Tsuda M, Matsumura M, Kubo M, Ishikawa F, Moon BG, Takatsu K, Nakanishi Y, Yoshimura A. Spred-1 negatively regulates allergen-induced airway eosinophilia and hyperresponsiveness. J Exp Med 2005;201:73-82.
[318] Arnold R, Brenner D, Becker M, Frey CR, Krammer PH. How T lymphocytes switch between life and death. Eur J Immunol 2006;36:1654-1658.
[319] Sun Y, Chen JH, Fu Y. Immunotherapy with agonistic anti-CD137: two sides of a coin. Cell Mol Immunol 2004;1:31-36.
[320] Alderson MR, Smith CA, Tough TW, Davis-Smith T, Armitage RJ, Falk B, Roux E, Baker E, Sutherland GR, Din WS. Molecular and biological characterization of human 4-1BB and its ligand. Eur J Immunol 1994;24:2219-2227.
[321] Pollok KE, Kim YJ, Hurtado J, Zhou Z, Kim KK, Kwon BS. 4-1BB T-cell antigen binds to mature B cells and macrophages, and costimulates anti-mu-primed splenic B cells. Eur J Immunol 1994;24:367-374.
[322] Wen T, Bukczynski J, Watts TH. 4-1BB ligand-mediated costimulation of human T cells induces CD4 and CD8 T cell expansion, cytokine production, and the development of cytolytic effector function. J Immunol 2002;168:4897-4906.
[323] Ma BY, Mikolajczak SA, Danesh A, Hosiawa KA, Cameron CM, Takaori-Kondo A, Uchiyama T, Kelvin DJ, Ochi A. The expression and the regulatory role of OX40 and 4-1BB heterodimer in activated human T cells. Blood 2005;106:2002-2010.
[324] Shao H, Fu Y, Liao T, Peng Y, Chen L, Kaplan HJ, Sun D. Anti-CD137 mAb treatment inhibits experimental autoimmune uveitis by limiting expansion and increasing apoptotic death of uveitogenic T cells. Invest Ophthalmol Vis Sci 2005;46:596-603.
[325] Ebata T, Mogi S, Hata Y, Fujimoto JI, Yagita H, Okumura K, Azuma M. Rapid induction of CD95 ligand and CD4+ T cell-mediated apoptosis by CD137 (4-1BB) costimulation. Eur J Immunol 2001;31:1410-1416.
[326] Bertram EM, Lau P, Watts TH. Temporal segregation of 4-1BB versus CD28-mediated costimulation: 4-1BB ligand influences T cell numbers late in the primary response and regulates the size of the T cell memory response following influenza infection. J Immunol 2002;168:3777-3785.
[327] Duttagupta PA, Boesteanu AC, Katsikis PD. Costimulation signals for memory CD8+ T cells during viral infections. Crit Rev Immunol 2009;29:469-486.

[328] Ayroldi E, Migliorati G, Bruscoli S, Marchetti C, Zollo O, Cannarile L, D'Adamio F, Riccardi C. Modulation of T-cell activation by the glucocorticoid-induced leucine zipper factor via inhibition of nuclear factor kappaB. Blood 2001;98:743-753.
[329] Asselin-Labat ML, David M, Biola-Vidamment A, Lecoeuche D, Zennaro MC, Bertoglio J, Pallardy M. GILZ, a new target for the transcription factor FoxO3, protects T lymphocytes from interleukin-2 withdrawal-induced apoptosis. Blood 2004;104:215-223.
[330] Quandt J, Dorovini-Zis K. The beta chemokines CCL4 and CCL5 enhance adhesion of specific CD4+ T cell subsets to human brain endothelial cells. J Neuropathol Exp Neurol 2004;63:350-362.
[331] Bystry RS, Aluvihare V, Welch KA, Kallikourdis M, Betz AG. B cells and professional APCs recruit regulatory T cells via CCL4. Nat Immunol 2001;2:1126-1132.
[332] Castellino F, Huang AY, Altan-Bonnet G, Stoll S, Scheinecker C, Germain RN. Chemokines enhance immunity by guiding naive CD8+ T cells to sites of CD4+ T cell-dendritic cell interaction. Nature 2006;440:890-895.
[333] Sironi M, Martinez FO, D'Ambrosio D, Gattorno M, Polentarutti N, Locati M, Gregorio A, Iellem A, Cassatella MA, Van Damme J, Sozzani S, Martini A, Sinigaglia F, Vecchi A, Mantovani A. Differential regulation of chemokine production by Fcgamma receptor engagement in human monocytes: association of CCL1 with a distinct form of M2 monocyte activation (M2b, Type 2). J Leukoc Biol 2006;80:342-349.
[334] Sebastiani S, Allavena P, Albanesi C, Nasorri F, Bianchi G, Traidl C, Sozzani S, Girolomoni G, Cavani A. Chemokine receptor expression and function in CD4+ T lymphocytes with regulatory activity. J Immunol 2001;166:996-1002.
[335] Freeman CM, Chiu BC, Stolberg VR, Hu J, Zeibecoglou K, Lukacs NW, Lira SA, Kunkel SL, Chensue SW. CCR8 is expressed by antigen-elicited, IL-10-producing CD4+CD25+ T cells, which regulate Th2-mediated granuloma formation in mice. J Immunol 2005;174:1962-1970.
[336] Miller MD, Krangel MS. The human cytokine I-309 is a monocyte chemoattractant. Proc Natl Acad Sci U S A 1992;89:2950-2954.
[337] Hubbe M, Altevogt P. Heat-stable antigen/CD24 on mouse T lymphocytes: evidence for a costimulatory function. Eur J Immunol 1994;24:731-737.
[338] Li O, Zheng P, Liu Y. CD24 expression on T cells is required for optimal T cell proliferation in lymphopenic host. J Exp Med 2004;200:1083-1089.
[339] Grela F, Aumeunier A, Bardel E, Van LP, Bourgeois E, Vanoirbeek J, Leite-de-Moraes M, Schneider E, Dy M, Herbelin A, Thieblemont N. The TLR7 agonist R848 alleviates allergic inflammation by targeting invariant NKT cells to produce IFN-gamma. J Immunol 2011;186:284-290.
[340] Tripp CH, Sparber F, Hermans IF, Romani N, Stoitzner P. Glycolipids injected into the skin are presented to NKT cells in the draining lymph node independently of migratory skin dendritic cells. J Immunol 2009;182:7644-7654.
[341] Porubsky S, Speak AO, Luckow B, Cerundolo V, Platt FM, Grone HJ. Normal development and function of invariant natural killer T cells in mice with isoglobotrihexosylceramide (iGb3) deficiency. Proc Natl Acad Sci U S A 2007;104:5977-5982.
[342] Colgan SP, Hershberg RM, Furuta GT, Blumberg RS. Ligation of intestinal epithelial CD1d induces bioactive IL-10: critical role of the cytoplasmic tail in autocrine signaling. Proc Natl Acad Sci U S A 1999;96:13938-13943.
[343] Rogers DF. Airway goblet cells: responsive and adaptable front-line defenders. Eur Respir J 1994;7:1690-1706.
[344] Devereux TR. Alveolar type II and Clara cells: isolation and xenobiotic metabolism. Environ Health Perspect 1984;56:95-101.
[345] Hajj R, Baranek T, Le Naour R, Lesimple P, Puchelle E, Coraux C. Basal cells of the human adult airway surface epithelium retain transit-amplifying cell properties. Stem Cells 2007;25:139-148.
[346] Singh G, Katyal SL. Clara cell proteins. Ann N Y Acad Sci 2000;923:43-58.
[347] Harkema JR. Comparative aspects of nasal airway anatomy: relevance to inhalation toxicology. Toxicol Pathol 1991;19:321-336.
[348] Cutz E, Yeger H, Pan J. Pulmonary neuroendocrine cell system in pediatric lung disease-recent advances. Pediatr Dev Pathol 2007;10:419-435.
[349] Basbaum CB, Madison JM, Sommerhoff CP, Brown JK, Finkbeiner WE. Receptors on airway gland cells. Am Rev Respir Dis 1990;141:S141-144.
[350] Basbaum CB, Jany B, Finkbeiner WE. The serous cell. Annu Rev Physiol 1990;52:97-113.

[351] Groneberg DA, Eynott PR, Oates T, Lim S, Wu R, Carlstedt I, Nicholson AG, Chung KF. Expression of MUC5AC and MUC5B mucins in normal and cystic fibrosis lung. Respir Med 2002;96:81-86.
[352] Jeffery PK. The origins of secretions in the lower respiratory tract. Eur J Respir Dis Suppl 1987;153:34-42.
[353] Wang YY, Cutz E. Localization of cholecystokinin-like peptide in neuroendocrine cells of mammalian lungs: a light and electron microscopic immunohistochemical study. Anat Rec 1993;236:198-205.
[354] McGuire JK, Li Q, Parks WC. Matrilysin (matrix metalloproteinase-7) mediates E-cadherin ectodomain shedding in injured lung epithelium. Am J Pathol 2003;162:1831-1843.
[355] Pearson CA, Lamar PC, Prozialeck WC. Effects of cadmium on E-cadherin and VE-cadherin in mouse lung. Life Sci 2003;72:1303-1320.
[356] Salon C, Moro D, Lantuejoul S, Brichon Py P, Drabkin H, Brambilla C, Brambilla E. E-cadherin-beta-catenin adhesion complex in neuroendocrine tumors of the lung: a suggested role upon local invasion and metastasis. Hum Pathol 2004;35:1148-1155.
[357] Nozawa N, Hashimoto S, Nakashima Y, Matsuo Y, Koga T, Sugio K, Niho Y, Harada M, Sueishi K. Immunohistochemical alpha- and beta-catenin and E-cadherin expression and their clinicopathological significance in human lung adenocarcinoma. Pathol Res Pract 2006;202:639-650.
[358] Bonner JC. Regulation of PDGF and its receptors in fibrotic diseases. Cytokine Growth Factor Rev 2004;15:255-273.
[359] Vestweber D. VE-cadherin: the major endothelial adhesion molecule controlling cellular junctions and blood vessel formation. Arterioscler Thromb Vasc Biol 2008;28:223-232.
[360] Litvinov SV, Velders MP, Bakker HA, Fleuren GJ, Warnaar SO. Ep-CAM: a human epithelial antigen is a homophilic cell-cell adhesion molecule. J Cell Biol 1994;125:437-446.
[361] Trzpis M, McLaughlin PM, Popa ER, Terpstra P, van Kooten TG, de Leij LM, Harmsen MC. EpCAM homologues exhibit epithelial-specific but different expression patterns in the kidney. Transgenic Res 2008;17:229-238.
[362] McQualter JL, Yuen K, Williams B, Bertoncello I. Evidence of an epithelial stem/progenitor cell hierarchy in the adult mouse lung. Proc Natl Acad Sci U S A 2010;107:1414-1419.
[363] Bertoncello I, McQualter J. Isolation and clonal assay of adult lung epithelial stem/progenitor cells. Curr Protoc Stem Cell Biol 2011;Chapter 2:Unit 2G 1.
[364] Ishikawa H, Tanaka K, Kutsukake E, Fukui T, Sasaki H, Hata A, Noda S, Matsumoto T. IFN-gamma production downstream of NKT cell activation in mice infected with influenza virus enhances the cytolytic activities of both NK cells and viral antigen-specific CD8+ T cells. Virology 2010;407:325-332.
[365] Ryckman C, Vandal K, Rouleau P, Talbot M, Tessier PA. Proinflammatory activities of S100: proteins S100A8, S100A9, and S100A8/A9 induce neutrophil chemotaxis and adhesion. J Immunol 2003;170:3233-3242.
[366] Ghavami S, Eshragi M, Ande SR, Chazin WJ, Klonisch T, Halayko AJ, McNeill KD, Hashemi M, Kerkhoff C, Los M. S100A8/A9 induces autophagy and apoptosis via ROS-mediated cross-talk between mitochondria and lysosomes that involves BNIP3. Cell Res 2010;20:314-331.
[367] Foell D, Wittkowski H, Ren Z, Turton J, Pang G, Daebritz J, Ehrchen J, Heidemann J, Borody T, Roth J, Clancy R. Phagocyte-specific S100 proteins are released from affected mucosa and promote immune responses during inflammatory bowel disease. J Pathol 2008;216:183-192.
[368] Vos JB, van Sterkenburg MA, Rabe KF, Schalkwijk J, Hiemstra PS, Datson NA. Transcriptional response of bronchial epithelial cells to Pseudomonas aeruginosa: identification of early mediators of host defense. Physiol Genomics 2005;21:324-336.
[369] Schmid KW, Lugering N, Stoll R, Brinkbaumer P, Winde G, Domschke W, Bocker W, Sorg C. Immunohistochemical demonstration of the calcium-binding proteins MRP8 and MRP14 and their heterodimer (27E10 antigen) in Crohn's disease. Hum Pathol 1995;26:334-337.
[370] Abtin A, Eckhart L, Glaser R, Gmeiner R, Mildner M, Tschachler E. The antimicrobial heterodimer S100A8/S100A9 (calprotectin) is upregulated by bacterial flagellin in human epidermal keratinocytes. J Invest Dermatol 2010;130:2423-2430.
[371] Henke MO, Shah SA, Rubin BK. The role of airway secretions in COPD--clinical applications. COPD 2005;2:377-390.
[372] Zelensky AN, Gready JE. The C-type lectin-like domain superfamily. FEBS J 2005;272:6179-6217.
[373] Graham LM, Brown GD. The Dectin-2 family of C-type lectins in immunity and homeostasis. Cytokine 2009;48:148-155.

[374] Yamasaki S, Ishikawa E, Sakuma M, Hara H, Ogata K, Saito T. Mincle is an ITAM-coupled activating receptor that senses damaged cells. Nat Immunol 2008;9:1179-1188.
[375] Yamasaki S, Matsumoto M, Takeuchi O, Matsuzawa T, Ishikawa E, Sakuma M, Tateno H, Uno J, Hirabayashi J, Mikami Y, Takeda K, Akira S, Saito T. C-type lectin Mincle is an activating receptor for pathogenic fungus, Malassezia. Proc Natl Acad Sci U S A 2009;106:1897-1902.
[376] Ishikawa E, Ishikawa T, Morita YS, Toyonaga K, Yamada H, Takeuchi O, Kinoshita T, Akira S, Yoshikai Y, Yamasaki S. Direct recognition of the mycobacterial glycolipid, trehalose dimycolate, by C-type lectin Mincle. J Exp Med 2009;206:2879-2888.
[377] Arce I, Martinez-Munoz L, Roda-Navarro P, Fernandez-Ruiz E. The human C-type lectin CLECSF8 is a novel monocyte/macrophage endocytic receptor. Eur J Immunol 2004;34:210-220.
[378] McGreal EP, Rosas M, Brown GD, Zamze S, Wong SY, Gordon S, Martinez-Pomares L, Taylor PR. The carbohydrate-recognition domain of Dectin-2 is a C-type lectin with specificity for high mannose. Glycobiology 2006;16:422-430.
[379] Sato K, Yang XL, Yudate T, Chung JS, Wu J, Luby-Phelps K, Kimberly RP, Underhill D, Cruz PD, Jr., Ariizumi K. Dectin-2 is a pattern recognition receptor for fungi that couples with the Fc receptor gamma chain to induce innate immune responses. J Biol Chem 2006;281:38854-38866.
[380] Aragane Y, Maeda A, Schwarz A, Tezuka T, Ariizumi K, Schwarz T. Involvement of dectin-2 in ultraviolet radiation-induced tolerance. J Immunol 2003;171:3801-3807.
[381] Chen ST, Lin YL, Huang MT, Wu MF, Cheng SC, Lei HY, Lee CK, Chiou TW, Wong CH, Hsieh SL. CLEC5A is critical for dengue-virus-induced lethal disease. Nature 2008;453:672-676.
[382] Wang KX, Denhardt DT. Osteopontin: role in immune regulation and stress responses. Cytokine Growth Factor Rev 2008;19:333-345.
[383] Renkl AC, Wussler J, Ahrens T, Thoma K, Kon S, Uede T, Martin SF, Simon JC, Weiss JM. Osteopontin functionally activates dendritic cells and induces their differentiation toward a Th1-polarizing phenotype. Blood 2005;106:946-955.
[384] Rollo EE, Hempson SJ, Bansal A, Tsao E, Habib I, Rittling SR, Denhardt DT, Mackow ER, Shaw RD. The cytokine osteopontin modulates the severity of rotavirus diarrhea. J Virol 2005;79:3509-3516.
[385] Abel B, Freigang S, Bachmann MF, Boschert U, Kopf M. Osteopontin is not required for the development of Th1 responses and viral immunity. J Immunol 2005;175:6006-6013.
[386] Ashkar S, Weber GF, Panoutsakopoulou V, Sanchirico ME, Jansson M, Zawaideh S, Rittling SR, Denhardt DT, Glimcher MJ, Cantor H. Eta-1 (osteopontin): an early component of type-1 (cell-mediated) immunity. Science 2000;287:860-864.
[387] Debets R, Timans JC, Homey B, Zurawski S, Sana TR, Lo S, Wagner J, Edwards G, Clifford T, Menon S, Bazan JF, Kastelein RA. Two novel IL-1 family members, IL-1 delta and IL-1 epsilon, function as an antagonist and agonist of NF-kappa B activation through the orphan IL-1 receptor-related protein 2. J Immunol 2001;167:1440-1446.
[388] Wang H, Ma S. The cytokine storm and factors determining the sequence and severity of organ dysfunction in multiple organ dysfunction syndrome. Am J Emerg Med 2008;26:711-715.
[389] Tudhope SJ, Catley MC, Fenwick PS, Russell RE, Rumsey WL, Newton R, Barnes PJ, Donnelly LE. The role of IkappaB kinase 2, but not activation of NF-kappaB, in the release of CXCR3 ligands from IFN-gamma-stimulated human bronchial epithelial cells. J Immunol 2007;179:6237-6245.
[390] Kennedy J, Vicari AP, Saylor V, Zurawski SM, Copeland NG, Gilbert DJ, Jenkins NA, Zlotnik A. A molecular analysis of NKT cells: identification of a class-I restricted T cell-associated molecule (CRTAM). J Leukoc Biol 2000;67:725-734.
[391] Garay E, Patino-Lopez G, Islas S, Alarcon L, Canche-Pool E, Valle-Rios R, Medina-Contreras O, Granados G, Chavez-Munguia B, Juaristi E, Ortiz-Navarrete V, Gonzalez-Mariscal L. CRTAM: A molecule involved in epithelial cell adhesion. J Cell Biochem 2010;111:111-122.
[392] Arase N, Takeuchi A, Unno M, Hirano S, Yokosuka T, Arase H, Saito T. Heterotypic interaction of CRTAM with Necl2 induces cell adhesion on activated NK cells and CD8+ T cells. Int Immunol 2005;17:1227-1237.
[393] Akbari O, Stock P, DeKruyff RH, Umetsu DT. Role of regulatory T cells in allergy and asthma. Curr Opin Immunol 2003;15:627-633.
[394] Rossi GA, Sacco O, Balbi B, Oddera S, Mattioni T, Corte G, Ravazzoni C, Allegra L. Human ciliated bronchial epithelial cells: expression of the HLA-DR antigens and of the HLA-DR alpha gene, modulation of the HLA-DR antigens by gamma-interferon and antigen-presenting function in the mixed leukocyte reaction. Am J Respir Cell Mol Biol 1990;3:431-439.

Appendix 1

Miltenyi Biotec

CD45 MicroBeads
mouse

Order No. 130-052-301

Index

1. Description

Components	2 mL CD45 MicroBeads, mouse: MicroBeads conjugated to monoclonal anti-mouse CD45 (Ly-5; isotype: rat IgG2b; clone: 30F11.1) antibody.
Size	For 2×10^9 total cells, up to 200 separations.
Product format	CD45 MicroBeads are supplied as a suspension containing stabilizer and 0.05% sodium azide.
Storage	Store protected from light at 4–8 °C. Do not freeze. The expiration date is indicated on the vial label.

1.1 Principle of MACS® separation

First, the CD45$^+$ cells are magnetically labeled with CD45 MicroBeads. Then, the cell suspension is loaded onto a MACS® Column which is placed in the magnetic field of a MACS Separator. The magnetically labeled CD45$^+$ cells are retained on the column. The unlabeled cells run through and this cell fraction is depleted of CD45$^+$ cells. After removal of the column from the magnetic field, the magnetically retained CD45$^+$ cells can be eluted as the positively selected cell fraction.

1.2 Background and product applications

CD45 MicroBeads are used for the positive selection or depletion of leukocytes from lymphoid and non-lymphoid tissues. The CD45 antigen is expressed on all cells of hematopoietic origin except erythrocytes and platelets.

Examples of applications

- Positive selection or depletion of CD45$^+$ leukocytes from spleen, lymph nodes, thymus, bone marrow, peripheral blood, body fluids or non-hematopoietic tissue.
- CD45 MicroBeads were used in combination with Anti-Ter-119 MicroBeads (# 130-049-901) for depletion of mouse leukocytes to enrich human cells from bone marrow of chimeric mice.[1]

1.3 Reagent and instrument requirements

- Buffer (degassed): Prepare a solution containing PBS (phosphate buffered saline) pH 7.2, 0.5% BSA and 2 mM EDTA by diluting MACS BSA Stock Solution (# 130-091-376) 1:20 in autoMACS™ Rinsing Solution (# 130-091-222). Keep buffer cold (4–8 °C).

  ▲ **Note:** EDTA can be replaced by other supplements such as anticoagulant citrate dextrose formula-A (ACD-A) or citrate phosphate dextrose (CPD). BSA can be replaced by other proteins such as mouse serum albumin, mouse serum or fetal calf serum. Buffers or media containing Ca^{2+} or Mg^{2+} are not recommended for use.

- MACS Columns and MACS Separators: CD45$^+$ cells can be enriched by using MS, LS or XS Columns (positive selection). CD45 MicroBeads can be used for depletion of CD45$^+$ cells on LD, CS or D Columns. Cells which strongly express the CD45 antigen can also be depleted using MS, LS or XS Columns. Positive selection or depletion can also be performed by using the autoMACS Separator.

Column	max. number of labeled cells	max. number of total cells	Separator
Positive selection			
MS	10^7	2×10^8	MiniMACS, OctoMACS, VarioMACS, SuperMACS
LS	10^8	2×10^9	MidiMACS, QuadroMACS, VarioMACS, SuperMACS
XS	10^9	2×10^{10}	SuperMACS
Depletion			
LD	10^8	5×10^8	MidiMACS, QuadroMACS, VarioMACS, SuperMACS
CS	2×10^8		VarioMACS, SuperMACS
D	10^9		SuperMACS
Positive selection or depletion			
autoMACS	2×10^8	4×10^9	autoMACS

▲ **Note:** Column adapters are required to insert certain columns into VarioMACS™ Separator or SuperMACS™ Separator. For details, see MACS Separator data sheets.

- (Optional) Fluorochrome-conjugated CD45 antibodies, e.g. CD45-FITC (# 130-091-609), CD45-PE (# 130-091-610) or CD45-APC (# 130-091-811).
- (Optional) PI (propidium iodide) or 7-AAD for the flow cytometric exclusion of dead cells.
- (Optional) Pre-Separation Filters (# 130-041-407) to remove cell clumps.

140-000-074.05

Miltenyi Biotec GmbH
Friedrich-Ebert-Straße 68, 51429 Bergisch Gladbach, Germany
Phone +49 2204 8306-0, Fax +49 2204 85197
macs@miltenyibiotec.de
www.miltenyibiotec.com

Miltenyi Biotec Inc.
2303 Lindbergh Street, Auburn, CA 95602, USA
Phone 800 FOR MACS, +1 530 888 8871, Fax +1 530 888 8925
macs@miltenyibiotec.com

2. Protocol

2.1 Sample preparation

Prepare a single-cell suspension from lymphoid organs, non-lymphoid tissue or peripheral blood using standard methods (see "General Protocols" in the User Manuals or visit www.miltenyibiotec.com).

▲ Dead cells may bind non-specifically to MACS MicroBeads. In case of high numbers of dead cells we recommend to remove dead cells by density gradient centrifugation or using the Dead Cell Removal Kit (# 130-090-101).

2.2 Magnetic labeling

▲ Work fast, keep the cells cold, and use pre-cooled solutions. This will prevent capping of antibodies on the cell surface and non-specific cell labeling.

▲ Volumes for magnetic labeling given below are for up to 10^7 total cells. When working with fewer than 10^7 cells, use the same volumes as indicated. When working with higher cell numbers, scale up all reagent volumes and total volumes accordingly (e.g. for 2×10^7 total cells, use twice the volume of all indicated reagent volumes and total volumes).

▲ For optimal performance it is important to obtain a single-cell suspension before magnetic separation. Pass cells through 30 µm nylon mesh (Pre-Separation Filters # 130-041-407) to remove cell clumps which may clog the column.

1. Determine cell number.
2. Centrifuge at 300×g for 10 minutes. Pipette off supernatant completely.
3. Resuspend cell pellet in 90 µL of buffer per 10^7 total cells.
4. Add 10 µL of CD45 MicroBeads per 10^7 total cells.
5. Mix well and incubate for 15 minutes at 4–8 °C.

   ▲ **Note:** Working on ice may require increased incubation times. Higher temperatures and/or longer incubation times lead to non-specific cell labeling.
6. (Optional) Add staining antibodies, e.g. add 10 µL of CD45-FITC (# 130-091-609), and incubate for 5 minutes at 4–8 °C.
7. Wash cells by adding 1–2 mL of buffer per 10^7 cells and centrifuge at 300×g for 10 minutes. Pipette off supernatant completely.
8. Resuspend up to 10^8 cells in 500 µL of buffer.

   ▲ **Note:** For higher cell numbers, scale up buffer volume accordingly.

   ▲ **Note:** For depletion with LD columns, resuspend cell pellet in 500 µL of buffer for up to 1.25×10^8 cells.
9. Proceed to magnetic separation (2.3).

2.3 Magnetic separation

▲ Choose an appropriate MACS Column and MACS Separator according to the number of total cells and the number of $CD45^+$ cells (see table in section 1.3).

Magnetic separation with MS or LS Columns

1. Place column in the magnetic field of a suitable MACS Separator (see "Column data sheets").
2. Prepare column by rinsing with appropriate amount of buffer:
   MS: 500 µL LS: 3 mL
3. Apply cell suspension onto the column.
4. Collect unlabeled cells which pass through and wash column with appropriate amount of buffer. Perform washing steps by adding buffer three times, each time once the column reservoir is empty.
   MS: 3×500 µL LS: 3×3 mL
   Collect total effluent. This is the unlabeled cell fraction.
5. Remove column from the separator and place it on a suitable collection tube.
6. Pipette appropriate amount of buffer onto the column. Immediately flush out fraction with the magnetically labeled cells by firmly applying the plunger supplied with the column.
   MS: 1 mL LS: 5 mL

   ▲ **Note:** To increase the purity of the magnetically labeled fraction, it can be passed over a new, freshly prepared column.

Magnetic separation with XS Columns

For instructions on the column assembly and the separation, refer to the "XS Column data sheet"

Depletion with LD Columns

1. Place LD Column in the magnetic field of a suitable MACS Separator (see "LD Column data sheet").
2. Prepare column by rinsing with 2 mL of buffer.
3. Apply cell suspension onto the column.
4. Collect unlabeled cells which pass through and wash column with 2×1 mL of buffer. Collect total effluent. This is the unlabeled cell fraction.

Depletion with CS Columns

1. Assemble CS Column and place it in the magnetic field of a suitable MACS Separator (see "CS Column data sheet").
2. Prepare column by filling and rinsing with 60 ml of buffer. Attach a 22G flow resistor to the 3-way-stopcock of the assembled column (see "CS Column data sheet").
3. Apply cell suspension onto the column.
4. Collect unlabeled cells which pass through and wash column with 30 mL buffer from top. Collect total effluent. This is the unlabeled cell fraction.

Depletion with D Columns

For instructions on column assembly and separation, refer to the "D Column data sheet"

Magnetic separation with autoMACS™ Separator

▲ Refer to the autoMACS™ User Manual for instructions on how to use the autoMACS Separator.

1. Prepare and prime autoMACS Separator.

140-000-074.05

2. Place tube containing the magnetically labeled cells in the autoMACS Separator. For a standard separation, choose following separation programs:

   Positive selection: "Possel"

   Depletion: "Depletes"

   ▲ **Note:** Program choice depends on the isolation strategy, the strength of magnetic labeling and the frequency of magnetically labeled cells. For details see autoMACS User Manual: "autoMACS Cell Separation Programs"

3. When using the program "Possel" collect positive fraction (outlet port "pos1"). This is the purified $CD45^+$ cell fraction.

   When using the program "Depletes" collect unlabeled fraction (outlet port "neg1"). This is the $CD45^-$ cell fraction.

3. Example of a separation using CD45 MicroBeads

$CD45^+$ cells were isolated from a mouse spleen cell suspension using CD45 MicroBeads, a MiniMACS™ Separator and an MS Column. The cells are fluorescently stained with CD45-FITC (# 130-091-609). Cell debris and dead cells were excluded from the analysis based on scatter signals and PI fluorescence.

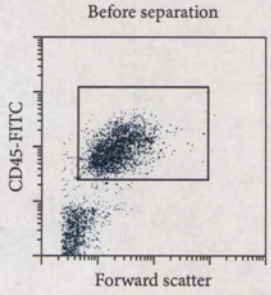

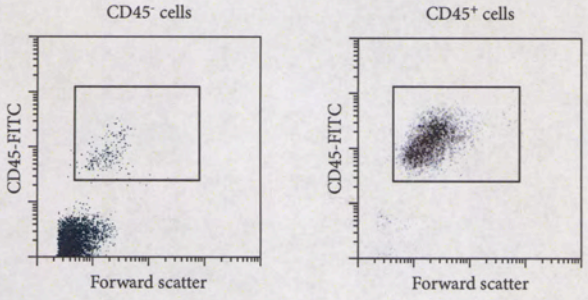

4. References

1. Schiedlmeier, B, Kühlicke, K; Eckert, HG; Baum, C; Zeller, WJ; Fruehauf, S (2000) Quantitative assessment of retroviral transfer of the human multidrug resistance 1 gene to human mobilized peripheral blood progenitor cells engrafted in nonobese diabetic/severe combined immunodeficient mice. Blood 95: 1237–1248.

Warnings

Reagents contain sodium azide. Under acidic conditions sodium azide yields hydrazoic acid, which is extremely toxic. Azide compounds should be diluted with running water before discarding. These precautions are recommended to avoid deposits in plumbing where explosive conditions may develop.

Warranty

The products sold hereunder are warranted only to be free from defects in workmanship and material at the time of delivery to the customer. MILTENYI BIOTEC GmbH makes no warranty or representation, either expressed or implied, with respect to the fitness of a product for a particular purpose. There are no warranties, expressed or implied, which extend beyond the technical specifications of the products. MILTENYI BIOTEC GmbH's liability is limited to either replacement of the products or refund of the purchase price. MILTENYI BIOTEC GmbH is not liable for any property damage, personal injury or economic loss caused by the product.

140-000-074.05

Miltenyi Biotec

Anti-PE MicroBeads

Order no. 130-048-801

Contents

1. Description

Components	2 mL Anti-PE MicroBeads: MicroBeads conjugated to monoclonal anti-PE antibodies (isotype: mouse IgG1)
Capacity	For 10^9 total cells, up to 100 separations.
Product format	Anti-PE MicroBeads are supplied in buffer containing stabilizer and 0.05% sodium azide.
Storage	Store protected from light at 2–8 °C. Do not freeze. The expiration date is indicated on the vial label.

1.1 Principle of MACS® Separation

First, the cells are stained with a R-Phycoerythrin (PE)-conjugated primary antibody or ligand. Subsequently, the cells are magnetically labeled with Anti-PE MicroBeads. Then the cell suspension is loaded on a MACS® Column which is placed in the magnetic field of a MACS Separator. The magnetically labeled cells are retained in the column while the unlabeled cells run through. After removal of the column from the magnetic field, the magnetically retained cells can be eluted as the positively selected cell fraction.

1.2 Background information

Anti-PE MicroBeads are developed for the separation of cells according to surface markers labeled with PE-conjugated antibodies, peptides or ligands. After separation the PE-labeled cells can be detected by flow cytometry or fluorescence microscopy.

▲ Fluorochrome tandem conjugates of R-Phycoerythrin and other fluorescent dyes that are often used in flow cytometry for third color analysis may also be recognized by Anti-PE MicroBeads, e.g. PE-Cy5 (Becton, Dickinson and Company), ECD and PC5 (Beckman Coulter). For separation of cells labeled with primary antibodies conjugated to PE-Cy5, it is recommended to use Anti-Cy5/Anti-Alexa Fluor® 647 MicroBeads (# 130-091-395).

1.3 Applications

- Positive selection or depletion of cells labeled with PE-conjugated antibodies.
- Positive selection or depletion of cells labeled with PE-conjugated peptides or ligands.

1.4 Reagent and instrument requirements

- Buffer: Prepare a solution containing PBS (phosphate-buffered saline) pH 7.2, 0.5% BSA and 2 mM EDTA by diluting MACS BSA Stock Solution (# 130-091-376) 1:20 with autoMACS™ Rinsing Solution (# 130-091-222). Keep buffer cold (2–8 °C). Degas buffer before use, as air bubbles could block the column

  ▲ **Note:** EDTA can be replaced by other supplements such as anticoagulant citrate dextrose formula-A (ACD-A) or citrate phosphate dextrose (CPD). BSA can be replaced by other proteins such as human serum albumin, human serum, or fetal calf serum. Buffers or media containing Ca^{2+} or Mg^{2+} are not recommended for use.

- MACS Columns and MACS Separators: Cells labeled with Anti-PE MicroBeads can be enriched by using MS, LS, or XS Columns or depleted with the use of LD, CS, or D Columns. Cells which strongly express the PE-labeled antigen can also be depleted using MS, LS, or XS Columns. Positive selection or depletion can also be performed by using the autoMACS or the autoMAC Pro Separator.

Column	Max. number of labeled cells	Max. number of total cells	Separator
Positive selection			
MS	10^7	2×10^8	MiniMACS, OctoMACS, VarioMACS, SuperMACS
LS	10^8	2×10^9	MidiMACS, QuadroMACS VarioMACS, SuperMACS
XS	10^9	2×10^{10}	SuperMACS
Depletion			
LD	10^8	5×10^8	MidiMACS, QuadroMACS VarioMACS, SuperMACS
CS	2×10^8		VarioMACS, SuperMACS
D	10^9		SuperMACS
Positive selection or depletion			
autoMACS	2×10^8	4×10^9	autoMACS, autoMACS Pro

▲ **Note:** Column adapters are required to insert certain columns into the VarioMACS™ or SuperMACS™ Separators. For details see the respective MACS Separator data sheet.

- PE-conjugated primary antibody, peptide or ligand.
- (Optional) Propidium iodide (PI) or 7-AAD for exclusion of dead cells.
- (Optional) Pre-Separation Filters (# 130-041-407) to remove cell clumps.
- (Optional) Dead Cell Removal Kit (# 130-090-101) for the depletion of dead cells.

140-000-698.56

Miltenyi Biotec GmbH
Friedrich-Ebert-Straße 68, 51429 Bergisch Gladbach, Germany
Phone +49 2204 8306-0, Fax +49 2204 85197
macs@miltenyibiotec.de
www.miltenyibiotec.com

Miltenyi Biotec Inc.
2303 Lindbergh Street, Auburn, CA 95602, USA
Phone 800 FOR MACS, +1 530 888 8871, Fax +1 530 888 8925
macs@miltenyibiotec.com

2. Protocol

2.1 Sample preparation

When working with anticoagulated peripheral blood or buffy coat, peripheral blood mononuclear cells (PBMCs) should be isolated by density gradient centrifugation, for example, using Ficoll-Paque™ For details see the General Protocols section of the respective separator user manual. The General Protocols are also available at www.miltenyibiotec.com/protocols.

▲ **Note:** To remove platelets after density gradient separation, resuspend cell pellet in buffer and centrifuge at 200×g for 10–15 minutes at 20 °C. Carefully aspirate supernatant. Repeat washing step.

When working with tissues or lysed blood, prepare a single-cell suspension using standard methods. For details see the General Protocols section of the respective separator user manual. The General Protocols are also available at www.miltenyibiotec.com/protocols.

▲ Dead cells may bind non-specifically to MACS MicroBeads. To remove dead cells, we recommend using density gradient centrifugation or the Dead Cell Removal Kit (# 130-090-101).

2.2 Magnetic labeling

▲ Work fast, keep the cells cold, and use pre-cooled solutions. This will prevent capping of antibodies on the cell surface and a non-specific cell labeling.

▲ Volumes for magnetic labeling given below are for up to 10^7 total cells. When working with fewer than 10^7 cells, use the same volumes as indicated. When working with higher cell numbers, scale up all reagent volumes and total volumes accordingly (e.g. for 2×10^7 total cells, use twice the volume of all indicated reagent volumes and total volumes).

▲ For optimal performance it is important to obtain a single-cell suspension before magnetic separation. Pass cells through 30 µm nylon mesh (Pre-Separation Filters, # 130-041-407) to remove cell clumps which may clog the column. Wet filter with buffer before use.

▲ Working on ice may require increased incubation times. Higher temperatures and/or longer incubation times may lead to non-specific cell labeling.

▲ The centrifugal force and centrifugation time mentioned below are recommendations. The optimal relative centrifugal force (RCF) and centrifugation time may be different depending on the cell sample.

▲ Primary PE-conjugated antibodies should be titrated to determine the optimal staining dilution. Staining should not increase fluorescence intensity of the negative population.

1. Determine cell number.
2. Centrifuge cell suspension at 300×g for 10 minutes. Aspirate supernatant completely.
3. Resuspend cell pellet and stain with the primary PE-conjugated antibody according to the manufacturer's recommendations. For MACS PE-conjugated antibodies, resuspend 10^7 total cells in 100 µL buffer and add 10 µL PE-conjugate.
4. Mix well and incubate for 10 minutes in the dark in the refrigerator (2–8 °C) or according to the manufacturer's recommendations.
5. Wash cells to remove unbound primary antibody by adding 1–2 mL of buffer per 10^7 cells and centrifuge at 300×g for 10 minutes.
6. (Optional) Repeat washing step.
7. Aspirate supernatant completely and resuspend cell pellet in 80 µL of buffer per 10^7 total cells.
8. Add 20 µL of Anti-PE MicroBeads per 10^7 total cells.
9. Mix well and incubate for 15 minutes in the refrigerator (2–8 °C).
10. Wash cells by adding 1–2 mL of buffer per 10^7 cells and centrifuge at 300×g for 10 minutes.
11. Aspirate supernatant completely.
12. Resuspend up to 10^8 cells in 500 µL of buffer.

    ▲ **Note:** For higher cell numbers, scale up buffer volume accordingly.

    ▲ **Note:** For depletion with LD Columns, resuspend up to 1.25×10^8 cells in 500 µL of buffer.
13. Proceed to magnetic separation (2.3).

2.3 Magnetic separation

▲ Choose an appropriate MACS Column and MACS Separator according to the number of total cells and the number of magnetically labeled cells. For details see table in section 1.4.

Magnetic separation with MS or LS Columns

1. Place column in the magnetic field of a suitable MACS Separator. For details see the respective MACS Column data sheet.
2. Prepare column by rinsing with the appropriate amount of buffer:
   MS: 500 µL LS: 3 mL
3. Apply cell suspension onto the column.
4. Collect unlabeled cells that pass through and wash column with the appropriate amount of buffer. Collect total effluent; this is the unlabeled cell fraction. Perform washing steps by adding buffer three times. Only add new buffer when the column reservoir is empty.
   MS: 3×500 µL LS: 3×3 mL
5. Remove column from the separator and place it on a suitable collection tube.
6. Pipette appropriate amount of buffer onto the column. Immediately flush out the magnetically labeled cells by firmly pushing the plunger into the column.
   MS: 1 mL LS: 5 mL
7. (Optional) To increase the purity of the magnetically labeled cells, the eluted fraction can be enriched over a second MS or LS Column. Repeat the magnetic separation procedure as described in steps 1 to 6 by using a new column.

Magnetic separation with XS Columns

For instructions on the column assembly and the separation, refer to the XS Column data sheet.

Depletion with LD Columns

1. Place LD Column in the magnetic field of a suitable MACS Separator. For details see LD Column data sheet.
2. Prepare column by rinsing with 2 mL of buffer.

130-000-598-06

3. Apply cell suspension onto the column.
4. Collect unlabeled cells that pass through and wash column with 2×1 mL of buffer. Collect total effluent; this is the unlabeled cell fraction. Perform washing steps by adding buffer two times. Only add new buffer when the column reservoir is empty.

Depletion with CS Columns

1. Assemble CS Column and place it in the magnetic field of a suitable MACS Separator. For details see CS Column data sheet.
2. Prepare column by filling and rinsing with 60 mL of buffer. Attach a 22G flow resistor to the 3-way-stopcock of the assembled column. For details see CS Column data sheet.
3. Apply cell suspension onto the column.
4. Collect unlabeled cells that pass through and wash column with 30 mL buffer from top. Collect total effluent; this is the unlabeled cell fraction.

Depletion with D Columns

For instructions on column assembly and separation refer to the D Column data sheet.

Magnetic separation with the autoMACS™ Separator or the autoMACS™ Pro Separator

▲ Refer to the respective user manual for instructions on how to use the autoMACS™ Separator or the autoMACS Pro Separator.

▲ Buffers used for operating the autoMACS Separator or the autoMACS Pro Separator should have a temperature of ≥ 10 °C.

▲ Program choice depends on the isolation strategy, the strength of magnetic labeling, and the frequency of magnetically labeled cells. For details refer to the section describing the cell separation programs in the respective user manual.

Magnetic separation with the autoMACS™ Separator

1. Prepare and prime the instrument.

2. Apply tube containing the sample and provide tubes for collecting the labeled and unlabeled cell fractions. Place sample tube at the uptake port and the fraction collection tubes at port neg1 and port pos1.

3. For a standard separation choose one of the following programs:

Positive selection: "Possel"
Collect positive fraction from outlet port pos1.

Depletion: "Deplete"
Collect negative fraction from outlet port neg1.

Magnetic separation with the autoMACS™ Pro Separator

1. Prepare and prime the instrument.

2. Apply tube containing the sample and provide tubes for collecting the labeled and unlabeled cell fractions. Place sample tube in row A of the tube rack and fraction collection tubes in rows B and C.

3. For a standard separation choose one of the following programs:

Positive selection: "Possel"
Collect positive fraction in row C of the tube rack.

Depletion: "Deplete"
Collect negative fraction in row B of the tube rack.

3. Example of a separation using Anti-PE MicroBeads

Separation of human peripheral blood mononuclear cells (PBMCs) using PE-conjugated CD28 antibody, Anti-PE MicroBeads and a MiniMACS™ Separator with an MS Column.

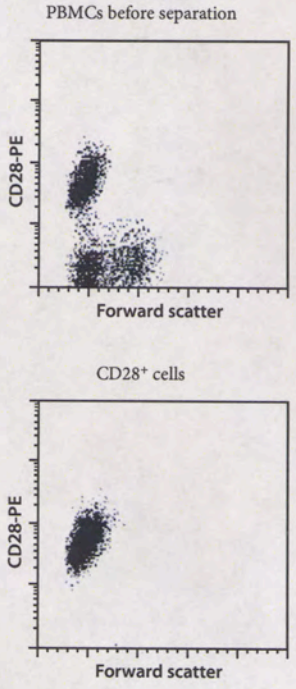

Warnings

Reagents contain sodium azide. Under acidic conditions sodium azide yields hydrazoic acid, which is extremely toxic. Azide compounds should be diluted with running water before discarding. These precautions are recommended to avoid deposits in plumbing where explosive conditions may develop.

Warranty

The products sold hereunder are warranted only to be free from defects in workmanship and material at the time of delivery to the customer. Miltenyi Biotec GmbH makes no warranty or representation, either expressed or implied, with respect to the fitness of a product for a particular purpose. There are no warranties, expressed or implied, which extend beyond the technical specifications of the products. Miltenyi Biotec GmbH's liability is limited to either replacement of the products or refund of the purchase price. Miltenyi Biotec GmbH is not liable for any property damage, personal injury or economic loss caused by the product.

140-000-098.06

Appendix 2

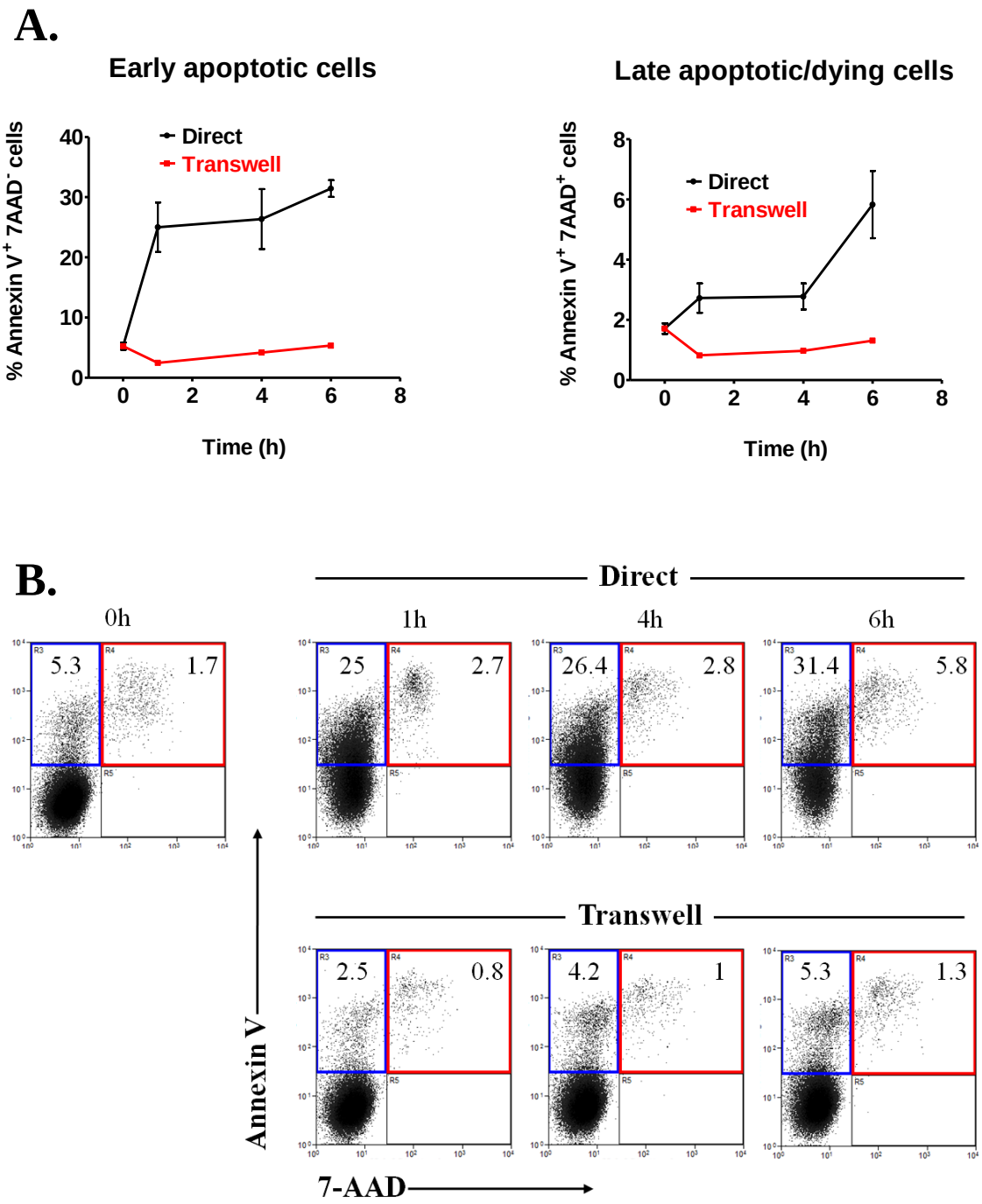

Direct interaction with epithelial CD1d induced apoptosis in *i*NKT cells. (A) 24h α–GC-pulsed Beas2B increased early (Annexin V^+ 7–AAD^-) and late (Annexin V^+ 7–AAD^+) apoptotic *i*NKT cell populations within 6h of co-culture. **(B)** Representative dot plot analyses are illustrated. N=2 independent experiments, 2-4 samples each.